2012

Implications of geothermal history on microbial gas generation and coalbed methane production in the Ninilchik Field, Cook Inlet basin, Alaska

Eric M. Hart
Louisiana State University and Agricultural and Mechanical College, ehart4@tigers.lsu.edu

IMPLICATIONS OF GEOTHERMAL HISTORY ON MICROBIAL GAS GENERATION AND COALBED METHANE PRODUCTION IN THE NINILCHIK FIELD, COOK INLET BASIN, ALASKA

A Thesis

Submitted to the Graduate Faculty of the
Louisiana State University and
Agricultural and Mechanical College
in partial fulfillment of the
requirements for the degree of
Master of Science

in

The Department of Geology and Geophysics

by
Eric M. Hart
B.S., Louisiana State University, 2010
December 2012

Acknowledgements

I would like to thank my committee chair and advisor, Dr. Jeffrey Nunn, for his Gandalf-like wisdom and guidance over the years, and my committee members, Dr. Alex Webb and Dr. Phil Bart, for their instruction throughout the course of my academic career at LSU. I also extend my appreciation to Richard Stanley of the USGS for the life-saving and very detailed explanation of his work on Cook Inlet stratigraphy, without which this study could not have been completed. Additionally, I would like to acknowledge Andrew Sampson's efforts in paving my way with his thesis on seismic attributes in the Ninilchik field, as well as for his continued assistance through his position at Marathon Oil Corporation. Furthermore, I was very fortunate in being selected for the Applied Depositional Geosystems (ADG) fellowship along with multiple installments of the Marathon Oil scholarship for academic excellence. The industry donors and members of LSU's Geology Department that strive to maintain these opportunities despite the seemingly endless budget cuts and weak economy warrant our sincere gratitude.

To my colleagues of the LSU graduate geology program, I hope to have offered you the same high levels of motivation and technical support that you have generously given me. And, of course, to my parents Tom and Paula, my sister Kelly, and all the members of my family, thank you for being there to show how much you love me every step of the way.

Last but unequivocally not least, my dearest, deepest thanks go out to my beautiful lab assistant/fiancée, Jance. You always stuck by my side, regardless of whether I deserved it or not. Getting through graduate school was the most challenging experience of my life, and if not for your help, encouragement and loving support, I most certainly would not have been capable of maintaining the mental fortitude necessary to see this project to fruition. I owe this achievement especially to you and will forever be in your debt.

Table of Contents

Abstract

Coalbed methane (CBM) production operations atop the Ninilchik anticline of Cook Inlet, Alaska pose intriguing questions regarding the nature of biogenic gas generation in a thermally complex forearc basin setting. This thermal complexity stems, in part, from its up to 30,000 ft thick Tertiary section, comprised of braided stream alluvium and expansive, interbedded coal deposits. Rapid accumulation of cold, glacial strata is documented as being capable of regionally suppressing the elevated heat flux values expected within a forearc basin. In addition, beds with high organic content, such as the coal layers, act as natural insulators from basinal heat flux and possibly cause a further increase to the thermal gradient (i.e. subsurface temperatures may be encountered at comparatively deeper depths relative to a basin with a more thermally conductive lithology). According to Head et al. (2003), 80 °C is the generally accepted maximum temperature that methanogenic bacteria can withstand before being pasteurized inside CBM reservoirs; therefore, the basin's geothermal history should play a pivotal role in determining which formations have sourced the highest amounts of methane and on what timescale this generation occurred. To investigate these questions, Ninilchik field's thermal and geohistories were calculated using the *PetroMod*® basin modeling software package to measure the changes in each layers' temperature with respect to time and depth. From these results, a sensitivity analysis of the controlling factors for biogenic gas generation (methanogenesis) was conducted to test the hypothesis that rapid Tertiary sedimentation has outpaced the basinal heat flux and is in fact the controlling variable for Ninilchik's natural gas potential. Results show that regionally, within the deepest parts of the basin that exhibit the highest sedimentation rates, this hypothesis is accurate. Locally, however, it is found that relative anticlinal uplift decreases both subsidence and sedimentation rates, and holds the coal-

bearing layers within the optimal temperature regime for extended periods of time. While it is previously understood that the anticlines create vast closures for hydrocarbon accumulation, it is concluded that, above all, relative anticlinal uplift gives rise to the most ideal reservoir conditions and instigates maximum methanogenesis within the Cook Inlet basin.

Introduction

Cook Inlet is a large estuarine basin in southern Alaska that has been producing hydrocarbons from Tertiary sandstone reservoirs since the discovery of the Swanson River field in 1957 (Boss et al., 1976; Haeussler & Saltus, 2011). As of 2010, >7.8 trillion cubic feet (Tcf) of natural gas and ~1.3 billion barrels of oil (BBO) have been extracted from the basin (Stanley et al., 2011), and since the late 1950's the population of south central Alaska, including the city of Anchorage, has relied on this production to fulfill their energy needs (Hartz et al., 2009). The Ninilchik field is located on the northwest coast of the Kenai Peninsula, approximately 90 miles southwest of Anchorage (Figures 1 & 2) (Hartz et al., 2009; Gorney, 2011). Although the ~27 km (16.8 mi) long, NE/SW-trending anticline that comprises Ninilchik was first identified in the 1960's as a potential oil play, it wasn't until the early 2000's that Marathon Oil brought renewed interest in the field for its accumulation of natural gas (Haeussler & Saltus, 2011; Gorney, 2011).

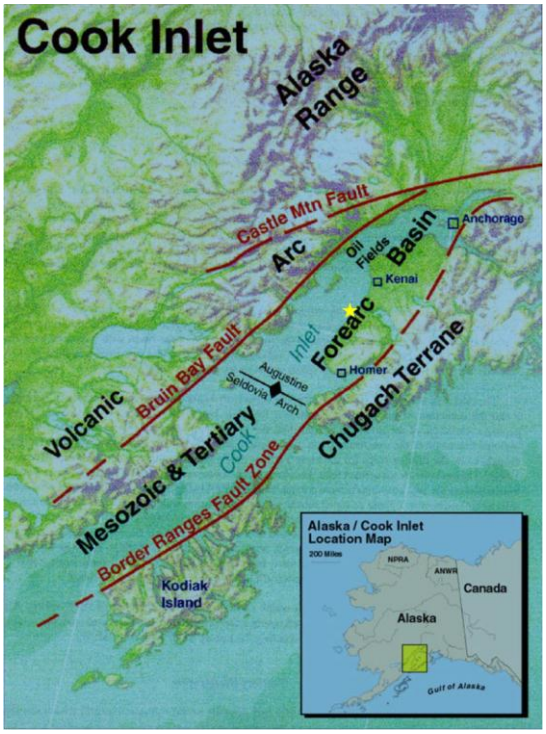

Figure 1: Map of Cook Inlet showing basin-bounding faults, mountain ranges, and more populated areas. The yellow star marks Ninilchik field. Image modified from Swenson, 2001.

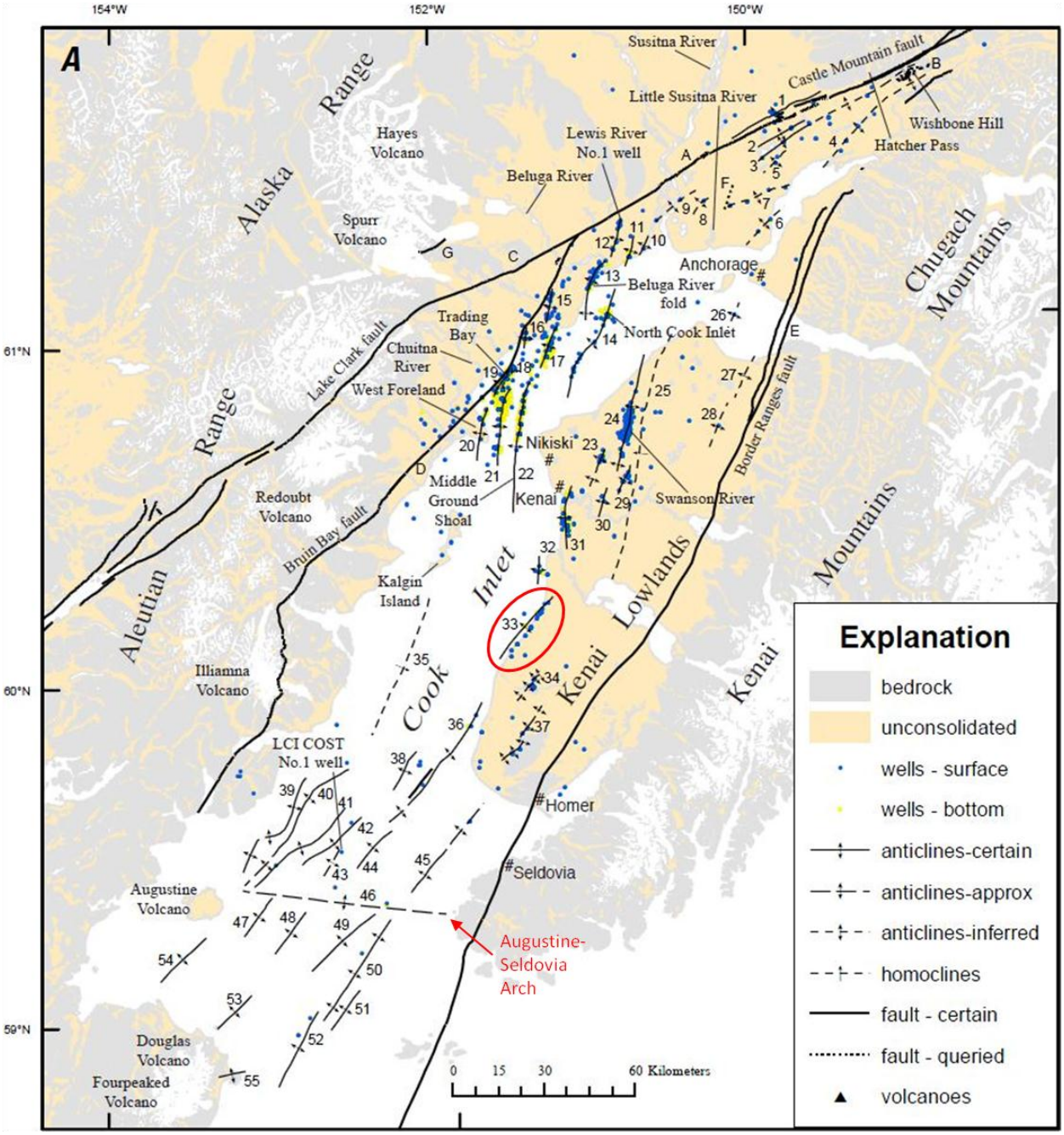

Figure 2: Map of Tertiary structures in Cook Inlet basin showing faults (lettered), folds (numbered, dashed if uncertain) and well locations (blue = surface, yellow = bottom hole). Note that the majority of wells trend with anticlinal features. The anticline that forms the Ninilchik field (#33) is circled in red and the Augustine-Seldovia Arch is labeled in red. Refer to Haeussler & Saltus (2011) for a more detailed description of the basinal structures. Image modified from Haeussler & Saltus, 2011.

Thick Tertiary coal deposits are the source of Cook Inlet's significant coalbed methane (CBM) resources, and all existing fields in the basin produce from structural traps atop anticlinal crests (Figure 2) (Haeussler & Saltus, 2011). Over 90% of the gas produced from Cook Inlet is very dry and light with respect to oil condensate and carbon isotopes (Figure 3) (Hartz et al., 2009; Strąpoć et al., 2011b). This implies that gas was biogenically generated *in situ* from the abundant coals, expelled directly into the interbedded Tertiary sands, and has since accumulated within the anticlinal folds (Figure 4) (Montgomery & Barker, 2003; Stanley et al., 2011).

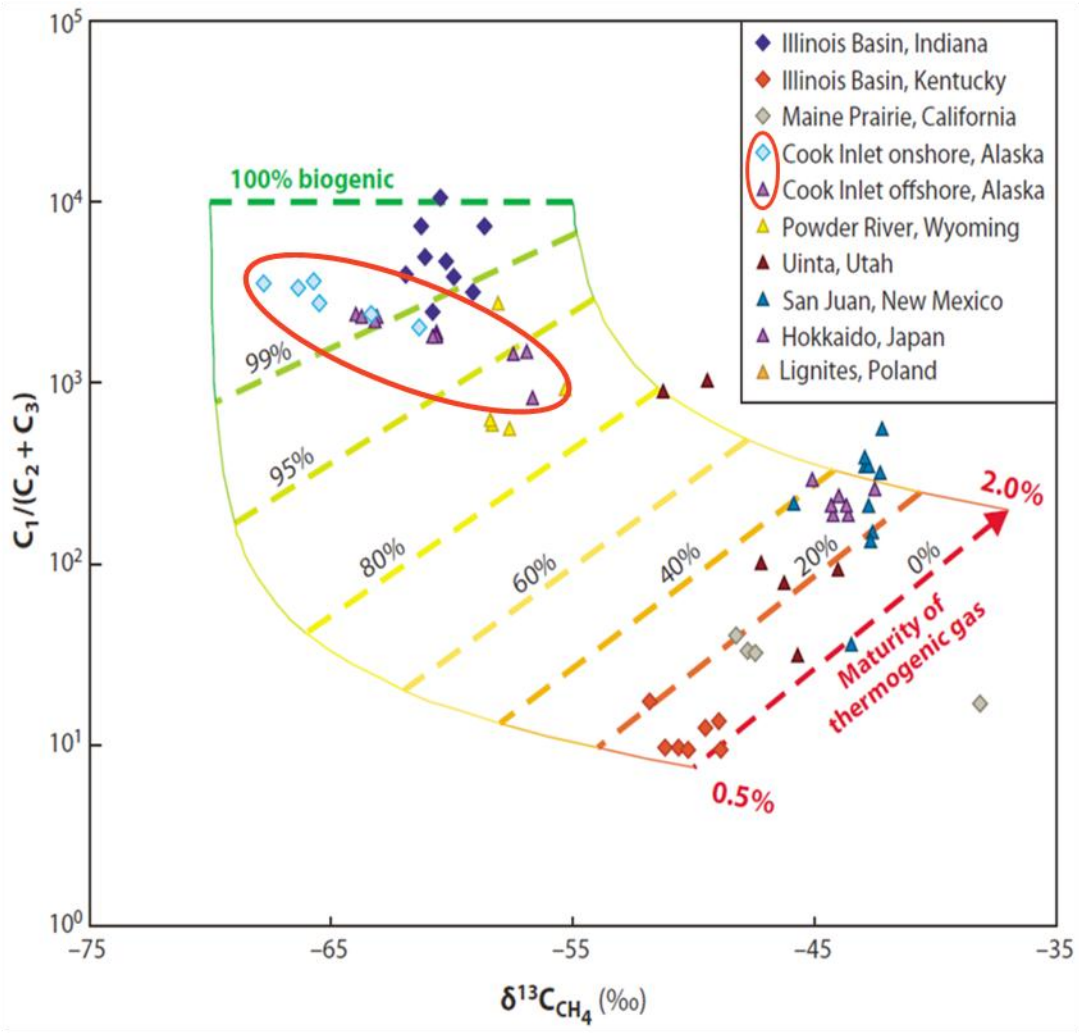

Figure 3: Distribution of biogenic and thermogenic gas accumulations from various basins based on gas dryness and Carbon isotope fractionation of methane. Ninilchik values correspond with the light blue diamonds circled in red. Image modified from Strąpoć et al., 2011b.

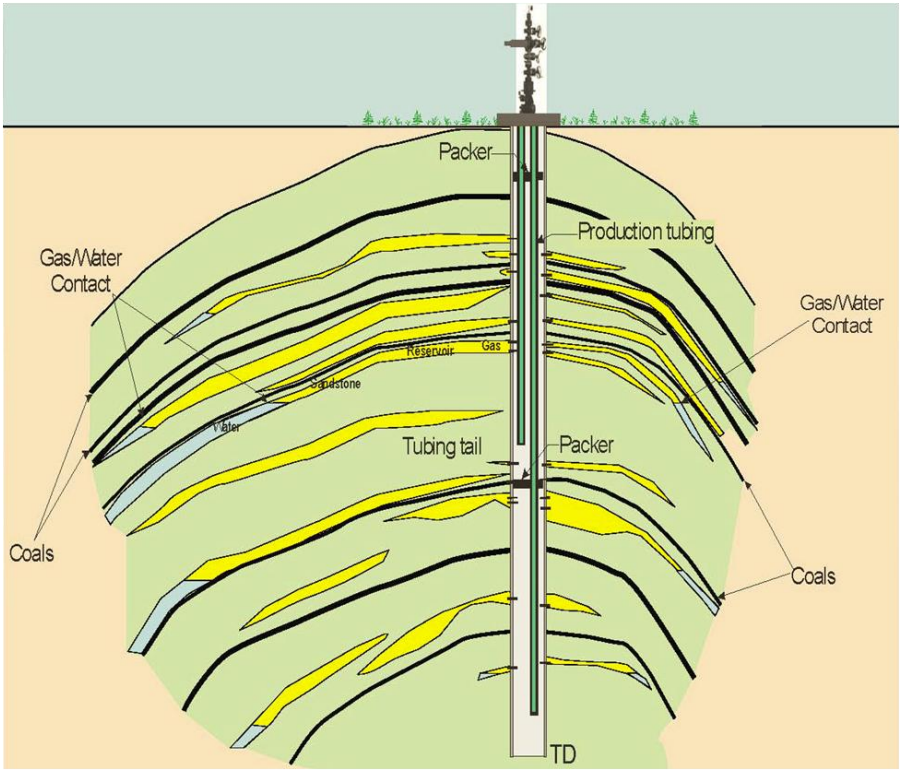

Figure 4: Schematic of petroleum system showing the *in situ* coals in which gas is generated and expelled directly into the interbedded sand units, then migrates updip toward the anticlinal crests, thus creating optimal drilling sites. Image modified from Stanley et al., 2011.

A small portion of the Cook Inlet gas is thermogenic in nature and found in association with oil reservoirs sourced from Jurassic marine shales. Oil production, however, occurs mainly in the basin's northeast fields, and is noticeably absent from the southern and central areas (e.g. Ninilchik) where the geothermal gradient is approximated as a relatively low 1 °F/100 ft (18 °C/1000 m) (Brimberry et al., 2001; Montgomery & Barker, 2003; Gorney, 2011). In addition, the presence of gas within coal beds is not a spontaneous occurrence; breakdown of coals' organic macerals releases methane gas particles through degradation of their constraining bonds, which requires either a biogenic process (i.e. methanogenesis) or a thermogenic process via increased reservoir temperature (Penner et al., 2010; Strapoć et al., 2007). Gas production in the Ninilchik field is sourced mainly from coals in the Tyonek Formation, with a minor amount obtained from the Beluga formation (Gorney, 2011; Sampson, 2011).

Since the reinitiation of the field in 2001, the twenty five wells drilled to target its reserves have produced over 127 billion cubic feet (Bcf) of natural gas, making Ninilchik the 5th largest gas-producing field in Cook Inlet. Additionally, high variation in gas production has been observed between wells across the anticline over the past decade, and the causes of this are not entirely understood (Gorney, 2011; Sampson, 2011). Possible explanations for these production variations include areas of higher coal deposition creating a larger source for gas generation, or portions of the anticline may have been subjected to the requisite gas generation temperatures for longer periods of time through differential structural deformation. Additionally, it is also proposed that the rapid rates of sediment deposition measured within the basin play a role in suppressing the basinal heat flow, which could increase the coal bearing formations' exposure times to the relatively low biogenic gas-forming temperatures (i.e. low temperature change with depth implies a longer period of gas generation). This study uses 3D seismic in conjunction with well logs and production data to characterize Ninilchik's regional variations in well production through an analysis of its geothermal and hydrocarbon generation history. To examine the extent of biogenic gas generation, exposure time for the coals' subjection to 'biogenic gas window' conditions were calculated, assuming reservoir pasteurization temperatures of 50 and 80 °C for the two types of microbial methane producers known as methanogens (Boone et al., 1993; Head et al., 2003; Hartz et al., 2009). Additionally, the field's thermal maturity was estimated to assess the likelihood for thermogenic hydrocarbon generation, or, more specifically, to explain the lack thereof. A sensitivity analysis was also conducted to test the precision of the final output data, as well as to further assess the controlling factors of gas generation. Lastly, using this geothermal history analysis, attempts were made to identify potential subsurface zones for CBM enhancement in the Ninilchik field.

Geologic Setting

Basin Formation

The Cook Inlet of southern Alaska is an elongate, northeast-trending, fault-bounded forearc basin that developed from tectonic coupling between the North American and Pacific plates along the Alaska-Aleutian subduction zone (Figure 5) (Haeussler et al., 2000; Swenson, 2001). Its structural configuration has evolved through multiple orogenic events that range from the Mesozoic to the Quaternary. Complex faulting of the Talkeetna anticline during the Mid Jurassic initiated the basin's emergence with the formation of a half graben on its northern edge (Kelly, 1963). Accretion of a microcontinent onto the North American plate during Cretaceous time created the Alaska Range and continued this half graben development across the basin's northwest flank (Figure 1) (Haeussler et al., 2000). From the Late Cretaceous to the Tertiary, uplift associated with early Laramide orogenesis generated a full graben by enclosing the basin's southeast margin with the Kenai and Chugach mountain ranges (Figure 2) (Kelly, 1963). The basin is bound to the northwest by the Bruin Bay fault, to the north by the Castle Mountain fault and to the southeast by the Border Ranges fault, and in many places these are thought to still be currently active as evidenced by the historical seismicity documented throughout the Cook Inlet region (Haeussler et al., 2000).

Structure

The basin is characterized by northeast/southwest-trending en echelon anticlines with westward asymmetry and intense local faulting (Kirschner & Lyon, 1973). While North American/Pacific plate convergence is the primary driving mechanism of deformation in Cook Inlet, the complex nature of these folds indicates that an additional right-transpressional component must be present (Haeussler et al., 2000). According to Haeussler and his colleagues,

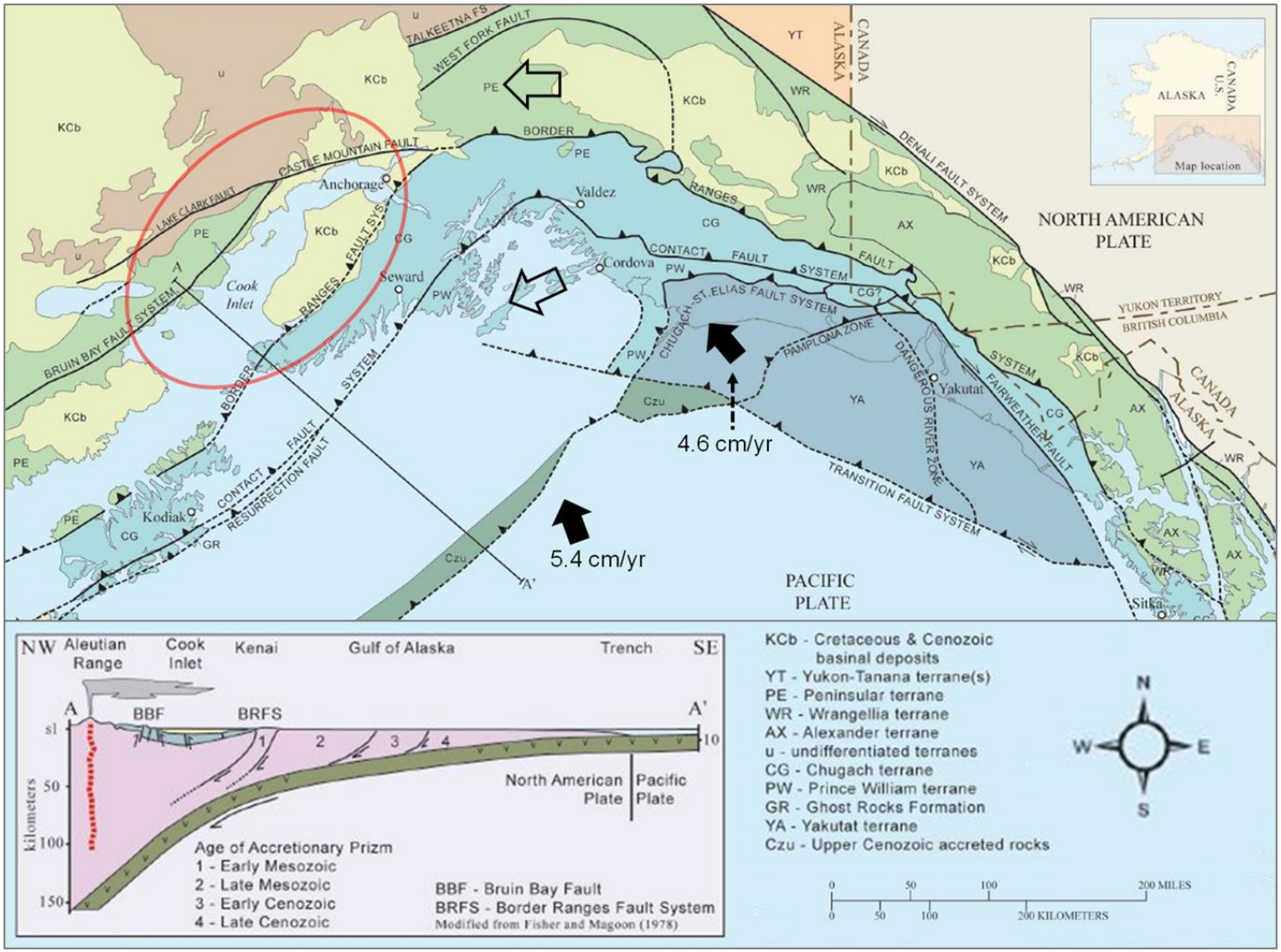

Figure 5: Geologic map of SE Alaska depicting the Alaska-Aleutian subduction zone and subsequent tectonic deformation. Velocity vectors (solid arrows) show motion of Pacific plate and Yakutat terrane (dark blue) relative to North America, as well as the interpreted dextral transpression (open arrows) (Haeussler et al., 2000). Cross section AA' illustrates a schematic view of Pacific Plate subduction beneath the Cook Inlet forearc basin (circled in red). Image modified from Haeussler & Saltus, 2011.

the source for this dextral transpression lies 300 km to the east with the Yakutat terrane's collision and indentation into the North American plate at an approximated rate of 46 mm/yr (Figure 5). Similar to Himalayan deformation models, the principal stress directions of the collision radiate outward from the Yakutat's point of impact, forcing the Cook Inlet forearc basin to escape obliquely to the southwest (Haeussler et al., 2000). As a result of this Late Oligocene-to-present microplate collision, basinal structures began to form in Cook Inlet as early as the Late Miocene, however, shallow termination points of deep-seated oblique-slip faults show that much of the deformation occurred after the deposition of Pliocene-aged strata (Haeussler et al., 2000; Haeussler & Saltus, 2011).

Depositional Environment

A wide range of volcanic, marine and nonmarine clastic sediments have been preserved in this rapidly subsiding intermontane basin from the Late Triassic to the Holocene (Kelly, 1963). Cook Inlet's stratigraphic record contains approximately 40,000 ft (12,195 m) of Mesozoic rock and 30,000 ft (9,150 m) of Tertiary beds in the deepest parts of the basin, however, due to Ninilchik's relative proximity to the Augustine-Seldovia Arch (Figure 2), the Tertiary section thins to around 12,000 ft (3658 m) across the field (Kirschner & Lyon, 1973; Gorney, 2011). The Mesozoic sediments were generated by 3 cycles of marine deposition in the progressively closing forearc basin and consist mainly of metamorphosed turbidite sequences, carbonates and volcanics (Kirschner & Lyon, 1973). Lying angularly unconformable above this Mesozoic section, the Tertiary strata formed through 2 cycles of estuarine to nonmarine deposition and are largely characterized by eroded, weathered or reworked volcanics and metamorphics which were deposited on extensive floodplains via braided, anastomosing and meandering streams (Kelly, 1963; Barker & Dallegge, 2001). Also interbedded with this

alluvium are thick deposits of coal that were derived from vast swamplands bordering the fluvial systems (Swenson, 2001).

Stratigraphy

Due to a lack of accessible outcrop data with which to compare the well logs, stratigraphic correlations of the Tertiary formations are widely variable. Nevertheless, the generalized stratigraphic model assembled by Stanley et al. (2011) honors all of the available biostratigraphic and geochronologic data and is adopted for this study (Figure 6). Based on $^{40}Ar/^{39}Ar$ and fission track dating of ash partings in coal beds, the Sterling/Beluga formation contact has been constrained at 8 Ma (Dallegge & Layer, 2004). Unfortunately, this radiometric dating was not continued through the rest of the Tertiary. The base of an undivided Beluga-Tyonek-Hemlock unit is shown at about 33.5 Ma and is interpreted as a regional unconformity that coincides with a prominent global drop in sea level between 33.5 to 35.7 Ma (Stanley et al., 2011; Miller et al., 2008). To differentiate between these undivided formations of the Kenai Group, ages have been extrapolated at 14.5 Ma and 31.7 Ma for the Beluga/Tyonek and Tyonek/Hemlock contacts. Assuming that the 9,800 ft undivided unit formed through constant deposition over its 25.5 Ma span, the resulting average accumulation rate of 11.7 cm/ka would have laid down the 2,500 ft Beluga, 6,600 ft Tyonek, and 700 ft Hemlock formations in ~6.5, 17.2 and 1.8 Ma, respectively (Gorney, 2011). Below the Hemlock formation, although not included in the Kenai Group because it lacks significant coal beds, the West Foreland formation lies atop Late Cretaceous strata on a regional angular unconformity which is thought to be related to uplift and erosion that accompanied the subduction of a spreading ridge beneath southern Alaska during the Early Tertiary (Swenson, 2001). The exact age of this basal Tertiary West Foreland formation is unclear, but based on the assumption that the oldest West Foreland is

as old as the oldest of its equivalent Chickaloon formation, it is estimated to be 56 Ma (Wilson et al., 2009). Although other stratigraphic models may interpret the Tertiary formations to be somewhat time transgressive throughout the basin, this model assumes that formational contacts are time constant within the study area.

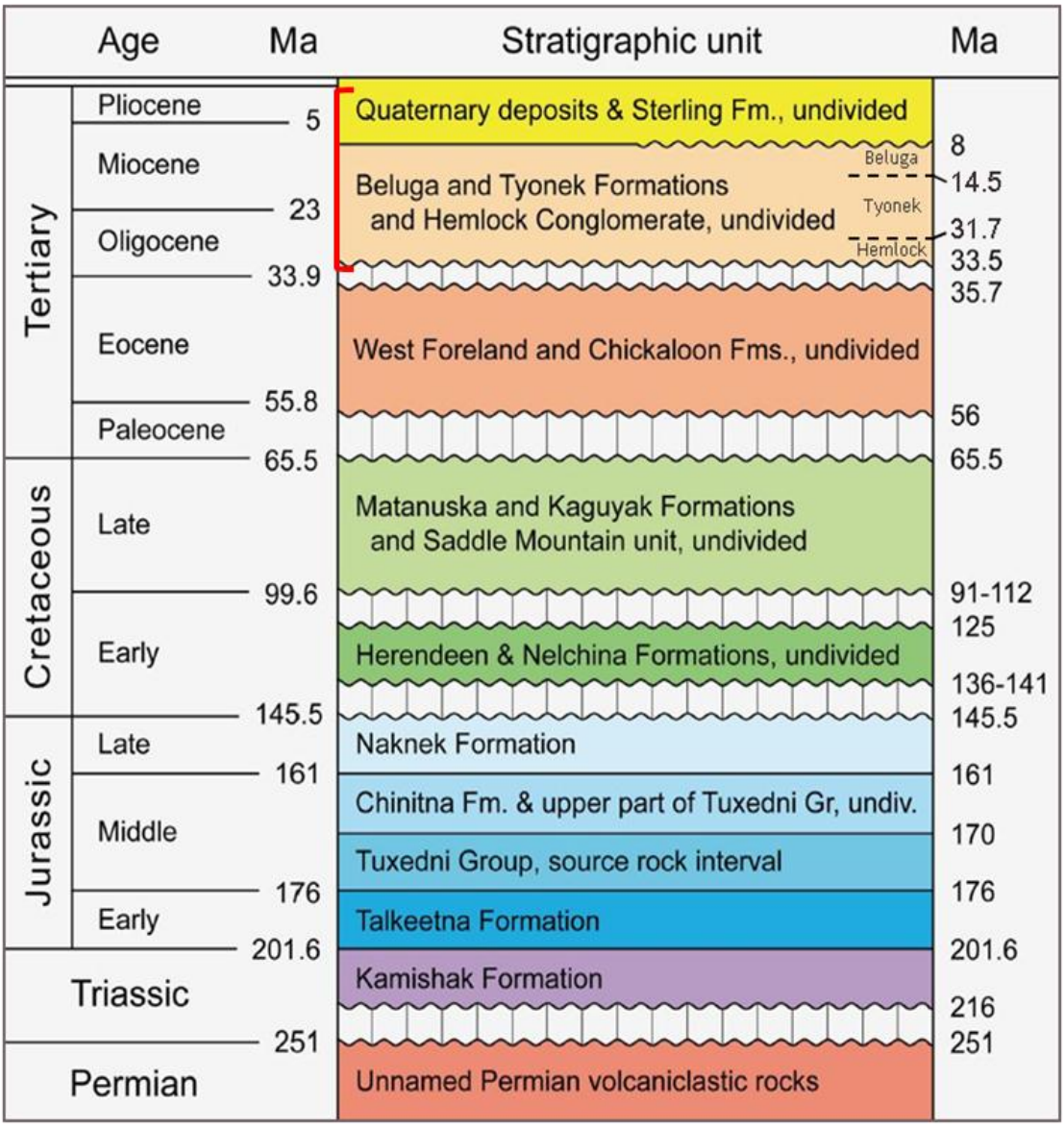

Figure 6: Model of Cook Inlet's Tertiary, Mesozoic, and uppermost Paleozoic stratigraphy with Kenai Group bracketed in red. Although generalized, this interpretation currently provides the most complete assessment for the timing of basinal deposition/erosion, and is based on the most recent biostratigraphic and geochronologic data available. Ages for the Tyonek's top and base were extrapolated using an average deposition rate for the undivided unit. Formation contacts are assumed to be time constant within the study area. Image modified from Stanley et al., 2011.

Data

Seismic Data

The available seismic data set for the Ninilchik field consists of a merged 3D survey donated to LSU by Marathon Oil Company, which was used to visualize and quantify the extent of structural deformation across the anticline. CGGVeritas merged two adjacent surveys (2003 & 2007) that together encompass a NE/SW-oriented rectangular area of 128 mi^2 along the NW coast of the Kenai Peninsula near the town of Ninilchik, Alaska (Figure 7). Since the modern day shoreline generally trends with the subsurface anticlinal fold axis, both onshore and offshore gathering techniques were employed. As seen in Figure 7, imaging complications were encountered while collecting the onshore data due to the inaccessible nature of the terrain at the water's edge (Figure 8). A '5D' processing method was developed by CGGVeritas to mitigate these processing difficulties. This new method utilized inline, crossline, offset, azimuth, and frequency data to interpolate signal in gaps where receivers were unable to be positioned. While pre-stack depth migration (PSDM) and post-stack time migration (PSTM) surveys were both available in this seismic package, only the PSDM was selected for further interpretation. The PSDM seismic volume was input into Schlumberger's *Petrel® 2011* software by, Andrew Sampson, whose M.S. thesis pertained to seismic interpretation of the Ninilchik anticline along with characterizing the field's well production using seismic attributes. For a more comprehensive description of the seismic data and incorporated fault and horizon interpretations, refer to Sampson (2011).

Well Data

In addition to seismic data, digital wireline logs were available through the Alaska Oil and Gas Conservation Commission (AOGCC) for 20 of the 24 wells inside the project area. 15

of these wells currently contribute to the field's gas production and have up-to-date cumulative production values accessible from www.drillinginfo.com. Each of the productive wells was drilled between 2001 and 2011 from one of five onshore well pads. Listed from NE to SW, these pads include: Falls Creek, Grassim Oskolkoff, Ninilchik State, Susan Dionne, and Paxton (Figure 9). To target the main anticlinal fold axis, an S-shaped drilling pattern was applied, which allowed for bottom-hole locations to be deviated by a mile or more between wells of a common pad. Surface coordinates and deviation paths were also acquired from the AOGCC website and plotted into *Petrel*®.

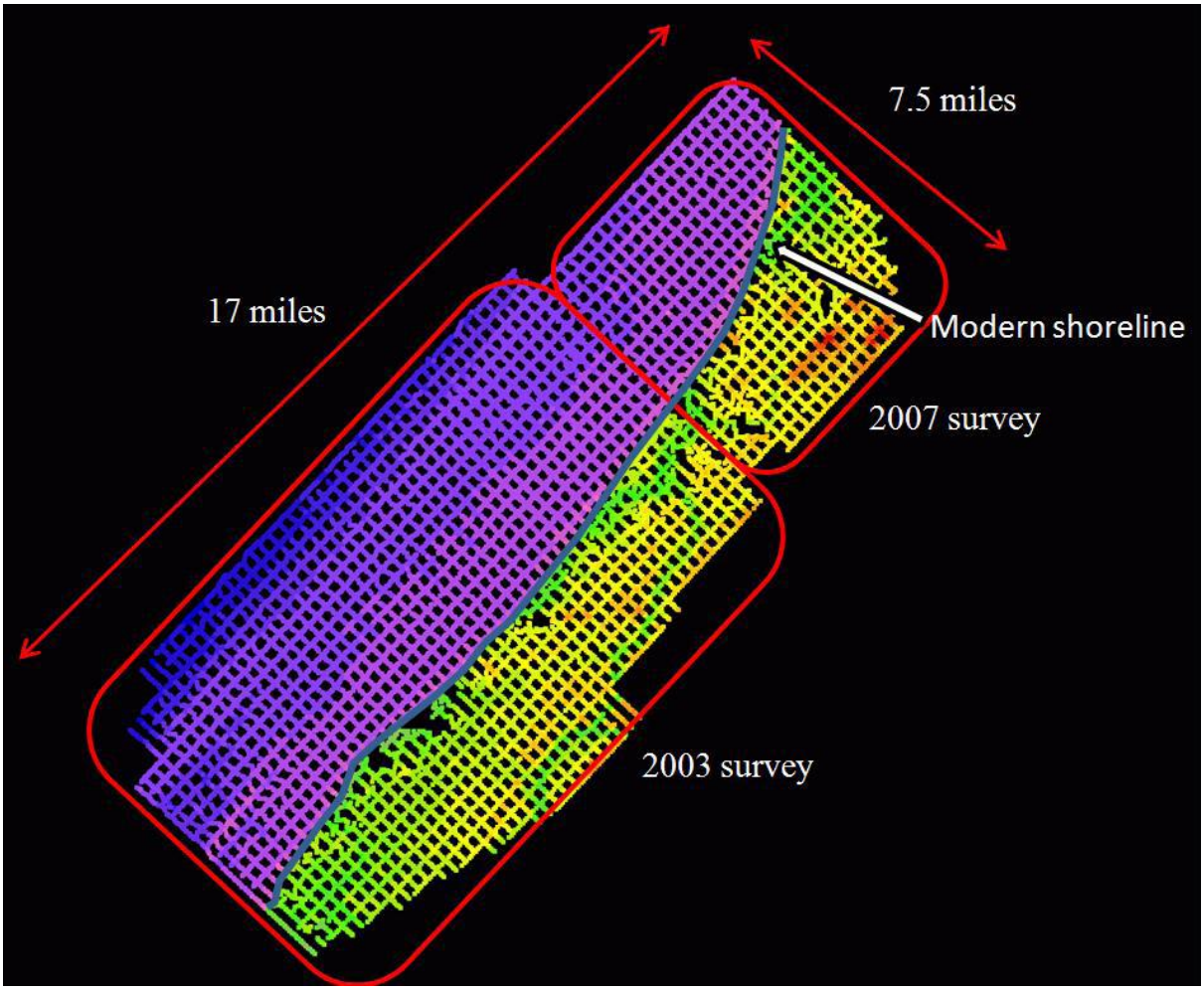

Figure 7: 3D seismic lines of Ninilchik's merged surveys. Purple lines signify offshore airgun acquisition and yellow lines signify an onshore dynamite source. Difficult areas to access are indicated by gaps in seismic lines near the coast. Image from Sampson, 2011.

Figure 8: Outcrop of Tyonek formation near Capps Glacier, Alaska showing a substantial coal layer encased in sandstone. No scale provided. Image from Stanley et al., 2011.

Of the wireline data obtained from the AOGCC, varying degrees of quantity and quality exist among the logging suites. The most inclusive package of digital logs for wells in the Ninilchik field consists of spontaneous potential, gamma ray, resistivity, sonic, and bulk density. Each of these logs were utilized to interpret formation boundaries as well as to compute the Net-to-Gross (NtG) coal thicknesses required to assess geothermal history and calculate biogenic gas generation. The spontaneous potential (SP) log measures naturally occurring electric potentials in the subsurface, and it is used to calculate formation water resistivity and determine bed boundaries. The gamma ray (GR) tool measures the natural emission of gamma rays by a formation and is widely used as a lithology indicator. Resistivity (ResD) tools measure a formation's resistance to electrical flow, which may signify the presence of hydrocarbons in the pore space. The sonic (Dt) tool records acoustic (P-wave) travel time through a medium and can be used to correlate the logs with seismic data as well as an additional lithology indicator. And finally, the bulk density (RhoB) tool utilizes a gamma ray source and receiver system to measure the density of a formation and is used to infer lithology, along with pore volume and contents. Appendix A provides a list of production and available logs for all the wells used in the study.

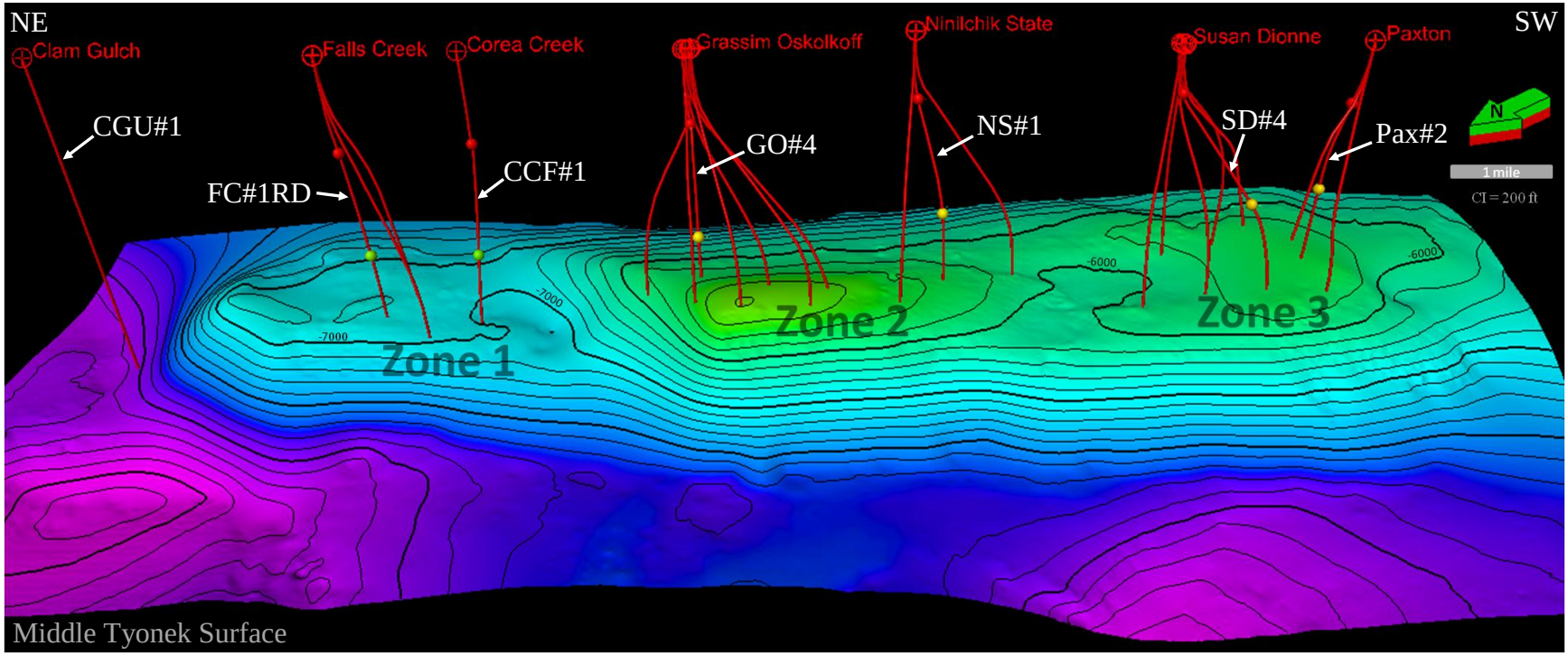

Figure 9: 3D seismic surface displaying the Ninilchik anticline on a middle Tyonek coal reflector. Brighter greens indicate higher points on the anticline, while the brighter pinks indicate deeper points off-structure. Well paths are shown in red from their surface location down to their point of intersection with the horizon, and the three separate fault blocks are labeled Zone 1, 2 & 3. White labels indicate the wells selected for the methanogenesis calculation study, and the red and yellow spheres indicate where they intersect the top of the Beluga and Tyonek formations. Image is oriented NE-SW to better illustrate the anticlinal structure.

Basin Heat Flow

In conjunction with the information obtained through the seismic and well data along with the depositional model from Stanley et al. (2011), basinal heat flux values are required to perform a geothermal history analysis. By the application of Fourier's Law, heat flux within a basin can be determined from geothermal gradient and thermal conductivity measurements (Turcotte & Schubert, 2002). Corrected bottom hole temperatures from wells are used to model present day heat flow and estimate the temperature gradient, while thermal conductivities can be obtained from formation lithologies (Li, 2006; Nunn & Lin, 2002). Values for heat flow in forearc basins are influenced by the age and depth of the subducting oceanic plate (Okubo et al., 2005). Muller et al. (2008) estimate the age of the Pacific plate under SE Alaska to be approximately 20-40 Ma, and Haeussler et al. (2000) establish that its depth of subduction reaches 50-60 km beneath the basin's center. A geothermal map of Alaska generated by Southern Methodist University places the Kenai Peninsula's heat flow between 40-44 mW/m^2 (Figure 10), and USGS data confirm this approximate value of 40 mW/m^2 (Blackwell & Richards, 2004; Lillis & Stanley, 2011).

Thermal Conductivity

Basinal heat flux can have a strong impact on the geothermal history of a region if given enough time to reach a state of equilibrium (Turcotte & Schubert, 2002). As cold, fluvial sediments are supplied to Cook Inlet, this basinal flux progressively transmits heat from below through each consecutive layer of deposition over the course of millions of years. Some sediments, however, are more efficient at conducting heat than others. According to Nunn & Lin (2002), organic rich rocks, such as the thick coal beds seen throughout the Tertiary section, have notably low thermal conductivities. These 'natural insulators' can cause elevated temperature

gradients and possibly even increase the thermal maturity of underlying units when heat flow is in equilibrium (Nunn & Lin, 2002). Additional factors that could affect the basin's heat transfer are fluid flow and radioactive heat decay. Further research may be necessary to determine the penetration depth of meteoric groundwater as well as the concentration of radioactive isotopes contained in the volcanics and fine-grained strata.

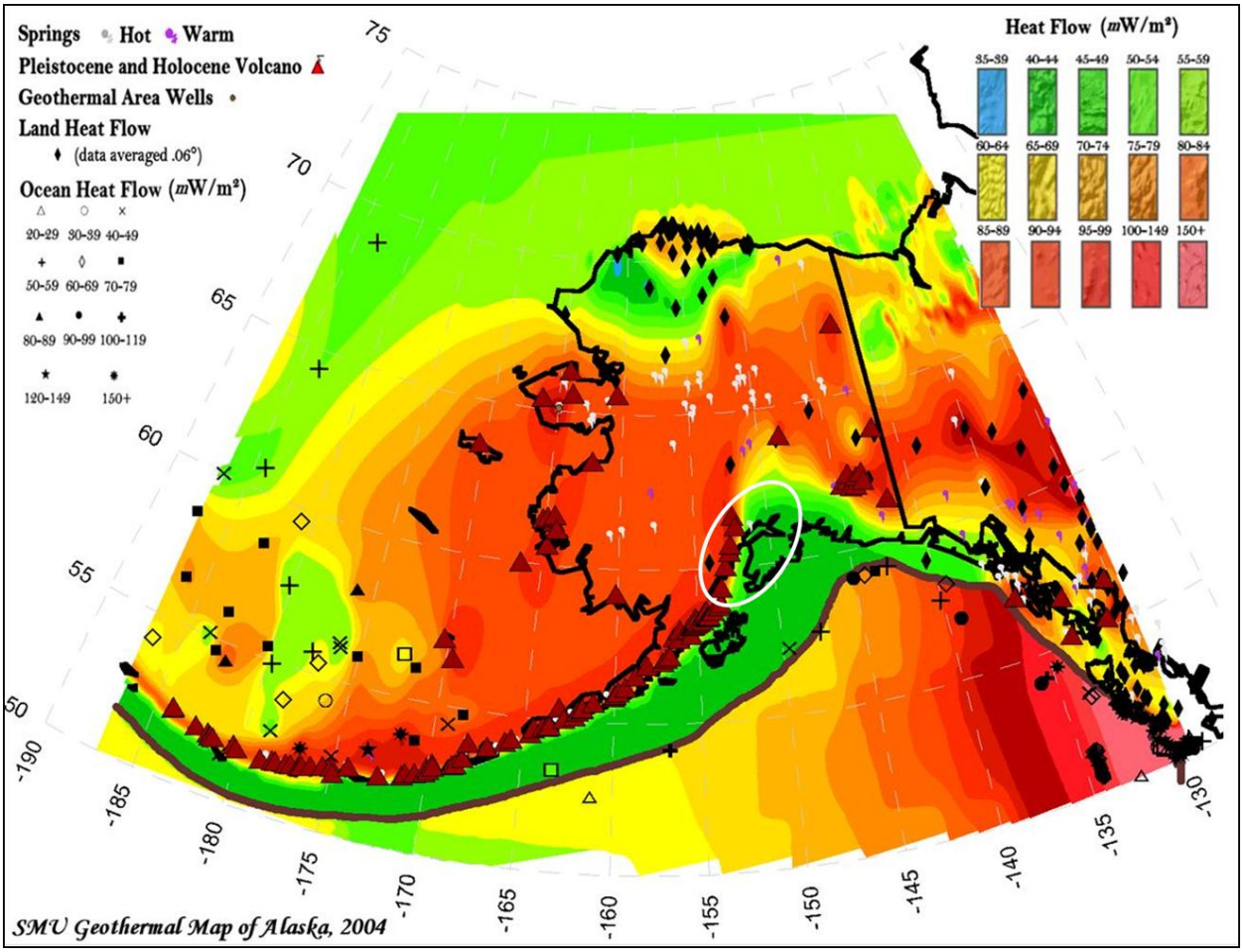

Figure 10: SMU's geothermal map of Alaska (an extension of the Geothermal Map of North America, 2004) showing surface heat flow in mW/m^2 from a combination of industry and USGS thermal data. Cook Inlet is circled in white. Image modified from Blackwell & Richards, 2004.

Kerogen

Aside from being natural insulators, coal layers exhibit large quantities of type III kerogen, making them a potentially significant source of natural gas (Figure 11) (Schlumberger

Oilfield Glossary). In each of the upper three formations of the Oligocene-to-Pliocene-aged Kenai Group, the net thickness of the source coals often exceeds 150 ft (46 m) at depths shallower than -6,000 ft (-1829 m) (Montgomery & Barker, 2003). Depth is significant to CBM exploration because increased temperature and overburden pressure heals coal cleats at depths greater than ~2 km, causing the hydraulic permeability of gas to drop substantially (Dallegge & Barker, 2000). Furthermore, as seen in Figure 12, the coals have a vitrinite reflectance of less than 0.6% (i.e. thermally immature) and are subbituminous in rank, but still manage to contain an average adsorbed gas content of 50 standard cubic feet per ton (scf/ton) (Montgomery & Barker, 2003). This value of 50 scf/ton was reduced by as much as 48% from its initial measurement to account for secondary gas emissions from renewed methanogenesis during coal desorption analyses (Barker & Dallegge, 2006).

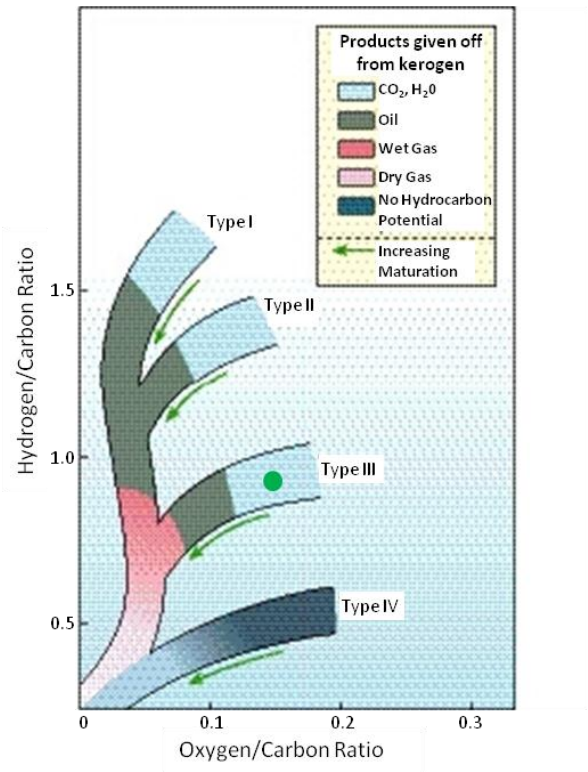

Figure 11: Graph of the H/C vs O/C maturation pathways for kerogens Type I-IV, along with the products given off through each stage of maturation. The green dot indicates an estimated H/C:O/C ratio for Ninilchik (HI ≈ 6). Image modified from the Schlumberger Oilfield Glossary.

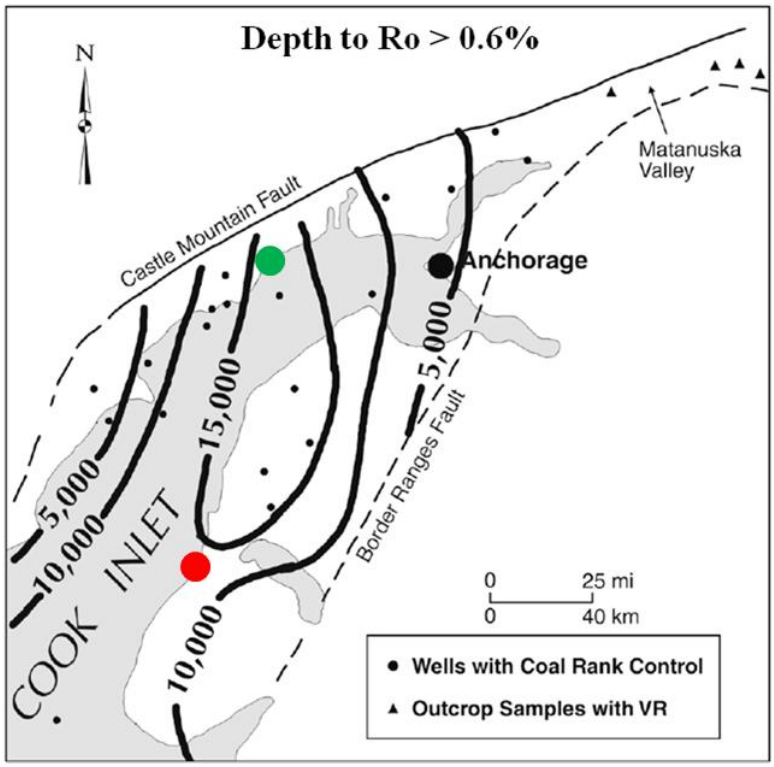

Figure 12: Contour map for depth (ft) to top of oil window showing Ninilchik field in red and the ConocoPhillips microbial diversity study in green. Both sites lie near the -15,000 ft contour and should have similar thermal histories. Image modified from Montgomery & Barker, 2003.

Biogenic Gas Generation (Methanogenesis)

Comparable to the thermogenic gas window that is encountered at subsurface temperatures between ~100-200 °C, the 'biogenic gas window' is also largely determined by reservoir temperatures and geothermal gradient (Ferry, 1993). Unlike thermogenic gas, however, since different microbes dominate at different temperatures ranges, the biogenic gas window can vary greatly depending on the specific assortment of microbes present in a particular subsurface zone (Ferry, 1993). Of the numerous types of microbes found in the subsurface, Methanogenic Archaea, or methanogens, are the group responsible for generating natural gas from coal (Figure 13); although certain types of bacteria and fungi also play a significant role by breaking down coal macerals into 'bite-size' pieces for the Archaea (Ferry, 1993; Penner et al., 2010). Methanogens are categorized as either mesophilic or thermophilic based on the

temperature range in which they live, and are also grouped according to their main metabolic pathway. Mesophilic methanogens are found between ~10-50 °C, with an optimum temperature of ~37 °C, while thermophilic methanogens can exist from ~40-80 °C, with a peak operation temperature of ~65 °C (Boone et al., 1993; McIntosh et al., 2010). Beyond temperatures of ~80 °C, reservoirs become effectively 'pasteurized' and biogenically-derived methane generation ceases (Head et al., 2003). The three metabolic pathways of methanogens consist of either CO_2 reduction, acetate fermentation, or methyl group utilization; however, some specimens have been documented as being capable of transitioning to the most efficient of the three in varied environments (Strąpoć et al., 2011a).

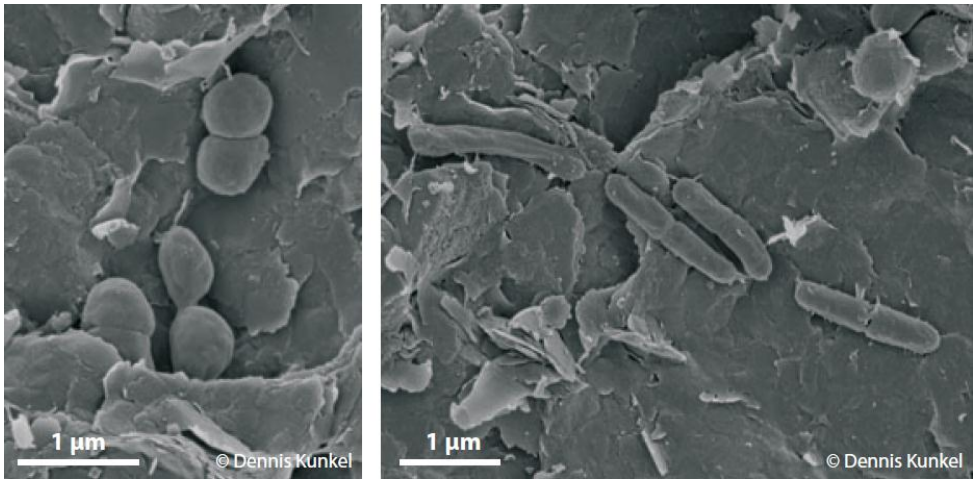

Figure 13: Spherical and Rod-shaped methanogens on coal matrices displayed through scanning electron microscopy. Image from Strąpoć et al., 2011b.

Ideal laboratory estimates for the rate of methanogenesis in Cook Inlet are approximately 7,500 scf per ton of coal a year, though it is important to keep in mind that a lack of resources can significantly inhibit microbial activity *in situ* and actual subsurface rates are generally orders of magnitude slower than in the laboratory (Strąpoć et al., 2011b; Penner et al., 2010). Other than temperature and nutrients, methanogenesis is also controlled by: pH, salinity, porosity/permeability, availability of electron donors/acceptors, toxicity of trace metals, quantity

of organic matter, and quality of organic substrates (Schlegel et al., 2011). Because of these wide ranging variables, accurate rates of subsurface methanogenesis are difficult to constrain. However, studies on the occurrence of methane production as a function of temperature in rice fields have been able to estimate the rates of methanogenesis between the temperatures of 0, 37 and 50 °C (Figure 14) (Yao & Conrad, 2000).

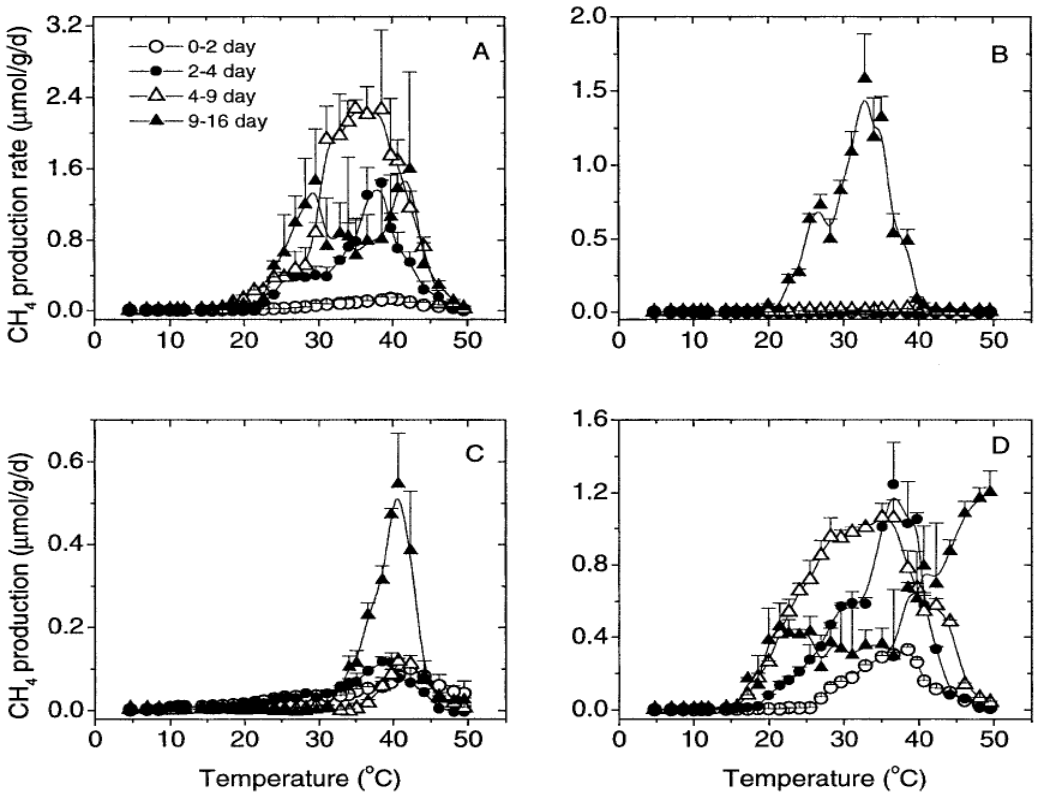

Figure 14: Rates of mesophilic methanogenesis at various temperatures and incubation durations for rice field soil samples from the Philippines (A-C) and Italy (D). Note that the peak rate centers upon ~37 °C and approaches zero at 10 °C and 50 °C. Image from Yao & Conrad, 2000.

Coalbed Methane (CBM) Enhancement

Despite the uncertainties surrounding *in situ* methanogenesis, attempts have been made to investigate the possibility of enhancing reservoir conditions to boost methanogenesis rates and overall gas production (Strąpoć et al., 2011a, b; McIntosh et al., 2010; Penner et al., 2010). According to Strąpoć et al. (2011b), the fraction of subbituminous coal that is biodegradable by

certain bacteria and fungi, and ultimately convertible to methane through methanogenesis, is ~30% of the total matrix by weight percent (wt%). Under ideal laboratory conditions, this entire 30 wt% of coal can be completely converted to methane in approximately two years, at the rate of 7,500 scf/ton per year. From this estimation, it is determinable that if given either an exceedingly sufficient conversion rate or duration of time for all of the 30 wt% convertible coal to be transformed into methane, the maximum generation potential of subbituminous coal would be an astronomical value of ~15,000 scf/ton. Any advancement that brings *in situ* methanogenesis closer to this ideal laboratory rate could have a significant impact on energy resources worldwide. For example, McIntosh et al. (2010) postulate that by simply sequestering CO_2 (a methanogen metabolic substrate) in CBM fields, the influx of resources might be capable of generating a potentially renewable hydrocarbon resource while simultaneously decreasing the amount of harmful greenhouse gases in the atmosphere.

To evaluate the specific requirements of a CBM enhancement operation in Cook Inlet, ConocoPhillips performed a gas isotope and microbial diversity assessment of a supposedly 'undisclosed' field (Beluga River) which happens to have a similar thermal maturity as Ninilchik (Figures 12 & 15) (Strąpoć et al., 2011a). While the effectiveness of their endeavor on overall well production has yet to be released, results from their study have been published which may provide intriguing insight into the nature of Cook Inlet methanogenesis. According to the deuterium and carbon isotope fractionations in the generated methane, gas accumulations of the field were more strongly attributed to the acetate and methyl/methanol utilizers rather than the CO_2 reducers (Figure 16). This data could be used as an example of what is needed to prove the lack of necessary nutrients for certain metabolic pathways, or even to indicate the presence of other microbes capable of out-competing the methanogens for metabolic substrates.

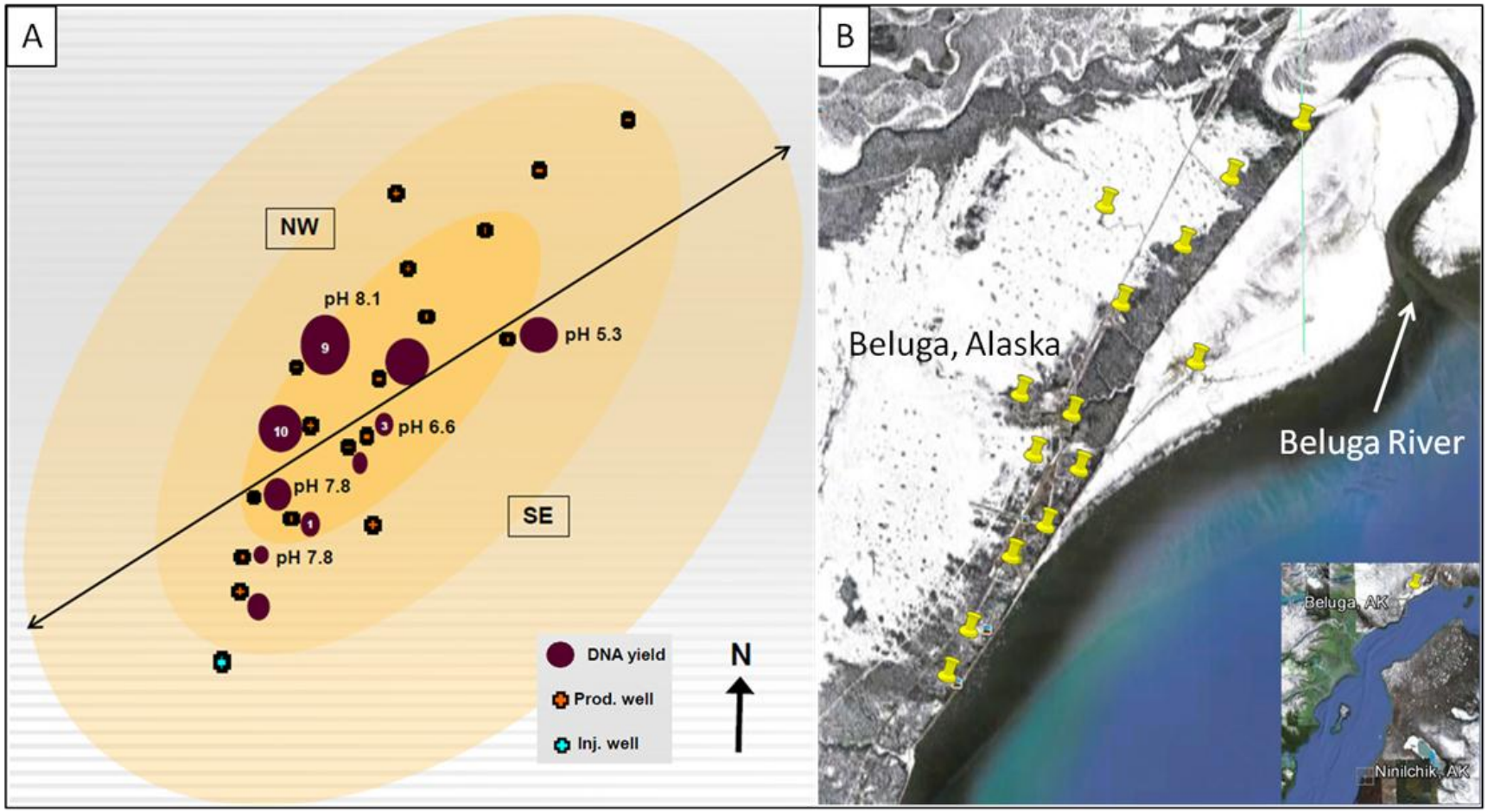

Figure 15: (**A**) Relative placement of wells in the ConocoPhillips microbial diversity study of an 'undisclosed' field location in Cook Inlet. Image modified from Lambo et al., 2011. (**B**) *Google Earth* image of Beluga River field with well sites marked by yellow pins.

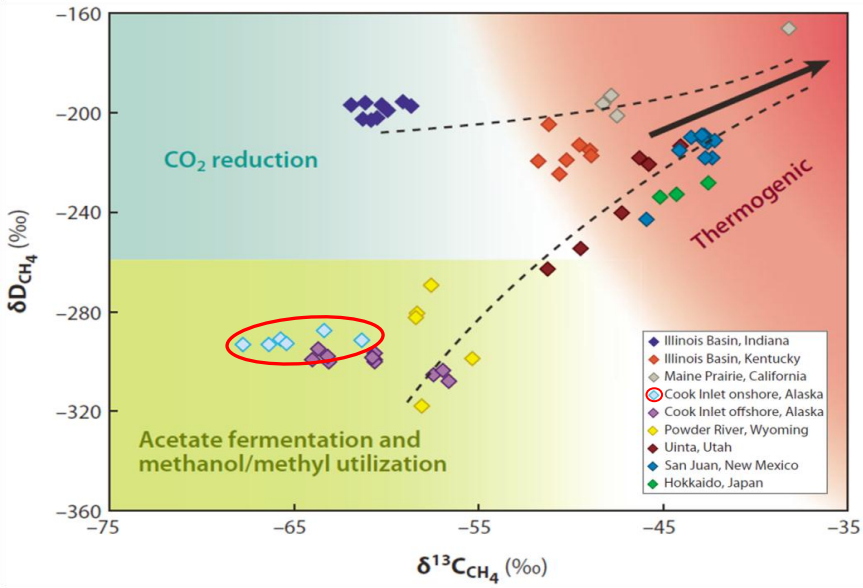

Figure 16: Distribution of biogenic and thermogenic gas accumulations from various basins based on the Deuterium and Carbon isotope fractionations of methane. Ninilchik values are expected to correspond with the light blue diamonds circled in red. Note the clustering toward Acetate and Methyl/Methanol pathways. Image modified from Strąpoć et al., 2011b.

In the microbial diversity study, ~86% of the methanogens were identified to be mesophilic and ~14% were thermophilic. Of the three mesophilic types found, *Methanolobus* sp. (an obligate methyl group utilizer) made up 43.75%, *Methanosarcina barkeri* (a universal CO_2, acetate and methyl utilizer) made up 34.72%, and *Methanocorpusculum* sp. (an obligate CO_2 reducer) made up 7.64%. The only identified thermophilic methanogen, *Methanobacterium* sp. (an obligate formate utilizer), made up the remaining 13.89% (Figure 17; Table 1) (Strąpoć et al., 2011a, b; Boone et al., 1993). There is a chance, however, that these data may be biased toward mesophilic methanogens since the studied field currently produces mostly from the Sterling and Beluga formations, while the Ninilchik field produces primarily from the Tyonek. Even so, based on the findings of the microbial diversity study, the temperatures of primary importance to track through the geothermal history analyses include the mesophilic optimum (37 °C) and maximum (50 °C). In addition, a secondary emphasis could be placed on the thermophilic optimum (65 °C) and maximum (80 °C).

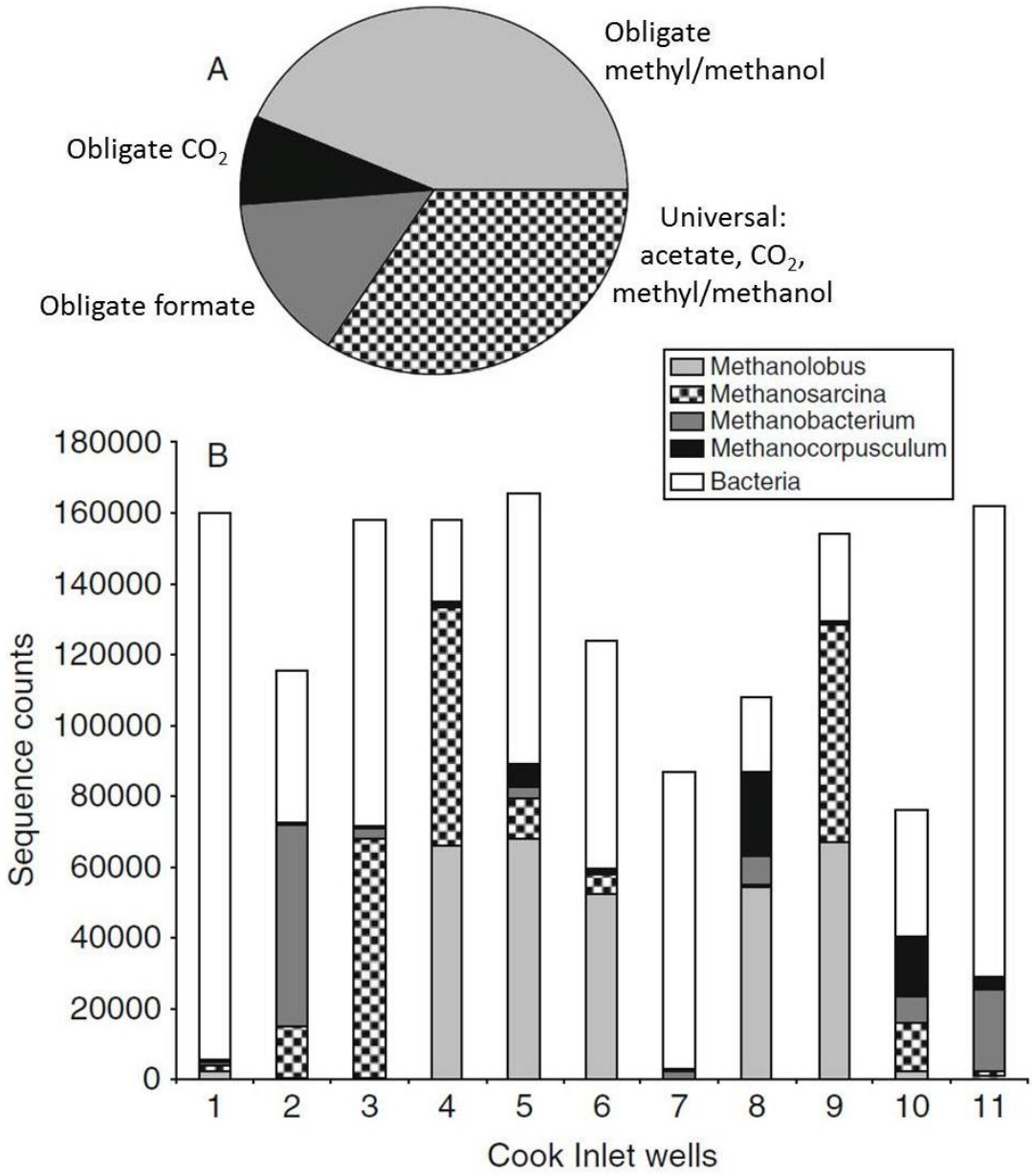

Figure 17: (**A**) Relative abundance of identified microbes in ConocoPhillips' diversity study. (**B**) 16S rRNA pyrosequencing data for 11 wells showing their specific distribution of methanogens and total bacterial counts. Although variations occur between wells, relative abundance is considered representative of the field. Image modified from Strąpoć et al., 2011a.

Table 1: Traits and Relative Abundance of Identified Methanogens

Methanogen	Metabolism	Type	T Range	T Optimum	% Identified
Methanolobus sp.	Methyl	Meso.	10-48 ˚C	~37 ˚C	43.75
Methanosarcina barkeri	Universal	Meso.	20-50 ˚C	~37 ˚C	34.72
Methanocorpusculum sp.	CO_2	Meso.	15-45 ˚C	~37 ˚C	7.64
Methanobacterium sp.	Formate	Thermo.	40-75 ˚C	~65 ˚C	13.89

Methods

In order to assess Ninilchik's geothermal history, *PetroMod*® software required values for formation tops, thicknesses and NtG coal, in addition to other boundary conditions which were obtained from the literature. Along with these input variables, as well as the results of the geothermal history analysis, fault block areas and rates of methanogenesis were also necessary to evaluate the extent of methanogenesis across each portion of the field. The following sections detail how these input parameters were obtained, utilized, and critiqued in the investigation of Ninilchik's regional well production variation.

Formation Tops and Thicknesses

Formation tops in each well were chosen according to the descriptions put forth in a paper by Marathon Oil Company (Gorney, 2011). Starting from the top of the stratigraphic column (Figure 6), the thick sands and thinly bedded shales and coals of the Late Miocene-Pliocene Sterling formation are grouped together with the overlying unnamed Quaternary sediments for the purpose of this study. Below this, the Miocene-aged Beluga formation transitions into a greater proportion of mud and silt, which is expressed on the GR log by higher API values. Following the Beluga, the top of the Oligocene-Miocene Tyonek formation is marked by the first thick, laterally continuous coal bed, as well as an increase in volcanic ash content. For each of these three shallow formations, thicknesses were recorded consistent with their individual top and base depths for each well. Unfortunately, none of the producing wells extend to the base of the Tyonek, thus the thickness of the Tyonek and subjacent Tertiary formations, the Hemlock conglomerate and the West Foreland, are assumed to be their average values reported by Marathon which are 6600 ft, 700 ft, and 1200 ft, respectively. For wells that lacked logs over a particular formation contact, or that lacked logs altogether, depths provided by

the USGS were used in conjunction with the seismic horizons from Sampson (2011). See Appendix A for a list of available logs in each well, and for a type log of Cook Inlet's Tertiary section, see Appendix B.

Net-to-Gross Coal and Fault Block Area

Seven wells with the most complete and best quality log data were selected for an in depth analysis of their coal content within the Tyonek formation. Moreover, these wells were chosen from different pad locations in an attempt to adequately represent the field's regional characteristics. According to Gorney (2011), the Ninilchik anticline is divided by normal faulting into three separate zones of production (Figures 9 & 18). Areas for these fault blocks were manually measured in *Petrel® 2011*'s 3D seismic visualizer based on the interpretation of coherency attribute volumes from Sampson (2011). Two wells were selected from each of these three zones, plus a supplementary off-structure well, Clam Gulch #1, was used as a control. This orientation matches the current field development structure with the Paxton and Susan Dionne pads covering Zone 3, and the Ninilchik State and Grassim Oskolkoff pads penetrating Zone 2. Because Zone 1 is produced only by wells from the Falls Creek pad, the solitary well, Corea Creek Federal #1, was added to uphold the organizational consistency (two wells per zone). The pad wells selected for further analysis include: Falls Creek #1RD, Grassim Oskolkoff #4, Ninilchik State #1, Susan Dionne #4, and Paxton #2 (Figures 9 & 18).

Collectively, the GR, ResD, Dt, and RhoB were utilized to carry out the logging analysis. Using *Petrel® 2011*, coals were manually picked in measured depth (MD) from the top of the Tyonek formation, down to the total drilled depth (TD). To aid in the identification of the coal beds, the GR color scheme was set to highlight values less than or equal to 45 API. Furthermore, because of its high resistance to the flow of electricity, as well as its tendency to decrease the

propagation velocity of sound waves, relative spikes in the ResD and Dt logs were also considered to be indicative of coal. Additionally, RhoB values below 2 g/cm^3 were taken to signify the presence of coal (Figure 19). Following this interpretation, cumulative NtG coal percentages for each of the seven wells were obtained by tabulating their coal layer thicknesses into 'discrete' (user defined) logs in MD. Next, depths and thicknesses for the identified coal beds were converted to true vertical depth (TVD) by *Petrel*® according to each wells' directional survey, and then the TVD NtG coal logs were manually transferred into *Microsoft Excel*.

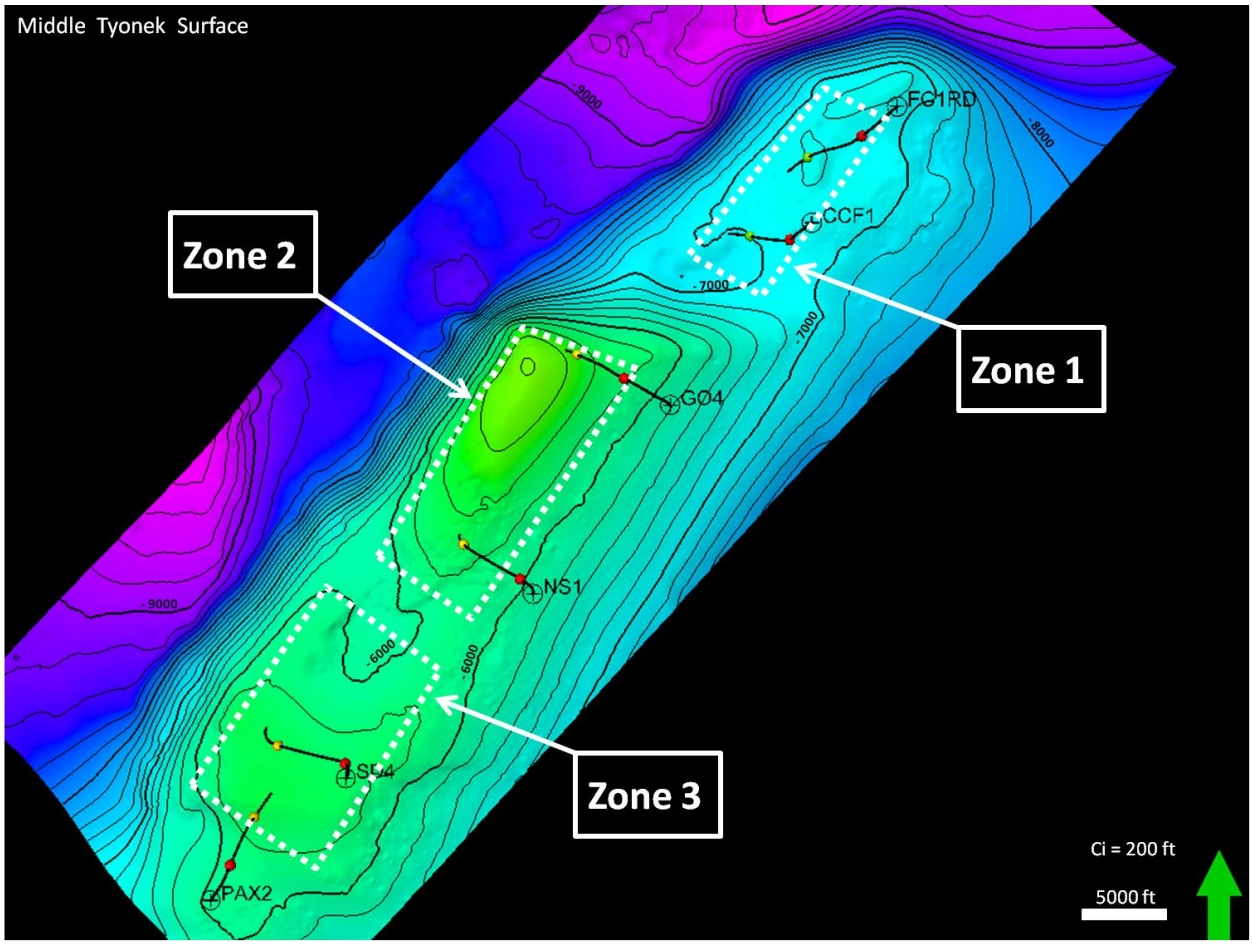

Figure 18: 3D seismic surface of the Ninilchik anticline on a middle Tyonek coal reflector in map view. Brighter greens indicate higher points on the anticline, while brighter pinks indicate deeper areas off-structure. Well paths are shown in black from their surface location (plus sign) down to their point of intersection with the horizon. Fault blocks are labeled Zone 1, 2 & 3, and their approximate areas are depicted by the dashed white polygons. To maintain simplicity on the display, fault interpretations are not shown. See Figure 9 for off-structure well CGU#1.

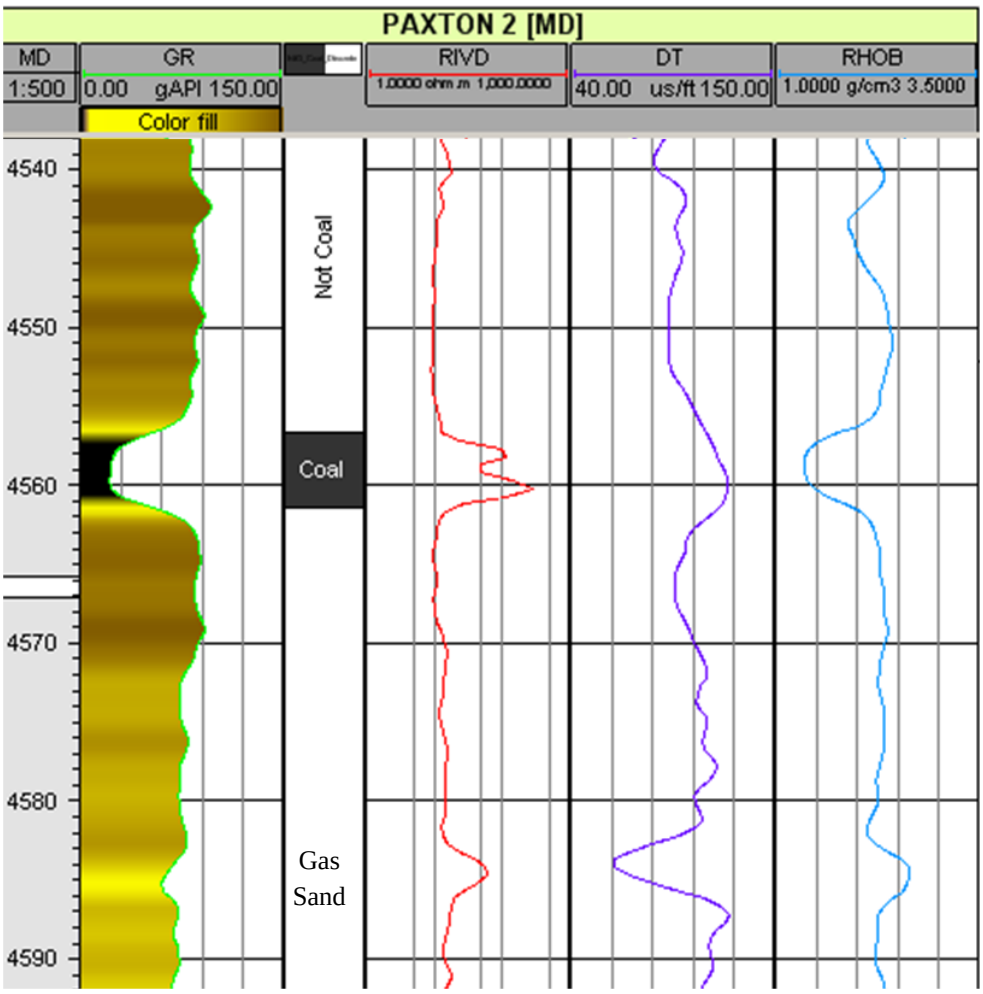

Figure 19: Example of the well log signature encountered for a coal bed (-4557 to -4561 ft MD). Note low gamma ray, spikes in resistivity and sonic, and drop in bulk density. A thin, potentially productive, gas sand is also seen from -4584 to -4586 ft MD. Image captured from *Petrel*®.

Once in *Excel*, average NtG coal percentages were calculated for each of the wells by dividing their total thickness of coal by the Tyonek formation's entire logged thickness. Additionally, in lieu of importing every individual coal bed directly into *PetroMod*®, to more closely represent the true percentage of coal at that specific depth range, each logged section of the Tyonek was broken down into 250 ft sections. These new sections were taken from the top of the Tyonek formation down to the base of the logged section, starting from the nearest successive 0, 250, 500 or 750 foot mark, and continuing from that point in 250 ft intervals. Any logged portion outlying this design was lumped together with an adjacent whole layer unless said

outlier was sufficiently large enough to constitute an individual layer on its own (≥150 ft). For example, the Falls Creek #1RD well's Tyonek formation starts at -5,061 ft TVD, so its first full 250 ft layer begins at -5,250 ft. Since the logged Tyonek portion above -5,250 ft measures 189 ft, it is able to form an individual layer. Conversely, if this extra portion had instead been <150 ft, it would have been tacked on to the layer at -5,250 ft and the first true 250 ft layer would have begun at -5,500 ft. After breaking down the wells' Tyonek sections into corresponding layers, NtG coal percents were then calculated by dividing each specific amount of coal by the total thickness of that layer. Any unlogged portion of the Tyonek formation below a well's TD was assumed to have the average NtG coal percentage calculated for that well. See Appendix C for a table of formation and layer depths, thicknesses, depositional ages, and NtG coal for the Tertiary section of the seven selected wells including the off-structure CGU#1 well.

PetroMod® Input Parameters

The *PetroMod*® basin modeling software package was used to investigate Ninilchik's thermal and geologic histories. In seven 1D models (one for each well), the present-day Tertiary section was decompacted with respect to time in order to account for the volume of porosity lost upon subsequent stages of burial. To accomplish this, depths for tops and bases were entered in feet below the surface for each Tertiary formation according to their thicknesses determined from the well logs and supporting data. Furthermore, the Tyonek formation was broken down into the 250 ft layers created in the NtG coal analysis. Ages of deposition were then added, consistent with the formation contacts illustrated in Figure 6. Constant deposition was assumed within each individual formation from base to top, and ages for the Tyonek formation's layers were extrapolated linearly from the upper and lower contact boundaries. Next, formation lithologies were manually set using the 'mixing' application of the *PetroMod*® *Lithology Editor*.

Because the Tertiary formations were laid down in a highly stratified terrestrial to estuarine environment, the generalized 'Silt and Sand' lithology in *PetroMod*® was initially set to 100%. Following this, average coal percentages were mixed in for the non-Tyonek formations according to their expected total coal thickness reported by Montgomery & Barker, 2003. In addition, the previously specified NtG coal percentages were input into each individual layer of the Tyonek's logged section, and each wells' NtG averages were assumed to be representative for their unlogged Tyonek sections below TD. Appendix C shows the coal percentages input for each formation and layer, with the remainder of their lithology mixtures kept as 'Silt and Sand'.

Even though kinetic models for hydrocarbon maturation deal with traditional thermogenic generation instead of biogenic coalbed methane production, the Burnham (1989) kinetic model was selected to estimate the thermal maturity, or potential for thermogenic gas, of each Tertiary formation with respect to both time and depth. A hydrocarbon index (HI) of 6 was assigned to signify that the kerogen present at Ninilchik is a generally thermally immature Type III. This value was approximated to be the median immature Type III hydrogen/carbon to oxygen/carbon ratio of 0.9/0.15 shown in Figure 11. Although the Burnham (1989) model was chosen on the main input screen, maturity in the form of vitrinite reflectance (%Ro) was actually calculated by *PetroMod*® using the Sweeney & Burnham (1990) Easy%Ro kinetic model according to the output plots.

The boundary conditions required for this simulation include paleo water depth (PWD), sediment water interface temperature (SWIT) and heat flow data. The PWD was set to zero since the majority of Tertiary deposition took place in a terrestrial or estuarine environment. The SWIT was automatically assigned using this PWD along with surface temperature estimates concordant with paleolatitude temporal regressions of Cook Inlet's current latitudinal position

and North America's tectonic history. This generated values that decreased from 17.24 to 5.00 °C over the duration of Tertiary deposition between 56 Ma to present. Lastly, heat flow was designated at the constant rate of 40 mW/m^2 (Figure 10) (Blackwell & Richards, 2004; Lillis & Stanley, 2011). Thermal conductivity was assigned in *PetroMod*® based on lithology and porosity, and temperature analyses were conducted through the application of Fourier's law by incorporating each underlying layers' thermal conductivity with the heat flux, thickness, and original temperature at their time of deposition. Heat flow is assumed to occur primarily by vertical conduction, and advective heat transport by fluid flow is ignored. The 1D models were simulated over five runs set at 100 meters maximum cell thickness and 1 Ma maximum time step duration, which successfully yielded optimizations on the order of 3.0 e^{-6} to 1.0 e^{-5} percent relative difference. Discussion of the time plots and burial histories produced in the output of this program can be found in the results section.

Methanogenesis Calculations

After measuring fault block areas and calculating NtG coal percentages in *Petrel*®, along with computing the geothermal histories in *PetroMod*®, it was then possible to delve into the relationships between coal, time, temperature and methanogenesis. Based on the mesophilic methanogenesis rates observed in the rice field study depicted in Figure 14, a 'bell curve' was generated to approximate the relative rate of subsurface methanogenesis, assuming that the rate hits 0% at the upper and lower boundaries of 10 and 50 °C and 100% at 37 °C (Figure 20). However, since the value 37 is not equidistant from 10 and 50, the curve is actually calculated by two polynomials, causing it to exhibit an offset or lopsided bell-shaped appearance. The formulae for these polynomials are provided with Figure 20. From this curve, percentages of the peak methanogenesis rate were averaged over each 5 °C temperature interval between 10 and 50

°C so that a time component (duration spent within each 5 °C interval) could be applied to the methanogenesis calculations shown in Equation 1. This equation was then computed for each layer that currently resides within the field's productive depths of -3,300 to -8,000 ft TVD (Gorney, 2011). In the event that this depth range extended beyond the logged portion of the Tyonek, the *PetroMod*® subhorizon function was used to approximate additional layers in the unlogged Tyonek or lower portion of the Beluga formation. For examples of these subhorizons, see Figures 23-29 and Appendix C.

Equation 1: Coal (ft) × Area (ft^2) × Density (ton/ft^3) × Rate ($scf \cdot ton^{-1} \cdot yr^{-1}$) × Time (yr) = Gas (scf)

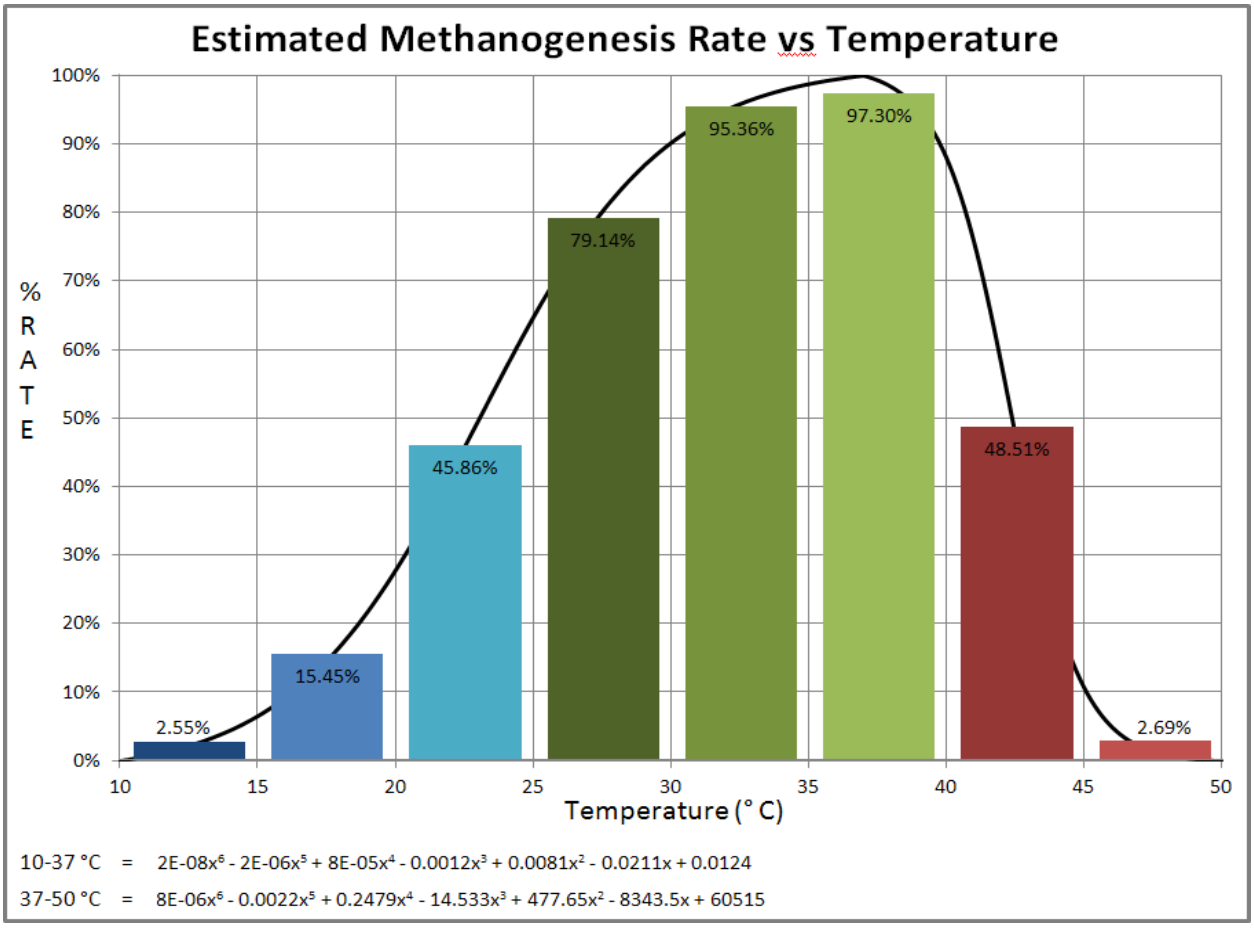

Figure 20: Estimated methanogenesis rate versus reservoir temperature based on the rice field methanogenesis studies from Yao & Conrad, 2000. Blues (10-25 °C) and reds (40-50 ° C) indicate temperatures are either too cold or too hot to be in the optimal generation window depicted in green (25-40 °C). Trendline formulae for both polynomials are also given.

Beginning with the data determined from *Petrel*®, for each individual layer of a well, when the net coal thickness (ft) is multiplied by the fault block area (ft^2), a coal volume (ft^3) is produced. This coal volume is then multiplied by the density of coal (~0.04 ton/ft^3) to obtain the total weight of coal (tons) inside that layer. This estimate is based on an average coal density of ~1.45 g/cm^3, which does not take changes due to burial and compaction into account (Sampson, 2011). Next, multiplying this weight by the rate of methanogenesis ($scf \cdot ton^{-1} \cdot yr^{-1}$) for that particular 5 °C temperature interval will yield the annual productivity of the layer (scf/yr) over that temperature range. Finally, a gas volume (scf) is acquired through multiplying the annual productivity by the duration of time the layer spent in this 5 °C interval, which is measured in the geothermal history output from *PetroMod*®.

Total gas generation for each layer is computed by repeating this process for the rest of the 5 °C intervals, making sure to use the appropriate rate, as well as the correct amount of time spent inside that temperature interval. When this is complete for a *single layer*, the process must then be repeated again for *each layer* of the well, and yet again for *each well* in the study, according to their respective NtG coal percentages, fault block areas and time spent within each 5 °C temperature interval. *Microsoft Excel* was used to organize and perform these calculations as well as to display the results.

Methanogenesis Rate Calculation

To determine a suitable 100% peak rate of methanogenesis for Ninilchik, the model's total generated methane volume was calibrated against a combination of the field's industry reserve estimate and a non-producible adsorbed gas volume. Expelled gas and adsorbed gas are treated as two separate, simultaneously generated accumulations (Figure 21). All of Cook Inlet's ~8 Tcf of produced gas comes from conventional sandstone reservoirs that are formed by mostly

structural and a few stratigraphic traps (Stanley et al., 2011). Because of this, the classification of the basin as a 'coalbed methane play' is a slight misnomer since, according to Stanley et al., 2011, there has been no commercial accumulation of continuous gas discovered within the coals. All 25 wells drilled to test the possibility of direct CBM production in Cook Inlet have proven unsuccessful, most likely due to the coals' low gas saturation values (Montgomery & Barker, 2003). A corrected adsorption value of 50 scf/ton was applied to the total weight of coal present in the field to calculate the amount of adsorbed gas trapped inside the coal beds (Barker & Dallegge, 2006). This volume of adsorbed gas was then added to Ninilchik's reserve estimate from Hartz et al. (2009) to obtain the total amount of gas for the industry estimate. The peak rate that brought the methanogenesis calculations closest to this estimated total volume produced was considered to be the field's rate. Values for this process are given in the Results and Discussion.

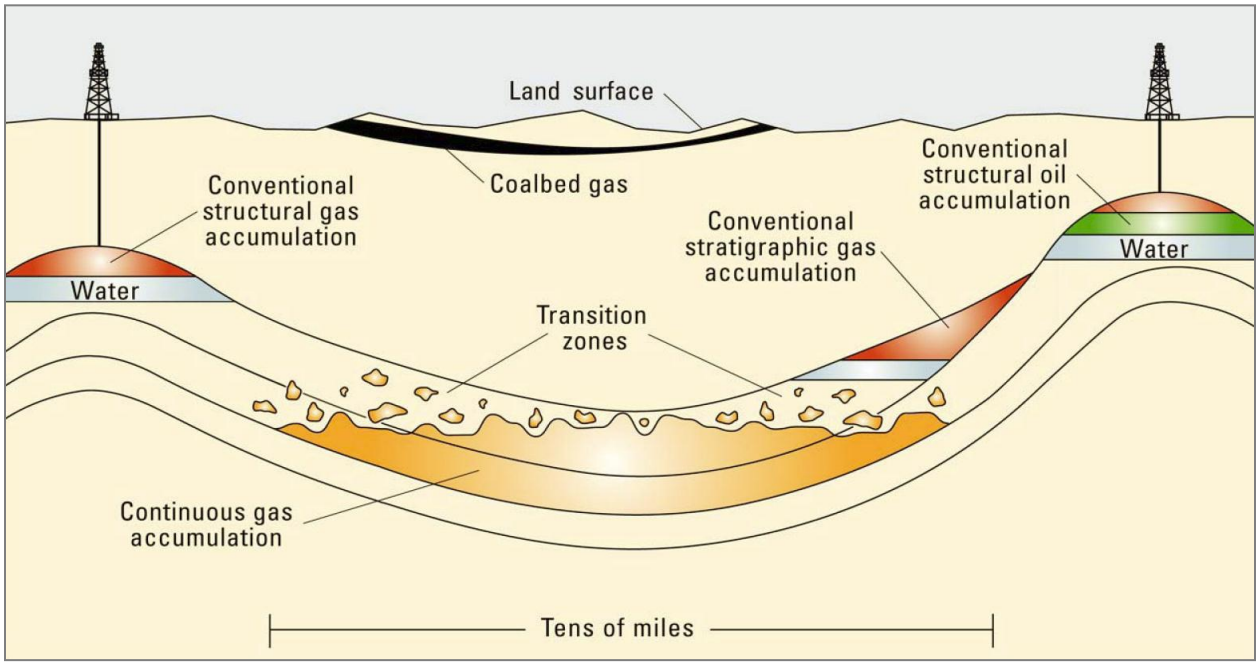

Figure 21: Diagram of the different types of hydrocarbon accumulations present in Cook Inlet. Continuous gas accumulations form from gas that is adsorbed onto the source coal matrix, while conventional accumulations form from expelled gas that migrates into a structural or stratigraphic trap. To date, all gas production in Cook Inlet occurs from conventional structural gas reservoirs found at the crest of anticlines and faulted anticlines throughout the basin. Image from Stanley et al., 2011.

Sensitivity Analysis

A sensitivity analysis was performed to establish the range of precision of the *PetroMod*® final output data as well as to determine what key factors affect Ninilchik's methanogenesis. The two main focus points that were tested in this analysis include the vertical distribution of subsurface temperature gradients along with the residence times of layers as they pass through the optimum temperature intervals. To evaluate these points, the *PetroMod*® input parameters for heat flow and depositional history were altered so that an overall high end and low end estimate of geothermal history could be generated. The pertinent variables that affect the temperature gradient are surface temperature at the time of deposition, basinal heat flux and thermal conductivity of the section. To produce the high end estimate, or hottest potential scenario, modern day surface temperature was raised to 10 °C (5 °C increase), heat flux was raised to 45 mW/m^2 (5 mW/m^2 increase), and thermal conductivity was boosted through multiplying the Sterling, Beluga and West Foreland formations' NtG coal % by a factor of 1.5 (150% of original). For the low end estimate, or coolest model, modern day surface temperature was lowered to 0 °C (5 °C decrease), heat flux was lowered to the forearc basin average of 35 mW/m^2 (5 mW/m^2 decrease), and thermal conductivity was dropped in the Sterling, Beluga and West Foreland formations by a factor of 0.5 (50% of original NtG coal). Although seemingly counterintuitive, these variations in thermal conductivity are justified by the hypothesis that sediments are being supplied to the basin too quickly to achieve thermal equilibrium.

Additionally, these temperature parameters were again tweaked, this time to match the 18 °C/1000 m thermal gradient assumed by Marathon Oil. This estimation was found to be a hybrid of the high and low end variables, with the surface temperature of the high model along with the heat flux and thermal conductivity of the low model. Since the industry estimate remained inside

the bounds of the high and low end sensitivity models, and shared the closest resemblance with the original model, the variation range was deemed to be geologically feasible (Figure 22). Furthermore, to assess the impact of an altered depositional history on layer residence times in the optimal window, ages of formation deposition were adjusted according to the stratigraphic column from Swenson (2001). This depositional model was chosen for comparison in the sensitivity analysis because it would have been used in the main model if not for the recent discovery of the much more detailed model proposed by Stanley et al. (2011). To continue the analysis, the modified ages from the Swenson stratigraphic column were then applied to the high and low end estimates, as well as to the original temperature parameters. In total, five permutations of the model were simulated: the high and low temperature estimates with the original deposition model, the alternate depositional model with the original temperature data, and, finally, the high and low estimates together with the alternate depositional model. Results of these models and their implications will be addressed in the following section.

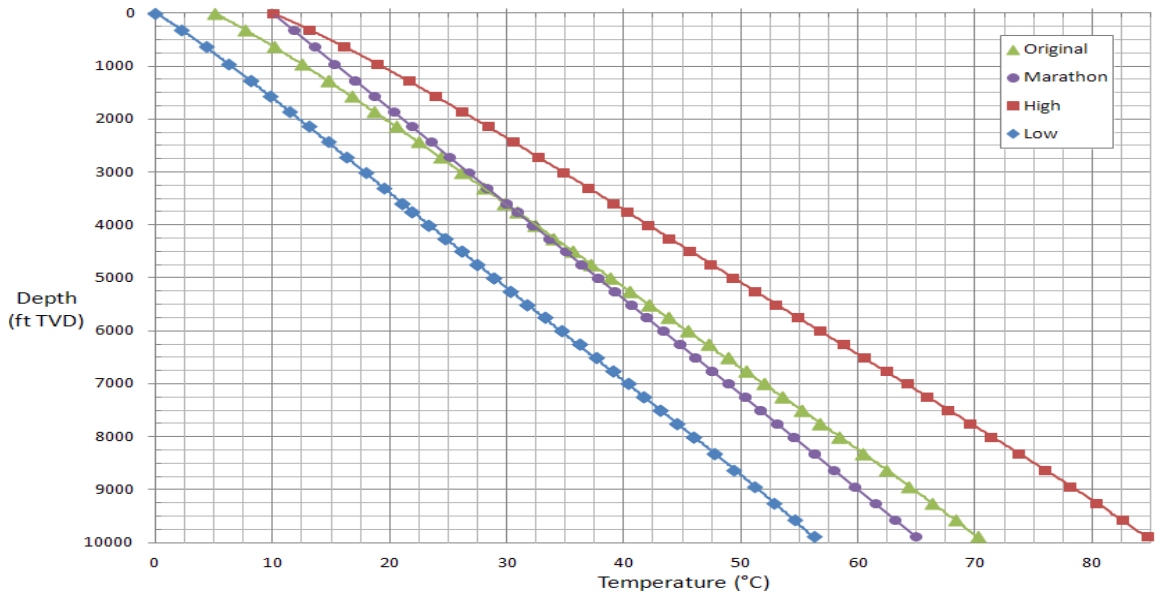

Figure 22: Graph of temperature vs depth showing the differing temperature gradients between each of the sensitivity models. 'Original' represents the thermal parameters used in the main study, while 'High' and 'Low' represent those used in the high end and low end estimates. Additionally, the Marathon Oil temperature gradient estimate is also depicted.

Results and Discussion

Geothermal History Analysis

Geothermal history curves produced in *PetroMod*® for each of the seven selected wells are shown in Figures 23-29. Depositional history is displayed from left to right, starting with the oldest Tertiary formation and continuing until present day. The thick black lines indicate each formational contact's path through the depositional history, while the thin black lines represent the layers of the logged Tyonek section used in the NtG coal calculations. Only Tyonek coal layers were directly measured; the rest of the Kenai Group's coal content was approximated from Montgomery & Barker (2003) and Gorney (2011). These Tyonek layers are labeled T1, T2, T3, etc., and those with higher coal percentages are marked with diagonal lithologic textures. Thin gray lines parallel to formation contacts represent subhorizons generated within *PetroMod*® to approximate layers between the productive depths of -3,300 to -8,000 ft when necessary for the methanogenesis calculations. Temperature distributions with respect to time and depth are also depicted on the plot in concordance with the 5 °C intervals designated in the 'Bell Curve' % rate graph. The temperature color scheme is set so that blues signify cool temperatures from the onset of methanogenesis at 10 °C to 25 °C, greens signify the optimal mesophilic biogenic gas window (MBGW) from 25-40 °C, and reds signify the hotter temperatures from 40 °C to the mesophilic pasteurization at 50 °C. Also, green and red lines are posted on each of the plots to mark the thermophilic methanogen optimum (65 °C) and maximum (80 °C), respectively. Cooling due to rapid sedimentation is observed from Miocene to present, shown by isotherms shifting deeper with time.

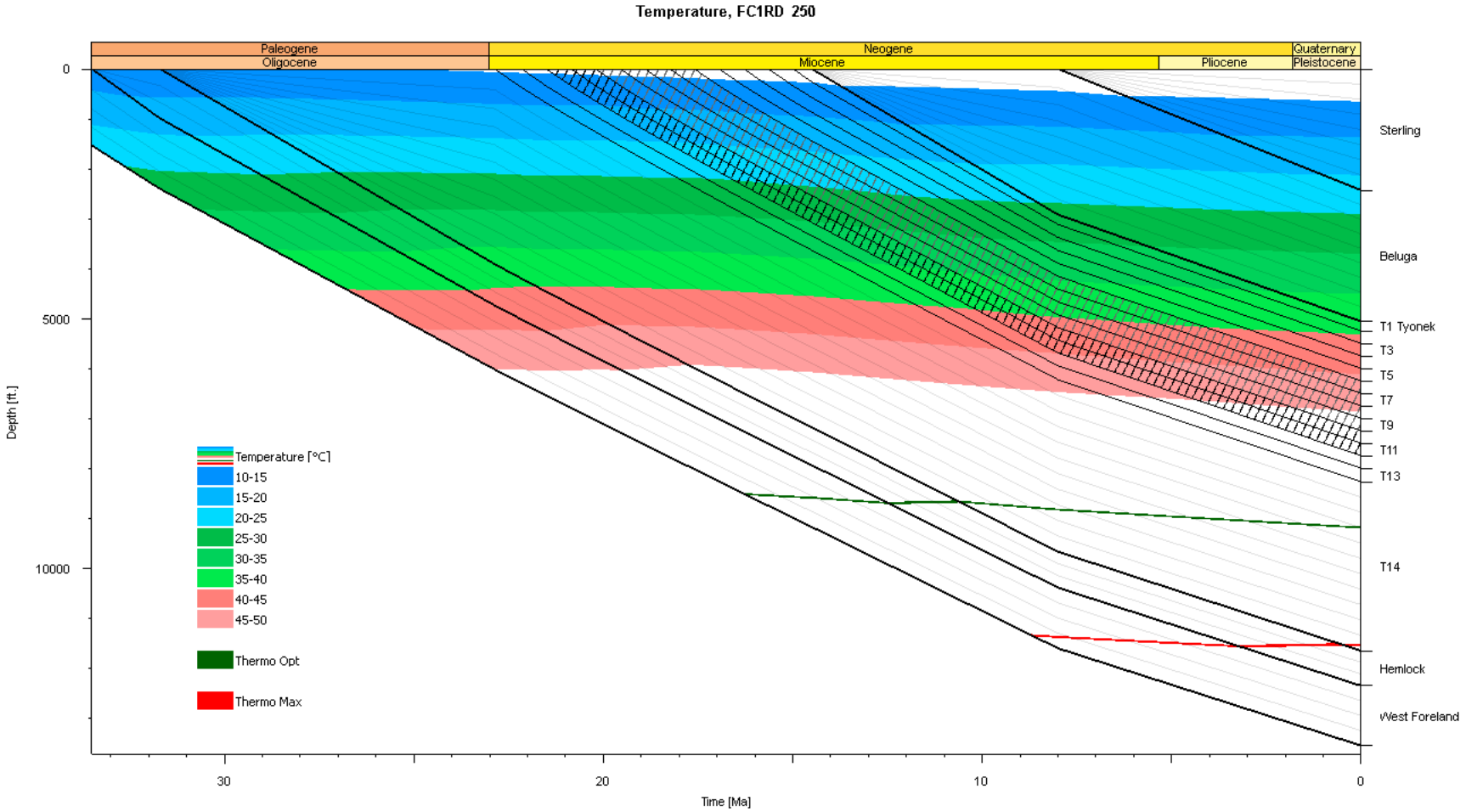

Figure 23: *PetroMod*® geothermal history output displaying Tertiary depositional history for the Falls Creek #1RD well of Zone 1 (see Figures 9 & 18 for location). Output data is plotted according to depth (ft) with respect to time (Ma). Formational contacts, Tyonek layers, and non-Tyonek subhorizons are marked by thick black lines, thin black lines, and thin gray lines, respectively. Temperature gradient color scheme is defined by the inset legend. 'Thermo Opt' and 'Thermo Max' refer to the optimum and maximum temperatures for thermophilic methanogenesis (65 and 80 °C). Diagonal lithology texture lines denote coal content, where black represents >15%, gray is 12.5-15%, and <12.5% remains unmarked. Cooling due to rapid sedimentation is observed from Miocene to present, shown by isotherms shifting deeper with time.

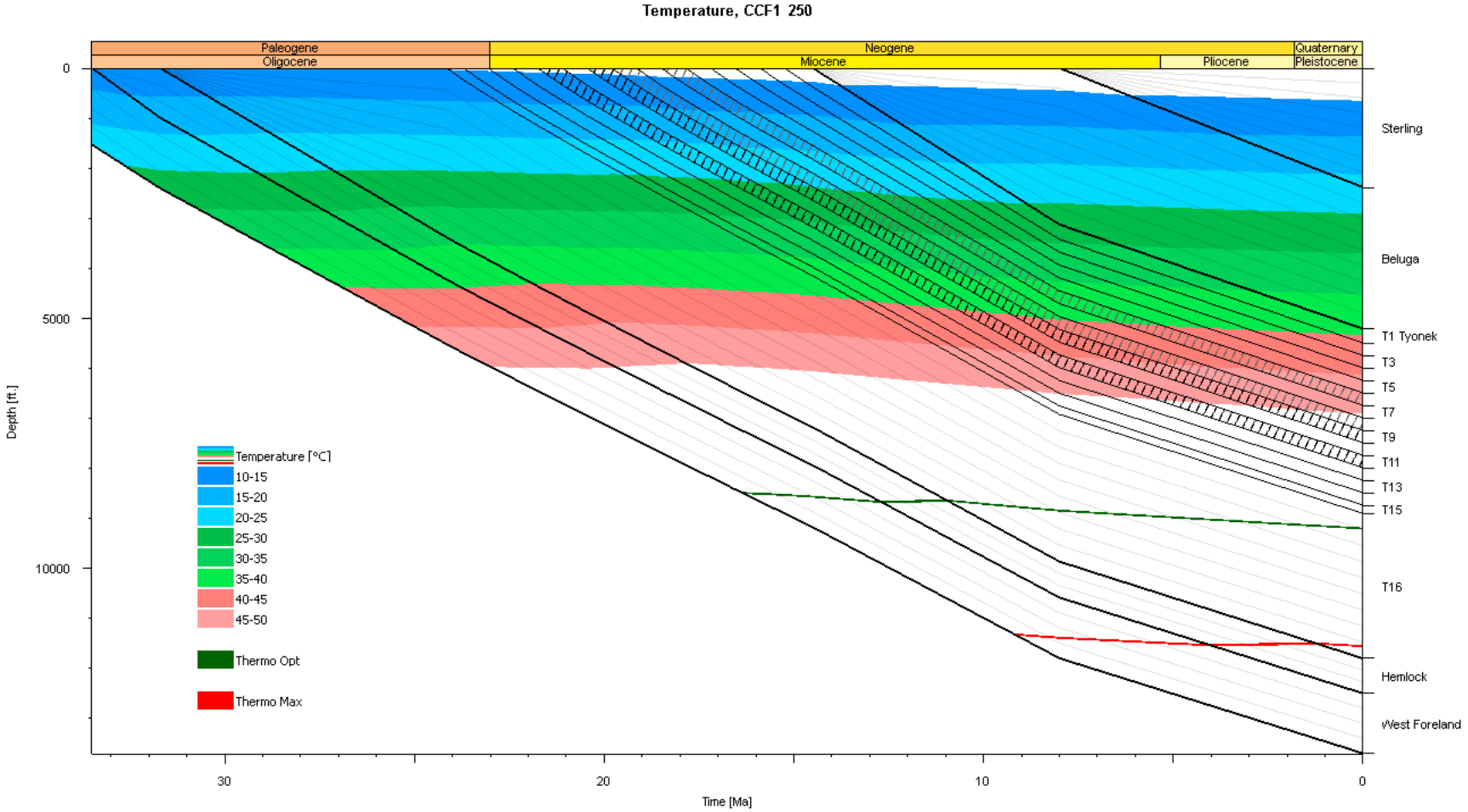

Figure 24: *PetroMod*® geothermal history output displaying Tertiary depositional history for the Corea Creek #1 well of Zone 1 (see Figures 9 & 18 for location). Cooling due to rapid sedimentation is observed from Miocene to present, shown by isotherms shifting deeper with time. Refer to Figure 23 for further description.

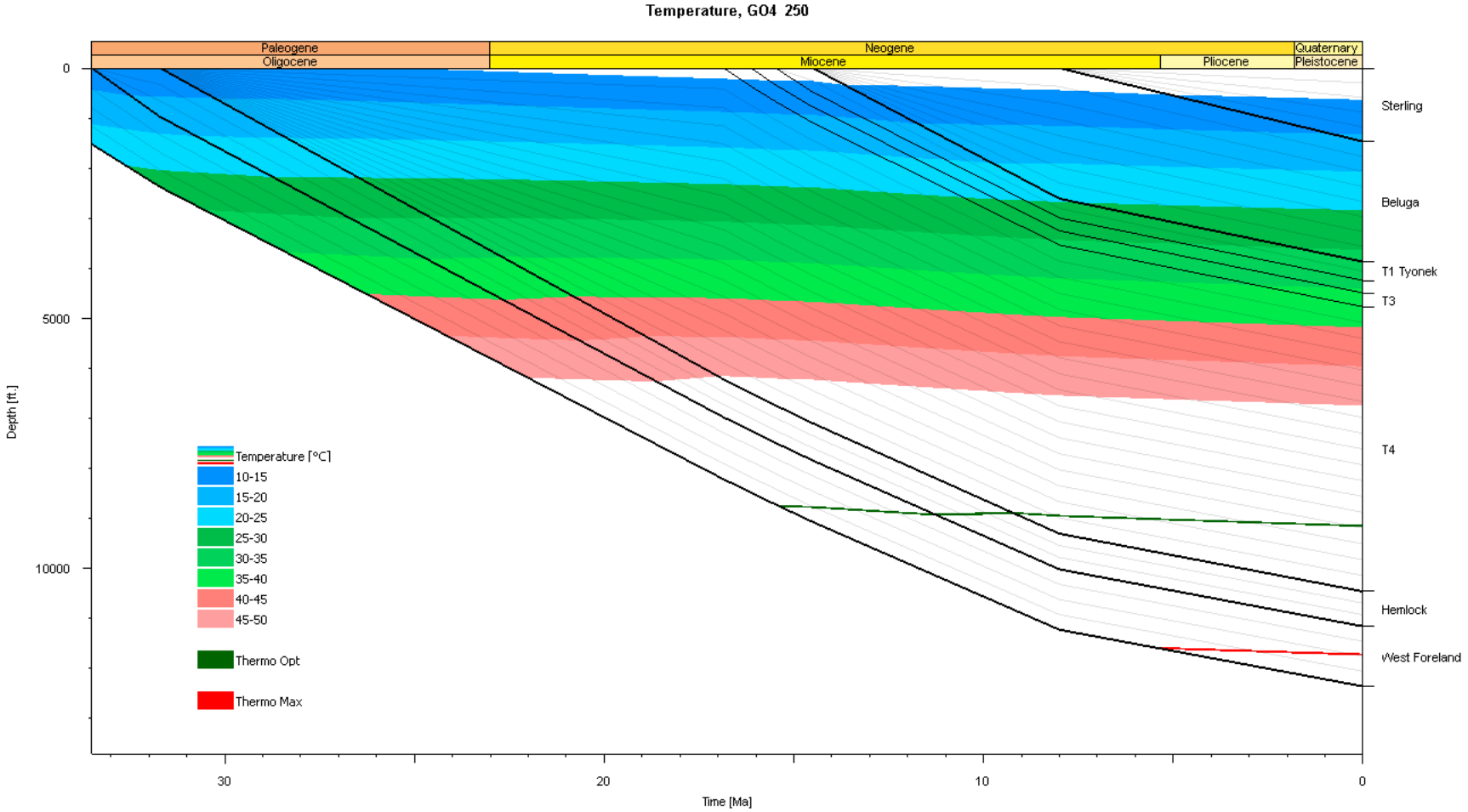

Figure 25: *PetroMod*® geothermal history output displaying Tertiary depositional history for the Grassim Oskolkoff #4 well of Zone 2 (see Figures 9 & 18 for location). Cooling due to rapid sedimentation is observed from Miocene to present, shown by isotherms shifting deeper with time. Refer to Figure 23 for further description.

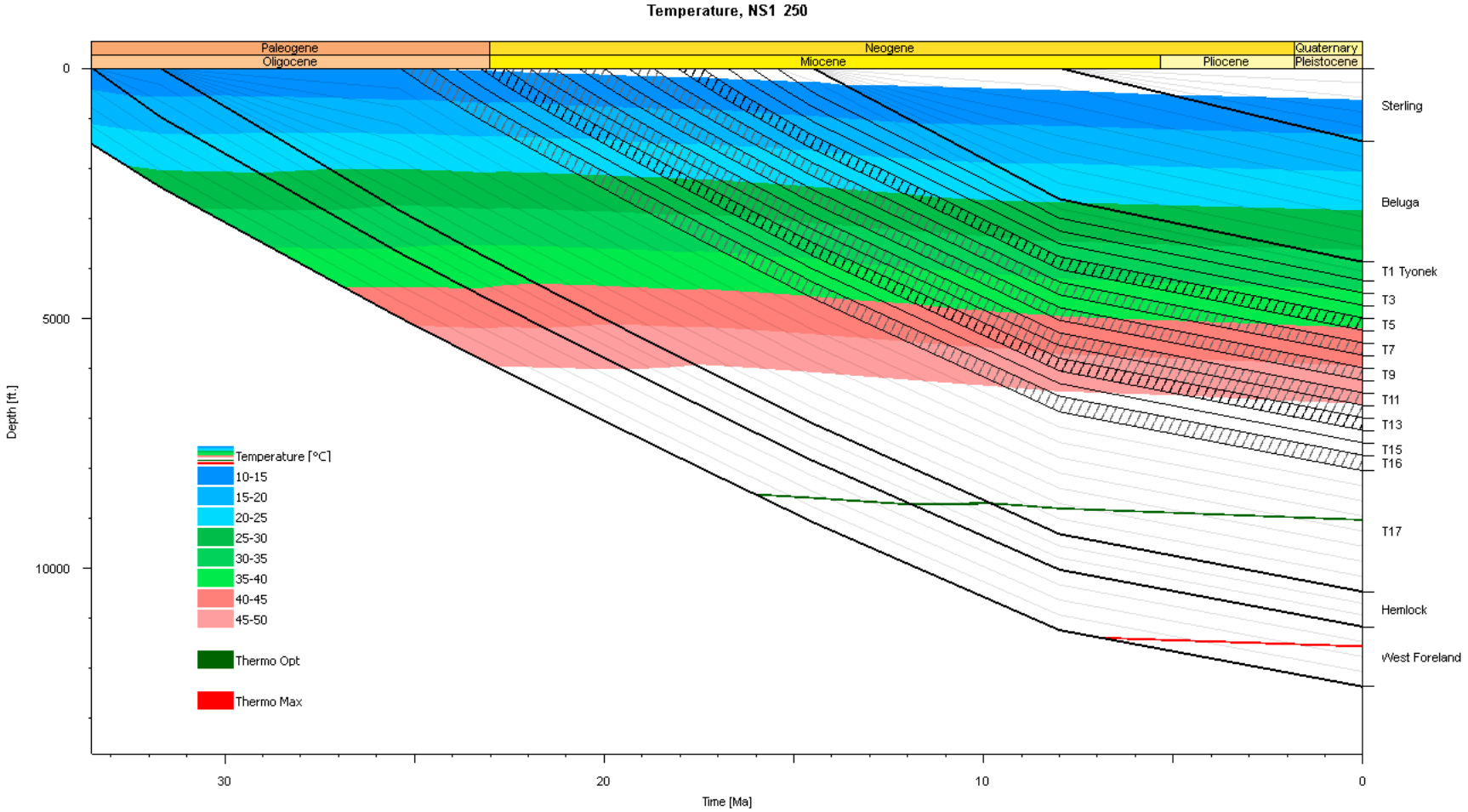

Figure 26: *PetroMod*® geothermal history output displaying Tertiary depositional history for the Ninilchik State #1 well of Zone 2 (see Figures 9 & 18 for location). Cooling due to rapid sedimentation is observed from Miocene to present, shown by isotherms shifting deeper with time. Refer to Figure 23 for further description.

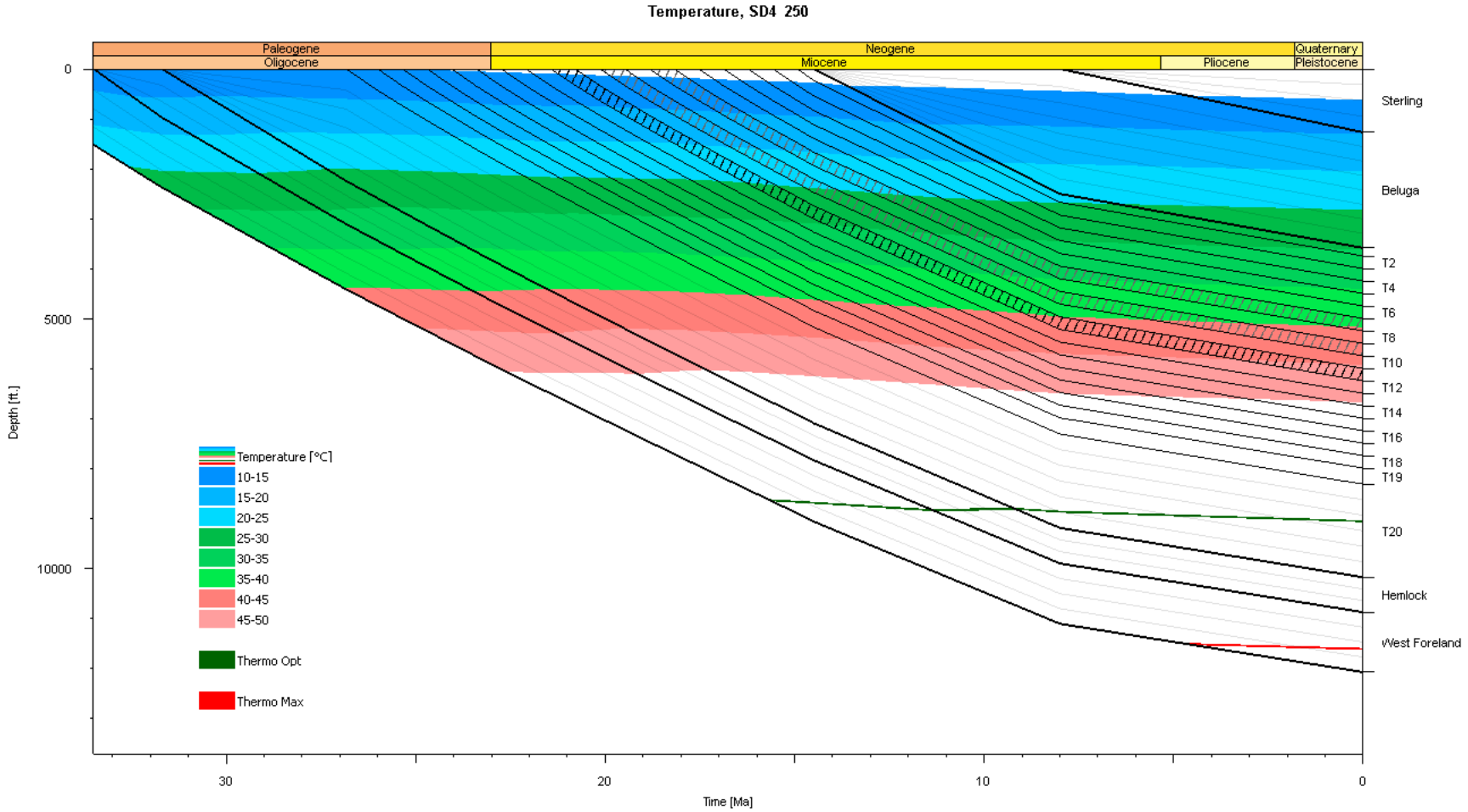

Figure 27: *PetroMod*® geothermal history displaying Tertiary depositional history output for the Susan Dionne #4 well of Zone 3 (see Figures 9 & 18 for location). Cooling due to rapid sedimentation is observed from Miocene to present, shown by isotherms shifting deeper with time. Refer to Figure 23 for further description.

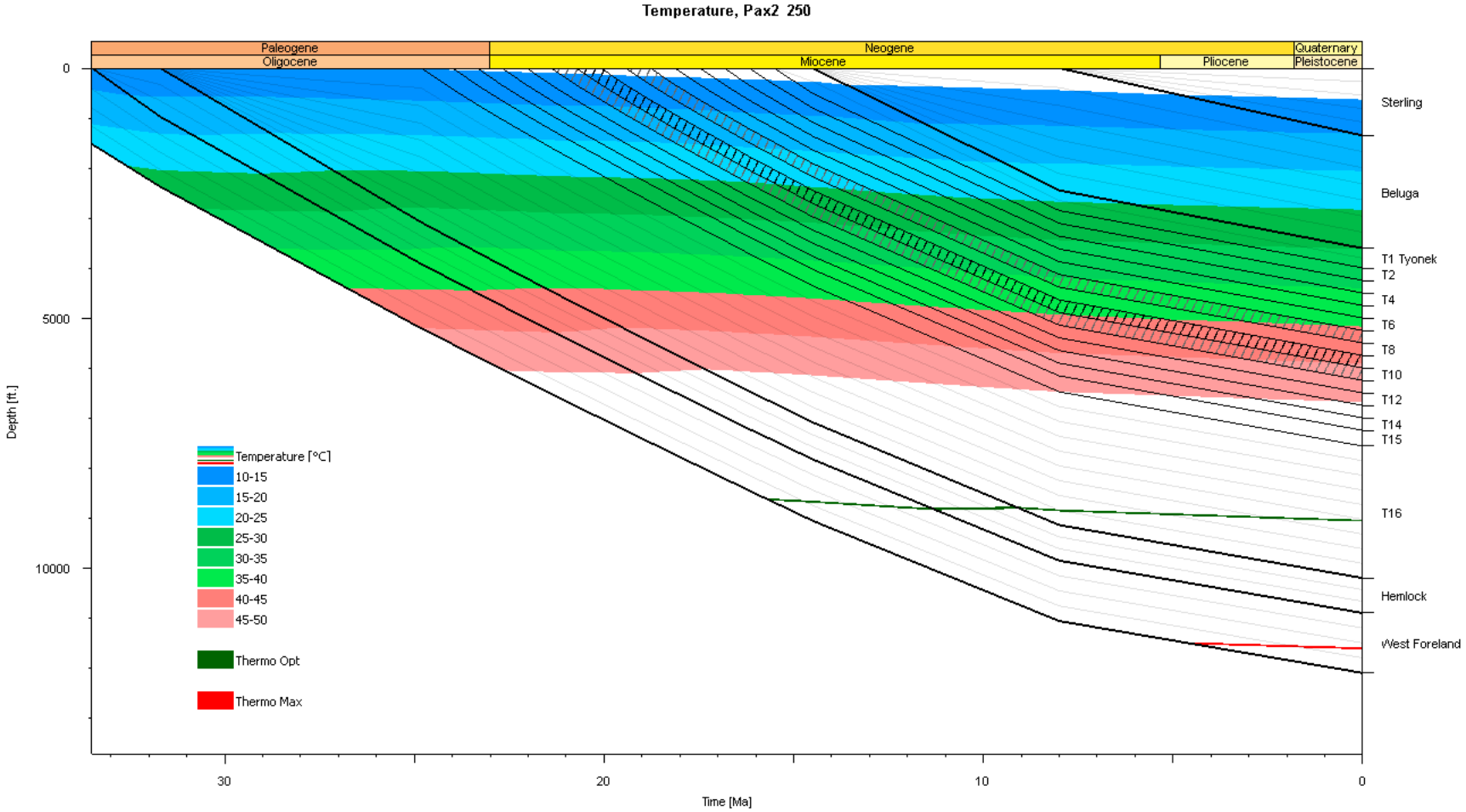

Figure 28: *PetroMod*® geothermal history output displaying Tertiary depositional history for the Paxton #2 well of Zone 3 (see Figures 9 & 18 for location). Cooling due to rapid sedimentation is observed from Miocene to present, shown by isotherms shifting deeper with time. Refer to Figure 23 for further description.

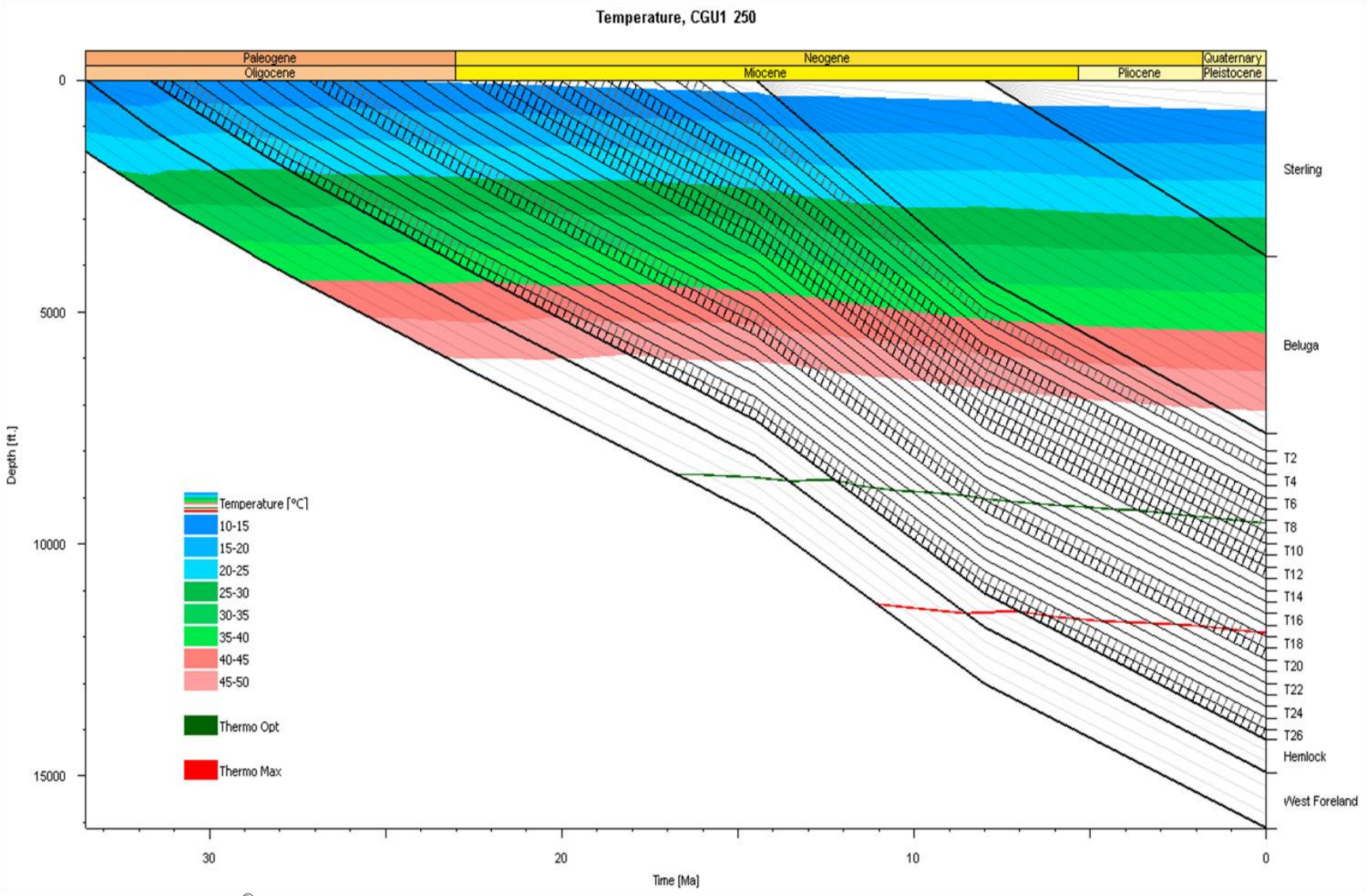

Figure 29: *PetroMod*® geothermal history output displaying Tertiary depositional history for the Clam Gulch #1 off-structure well (see Figures 9 & 18 for location). Cooling due to rapid sedimentation is observed from Miocene to present, shown by isotherms shifting deeper with time. Vertical scale is maintained with Figures 23-28. Refer to Figure 23 for further description.

Temperature distribution with respect to depth, or temperature gradient, stays relatively constant through time between each of the wells atop the anticline (refer to Figures 9 & 18). Given that the heat flow is constant and sedimentation rates are similar in each model, this is to be expected. Contrary to this mostly constant thermal gradient, though, individual depositional histories are seen to be somewhat varied in formation thickness and sedimentation rate between the wells of different zones. To maintain scale, the range of each on-structure plot was set from 0 to -13,725 ft depth and 33.5 to 0 Ma. This depth was obtained from the Corea Creek #1 well of Zone 1 which holds the deepest Tertiary on-structure section, and the ages coincide with the onset of Hemlock deposition to present. Since the Tertiary depths recorded for the off-structure well are around 2,500 ft deeper than the on-structure wells, the Figure 29 was expanded to uphold vertical proportion with the previous figures.

Within a formation, deposition rate is assumed to be constant; so subsidence versus time appears as a series of linear line segments. By observing the angles that these linear segments form, the relationship of deposition between adjacent formations and the relative rates of basinal subsidence, or inversely of anticlinal uplift, can be inferred. Additionally, it is the contrast in these depositional histories that causes variation in the durations of time each layer spends within a certain temperature range. By tracking the depositional history across the temperature gradient, these durations of time were measured for each layer's path through the 5 °C temperature intervals. As a layer passes over a particular temperature interval, the steepness of its trajectory will determine the amount of time it spends in that interval; i.e., a steep slope takes less time while a shallow slope takes more time to travel through the temperature range. It is important to note, however, that the plots aren't displaying lateral displacement, as the slopes are instead used to show the rate of deposition, compaction and subsidence at a single vertical point.

An example of this process is demonstrated in the model of the Susan Dionne #4 well between its Tyonek layers T7 and T11 (Figure 27). The deeper layer T11 enters the MBGW (25-40 °C) at around 16 Ma and continues through at a constant rate of subsidence until it exits the window around 8.5 Ma. The shallower layer T7, however, enters the MBGW around 12.5 Ma and continues at that same rate of subsidence until the rate decreases at the onset of Sterling deposition, thus changing its depositional trajectory. From here, it then follows this shallower trajectory and remains in the MBGW up to very near the present day. Because of this altered depositional history, layer T7 spends a total of 12.5 Ma in the MBGW while layer T11 spends only 7.5 Ma. The relationship between depositional history and times spent within the MBGW according to each layers' current TVD are displayed in Figure 30 for the seven models.

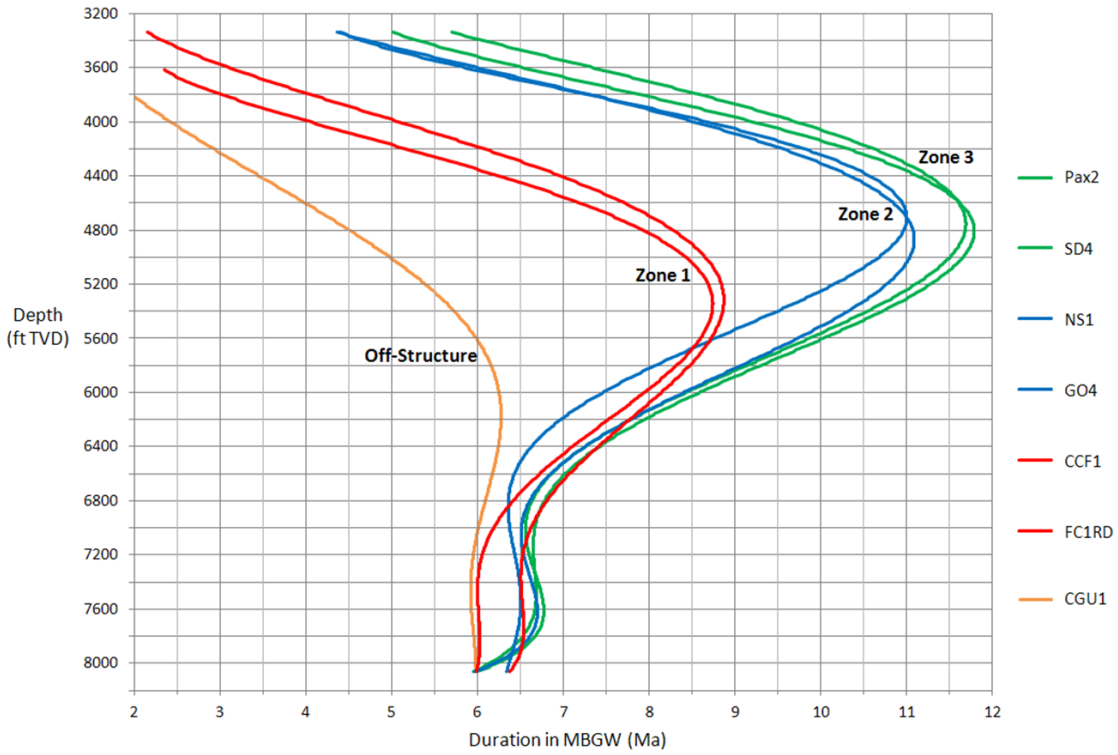

Figure 30: Durations of time spent within the MBGW (25-40 °C) for the layers of each modeled well with respect to their current TVD. Zone 1 is represented in red, Zone 2 in blue, Zone 3 in green, and off-structure in orange. The extended durations for layers from -6,000 to -4,000 ft TVD are attributed to anticlinal uplift, and the rapid declines above -4,000 ft occur because the shallow layers have yet to reach or fully pass through the MBGW.

In addition to the geothermal history plots, graphs for temperature versus time as well as maturity versus time were created in *PetroMod*® (Figures 31 & 32). Curves for each of the seven wells were displayed together for both of these graphs to allow for the identification of trends in the data over the course of Tertiary deposition. One such trend is evidenced by the separation of temperatures and vitrinite reflectance (%Ro) values between the off-structure area and Zone 1, as well as between those of Zone 1 and Zones 2-3. While each of the curves remain consistently spaced throughout the Tyonek formation's deposition, a disparity begins to occur at the onset of Beluga deposition and becomes increasingly pronounced past the onset of Sterling deposition. The highest values are reached in the off-structure well, which peak at just over 100 °C and 0.60 %Ro for the basal Tertiary horizon. Additionally, Zone 1 records intermediate basal Tertiary values of 90 °C and 0.52 %Ro, while Zones 2-3 remain the coolest and least thermally mature with temperatures between 80-85 °C and %Ro of less than 0.5%.

To correlate this trend with the observed changes in depositional history both chronologically and spatially, the timing of the anticline's formation must be considered in conjunction with specific positioning atop its structure. The timing for the curves' divergence is explained by the Yakutat block's dextral transpression of Cook Inlet that initiated the formation of the Ninilchik anticline from the mid to late Miocene. From this deformation, uplift along the anticline caused a reduction in deposition rates for the Beluga and Sterling formations in Zones 1-3, thus altering the trajectory of their depositional histories shown in Figures 23-28. Since no relative anticlinal uplift occurred to offset basinal subsidence in the location of the off-structure well, accumulation of the Beluga and Sterling formations remained unaltered (Figure 29). This greater depth of burial is used to explain the higher temperature and %Ro values seen in the off-structure section surrounding the Ninilchik anticline when compared to the on-structure wells.

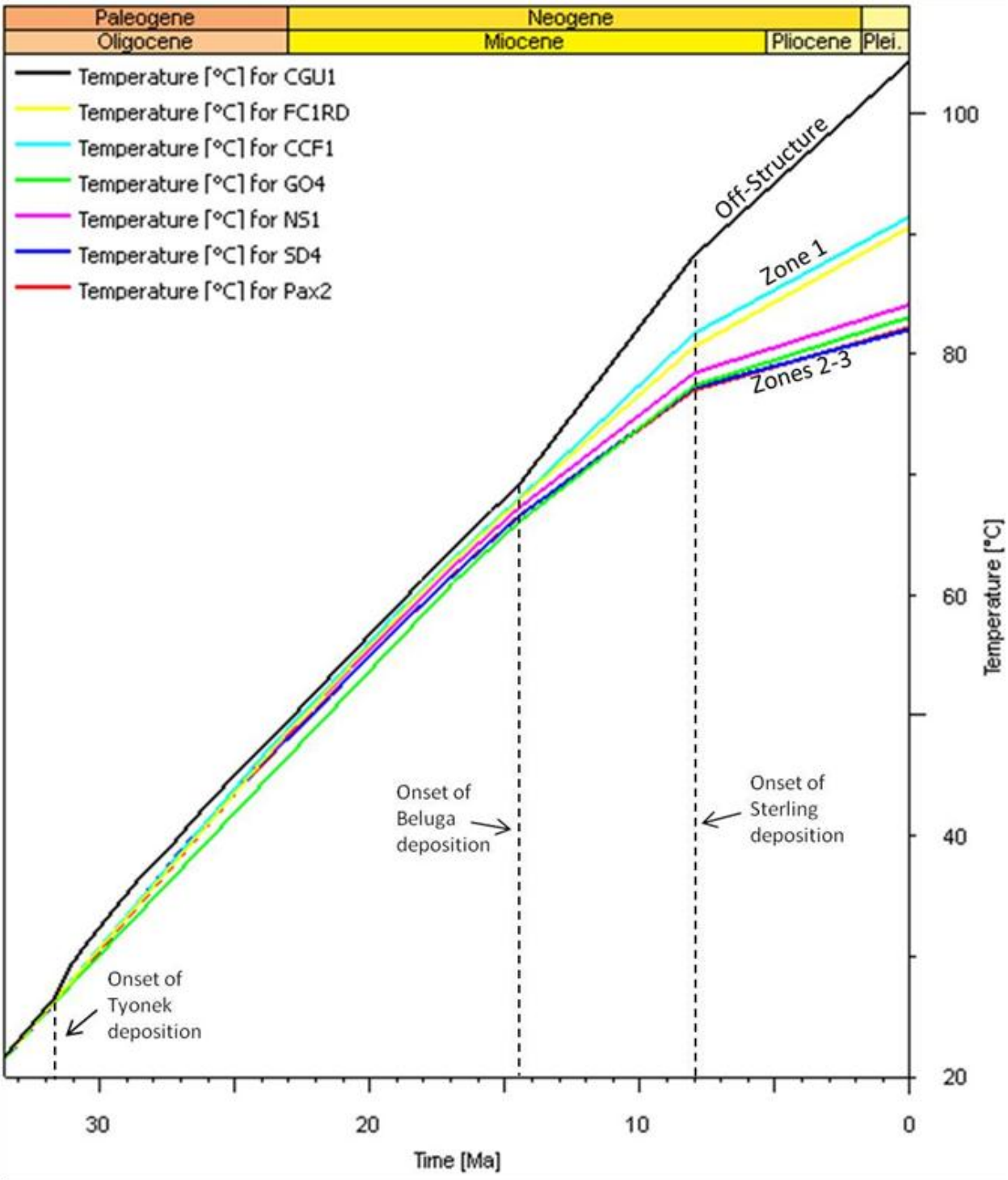

Figure 31: *PetroMod*® thermal history graph showing the temperatures reached with respect to time for each of the seven modeled wells at the basal Tertiary horizon. Ages for the onset of formation deposition are marked by the dashed lines. Models are labeled on the upper right hand side according to their location within the Ninilchik field to exemplify the divergence of maximum temperature values between different regions (see Figures 9 & 18 for locations).

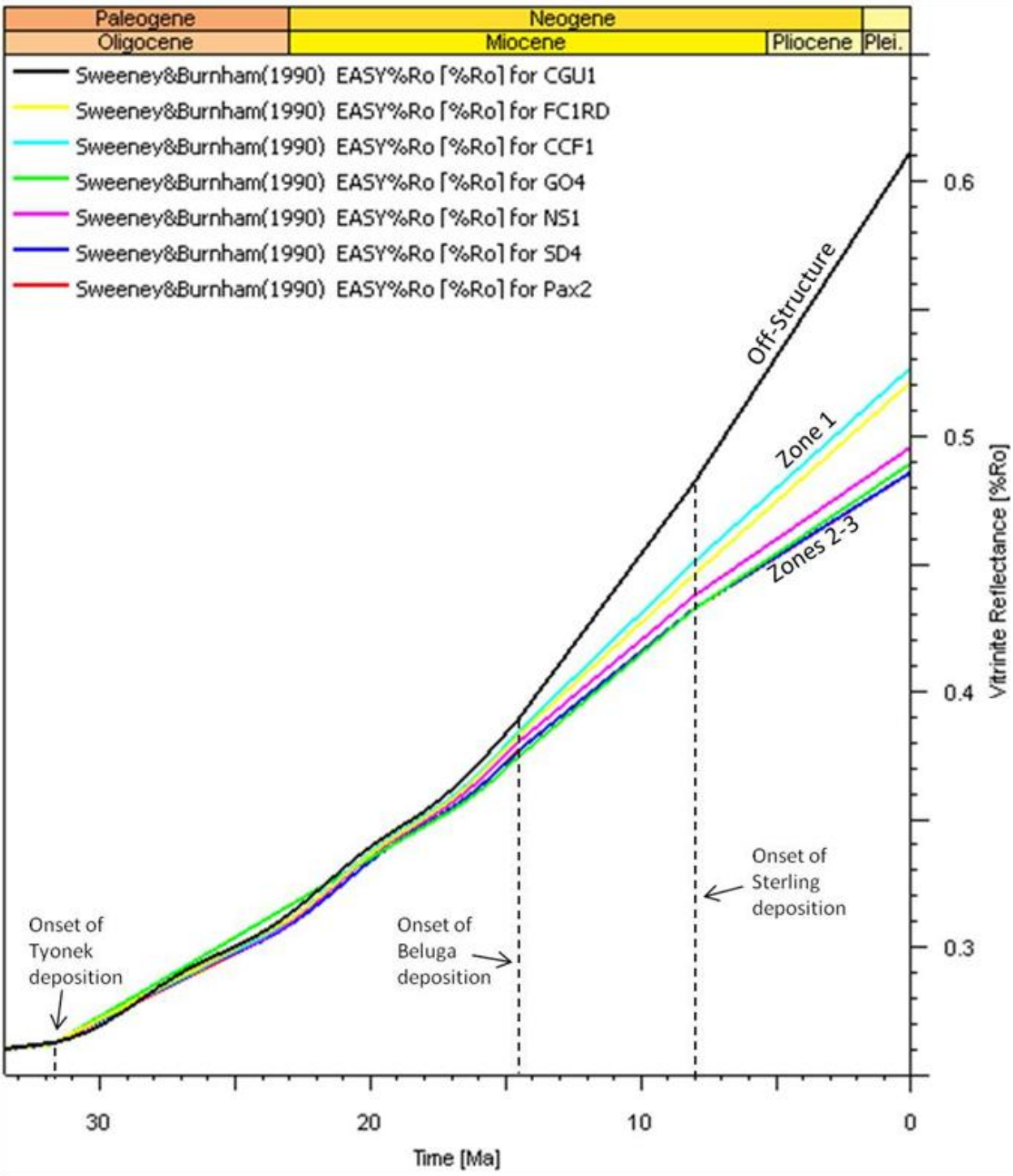

Figure 32: *PetroMod*® maturation history graph showing the vitrinite reflectance (%Ro) reached with respect to time for each of the seven modeled wells at the basal Tertiary horizon according to the Sweeney&Burnham (1990) EASY%Ro kinetic model. Ages for the onset of formation deposition are marked by dashed lines. Models are labeled on the right hand side according to their location within the Ninilchik field to exemplify the divergence of maximum vitrinite reflectance (%Ro) values between different regions (see Figures 9 & 18 for locations).

Judging from Figures 32 & 29, the off-structure basal Tertiary section only recently entered the oil window (0.6%Ro) during the mid Pleistocene at a depth of just over -15,000 ft. These results conform well with the depth to oil window map shown in Figure 12 where Ninilchik is depicted as being slightly short of the -15,000 ft mark. If further testing of off-structure wells near the Ninilchik anticline proves similar results, the map contour may need to be adjusted southward to include the Ninilchik field. Furthermore, through comparison of Figure 12 with Figure 2, it is apparent that the best fields in the basin coincide with the region encompassed by this contour which exhibit depths to the oil window of over -15,000 ft. This implies that rapid sediment influx is a significant factor in suppressing the geotherm, and, consequently, in creating the conditions for maximum methanogenesis.

Locally, to distinguish between the zones on top of the anticline structure, their particular locations and relative difference in subsurface elevation are shown in Figures 9 & 18. From this image, it is interpreted that the intermediate temperature and %Ro values of Zone 1 occur because the fault block is downthrown about 1,000 ft from Zones 2-3 by an E/W-trending normal fault. Due to this lower relative depth in the subsurface, Zone 1's Beluga and Sterling sections are slightly thicker than those of Zones 2-3, and each of its coal layers were subjected to the higher temperatures present at that deeper/hotter portion of the thermal gradient. Finally, given that the equivalent horizons of Zones 2-3 sit shallowest in the subsurface atop the peak of the structure, they have been held to the lowest possible temperatures and %Ro values by maximum uplift of the anticline. This signifies that anticlinal uplift not only forms fault blocks and structural closures for gas accumulation, but it also actively forces layers of Zones 2-3 to experience prolonged exposure to the mesophilic optimum temperature range from -4,000 to -6,000 ft TVD (Figure 30).

Characterizing Methanogenesis

According to Schlegel et al. (2010), there are two possible methods in which methanogenesis can become established in the subsurface: (1) methanogens present at the point of sediment deposition maintain a continued presence through burial and subsidence, and/or (2) microbial communities colonize uninhabited reservoirs via advective hydraulic transport from surface aquifers. Additionally, these processes are not necessarily mutually exclusive. The first possibility implies that methanogenesis is an independent, ongoing process that takes place over the entirety of a reservoir's existence until it undergoes pasteurization, while the second possibility is dependent on the timing of basinal uplift and, more importantly, of freshwater recharge. In the case of the Illinois basin, for example, the original population present at deposition was pasteurized through deep basin burial. Eventually, the basin became uplifted and reservoir temperatures decreased, but it was not until the end of the last glacial maximum that microbes were reintroduced through an influx of deglacial meltwater that resumed methanogenesis (McIntosh et al., 2010; Strąpoć et al., 2011b).

To determine the nature of hydrocarbon generation for the Ninilchik field, multiple elements of the geothermal history and production data must be considered. Firstly, the maturation values for the Tertiary sections shown in Figure 32 signify that no area of the anticline has yet passed into the oil window (0.6 %Ro). This is in concordance with the isotope data depicted in Figures 3 and 11, and confirms the previous assumption that the vast majority of hydrocarbons found in the field are biogenic in origin. Secondly, judging from the thermophilic optimum and maximum temperatures displayed on the geothermal history diagrams (Figures 23-29), the optimum resides at least 1,000 feet deeper than the well production's lower bound of -8,000 ft TVD, and the shallowest depth that undergoes total reservoir pasteurization is the base

of the Tyonek formation. Because of these two points, along with a low abundance shown in the microbial diversity study, thermophilic methanogens are only of minor significance to the overall production of gas and therefore are omitted from further consideration in the gas generation calculations. Conversely, the mesophilic optimum occurs between -4,700 to -4,900 ft TVD, placing it well within the range of production observed at Ninilchik. In addition, the mesophilic maximum is found from -6,650 to -6,950 ft TVD, which signifies that much of the coal bearing section is still undergoing biogenic gas generation. Finally, while meteoric groundwater recharge may play a significant role in older, pasteurized basins, based on the observations accumulated from this geothermal history analysis, it can be reasonably established that the Tertiary formations of Cook Inlet are simply too young and cool for this microbe recolonization process to be necessary. Methanogenesis in the Ninilchik field has likely occurred continuously over the epochs as coal-bearing Kenai Group strata successively pass through the mesophilic biogenic gas window, and, depending on the *in situ* rate of methano-genesis, all or some percentage of the 30 wt% of total coal matrices were converted to methane.

Calculating Methanogenesis

Through further investigation of the equation used to calculate gas generation (Equation 1), a relationship between the amount of coal and the duration of time spent within a 5 °C interval was devised. To evaluate the difference in relative generation between two or more layers of a well, the layer with the highest multiplied value of net coal (ft) and time (Ma) in the interval will generate the most gas (Figure 33). For example, say layer 1 has 5 ft of coal and a duration of 10 Ma, layer 2 has 50 ft of coal and a duration of 1 Ma, and layer 3 has 25 ft of coal and a duration of 5 Ma. By multiplying each of these two values, their respective products are 50, 50, and 125. This signifies that layers 1 and 2 will both produce the same amount of gas,

while layer 3 produces 2.5 times more. Even though neither of layer 3's input values are singly the highest, together they combine to make layer 3 the greatest methane producer. This same premise is used on the data obtained for each of the layers in all seven models to identify which layers have sourced the most gas across the field, with the added improvement that actual gas volumes are calculated instead of a hypothetical relative proportion.

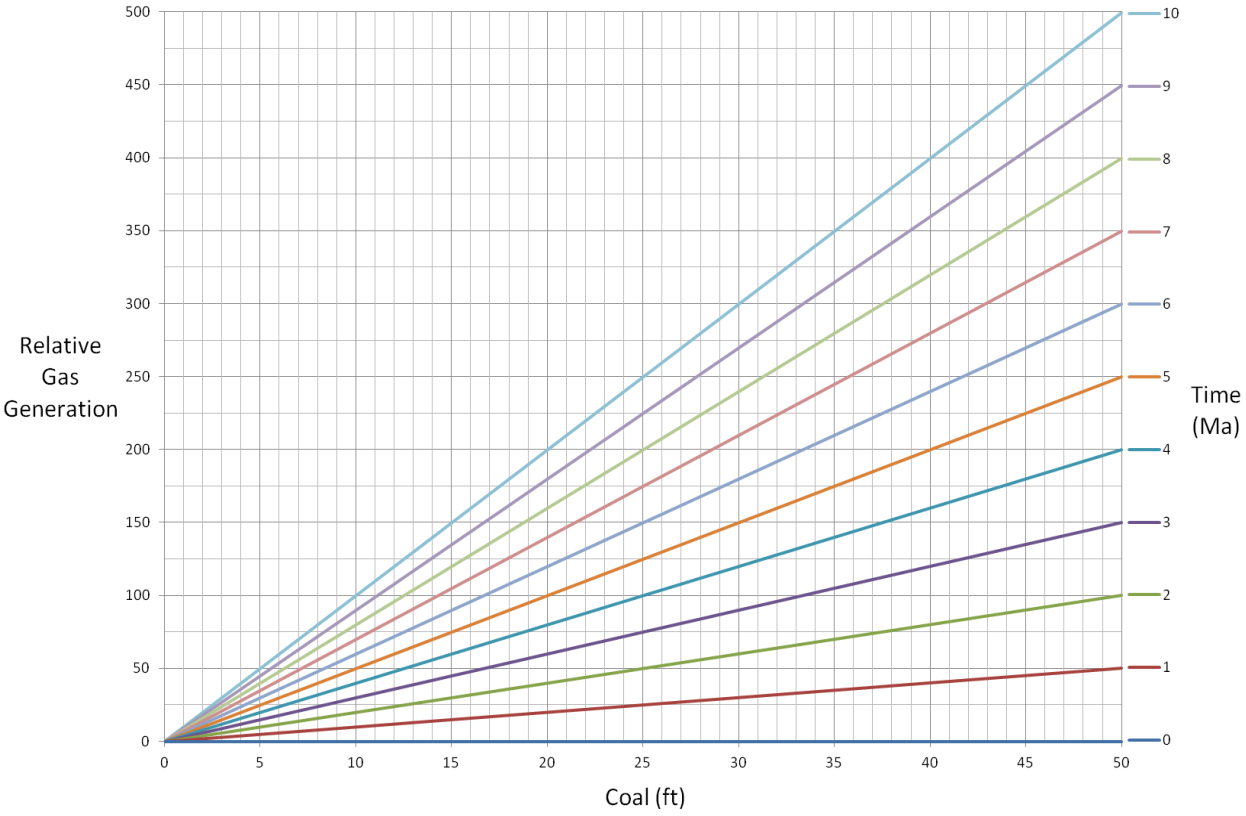

Figure 33: Relationship between relative gas generation with respect to net coal and time, based on the proportionalities of Equation 1. Graph can be used to determine the highest gas producer of two or more coal layers, assuming constant methanogenesis rate and fault block area.

The average Tyonek NtG coal value for each modeled well across the field was calculated to be 10.7%, with a range of 9.3-11.6%. Although net coal values among individual layers had much larger deviations (Appendix C), since each composite NtG coal value fell within ~2%, it is assumed that the seven sampled wells adequately represent the average coal content for each portion of the anticline. Calculating NtG coal % in the remaining unmodelled wells

would help to confirm this assumption. To complete the procedure outlined in Equation 1, the calculated net coal thicknesses were extrapolated to total coal weight, and those values were then multiplied by their respective times spent in the 5 °C intervals (Appendix D) and the corresponding percent rates of methanogenesis (Figure 20). At this point, the only major variable remaining for the gas generation calculations was the overall 100% peak rate at which methanogenesis occurs *in situ* at the optimum temperature of 37 °C. Due to the broad variety of factors that influence methanogenesis, each coalbed methane basin in the world (and probably down to the scale of each field in a basin, each well in a field, or even each reservoir in a well) could potentially possess drastically diverse rates according to each of their unique sets of *in situ* reservoir conditions. In this study, the same peak rate is assumed for all of the layers and wells across the Ninilchik field.

Initially, this rate was set as the *in situ* rate estimated for the Illinois basin, 0.01 $scf \cdot ton^{-1} \cdot yr^{-1}$ (Strąpoć et al., 2007), but this produced results vastly exceeding the amount of gas expected for the Ninilchik field. In fact, this rate produced higher gas volumes than the total amount of gas that has been produced across the entire basin. This overestimate likely occurs because, unlike in the Cook Inlet, methanogenesis in the Illinois basin is a very recent process, primarily driven through an influx of deglacial meltwater near the end of the Pleistocene (McIntosh et al., 2010; Strąpoć et al., 2011b). To obtain a rate more appropriate for Cook Inlet methanogenesis, the total methane volume produced by the models was balanced with an industry estimate of expected gas which was based on a combination of Ninilchik's reserve estimate (conventional) along with a calculated amount of adsorbed gas (continuous). According to Hartz et al. (2009), the estimated reserves for the Ninilchik field total 350 Bcf, and the adsorbed gas is computed to be 324 Bcf based on a gas saturation value of 50 scf/ton. This

brings the industry estimate of total generated gas within the Ninilchik field to 674 Bcf. Next, the peak rate used in the methanogenesis calculations was decreased until the total modeled gas volume matched this industry estimate. The final rate that produced the most similar results was determined to be $1.06e^{-5}$ $scf \cdot ton^{-1} \cdot yr^{-1}$. This value is three orders of magnitude less than the *in situ* rate estimated for the Illinois basin, and nine orders of magnitude lower than the maximum laboratory rates observed under ideal conditions (Strąpoć et al., 2007; Strąpoć et al., 2011b). Also, this is a low end rate estimate as it assumes that all produced gas is retained in the system.

Once this peak rate was determined, gas generation volumes were calculated for each layer over each 5 °C interval. These interval volumes were then added to get the total for that layer, and the layer volumes were added to get the total for that modeled well. Because these calculations were performed in a stepwise process, Appendix E displays each model's results in numerous variations to aid in their interpretation. Each model's net coal thickness, time in the MBGW and total gas generation are displayed across the range of productive depths, with the layers listed in descending order according to their relative depths TVD. From these graphs, the most productive layers can be easily identified in each model, and their relative volumes of gas can be qualitatively explained by visually evaluating their particular combination of net coal and MBGW time. These results confirm the notion that the most productive layers are not defined by just one variable. The highest combined value of both net coal and MBGW duration must be determined to characterize which layers have sourced the most gas. In addition, to evaluate production with respect to the temperature gradient, gas generation is broken down into its corresponding 5 °C intervals. On average, nearly 75% of production is sourced within the optimal window from 25-40 °C. This is to be expected due to the distribution of the '% Rate' curve (Figure 20) utilized in the calculations. Furthermore, to assess the timing of maximum

methanogenesis, each layer's total gas volume is separated into 5 Ma spans according to when the gas was produced. These results indicate that while some methanogenesis does take place as early as 25 Ma, significant production does not occur until 20 Ma before present at the earliest. In general, the highest volumes of methane were produced between 15-5 Ma, which roughly coincides with the maximum stages of anticlinal deformation. Lastly, cumulative generation versus time curves are displayed so that each layer's contribution of gas, as well as the timing of its contribution, can be compared to the total volume of gas produced.

Since the spatial distribution of the wells was chosen so that they each represented half of their particular fault block, gas volumes for the two wells in each zone were added to obtain its total amount of gas produced. Figure 34 provides a comparison of gas generation with respect to time for each of the zones, as well as for the field's cumulative total. The results indicate that coals within the productive section (-3,300 to -8,000 ft TVD) of Zone 3 sourced the most gas with a total of 331 Bcf (49%), Zone 2 came in a relatively close second with 255 Bcf (38%), and Zone 1 produced considerably less, with a total generation of only 88 Bcf (13%). To understand why this generation gap occurs, the differences between each zones' net coal %, time spent in the MBGW, and fault block area were analyzed.

The average net coal % in Zones 1, 2, and 3 were calculated to be 11.5%, 10.25%, and 10.35%, respectively. In addition, the peak durations of time spent in the MBGW shown in Figure 30 range from ~9 Ma for Zone 1, ~11 Ma for Zone 2, and ~12 Ma for Zone 3. Furthermore, the computed fault block areas used in the methanogenesis calculation are $5.6e^7$ ft^2 (17% of the field) for Zone 1, $12.8e^7$ ft^2 (38% of the field) for Zone 2, and $15e^7$ ft^2 (45% of the field) for Zone 3. Although the trend in combined values for net coal and duration matches the distribution of generated gas volumes across the field from low in Zone 1 to high in Zone 3, their

relative proportions don't seem likely to produce such a significant dispersion in the data. The area values, on the other hand, appear very similar in magnitude to the distribution seen in the gas generation. This suggests that the size of the structural closure plays the most significant role in determining which general regions should contain the most gas on a field-wide scale.

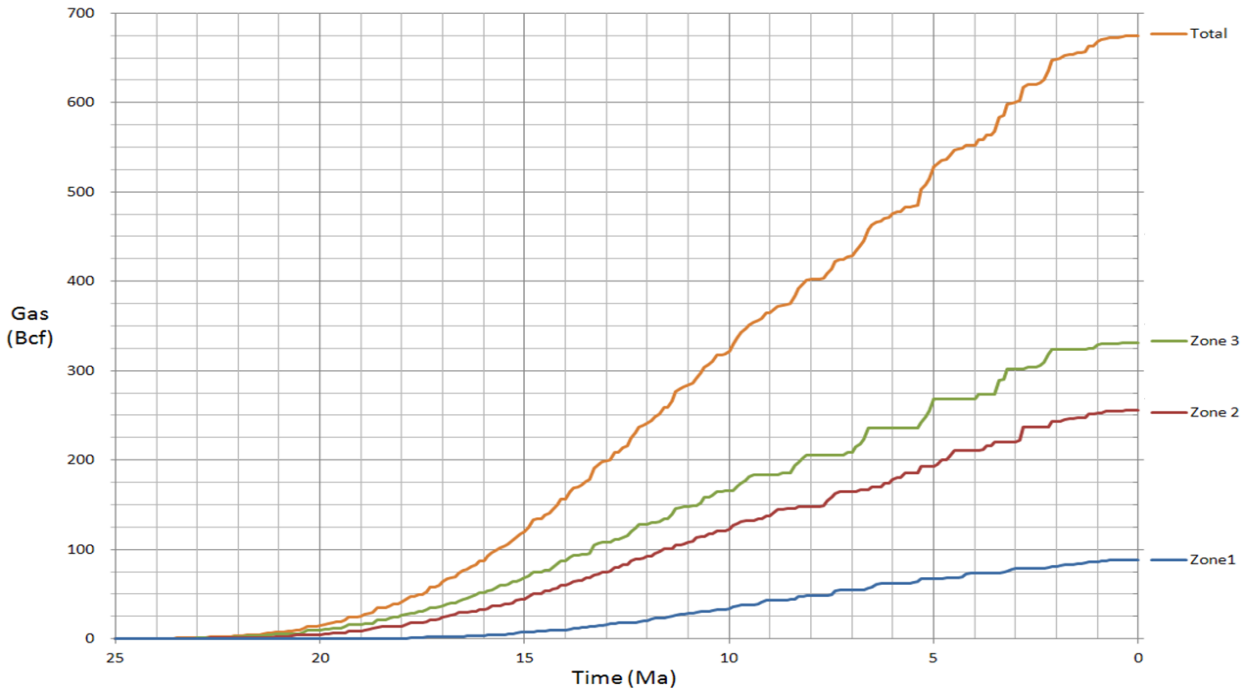

Figure 34: Cumulative gas generation (Bcf) with respect to time (Ma) for the field as well as each individual zone (see Figures 9 & 18 for locations).

However, while a larger fault block closure will in all probability contain a higher total gas volume due to its greater size, this does not automatically signify that it will possess the overall highest gas productivity per unit area. To focus this investigation on a more relevant scale, the total gas generated in each zone was divided by its fault block area. After an additional conversion from ft^2 to the desired unit of acres, efficiency of gas generation was able to be directly compared between zones of different size. The regional surface map in Figure 35 shows that Zones 2-3 are at least 18 MMcf/acre more productive that Zone 1. Judging from each model's roughly similar Tyonek NtG coal values, this lower productivity cannot be explained by

any trend in coal content towards a particular region of the field. Because of this, and since gas generation cannot be wholly defined by just coal content alone, duration in the MBGW is also taken into consideration. As determined through the analysis of Ninilchik's depositional history, the limited burial associated with anticlinal deformation is responsible for exposing the coal-bearing layers of Zone 3 to the optimal temperature window for the longest period of time. Based on these methane generation results, the field's highest average productivity exists in Zone 3 due to its superior combined values of net coal % and duration inside the MBGW.

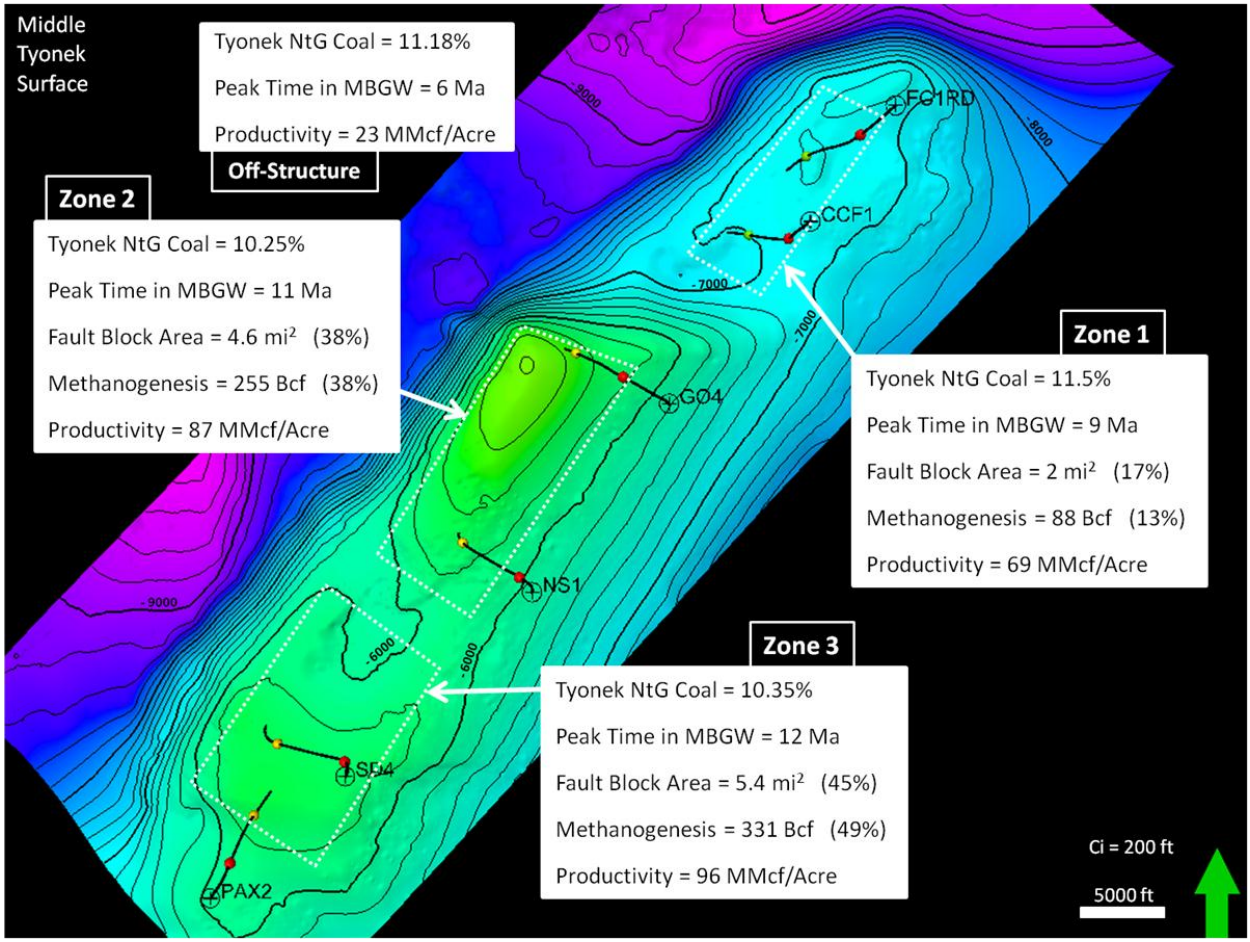

Figure 35: 3D seismic surface of the Ninilchik anticline on a middle Tyonek coal reflector. Tyonek NtG coal content, peak time in the MBGW, fault block area, volume of methanogenesis, and productivity per acre are given for each zone, along with applicable values for the off-structure well. Percentages for fault block area and methanogenesis refer to each zones' contribution to the overall field values. See Figure 18 for further seismic description.

Testing Methanogenesis

To test the accuracy and significance of the methanogenesis models, their results were compared against Ninilchik's actual well production history (Appendix A). According to these production data, ~53% of the total produced gas has come from Zone 3, while Zones 1 and 2 have produced ~22% and 25%, respectively. While gas production at the wellhead does not necessarily relate directly to methanogenesis, the trend in ascending productivity from north to south is preserved. Because Zone 1 possessed only slightly more net coal but spent considerably less time in the MBGW than Zones 2-3, it comes as no surprise that its cumulative well production is the lowest for the field. The only major producing well in Zone 1 is the Falls Creek #1RD, which is believed to have better total production compared to the other wells in this fault block because it came online first and is positioned structurally updip at the crest of the anticline (Sampson, 2011) (Figure 36). Similarly, the high producing well in Zone 2 also happens to have been the first drilled in that fault block, but unlike the FC#1RD, this Grassim Oskolkoff #1 well doesn't show any distinct structural advantage over the other wells drilled from this pad. Compared to the Ninilchik State pad, however, the GO wells are all drilled structurally updip in Zone 2, which could be used to explain its higher cumulative gas production than the NS wells. Additionally, this updip movement of gas from a region of higher methanogenesis productivity would signify that migration also plays a key role in overall gas production.

The fact that Zone 3 accounts for over half of Ninilchik's cumulative gas production correlates well with its maximal values of net coal, MBGW duration, and fault block area (Figure 35). Its largest producers each encompass at least one of the characteristics seen in the previous big wells, with the Susan Dionne #4 & #5 wells showing optimal updip placement on the front and back sides of the anticline, respectively, while the Susan Dionne #3 well was

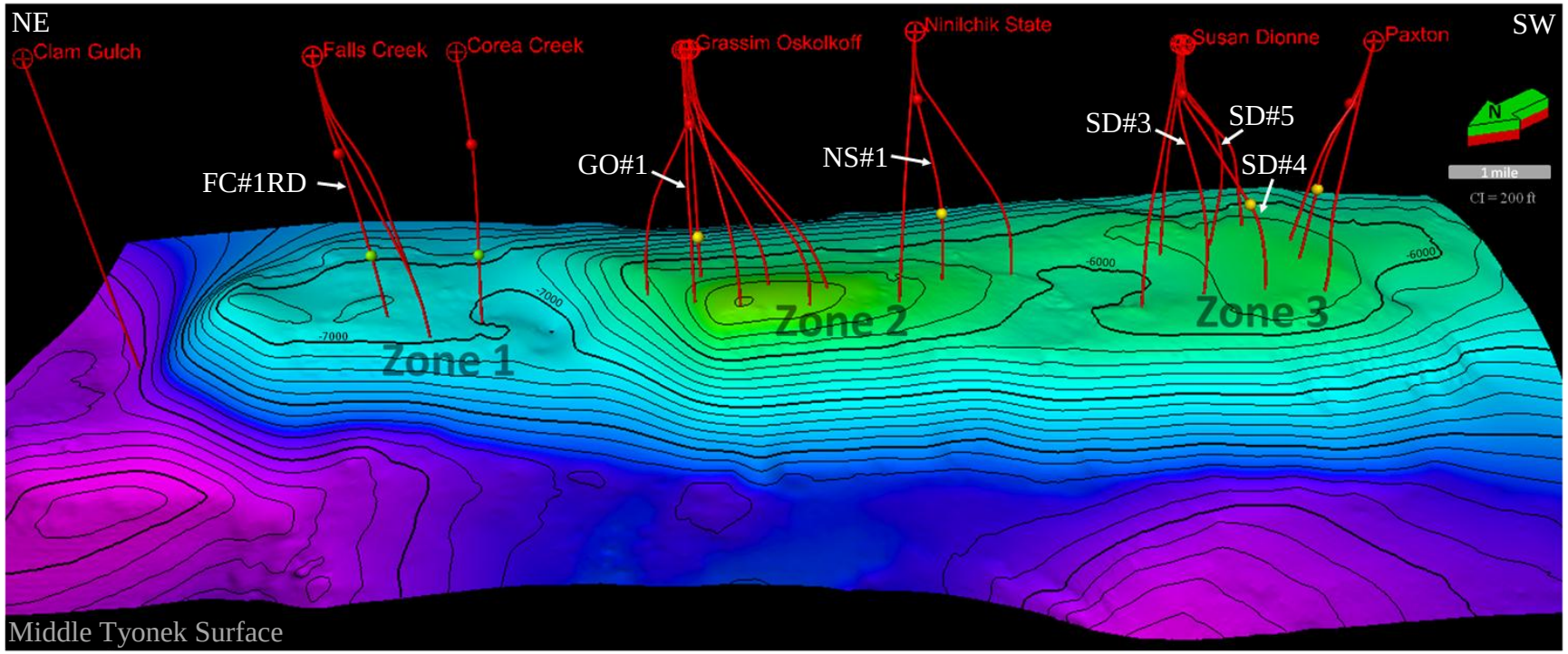

Figure 36: 3D seismic surface displaying the Ninilchik anticline on a middle Tyonek coal reflector. Well paths are shown in red from their surface location down to their point of intersection with the horizon, and the three fault blocks are labeled Zone 1, 2 & 3. White labels indicate the larger producing wells of the field. See Appendix A for production values and Figure 14 for seismic description.

completed at an earlier date (Figure 36 & Appendix A). However, the Paxton pad exhibits considerably less well production even though it produces from the same zone that contains the highest calculated productivity. This could be explained by the fact that an East/West-trending normal fault cuts the Paxton wells off from the larger portion of Zone 3 (Sampson, 2011). While the fault's presence doesn't affect the gas generation calculations for Zone 3, its potential impact on well production reiterates the fact that gas migration and fetch area may be significantly influential in determining where to find the generated gas after its expulsion from the source coals. More recently generated gas would have a larger chance of being found near its source, whereas older gas would have had more time to migrate elsewhere. By investigating the graphs in Appendix E that express each layer's methanogenesis over 5 Ma time spans, the current depths which have most recently generated the largest volumes of gas may be determined. For example, it is likely that the Susan Dionne region currently possesses a large portion of its generated gas because the highest amounts of methanogenesis took place from 10 to 5 Ma. Conversely, the Ninilchik State model indicates that its greatest generation occurred from 15 to 10 Ma, thus inducing a statistically higher risk of gas escapement from the system.

It is assumed in the methanogenesis calculations to this point that all of the generated gas has remained trapped within the system and only exits at the wellhead. To consider the effects of leakage, the calculations were recalibrated with an additional gas leakage volume equivalent to the total methane used in the initial tests (i.e., twice the amount of gas generation was input into the calculation and half was proposed to have leaked out). Based on this arbitrary twofold increase in gas generation volume, the calculated methanogenesis rates rose to $2.12e^{-5}$ $scf \cdot ton^{-1} \cdot yr^{-1}$; still three orders of magnitude less than the Illinois Basin and nine orders less than the ideal laboratory rates. With no structural or stratigraphic reason to believe that any zone of

the anticline would be leakier than the rest, the ratio of gas generation volumes between each zone stays consistent. Further studies on whether faults are impermeable barriers or conduits in the Ninilchik field would help to define gas migration and leakage characteristics. From this knowledge, after identifying a prolific source coal that possesses a high thickness and long but relatively recent duration in the MBGW, it may be possible to track probable pathways of migration away from this source to locate structural traps with a high potential gas volume.

Sensitivity Analysis

A sensitivity analysis was conducted to further test the methanogenesis calculations by adjusting input parameters within *PetroMod*®. Because the majority of well production comes from the Susan Dionne pad, the SD#4 model was chosen to be representative of how such variations would affect the field. The high end estimate resulted in a 23% decrease of both total gas volume and productivity to 123 Bcf and 72 mmcf/acre, respectively (Appendix F). In addition, to recalibrate the generated gas total with the industry reserve estimate, the rate of methanogenesis had to be increased by 30% to equal $1.38e^{-5}$ $scf \cdot ton^{-1} \cdot yr^{-1}$. Since the net coal thickness of the Tyonek formation was left unchanged, these results indicate that the collective time each of the layers spent in the MBGW was decreased due to the model's hotter near-surface temperatures. Conversely, the low end temperature estimate showed a 5% increase in gas generation and productivity (168 Bcf and 98 mmcf/acre), which necessitated a 5% decrease in methanogenesis rate ($1.01e^{-5}$ $scf \cdot ton^{-1} \cdot yr^{-1}$) to match the reserve estimate. The greater gas total in this low end model signifies that its cooler thermal regime induces extended residence times within the MBGW.

Next, an alternate stratigraphic column was applied to the original, high end and low end thermal models to evaluate how a change in depositional history would affect methanogenesis

calculations. The new ages of formational contacts together with the high end temperature parameters resulted in a 25% decrease in total gas and productivity (120 Bcf and 70 mmcf/acre), with a 34% increase in methanogenesis rate ($1.42e^{-5}$ scf·ton^{-1}·yr^{-1}) required to balance the reserves. This was the largest variation seen in the sensitivity analysis, which implies that the combination of a high temperature regime and the substituted depositional history create the least favorable conditions for methanogenesis. Furthermore, when the alternate ages were applied to the original and low end models, their total gas and productivity values each coincidentally decreased by 11% (143 Bcf and 83 mmcf/acre), and the rate needed to balance their production rose by 12% to 1.19 e^{-5} scf·ton^{-1}·yr^{-1}. While both of these modeled wells generated approximately the same total volume of gas, the corresponding graphs in Figure 37 show that this methanogenesis takes place within different layers and at different times. This occurrence demonstrates that in formations containing relatively homogenized vertical coal distribution, if the temperature gradient is adjusted so that the duration of time spent within the MBGW is decreased in some layers, other layers might actually benefit from the shift to cause only modest variations in the total gas generation.

Figure 38 illustrates how all of these models compare in total volumes of methanogenesis. Overall, the various rates determined in these sensitivity analyses may prove to be the most valuable bits of information for use in future studies by supplying ballpark estimates for Cook Inlet *in situ* methanogenesis. Based on the results of this investigation, methanogenesis rates for the Ninilchik field could range from $1.01e^{-5}$ scf·ton^{-1}·yr^{-1} to $1.42e^{-5}$ scf·ton^{-1}·yr^{-1}, with an emphasis on the original model's rate of 1.06 e^{-5} scf·ton^{-1}·yr^{-1} since it was produced via the most reasonable set of parameters. However, these results should be considered as baseline values since they assume no leakage of gas from the system.

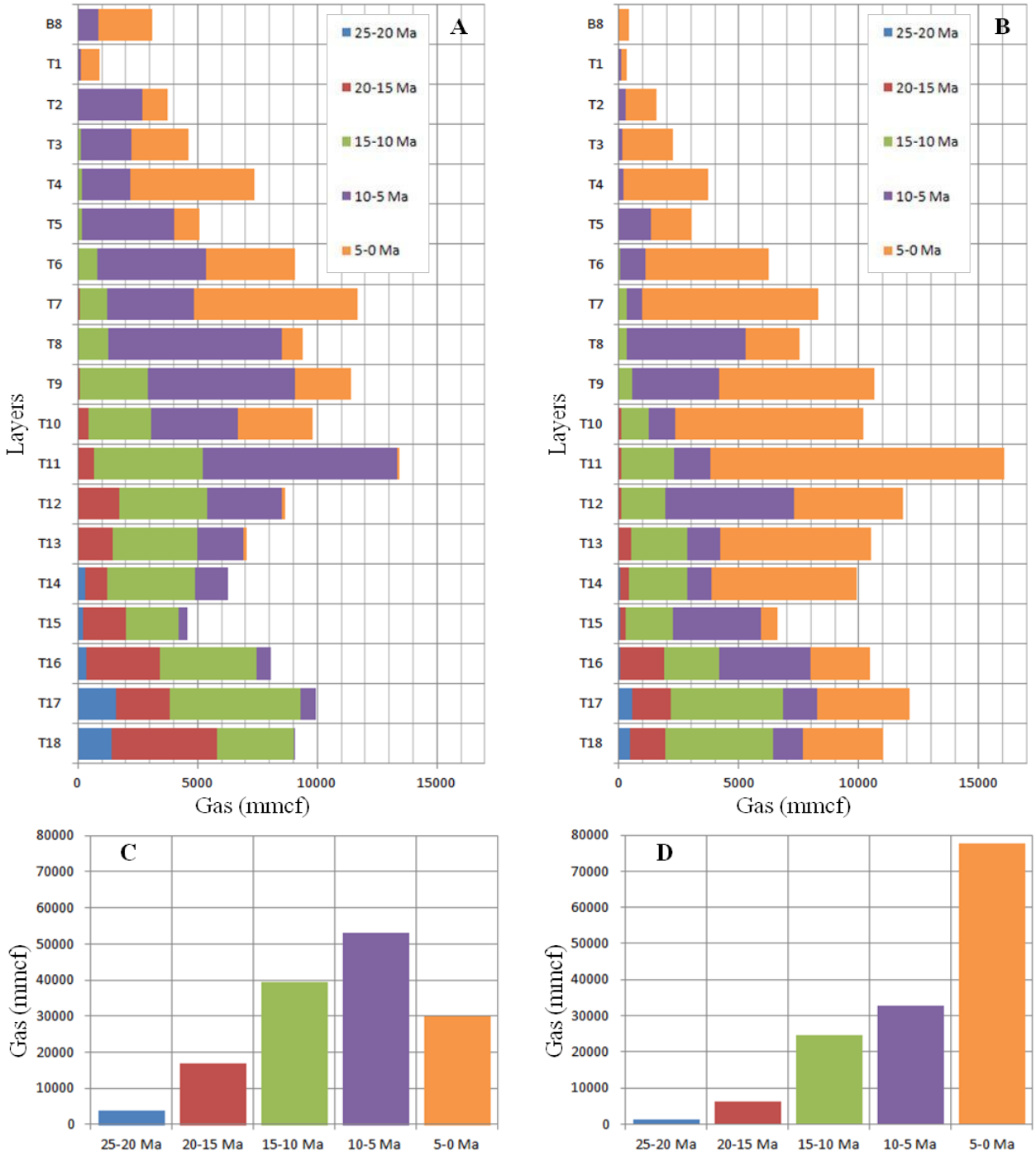

Figure 37: Graphs depicting gas generation per layer and 5 Ma interval for the two sensitivity models which similarly resulted in total gas generations of ~143 Bcf. The model calculated with original temperature parameters and alternate depositional ages is shown on left (A & C), and the model with low end temperatures and alternate depositional ages is shown on right (B & D). Note how the highest proportion of the gas in graphs A & C comes from the middle to upper modeled layers between 10-5 Ma, while the vast majority of gas in graphs B & D was produced from 5-0 Ma in the middle to lower layers. This implies that even if the basinal heat flow and thermal regime is slightly altered, total gas generation values may remain essentially constant due to the relatively even distribution of coal beds seen throughout the Tyonek formation.

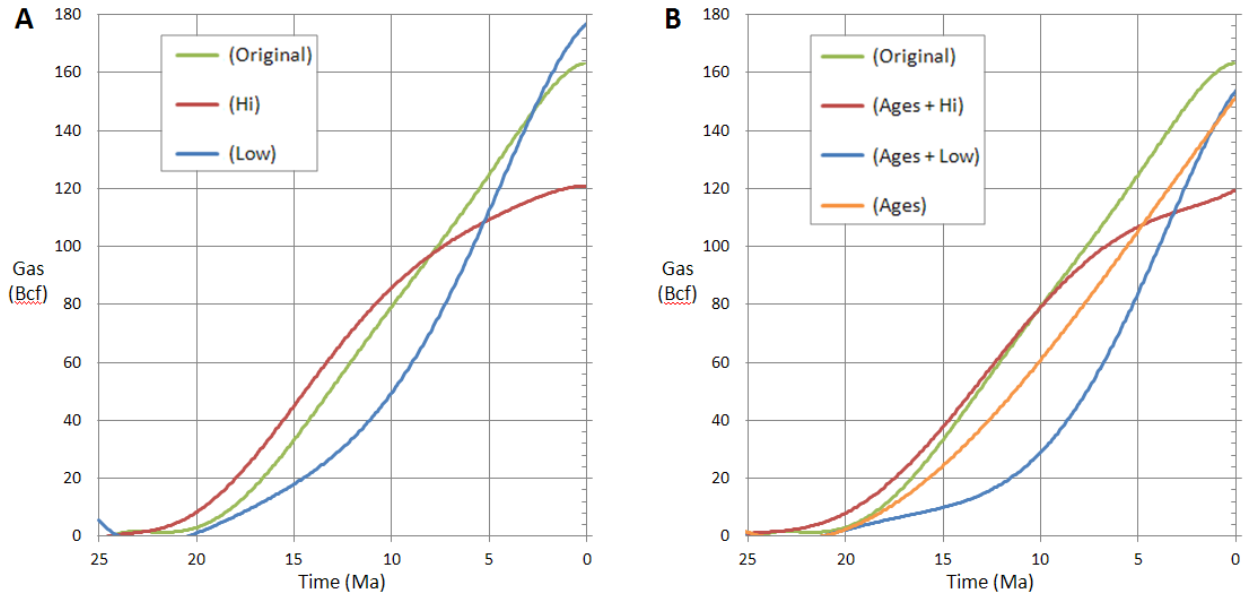

Figure 38: Cumulative gas generation (Bcf) vs time (Ma) for the original Susan Dionne #4 model compared to (**A**) the high and low end temperature estimates and (**B**) the altered depositional ages with the high and low end temperature estimates of the Sensitivity Analysis.

Future Work – CBM Enhancement

Natural methanogenesis enhancement has occurred in particular basins which might be used as an analog to guide anthropogenic CBM enhancement. Large volumes of biogenic methane have been discovered in midcontinent plays such as the Illinois, Michigan and Appalachian basins (McIntosh et al., 2010; Strąpoć et al., 2011b). These basins, however, are Paleozoic in age and have been subjected to temperatures far beyond total pasteurization, seemingly making them unlikely candidates to generate biogenic gas. Their methanogenesis is explained by uplift into a less severe temperature range, along with a late stage (Pleistocene) hydraulic recharge by inter and post-glacial meltwater that diluted and flushed the basinal brines (McIntosh et al., 2010; Schlegel et al., 2011). This freshwater influx additionally brought renewed populations of microbes as well as a replenished supply of nutrients for them to consume. Because of this process, methanogenesis in these continental basins is believed to be a very recent occurrence.

Conversely, the Kenai Group formations of Cook Inlet are much younger than the continental basin strata and have never subsided deep enough to reach the pasteurization temperature of ~80 °C (Figures 23-28). Additionally, well production at Ninilchik has been shown to include a range of depths that extends deeper than the mesophilic methanogen optimum temperature, yet too shallow to be associated with the thermophilic optimum (Gorney, 2011). If Cook Inlet methanogenesis operated on the same timescales as the continental basins, these intermediate layers would not have possessed the necessary resources to generate gas as they passed through the mesophilic optimum temperatures during the millennia preceding Pleistocene deglacial melting. Therefore, Cook Inlet methanogenesis is believed to be an ongoing process that has taken place since the co-deposition of methanogenic microbes within the Tertiary coal-bearing strata, and the temperature range used in the methanogenesis calculations is confirmed.

By evaluating the specific reservoir conditions present at Ninilchik, its rate of methanogenesis can be extrapolated into the past to help explain the field's current reserves. Furthermore, this information could also be applied to CBM enhancement operations so that the rate of gas generation might be amplified to function on human timescales. While an in-depth industry study would be required to fully investigate these specific reservoir conditions, at least one piece of information can be gleaned from preexisting knowledge of the subsurface. It is known that methanogens become highly inhibited at salinities above 2 mol/L and their growth rates are exceedingly slow above 4 mol/L (McIntosh et al., 2010). Based on the well data provided by Marathon Oil, reservoir salinities are measured to be $\leq$ 15,000 ppm, signifying that connate waters are brackish at most and are even fresher than the drilling mud. This places the salinity at ~0.2 mol/L; an order of magnitude less than the harmful values, so the earlier assumption of continuous biogenic gas generation is confirmed.

Other reservoir conditions not directly considered in this study that should be tested are pH, porosity/permeability, and the presence of supplementary microbe populations. According to McIntosh et al. (2010), pH values between 4 and 9 are required for methanogenesis, with optimal rates occurring around neutral, but variations in pH are likely in Cook Inlet due to high volcanic ash content in the Kenai Group. Additionally, methanogens measure ~0.4 μm in diameter, which could severely limit their mobility and food source access through coal matrices in areas where natural fracture networks are not present. Hydraulic fracturing may be considered to open up extra avenues for the methanogens, as well as to flush fluid into the reservoir which could bring it closer to a neutral pH if future pH testing deems it necessary. However, this hydraulic fracturing process might not be that effective in such a coal-filled basin. Furthermore, the presence of sulfate reducing bacteria can drastically limit methanogenesis by their ability to outcompete the methanogens for metabolic substrates (Schlegel et al., 2011). For this reason, as well as for the risk of inducing the production of H_2S, sulfate content should be closely monitored if any fluids are to be injected into the reservoir. Moreover, the microbes responsible for the initial fragmentation of the macromolecular network of coal are cited to be the limiting factor the rate of methanogenesis (Strąpoć et al., 2008). If these microbes can be identified, boosting their *in situ* rate of biodegradation could provide the methanogens with a more rapidly replenished food supply. Also, by studying how their extracellular excretions break down the coal, it may be possible to artificially manufacture the enzymes and directly inject them into the reservoir on an industrial scale. Lastly, the microbial assortment data in Figure 17 and Table 1 illustrate that the methyl/methanol utilizers are the most abundant producers of gas elsewhere in the basin (possibly because they don't compete with sulfate reducing bacteria for metabolic

substrates). If this proportion holds true for Ninilchik, experiments should be geared to fulfill the specific metabolic requirements of the obligate methyl/methanol utilizer, *Methanolobus* sp.

Because the coal-bearing formations of the Kenai Group are still passing through the MBGW, the best target for a CBM enhancement would be the reservoir with the most ideal of these specified conditions that is located in the region of the field that contains the largest amount of coal at the mesophilic optimum of 37 °C. To evaluate the amount remaining of the 30 wt% convertible coal, consumption values were calculated according to the volume of gas generated in each model. It was determined that a meager ~100 scf of methane has been generated per ton of coal out of the 15,000 scf/ton achievable. Based on these results, only 0.67% of the convertible coal has been transformed into methane (Figure 39). This implies that if the 674 Bcf of gas generated to this point only makes up 0.67% of the total potential, in uninhibited ideal circumstances, the Ninilchik field alone would be responsible for producing ~100 Tcf of gas. The significance of this is if generation can theoretically be raised another 0.1 % through an enhancement operation, gas reserves for the Ninilchik field could be increased by ~50 Bcf. In addition, these calculations indicate that practically the entire net coal wt% is expected to still be in place across the anticline, so the Ninilchik field would be a superb target for CBM enhancement if near-laboratory rates of methanogenesis could be achieved.

To pinpoint which region is best fit for a CBM enhancement, NtG coal percentages were calculated over the depths 300 ft above and below the 37 °C mark in each modeled well. This depth range roughly corresponds to the optimal temperatures of 35-39 °C. It was found that the Tyonek formation had already passed through the MBGW in Zone 1, and the Grassim Oskolkoff modeled well's TD was too shallow to properly evaluate this entire section. Of the three remaining wells, the Ninilchik State and Susan Dionne models showed 7.33% and 7.67% of NtG

coal within the 600 ft focus window, while the Paxton #2 well showed the highest percentage with 9.67%. Based on this higher percentage of coal at the mesophilic optimum temperature, along with its relatively mediocre well production history, the Paxton pad would make the most ideal target for CBM enhancement.

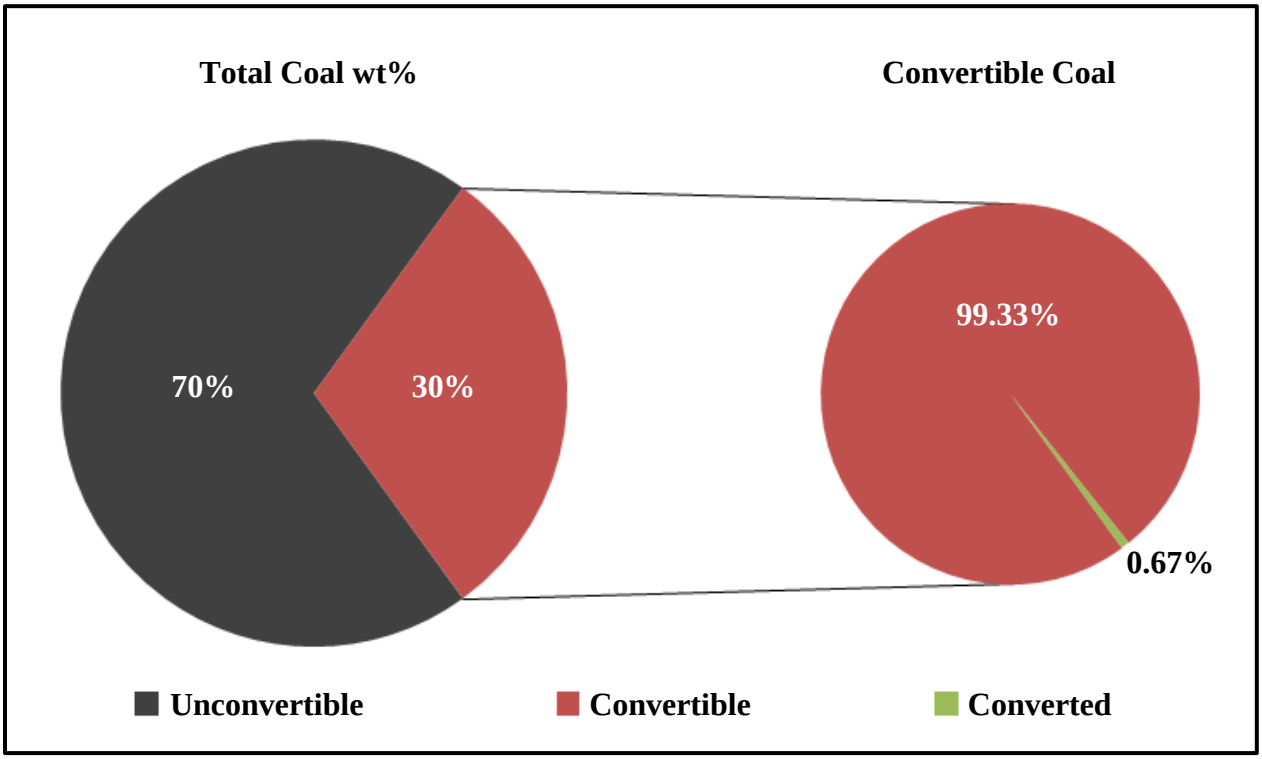

Figure 39: Distribution of convertible/unconvertible coal by wt%, along with the field's average percentage of converted methane out of the 30 wt% convertible coal.

Conclusions

Methanogenesis in the Ninilchik field has been an ongoing process taking place over millions of years since the co-deposition of microbes with the coal-bearing Kenai Group strata. Unlike midcontinent basins, late stage deglacial meltwater flushing does not fundamentally drive Cook Inlet methanogenesis, though any recent influx of meteoric groundwater may promote shallow CBM enhancement. Biogenic natural gas is generated primarily by mesophilic methanogens as the coal layers pass through their habitable temperature range of 10-50 °C. Although thermophilic methanogens are capable of withstanding temperatures up to 80 °C, they do not significantly contribute to the field's overall methane production because the majority of producing wells were not drilled to the greater depths required to reach the thermophilic temperature range. Based on the results of the geothermal history analyses, depths for the mesophilic methanogens' absolute optimum of 37 °C vary from -4,700 to -4,900 ft TVD across the anticline, while the expanded mesophilic biogenic gas window (25-40 °C) currently ranges from about -2,800 to -5,300 ft TVD. Additionally, computed vitrinite reflectance values indicate that the Tertiary coals are too thermally immature to generate thermogenic gas.

This study also demonstrates that differences in methanogenic output occur between the anticline and off-structure, as well as between the three separate fault blocks that make up the anticline structure. It was determined that 49% of the total volume of Ninilchik's methane was sourced in Zone 3, while Zone 2 sourced 38% and Zone 1 sourced 13% (Figure 34). Superficially, these proportions appear to mainly reflect the differences in fault block area, with Zones 3, 2 & 1 measuring 45%, 38% and 17% of the anticline's aerial extent, respectively. Upon further inspection, however, it was observed that while Zone 3 contains only an average NtG coal value, it maintains a 1-3 Ma higher peak MBGW duration (Figure 30). Together, these

two trends create a productivity per unit area of 96 mmcf/acre in Zone 3, compared to 87 mmcf/acre in Zone 2 and 69 mmcf/acre in Zone 1. Furthermore, no trend in the Tyonek formation's coal thicknesses towards any part of the field was found to explain the regional variation in productivity. Instead, the key factor controlling Zone 3's superior productivity is proposed to be its extended MBGW duration, which is caused by its highest relative placement atop the anticline (Figure 36). Figures 31 and 32 confirm that zones sitting at shallower depths are relegated to less severe temperatures and lower thermal maturity. Additionally, thermal differentiation of these fault blocks did not occur until the onset of Beluga deposition, and gained further disparity with the onset of Sterling deposition. This signifies that the anticline is not only responsible for housing fault blocks and closures for gas accumulation; the deformation that decreases subsidence of the Tertiary section and brings about relative anticlinal uplift also prolongs methanogenesis by holding the source coals within the optimum temperature window for longer periods of time.

Through comparison of Ninilchik's well production with the methanogenesis calculations, it was found that the same trends in productivity are preserved. 53% of the field's gas production has been extracted out of Zone 3, along with 25% out of Zone 2, and 22% from Zone 1. It is also observed that better well production generally occurs in the updip wells or first completed wells of each fault block. This indicates that migration may be a significant factor in gas production. It is hypothesized that recently generated gas is more likely to be found near its source, possibly within a transition zone between continuous and conventional accumulations. Further investigation is required to determine the nature of faults as being either impermeable barriers or gas chimney conduits. By using that information in conjunction with this study, it

may be possible to identify a prolific source coal and then track the probable migration pathways to find a productive structural trap.

Results from the sensitivity analysis reiterate that within *PetroMod*®, a fault block's depositional history controls its rate of subsidence, with a more rapid rate allowing for less time at a particular temperature in a stable geothermal gradient and vice versa. This, however, only determines when the layers were held longer at a constant depth through relative anticlinal uplift and does not define which layers happened to be inside the optimal temperature window at that point in time. It is the basinal heat flux that controls the temperature gradient and ultimately which layers fell inside the MBGW when the uplift occurred. This implies that a combination of relative anticlinal uplift (or reduced subsidence) and low heat flow values were required to create the right conditions for maximum methanogenesis.

Judging from Figure 12, the greatest depths to the oil window (%Ro > 0.6) exist in the deepest parts of the basin, north of Ninilchik and west of Anchorage. The more rapid subsidence present throughout this area brings about higher rates of sedimentation, which suppresses the effectiveness of basinal heat flux warming. Regionally, this cooler temperature regime stimulates prolonged methanogenesis by allowing the coal bearing Kenai Group formations to reside at MBGW conditions for extended durations of time. Moreover, the results of this study indicate that locally within this region, the relative anticlinal uplift actively bolsters this methanogenesis to the fullest possible natural extent on the most highly uplifted structures through inducing maximum residence times in the MBGW. These facts are evidenced in Figure 2 by noting that all major Cook Inlet gas fields occur inside the deepest region of the basin, each centered upon the crest of a major anticline.

Lastly, it was determined that the Paxton pad would make the best candidate for a CBM enhancement operation based on a combination of its higher values of net coal around the optimum temperature of 37 °C and its less than prevalent well production history (i.e. lack of reserves to risk). Its modeled geothermal history shows that this optimum temperature was encountered in the upper Tyonek formation at -4,700 ft TVD. Furthermore, the methanogenesis calculations established that <1% of the 30 wt% convertible coal has been biogenically transformed to methane, which indicates that nearly all of the field's potential resources for gas generation could still remain. These calculations imply that if the converted wt% of coal can be raised by just 0.1% through CBM enhancement, Ninilchik's producible gas reserve estimate could increase by ~50 Bcf. Finding a way to harvest this giant potential resource by initiating large scale hydrocarbon generation on human timescales, both in the Cook Inlet basin and in others like it, would fulfill the world's rising energy needs for many years to come.

References

Barker, C.E. & Dallegge, T.A. (2001). High-resolution Chronostratigraphic Analyses of the Tertiary Kenai Group, South-central Alaska: Applications to Basin Analysis and Coal-bed Methane Assessment: An Update. Division of Geological & Geophysical Survey, Miscellaneous Publication 128, p. 29-39.

Barker, C.E. & Dallegge, T.A. (2006). Secondary gas emissions during coal desorption, Marathon Grassim Oskolkoff-1 Well, Cook Inlet Basin, Alaska: implications for resource assessment. Bulletin of Canadian Petroleum Geology, v. 54, no. 3, p. 273-291.

Blackwell, D.D. & Richards, M. (2004). Geothermal Map of North America. American Association of Petroleum Geologists, 1 sheet, scale 1:6,500,000.

Boone, D.R., Whitman, W.B., & Rouvière, P. (1993). Diversity and Taxonomy of Methanogens. in Methanogens: Ecology, Physiology, Biochemistry & Genetics, p. 35-80. Chapman & Hall. 1 Penn Plaza, New York, NY 10119.

Boss, R.F., Lennon, R.B., & Wilson, B.W. (1976). Middle Ground Shoal oil field, Alaska. in North American oil and gas fields: AAPG Mem. 24, p. 1-22.

Brimberry, D.L., Gardner, P.S., McCullough, M.L., & Trudell, S.E. (2001). Kenai Field, the Kenai Peninsula's Largest Gas Field. Division of Geological & Geophysical Survey, Miscellaneous Publication 128, p. 20-28.

Dallegge, T.A. & Barker, C.E. (2000). Coal-bed methane gas-in-place resource estimates using sorption isotherms and burial history reconstruction: An example from the Ferron Sandstone member of the Mancos Shale, Utah. U.S. Geological Survey Professional Paper 1625-B, ch. L.

Dallegge, T.A. & Layer, P.W. (2004). Revised chronostratigraphy of the Kenai Group from $^{40}Ar/^{39}Ar$ dating of low-potassium bearing minerals, Cook Inlet Basin, Alaska. Canadian Journal of Earth Science, v. 41, p. 1159-1179

Ferry, J.G. (1993). Methanogens: Ecology, Physiology, Biochemistry & Genetics. Chapman & Hall. 1 Penn Plaza, New York, NY 10119, USA.

Gorney, D. (2011). Overview of Ninilchik Gas Field. Marathon Oil Company. Unpublished Industry Data.

Haeussler, P.J., Bruhn, R.L., & Pratt, T.L. (2000). Potential seismic hazards and tectonics of the upper Cook Inlet basin, Alaska, based on analysis of Pliocene and younger deformation. Geological Society of America Bulletin, v. 112, no. 9, p. 1414-1429.

Haeussler, P.J. & Saltus, R.W. (2011). Location and extent of Tertiary structures in Cook Inlet Basin, Alaska, and mantle dynamics that focus deformation and subsidence. Studies by the U.S. Geological Survey in Alaska 2008–2009: U.S. Geological Survey Professional Paper 1776–D, p. 26.

Hartz, J.D., Kremer, M.C., Krouskop, D.L., Silliphant, L.J., Houle, J.A., Anderson, P.C., & LePain, D.L. (2009). Preliminary engineering and geological evaluation of remaining Cook Inlet gas reserves. Alaska Division of Oil and Gas, report 37.

Head, I.M., Jones, D.M., & Larter, S.R. (2003). Biological activity in the deep subsurface and the origin of heavy oil. Nature, v. 426, p. 344-352.

Kelly, T.E. (1963). Geology and Hydrocarbons in Cook Inlet Basin, Alaska. American Association of Petroleum Geologists, Mem. 2, p. 278-296.

Kirschner, C.E. & Lyon, C.A. (1973). Stratigraphic and Tectonic Development of Cook Inlet Petroleum Province. American Association of Petroleum Geologists, mem. 19, p. 396-407.

Lambo, A.J., Strąpoć, D., Pittenger, M., Wood, L., Ashby, M., & Huizinga, B. (2011). Molecular and Risk-Based Approach to Nutrient Development for a Proposed Sub-Surface Biogasification Field Trial in a Biogenic Gas Field. ConocoPhillips and Taxon Biosciences.

Li, P. (2006). Modeling of thermal maturity history of strata in the North Louisiana Salt Basin area. Gulf Coast Association of Geological Societies Transactions, v. 56, p. 439-454.

Lillis, P.G. & Stanley, R.G. (2011). Petroleum generation modeling for Cook Inlet basin, Alaska (abstract). Program with Abstracts, 2011 Western Region Meeting, Society of Petroleum Engineers and Pacific Section. American Association of Petroleum Geologists, Anchorage, Alaska, May 6-14, 2011, p. 72.

McIntosh, J.C., Warwick, P.D., Martini, A.M., & Osborn, S.G. (2010). Coupled hydrology and biogeochemistry of Paleocene-Eocene coal beds, northern Gulf of Mexico. Geological Society of America Bulletin, v. 122, no. 7-8, p. 1248-1264.

Miller, K.G., Browning, J.V., Aubry, M.P., Wade, B.S., Katz, M.E., Kulpecz, A.A., & Wright, J.D. (2008). Eocene-Oligocene global climate and sea-level changes: St. Stephens quarry, Alabama. Geological Society of America Bulletin, v. 120, p. 34-53.

Montgomery, S.L. & Barker, C.E. (2003). Coalbed Methane, Cook Inlet, south-central Alaska: A potential giant gas resource. American Association of Petroleum Geologists Bulletin, v. 87, no. 1, p. 1-13.

Muller, R.D., Sdrolias, M., Gaina, C., & Roest, W.R. (2008). Age, spreading rates and spreading symmetry of the world's ocean crust. Geochemical, Geophysical, Geosystems, v. 9, in Seafloor Age Map (2009), California Institute of Technology – Tectonics Observatory.

Nunn, J.A. & Lin, G. (2002). Insulating effect of coals and organic rich shales: Implications for topography-driven fluid flow, heat transport, and genesis of ore deposits in the Arkoma Basin and Ozarka Plateau. Basin Research, v. 14, p. 129-145.

Okubo, Y., Uchida, Y., Taniguchi, M., Miyakoshi, A., & Safanda, J. (2005). Statistical analysis for thermal data in the Japanese Islands. Physics of the Earth and Planetary Interiors, v. 152, p. 277-291.

Penner, T.J., Foght, J.M., & Budwill, K. (2010). Microbial diversity of western Canadian subsurface coal beds and methanogenic coal enrichment cultures. International Journal of Coal Geology, v. 82, p. 81-93.

Sampson, A. (2011). A Seismic Attribute Study to Assess Well Productivity in the Ninilchik Field, Cook Inlet Basin, Alaska. Master's Thesis, Louisiana State University.

Schlegel, M.E., McIntosh, J.C., Bates, B.L., Kirk, M.F., & Martini, A.M. (2011). Comparison of fluid geochemistry and microbiology of multiple organic-rich reservoirs in a sedimentary basin: Evidence for controls on methanogenesis and microbial transport. Geochimica et Cosmochimica Acta, v. 75, p. 1903-1919.

Schlumberger Oilfield Glossary (1998). Schlumberger Limited. 12/12/2011 <www.glossary.oilfield.slb.com>

Stanley, R.G., Pierce, B.S., & Houseknecht, D.W. (2011). USGS 2011 assessment of undiscovered oil and gas resources of Cook Inlet region, south-central Alaska: U.S. Geological Survey Open-File Report 1237.

Strąpoć, D., Mastalerz, M., Eble, C., & Schimmelmann, A. (2007). Characterization of the origin of coalbed gases in south-eastern Illinois Basin by compound-specific carbon and hydrogen stable isotope ratios. Organic Geochemistry, v. 38, p. 267-287.

Strąpoć, D., Picardal, F.W., Turich, C., Schaperdoth, I., Macaladay, J.L., Lipp, J.S., Lin, Y., Ertefai, T.F., Schubotz, F., Hinrichs, K., Mastalerz, M., & Schimmelmann, A. (2008). Methane-Producing Microbial Community in a Coal Bed of the Illinois Basin. Applied and Environmental Microbiology, v. 74, no. 8, p. 2424-2432.

Strąpoć, D., Ashby, M., Wood, L., Levinson, R., Huizinga, B. (2011a). How Specific Microbial Communities Benefit from the Oil Industry: Significant Contribution of Methyl/Methanol Utilizing Methanogenic Pathway in a Subsurface Biogas Environment. in Applied Microbiology and Molecular Biology in Oilfield Systems, ch. 25, p. 211-216. Springer Science + Business Media.

Strąpoć, D., Mastalerz, M., Dawson, K., Macalady, J.L., Callaghan, A.V., Wawrik, B., Turich, C., & Ashby, M. (2011b). Biogeochemistry of Microbial Coal-Bed Methane. Annual Review of Earth and Planetary Sciences, v. 39, p. 617-656.

Swenson, R. (2001). Introduction to Tertiary Tectonics and Sedimentation in the Cook Inlet Basin. Division of Geological & Geophysical Survey, Miscellaneous Publication 128, p. 10-19.

Turcotte, D.L. & Schubert, G. (2002). Geodynamics, 2 ed. Cambridge University Press. 40 West 20th Street, New York, NY 10011.

Wilson, F.H., Hults, C.P., Schmoll, H.R., Haeussler, P.J., Schmidt, J.M., Yehle, L.A., & Labay, K.A. (2009). Preliminary geologic map of the Cook Inlet region, Alaska: U.S. Geological Survey Open-File Report 1108, scale 1:250,000.

Yao, H. & Conrad, R. (2000). Effect of temperature on reduction of iron and production of carbon dioxide and methane in anoxic wetland rice soils. Biology of Fertile Soils, v. 32, p. 135-141.

Appendix A: Wells Used in Study

(Modeled wells shown in bold)

Well Name	Location*	Date Completed	MD (ft)	TVD (ft)	Logs Available**	Gas Cum. (Mcf)***
Clam Gulch Unit #1	28, 2N, 12W	08/24/1978	14,200	14,200	SP, GR, ResD, Dt, RhoB	N/A
Falls Creek #1RD	6, 1N, 12W	04/09/2002	8,900	8,322	SP, GR, ResD, Dt, RhoB	18,812,983
Falls Creek #3	6, 1N, 12W	08/11/2003	10,668	8,466	GR, ResD, Dt, RhoB	3,807,552
Falls Creek #4	6, 1N, 12W	03/26/2004	7,910	6,047	GR, ResD, Dt, RhoB	5,098,017
Corea Creek Fed #1	12, 1N, 13W	05/31/1996	9,738	9,052	SP, GR, Dt, RhoB	N/A
Grassim Oskolkoff #1	23, 1N, 13W	07/31/2001	11,600	8,510	GR, Dt	16,958,170
Grassim Oskolkoff #2	23, 1N, 13W	11/29/2001	12,026	8,483	GR, ResD, Dt, RhoB	2,008,522
Grassim Oskolkoff #3	23, 1N, 13W	09/01/2005	13,771	8,147	SP, GR, RhoB	2,906,826
Grassim Oskolkoff #4	23, 1N, 13W	02/03/2006	8,175	4,828	GR, ResD, Dt, RhoB	N/A
Grassim Oskolkoff #5	23, 1N, 13W	05/31/2007	10,384	7,987	GR, Dt, RhoB	N/A
Grassim Oskolkoff #6	23, 1N, 13W	11/22/2007	12,069	7,429	N/A	1,317,894
Grassim Oskolkoff #7	23, 1N, 13W	06/12/2008	13,500	7,325	N/A	N/A
Ninilchik State #1	34, 1N, 13W	08/25/2005	10,221	8,104	SP, GR, ResD, Dt, RhoB	7,144,413
Ninilchik State #2	34, 1N, 13W	02/13/2007	11,500	8,311	SP, GR, ResD, Dt, RhoB	N/A
Ninilchik State #3	34, 1N, 13W	10/05/2007	11,962	8,005	GR, ResD, Dt, RhoB	1,298,835
Susan Dionne #2	6, 1S, 13W	12/06/2004	11,094	8,007	SP, GR, ResD, Dt, RhoB	N/A
Susan Dionne #3	6, 1S, 13W	07/03/2002	10,255	8,102	GR, Dt	14,426,152
Susan Dionne #4	6, 1S, 13W	03/18/2005	11,953	8,367	GR, ResD, Dt, RhoB	21,690,649
Susan Dionne #5	6, 1S, 13W	10/03/2006	9,600	7,987	GR, ResD, Dt, RhoB	15,977,425
Susan Dionne #6	6, 1S, 13W	12/21/2008	6,737	4,520	N/A	7,440,540
Paxton #1	13, 1S, 14W	05/29/2004	10,115	8,320	GR, ResD, Dt, RhoB	1,778,274
Paxton #2	13, 1S, 14W	03/08/2008	8,436	7,985	GR, ResD, Dt, RhoB	3,851,617
Paxton #3	13, 1S, 14W	04/19/2010	7,414	4,179	GR, Dt, RhoB	1,652,681

* Locations given in Section, Township, & Range format

** SP = Spontaneous Potential, GR = Gamma Ray, ResD = Resistivity, Dt = Sonic, RhoB = Bulk Density

*** Cumulative volumes last updated 10/2011

Appendix B: Cook Inlet Type Log with Example Picks of Beluga and Tyonek Fm.

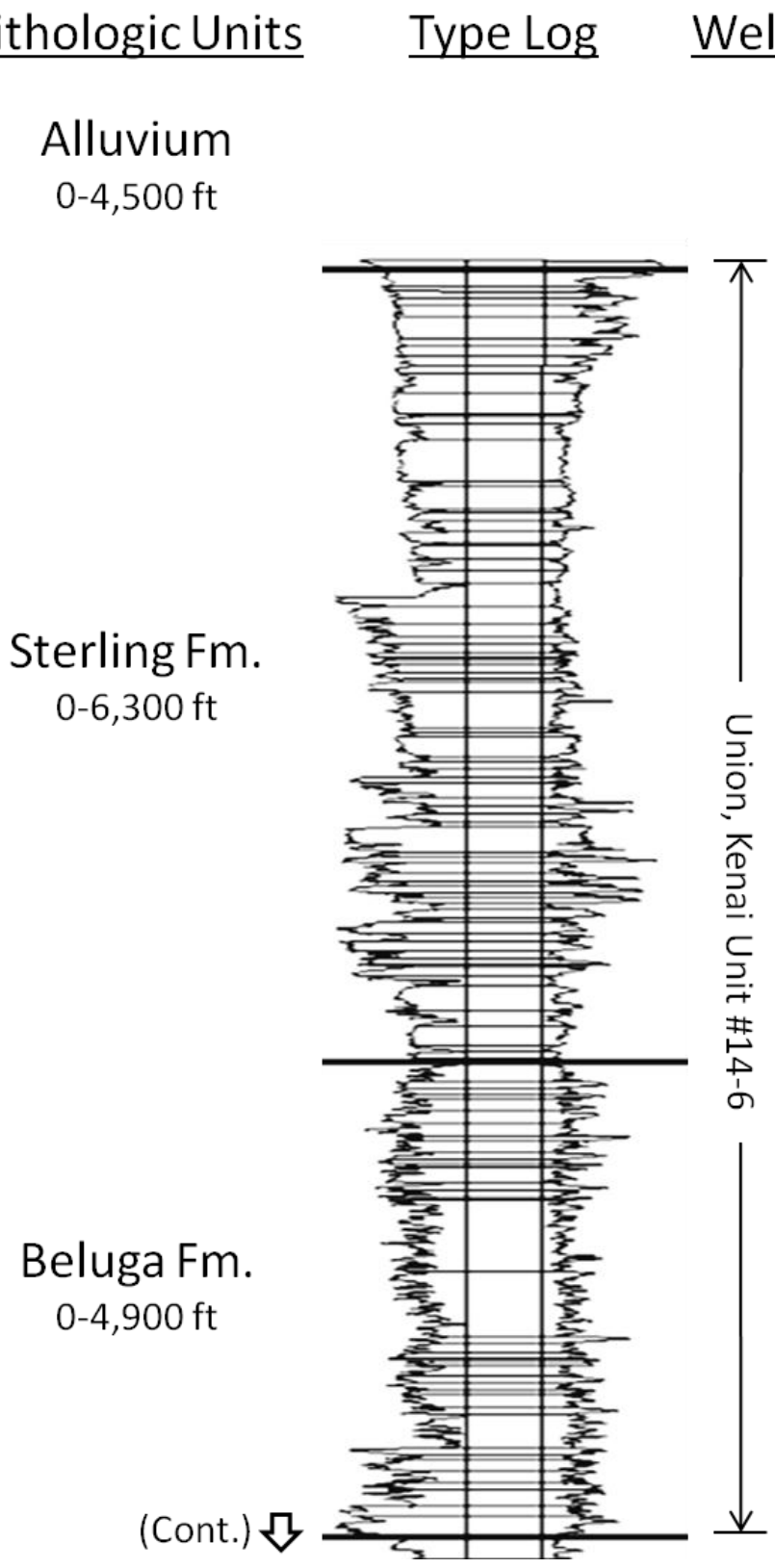

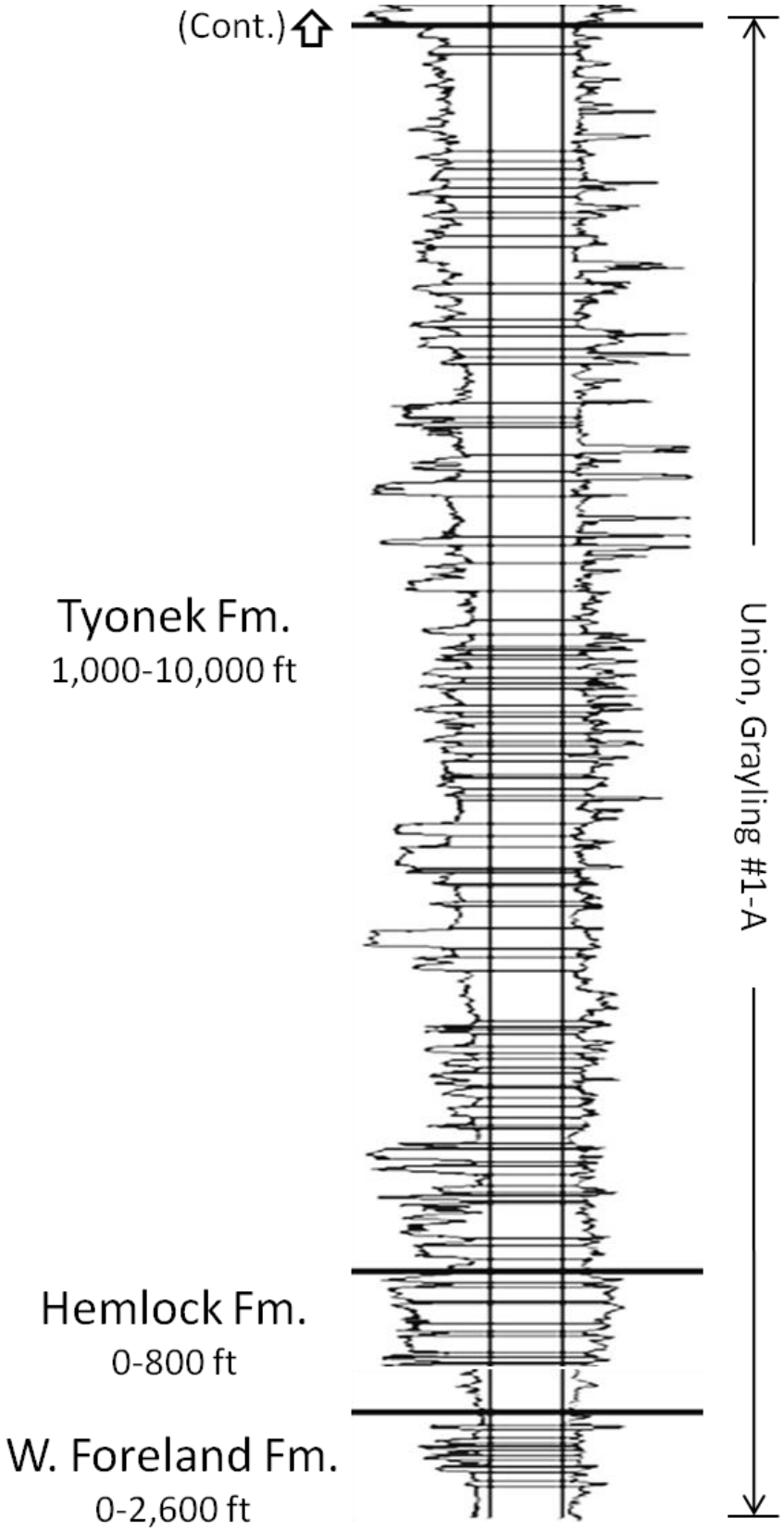

Image modified from Montgomery & Barker, 2003. No log scales were provided.

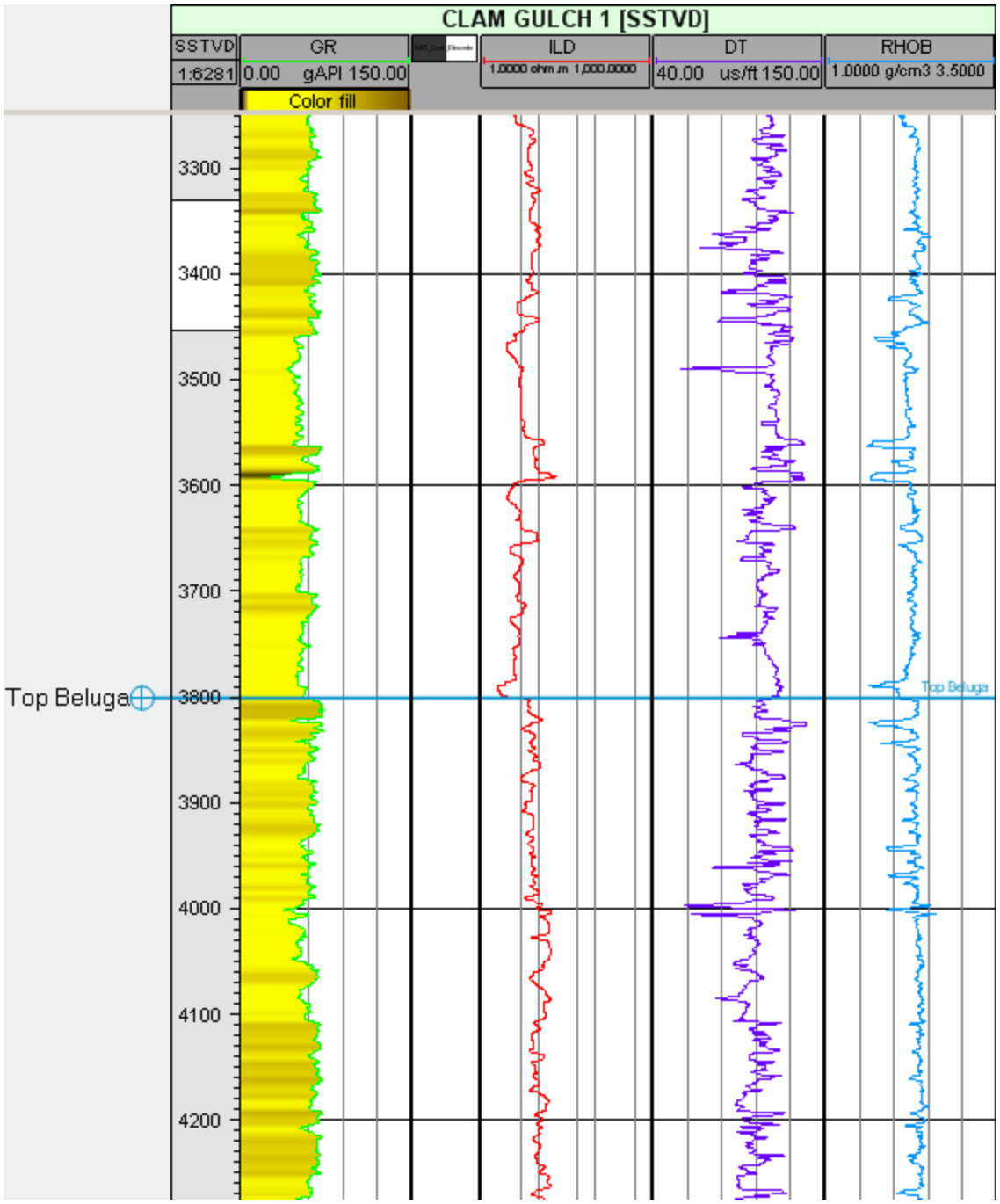

Example well log character of the Sterling/Beluga contact for the Clam Gulch #1 well showing subsea true vertical depth, gamma ray, coal, resistivity, sonic and bulk density from left to right. Beluga top is picked on first package of thin coal and shale beds. Image captured from *Petrel*®.

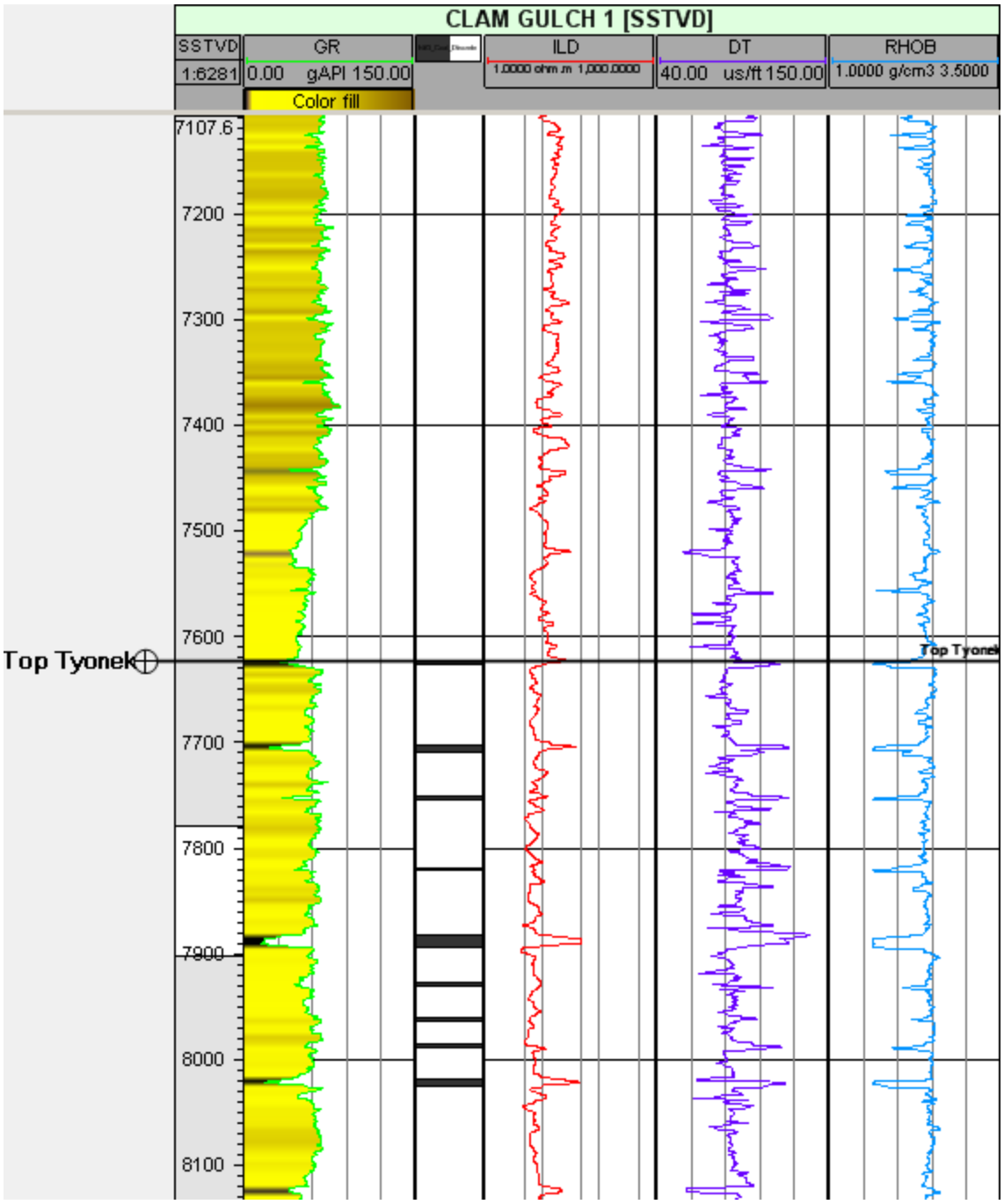

Example well log character of the Beluga/Tyonek contact for the Clam Gulch #1 well showing subsea true vertical depth, gamma ray, coal, resistivity, sonic and bulk density from left to right. Tyonek top is picked on first thick, laterally correlative coal bed. Image captured from *Petrel*®.

Appendix C: Input Data for *PetroMod*® and Methanogenesis Calculations

Clam Gulch #1

Layer	Top	Base	Thick.	Depo. From	Depo. To	NtG Coal
Sterling	0	3800	3800	8.00	0.00	3.90%
Beluga	3800	7623	3823	14.50	8.00	3.30%
T1 Tyonek	7623	8000	377	15.48	14.50	9.40%
T2	8000	8250	250	16.13	15.48	2.54%
T3	8250	8500	250	16.79	16.13	13.86%
T4	8500	8750	250	17.44	16.79	11.22%
T5	8750	9000	250	18.09	17.44	10.40%
T6	9000	9250	250	18.74	18.09	15.60%
T7	9250	9500	250	19.39	18.74	13.60%
T8	9500	9750	250	20.04	19.39	12.80%
T9	9750	10000	250	20.69	20.04	16.80%
T10	10000	10250	250	21.35	20.69	13.60%
T11	10250	10500	250	22.00	21.35	15.20%
T12	10500	10750	250	22.65	22.00	16.00%
T13	10750	11000	250	23.30	22.65	3.60%
T14	11000	11250	250	23.95	23.30	10.80%
T15	11250	11500	250	24.60	23.95	6.00%
T16	11500	11750	250	25.26	24.60	10.80%
T17	11750	12000	250	25.91	25.26	10.80%
T18	12000	12250	250	26.56	25.91	14.40%
T19	12250	12500	250	27.21	26.56	19.20%
T20	12500	12750	250	27.86	27.21	6.80%
T21	12750	13000	250	28.51	27.86	5.60%
T22	13000	13250	250	29.16	28.51	1.20%
T23	13250	13500	250	29.82	29.16	2.40%
T24	13500	13750	250	30.47	29.82	11.60%
T25	13750	14000	250	31.12	30.47	13.60%
T26	14000	14223	223	31.70	31.12	28.96%
Hemlock	14223	14923	700	33.50	31.70	0.00%
W. Foreland	14923	16123	1200	56.00	35.70	8.30%
	(ft)	(ft)	(ft)	(Ma)	(Ma)	

Falls Creek #1RD

	Layer	Top	Base	Thick.	Depo. From	Depo. To	NtG Coal
	Sterling	0	2433	2433	8.00	0.00	6.20%
*	Beluga 1-3	2433	3309	876	10.17	8.00	4.79%
*	B4	3309	3601	292	10.89	10.17	4.79%
*	B5	3601	3893	292	11.61	10.89	4.79%
*	B6	3893	4185	292	12.33	11.61	4.79%
*	B7	4185	4477	292	13.06	12.33	4.79%
*	B8	4477	4769	292	13.78	13.06	4.79%
*	B9	4769	5061	292	14.50	13.78	4.79%
	T1 Tyonek	5061	5250	189	14.99	14.50	8.99%
	T2	5250	5500	250	15.64	14.99	7.20%
	T3	5500	5750	250	16.30	15.64	8.40%
	T4	5750	6000	250	16.95	16.30	8.40%
	T5	6000	6250	250	17.60	16.95	8.80%
	T6	6250	6500	250	18.25	17.60	14.80%
	T7	6500	6750	250	18.90	18.25	10.80%
	T8	6750	7000	250	19.55	18.90	12.80%
	T9	7000	7250	250	20.20	19.55	13.20%
	T10	7250	7500	250	20.86	20.20	16.40%
	T11	7500	7750	250	21.51	20.86	16.80%
	T12	7750	8000	250	22.16	21.51	11.20%
	T13	8000	8272	272	22.87	22.16	9.93%
	T14	8272	11661	3389	31.70	22.87	11.40%
	Hemlock	11661	12361	700	33.50	31.70	0.00%
	W. Foreland	12361	13561	1200	56.00	35.70	8.30%
		(ft)	(ft)	(ft)	(Ma)	(Ma)	

* Subhorizon estimated from *PetroMod*®

Corea Creek #1

	Layer	Top	Base	Thick.	Depo. From	Depo. To	NtG Coal
	Sterling	0	2386	2386	8.00	0.00	6.30%
*	Beluga 1-3	2386	3329	943	10.17	8.00	4.45%
*	B4	3329	3644	314.5	10.89	10.17	4.45%
*	B5	3644	3958	314.5	11.61	10.89	4.45%
*	B6	3958	4273	314.5	12.33	11.61	4.45%
*	B7	4273	4587	314.5	13.06	12.33	4.45%
*	B8	4587	4902	314.5	13.78	13.06	4.45%
*	B9	4902	5216	314.5	14.50	13.78	4.45%
	T1 Tyonek	5216	5500	284	15.24	14.50	6.69%
	T2	5500	5750	250	15.89	15.24	8.40%
	T3	5750	6000	250	16.54	15.89	10.40%
	T4	6000	6250	250	17.19	16.54	6.40%
	T5	6250	6500	250	17.85	17.19	10.80%
	T6	6500	6750	250	18.50	17.85	13.60%
	T7	6750	7000	250	19.15	18.50	6.80%
	T8	7000	7250	250	19.80	19.15	14.40%
	T9	7250	7500	250	20.45	19.80	21.60%
	T10	7500	7750	250	21.10	20.45	9.20%
	T11	7750	8000	250	21.76	21.10	16.80%
	T12	8000	8250	250	22.41	21.76	12.40%
	T13	8250	8500	250	23.06	22.41	10.40%
	T14	8500	8750	250	23.71	23.06	14.40%
	T15	8750	8916	166	24.14	23.71	12.65%
	T16	8916	11816	2900	31.70	24.14	11.60%
	Hemlock	11816	12516	700	33.50	31.70	0.00%
	W. Foreland	12516	13716	1200	56.00	35.70	8.30%
		(ft)	(ft)	(ft)	(Ma)	(Ma)	

* Subhorizons estimated from *PetroMod*®

Grassim Oskolkoff #4

	Layer	Top	Base	Thick.	Depo. From	Depo. To	NtG Coal
	Sterling	0	1470	1470	8.00	0.00	10.20%
*	Beluga 1-6	1470	3273	1803	12.88	8.00	5.32%
*	B7	3273	3574	301	13.69	12.88	5.32%
*	B8	3574	3875	301	14.50	13.69	5.32%
	T1 Tyonek	3875	4250	375	15.48	14.50	11.20%
	T2	4250	4500	250	16.13	15.48	5.60%
	T3	4500	4778	278	16.85	16.13	10.07%
*	T4_1	4778	5095	316.5	17.68	16.85	9.30%
*	T4_2	5094.5	5411	316.5	18.50	17.68	9.30%
*	T4_3	5411	5728	316.5	19.33	18.50	9.30%
*	T4_4	5727.5	6044	316.5	20.15	19.33	9.30%
*	T4_5	6044	6361	316.5	20.98	20.15	9.30%
*	T4_6	6360.5	6677	316.5	21.80	20.98	9.30%
*	T4_7	6677	6994	316.5	22.63	21.80	9.30%
*	T4_8	6993.5	7310	316.5	23.45	22.63	9.30%
*	T4_9	7310	7627	316.5	24.28	23.45	9.30%
*	T4_10	7626.5	7943	316.5	25.10	24.28	9.30%
*	T4_11-18	7943	10475	2532	31.70	25.10	9.30%
	Hemlock	10475	11175	700	33.50	31.70	0.00%
	W. Foreland	11175	12375	1200	56.00	35.70	8.30%
		(ft)	(ft)	(ft)	(Ma)	(Ma)	

* Subhorizon estimated from *PetroMod*®

Ninilchik State #1

	Layer	Top	Base	Thick.	Depo. From	Depo. To	NtG Coal
	Sterling	0	1468	1468	8.00	0.00	10.20%
*	Beluga 1-6	1468	3277	1809	12.87	8.00	5.30%
*	B7	3277	3579	302	13.69	12.87	5.30%
*	B8	3579	3881	302	14.50	13.69	5.30%
	T1 Tyonek	3881	4250	369	15.46	14.50	5.15%
	T2	4250	4500	250	16.11	15.46	7.60%
	T3	4500	4750	250	16.76	16.11	8.40%
	T4	4750	5000	250	17.42	16.76	6.00%
	T5	5000	5250	250	18.07	17.42	18.80%
	T6	5250	5500	250	18.72	18.07	10.40%
	T7	5500	5750	250	19.37	18.72	12.80%
	T8	5750	6000	250	20.02	19.37	8.80%
	T9	6000	6250	250	20.67	20.02	14.40%
	T10	6250	6500	250	21.33	20.67	10.80%
	T11	6500	6750	250	21.98	21.33	12.80%
	T12	6750	7000	250	22.63	21.98	12.80%
	T13	7000	7250	250	23.28	22.63	19.60%
	T14	7250	7500	250	23.93	23.28	9.20%
	T15	7500	7750	250	24.58	23.93	9.60%
	T16	7750	8059	309	25.39	24.58	13.92%
	T17	8059	10481	2422	31.70	25.39	11.20%
	Hemlock	10481	11181	700	33.50	31.70	0.00%
	W. Foreland	11181	12381	1200	56.00	35.70	8.30%
		(ft)	(ft)	(ft)	(Ma)	(Ma)	

* Subhorizon estimated from *PetroMod*®

Susan Dionne #4

	Layer	Top	Base	Thick.	Depo. From	Depo. To	NtG Coal
	Sterling	0	1271	1271	8.00	0.00	11.80%
*	Beluga 1-7	1271	3297	2026	13.69	8.00	5.52%
*	B8	3297	3587	290	14.50	13.69	5.52%
	T1 Tyonek	3587	3750	163	14.92	14.50	2.45%
	T2	3750	4000	250	15.58	14.92	6.00%
	T3	4000	4250	250	16.23	15.58	6.80%
	T4	4250	4500	250	16.88	16.23	10.00%
	T5	4500	4750	250	17.53	16.88	6.40%
	T6	4750	5000	250	18.18	17.53	10.80%
	T7	5000	5250	250	18.83	18.18	13.20%
	T8	5250	5500	250	19.49	18.83	10.80%
	T9	5500	5750	250	20.14	19.49	13.60%
	T10	5750	6000	250	20.79	20.14	12.00%
	T11	6000	6250	250	21.44	20.79	17.60%
	T12	6250	6500	250	22.09	21.44	12.00%
	T13	6500	6750	250	22.74	22.09	10.00%
	T14	6750	7000	250	23.39	22.74	8.80%
	T15	7000	7250	250	24.05	23.39	6.00%
	T16	7250	7500	250	24.70	24.05	10.00%
	T17	7500	7750	250	25.35	24.70	11.60%
	T18	7750	8000	250	26.00	25.35	10.00%
	T19	8000	8322	322	26.84	26.00	13.04%
	T20	8322	10187	1865	31.70	26.84	10.20%
	Hemlock	10187	10887	700	33.50	31.70	0.00%
	W. Foreland	10887	12087	1200	56.00	35.70	8.30%
		(ft)	(ft)	(ft)	(Ma)	(Ma)	

* Subhorizon estimated from *PetroMod*®

Paxton #2

	Layer	Top	Base	Thick.	Depo. From	Depo. To	NtG Coal
	Sterling	0	1352	1352	8.00	0.00	11.10%
*	Beluga 1-6	1352	3285	1933	13.57	8.00	5.59%
*	B7	3285	3607	322	14.50	13.57	5.59%
	T1 Tyonek	3607	4000	393	15.52	14.50	7.12%
	T2	4000	4250	250	16.18	15.52	10.40%
	T3	4250	4500	250	16.83	16.18	4.40%
	T4	4500	4750	250	17.48	16.83	10.80%
	T5	4750	5000	250	18.13	17.48	11.20%
	T6	5000	5250	250	18.78	18.13	10.00%
	T7	5250	5500	250	19.43	18.78	14.80%
	T8	5500	5750	250	20.08	19.43	9.20%
	T9	5750	6000	250	20.74	20.08	16.40%
	T10	6000	6250	250	21.39	20.74	12.80%
	T11	6250	6500	250	22.04	21.39	9.60%
	T12	6500	6750	250	22.69	22.04	11.20%
	T13	6750	7000	250	23.34	22.69	9.20%
	T14	7000	7250	250	23.99	23.34	10.80%
	T15	7250	7566	316	24.82	23.99	11.08%
*	T16_1	7566	7860	293.5	25.59	24.82	10.56%
*	T16_2	7860	8153	293.5	26.35	25.59	10.56%
*	T16_3-9	8153	10207	2054	31.70	26.35	10.56%
	Hemlock	10207	10907	700	33.50	31.70	0.00%
	W. Foreland	10907	12107	1200	56.00	35.70	8.30%
		(ft)	(ft)	(ft)	(Ma)	(Ma)	

* Subhorizon estimated from *PetroMod*®

Appendix D: Time (Ma) Each Layer Spent within the 5 °C Temperature Intervals

Falls Creek #1RD

	Layer	10-15 °C	15-20 °C	20-25 °C	25-30 °C	30-35 °C	35-40 °C	40-45 °C	45-50 °C
*	B4 Beluga	1.8	2.4	3.1	2.1	0	0	0	0
*	B5	1.7	2.1	3.1	3.1	0.2	0	0	0
*	B6	1.7	1.5	3.1	3.2	1.4	0	0	0
*	B7	1.7	1.7	2.4	3.2	2.6	0	0	0
*	B8	1.7	1.7	1.9	3.2	3.3	0.5	0	0
*	B9	1.6	1.6	1.6	3.2	3.3	1.7	0	0
	T1 Tyonek	1.8	1.7	1.8	2.7	3.4	2.7	0	0
	T2	1.7	1.9	1.9	2.1	3.4	3.4	0.4	0
	T3	1.6	1.9	1.9	2.1	3.2	3.5	1.3	0
	T4	1.6	1.9	1.9	2.1	2.8	3.4	2.5	0
	T5	1.5	1.8	2	2.1	2.4	3.3	3.7	0
	T6	1.5	1.8	2	2.1	2.2	3.1	3.7	1.2
	T7	1.4	1.7	2	2.1	2.2	2.8	3.7	2.3
	T8	1.4	1.7	2	2.1	2.2	2.4	3.6	3.4
	T9	1.4	1.7	1.9	2.1	2.2	2.2	3.4	3.5
	T10	1.4	1.6	1.9	2.1	2.2	2.2	3	3.5
	T11	1.4	1.6	1.8	2.1	2.2	2.2	2.5	3.5
	T12	1.3	1.6	1.8	2	2.2	2.2	2.2	3.4
		(Ma)	(Ma)	(Ma)	(Ma)	(Ma)	(Ma)	(Ma)	(Ma)

* Subhorizon estimated from *PetroMod*®

Corea Creek #1

	Layer	10-15 °C	15-20 °C	20-25 °C	25-30 °C	30-35 °C	35-40 °C	40-45 °C	45-50 °C
*	B4 Beluga	1.7	2.4	3.1	2.3	0	0	0	0
*	B5	1.6	1.8	3.2	3.2	0.4	0	0	0
*	B6	1.6	1.8	2.5	3.3	1.7	0	0	0
*	B7	1.6	1.6	2	3.4	3	0	0	0
*	B8	1.4	1.5	1.5	3.3	3.4	1	0	0
*	B9	1.6	1.6	1.6	2.4	3.4	2.4	0	0
	T1 Tyonek	1.6	1.8	1.7	2.1	3.4	3.7	0	0
	T2	1.5	1.8	1.7	1.8	3.3	3.5	1.4	0
	T3	1.5	1.8	1.8	1.8	2.8	3.5	2.5	0
	T4	1.5	1.8	1.9	1.8	2.3	3.5	3.6	0
	T5	1.5	1.8	1.9	1.8	2	3.3	3.7	1.1
	T6	1.5	1.7	1.9	1.9	2	2.8	3.6	2.4
	T7	1.5	1.7	1.9	2	2	2.3	3.6	3.5
	T8	1.5	1.6	1.9	2	2	2	3.6	3.6
	T9	1.5	1.6	1.9	2	2	2	2.9	3.7
	T10	1.4	1.6	1.9	2	2	2	2.4	3.7
	T11	1.4	1.6	1.9	2	2	2	2.2	3.4
		(Ma)	(Ma)	(Ma)	(Ma)	(Ma)	(Ma)	(Ma)	(Ma)

* Subhorizon estimated from *PetroMod*®

Grassim Oskolkoff #4

	Layer	10-15 °C	15-20 °C	20-25 °C	25-30 °C	30-35 °C	35-40 °C	40-45 °C	45-50 °C
*	B7 Beluga	1.9	2	4	4.2	0	0	0	0
*	B8	2	1.9	2.6	5.8	0.6	0	0	0
	T1 Tyonek	2	2	2	5.7	2.4	0	0	0
	T2	1.7	2.1	2.2	3.6	5.7	0	0	0
	T3	1.5	2.1	2.3	2.3	5.9	1.9	0	0
*	T4_1	1.5	2.1	2.2	2.3	4.7	4.1	0	0
*	T4_2	1.5	1.8	2.3	2.3	3.1	6	0.7	0
*	T4_3	1.7	1.7	2	2.4	2.3	5.6	2.9	0
*	T4_4	1.9	1.9	1.9	2.4	2.4	3.9	5.6	0
*	T4_5	1.8	1.8	1.8	2.2	2.5	2.5	6.1	1.9
*	T4_6	1.8	1.8	1.8	2.2	2.4	2.5	4.5	4.6
*	T4_7	2	2.1	1.9	1.9	2.4	2.5	3.1	6.3
*	T4_8	2	1.9	1.9	1.9	2.2	2.5	2.6	5.4
*	T4_9	2	2	2	2	2.1	2.4	2.6	3.9
*	T4_10	2	2	2	2	2	2.4	2.5	2.6
		(Ma)	(Ma)	(Ma)	(Ma)	(Ma)	(Ma)	(Ma)	(Ma)

* Subhorizon estimated from *PetroMod*®

Ninilchik State #1

	Layer	10-15 °C	15-20 °C	20-25 °C	25-30 °C	30-35 °C	35-40 °C	40-45 °C	45-50 °C
*	B7 Beluga	1.9	2	4	4.2	0	0	0	0
*	B8	1.9	2	2.5	5.7	0.7	0	0	0
	T1 Tyonek	2	2	2	5.7	2.4	0	0	0
	T2	1.8	2.1	2.2	3.7	5.5	0	0	0
	T3	1.7	2.1	2.3	2.4	6.1	1.5	0	0
	T4	1.6	2.1	2.3	2.4	5	3.4	0	0
	T5	1.6	1.8	2.3	2.4	3.8	5.5	0	0
	T6	1.5	1.8	2.3	2.4	2.5	6	1.6	0
	T7	1.4	1.7	2.2	2.3	2.5	5.1	3.5	0
	T8	1.4	1.7	2	2.3	2.5	4	5.5	0
	T9	1.3	1.7	1.9	2.3	2.5	2.7	6.2	1.4
	T10	1.3	1.7	1.9	2.1	2.5	2.5	5.1	3.6
	T11	1.2	1.7	1.9	2	2.4	2.5	4.1	5.5
	T12	1.2	1.7	1.8	2	2.4	2.5	2.7	6.4
	T13	1.1	1.7	1.8	2	2.2	2.5	2.6	5.2
	T14	1.1	1.6	1.8	1.9	2.2	2.4	2.6	4
	T15	1	1.6	1.8	1.9	2.1	2.4	2.6	2.7
	T16	1	1.6	1.8	1.9	2	2.2	2.6	2.6
		(Ma)	(Ma)	(Ma)	(Ma)	(Ma)	(Ma)	(Ma)	(Ma)

* Subhorizon estimated from *PetroMod*®

Susan Dionne #4

	Layer	10-15 °C	15-20 °C	20-25 °C	25-30 °C	30-35 °C	35-40 °C	40-45 °C	45-50 °C
*	B8 Beluga	2.1	2.1	3.5	5.3	0	0	0	0
	T1 Tyonek	2.1	2.1	2.5	6.8	0.5	0	0	0
	T2	2	2.1	2.2	6.1	2.3	0	0	0
	T3	1.7	2.3	2.3	4.5	4.6	0	0	0
	T4	1.5	2.3	2.4	3.1	6.8	0	0	0
	T5	1.5	2.1	2.5	2.5	6.2	2	0	0
	T6	1.5	2	2.4	2.5	4.8	4.3	0	0
	T7	1.5	1.8	2.3	2.5	3.3	6.8	0	0
	T8	1.4	1.8	2.2	2.5	2.6	6.3	2	0
	T9	1.4	1.7	2	2.5	2.6	4.9	4.4	0
	T10	1.3	1.7	2	2.4	2.6	3.3	6.8	0
	T11	1.3	1.7	1.9	2.2	2.6	2.6	6.4	2.1
	T12	1.2	1.7	1.8	2.1	2.6	2.6	4.7	4.7
	T13	1.2	1.7	1.8	2	2.5	2.6	3.2	7.1
	T14	1.1	1.7	1.8	1.9	2.4	2.6	2.7	6.6
	T15	1.1	1.7	1.8	1.9	2.3	2.6	2.7	5.1
	T16	1.1	1.7	1.8	1.9	2.2	2.5	2.7	3.6
	T17	1.1	1.6	1.8	1.9	2.1	2.3	2.7	2.8
	T18	1.1	1.6	1.8	1.9	2	2.3	2.6	2.8
		(Ma)	(Ma)	(Ma)	(Ma)	(Ma)	(Ma)	(Ma)	(Ma)

* Subhorizon estimated from *PetroMod*®

Paxton #2

	Layer	10-15 °C	15-20 °C	20-25 °C	25-30 °C	30-35 °C	35-40 °C	40-45 °C	45-50 °C
*	B7 Beluga	2.1	1.8	3.8	4.8	0	0	0	0
	T1 Tyonek	2.1	2.1	2.8	6.2	0.8	0	0	0
	T2	1.8	2.3	2.4	4.6	4.3	0	0	0
	T3	1.6	2.4	2.4	3.3	6.4	0	0	0
	T4	1.5	2.1	2.4	2.5	6.3	1.9	0	0
	T5	1.5	1.9	2.4	2.5	5	4.1	0	0
	T6	1.5	1.8	2.4	2.5	3.6	6.3	0	0
	T7	1.4	1.8	2.2	2.5	2.8	6.3	1.8	0
	T8	1.4	1.7	2	2.5	2.7	5	4.1	0
	T9	1.4	1.7	1.9	2.4	2.7	3.6	6.4	0
	T10	1.2	1.7	1.9	2.2	2.7	2.7	6.4	1.9
	T11	1.2	1.7	1.9	2	2.7	2.7	4.8	4.4
	T12	1.2	1.7	1.8	2	2.5	2.7	3.6	6.5
	T13	1.2	1.7	1.8	2	2.3	2.7	2.8	6.5
	T14	1.1	1.7	1.8	1.9	2.2	2.7	2.7	5.2
	T15	1	1.7	1.8	1.9	2.1	2.5	2.7	3.7
*	T16_1	1	1.6	1.8	1.9	2.1	2.3	2.7	2.9
*	T16_2	1	1.6	1.8	1.9	2	2.2	2.6	2.9
		(Ma)	(Ma)	(Ma)	(Ma)	(Ma)	(Ma)	(Ma)	(Ma)

* Subhorizon estimated from *PetroMod*®

Appendix E: Output of Methanogenesis Calculations

Explanation of Appendix E abbreviations and labels:

FC1RD = Falls Creek #1RD modeled well

CCF1 = Corea Creek #1 modeled well

GO4 = Grassim Oskolkoff #4 modeled well

NS1 = Ninilchik State #1 modeled well

SD4 = Susan Dionne #4 modeled well

PAX2 = Paxton #2 modeled well

Zone 1, 2, & 3 = Fault block in which modeled well is located

Layers = ~250 ft layers of Tyonek (T) and Beluga (B) formations; orientation represents relative depths along wellbore

Net Coal (ft) = Thickness of coal measured within the layer

Graph of 'Time (Ma)' = Duration each layer spent within MBGW (25-40 °C)

Gas (mmcf) = Total gas generation for each layer in millions of cubic feet; colors designate distributions per 5 °C and 5 Ma

Graph of 'Gas (Bcf) vs Time (Ma)' = Each layers' cumulative gas contribution to the modeled well volume with time

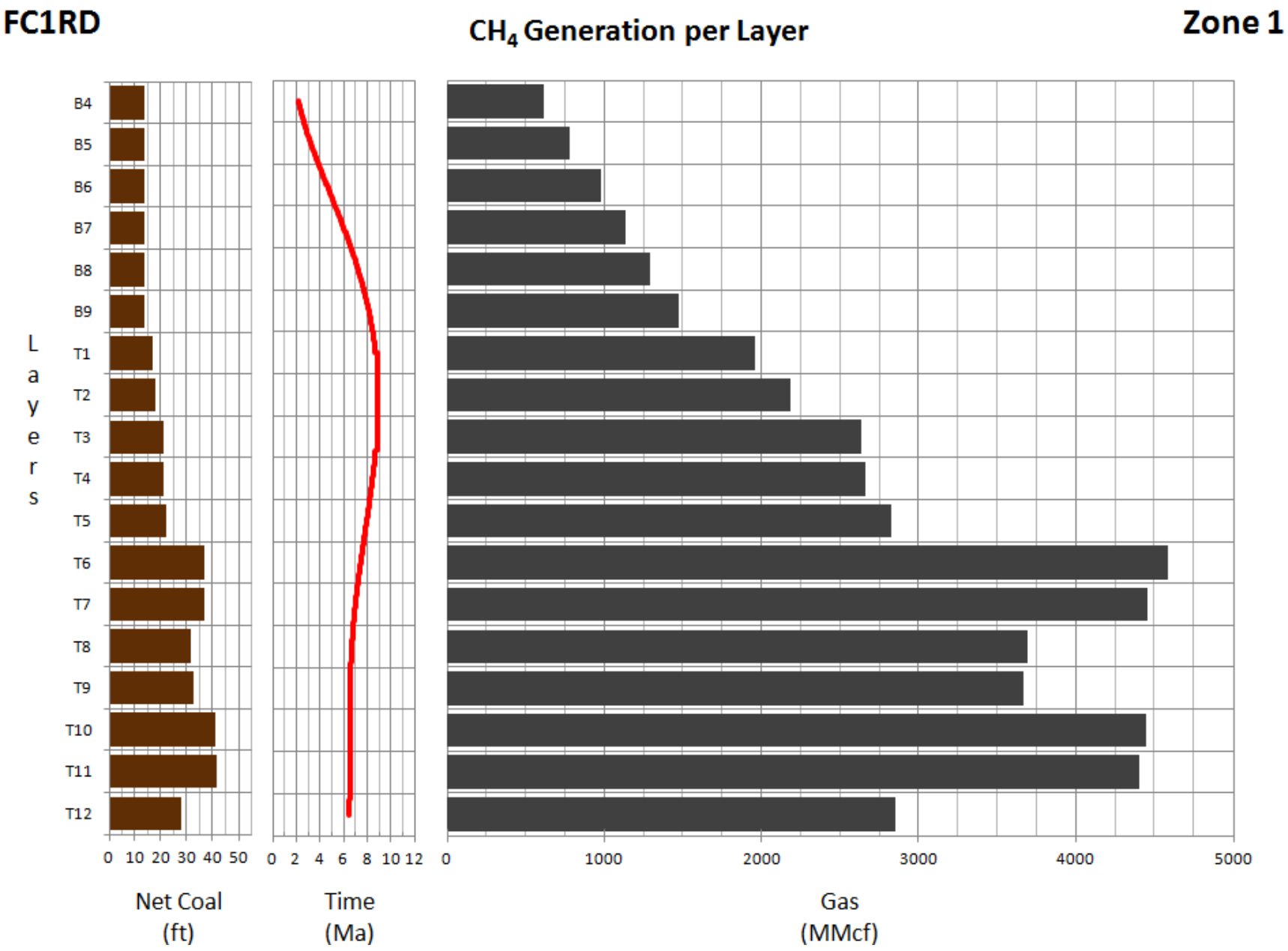
FC1RD
CH4 Generation per Layer
Zone 1
Layers
B4
B5
B6
B7
B8
B9
T1
T2
T3
T4
T5
T6
T7
T8
T9
T10
T11
T12
0 10 20 30 40 50
Net Coal (ft)
0 2 4 6 8 10 12
Time (Ma)
0 1000 2000 3000 4000 5000
Gas (MMcf)

FC1RD **Zone 1**

CH_4 Generation per Layer (5 °C Temp Intervals)

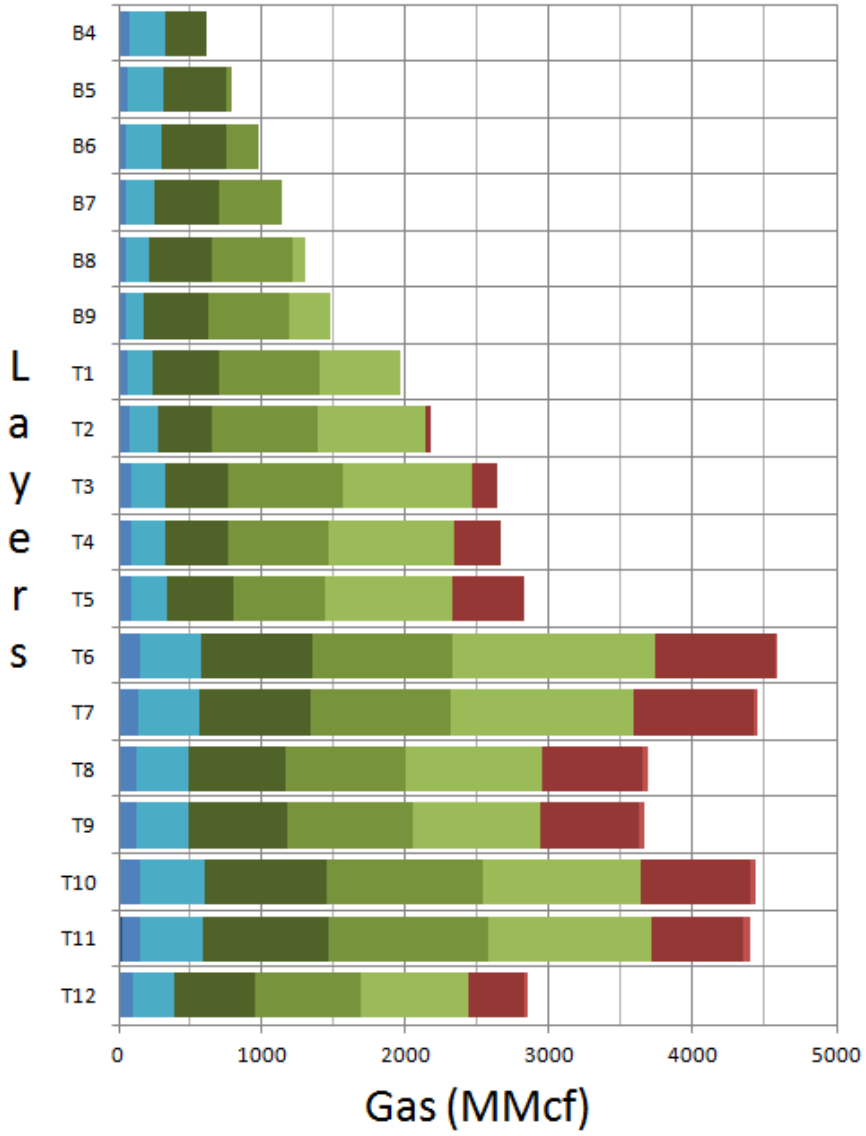

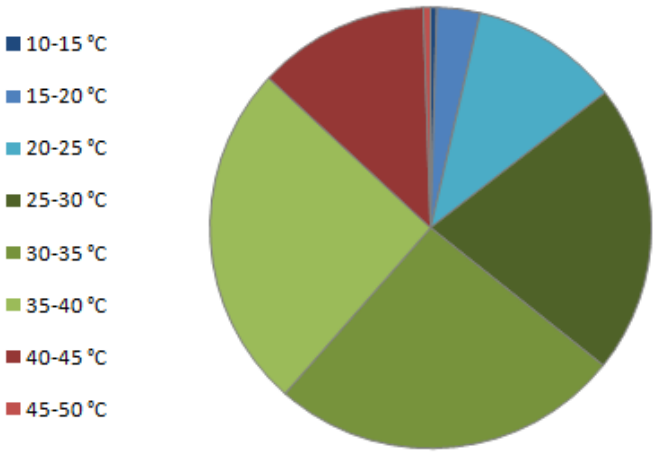

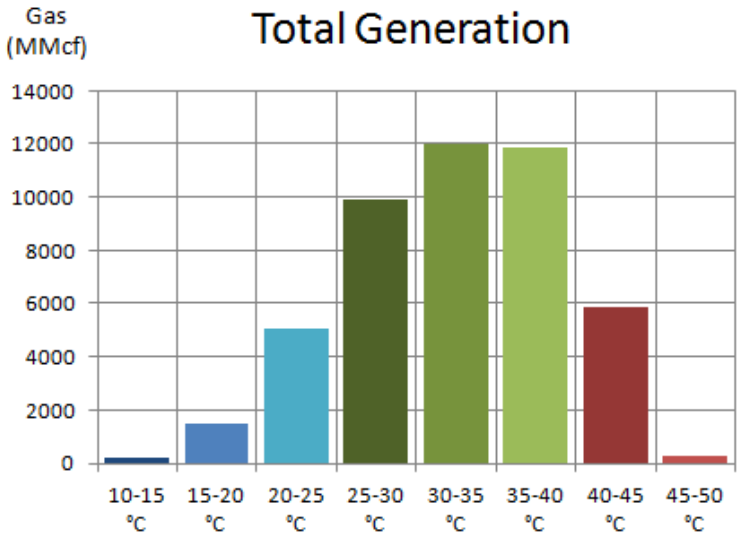

FC1RD **Zone 1**

CH_4 Generation per Layer (5 Ma Time Intervals)

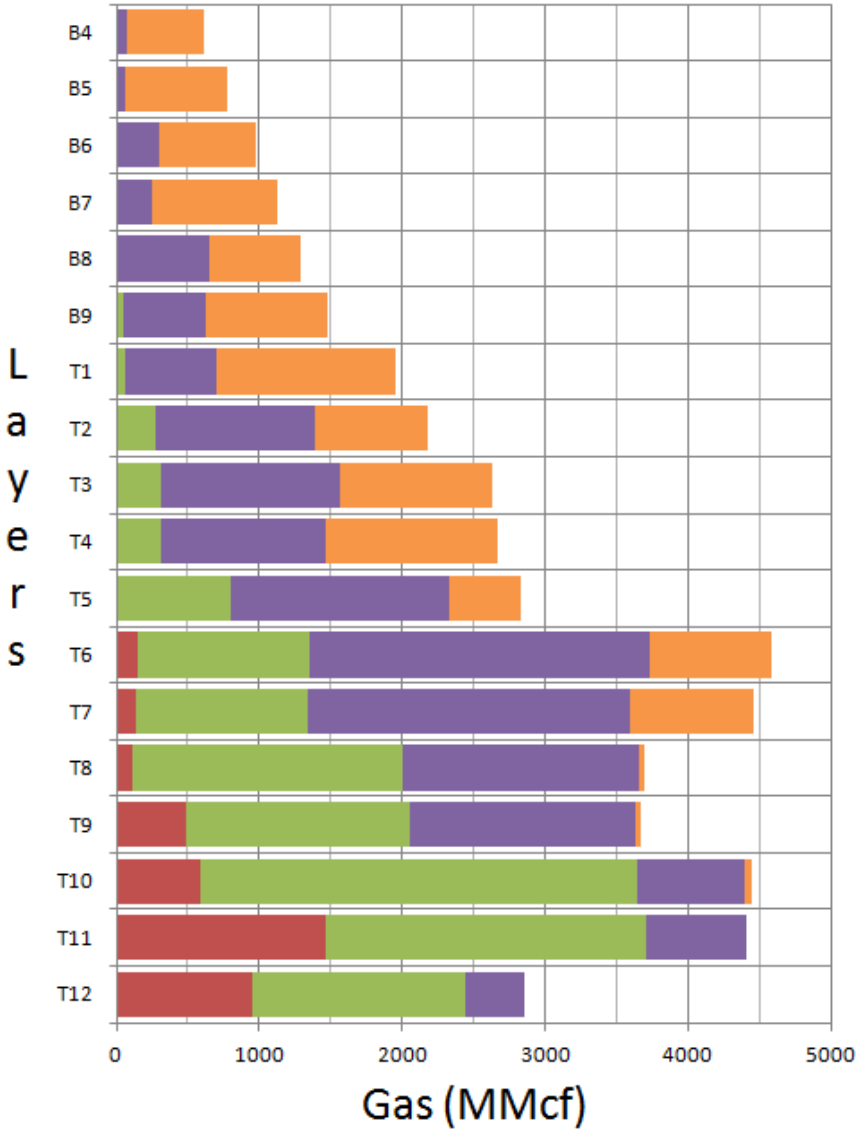

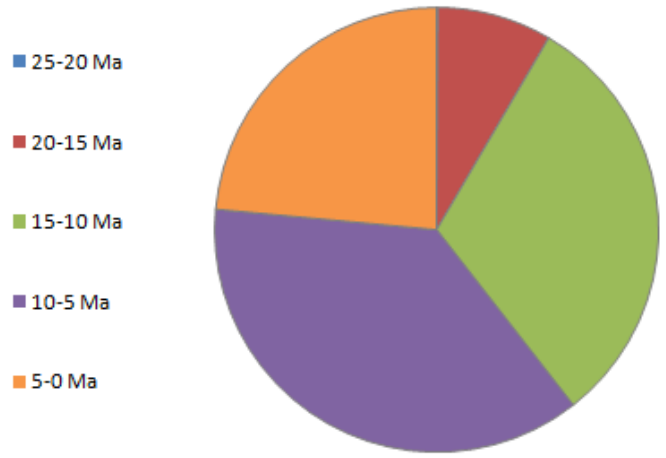

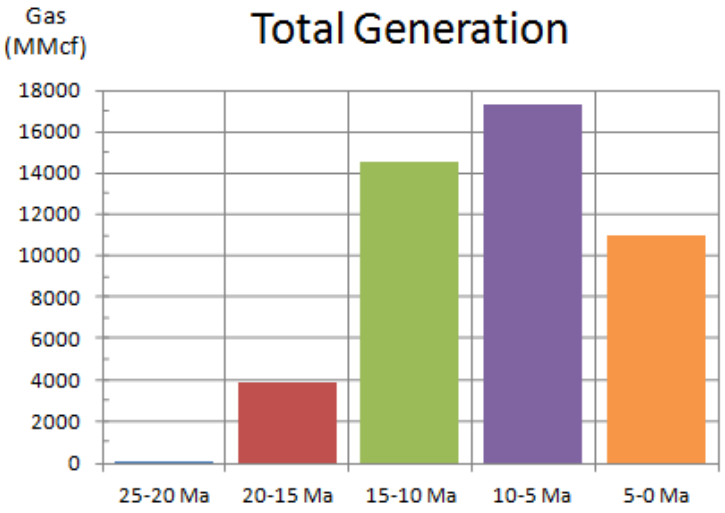

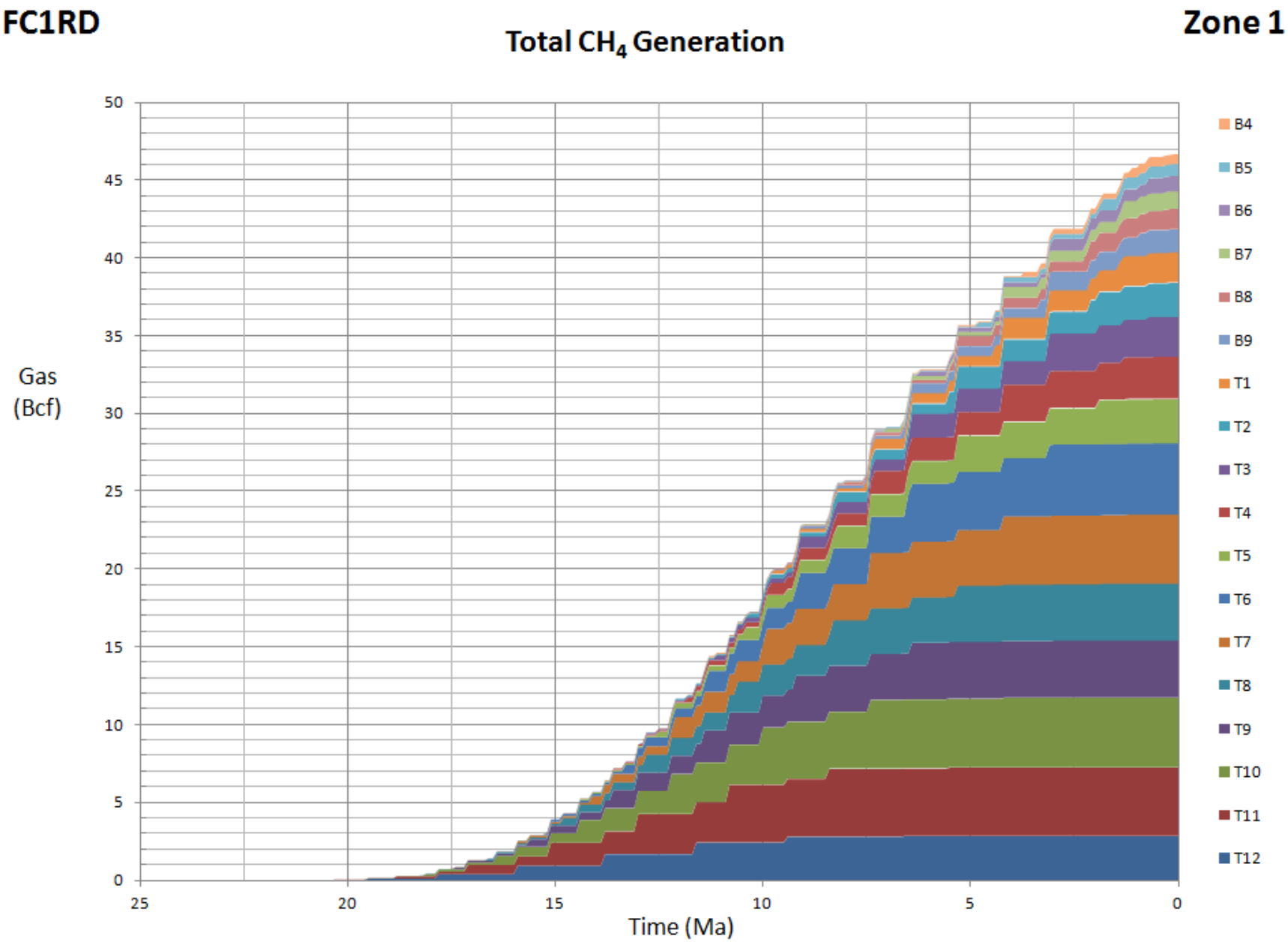
FC1RD
Total CH_4 Generation
Zone 1
Gas (Bcf)
50
45
40
35
30
25
20
15
10
5
0
25
20
15
10
5
0
Time (Ma)
B4
B5
B6
B7
B8
B9
T1
T2
T3
T4
T5
T6
T7
T8
T9
T10
T11
T12

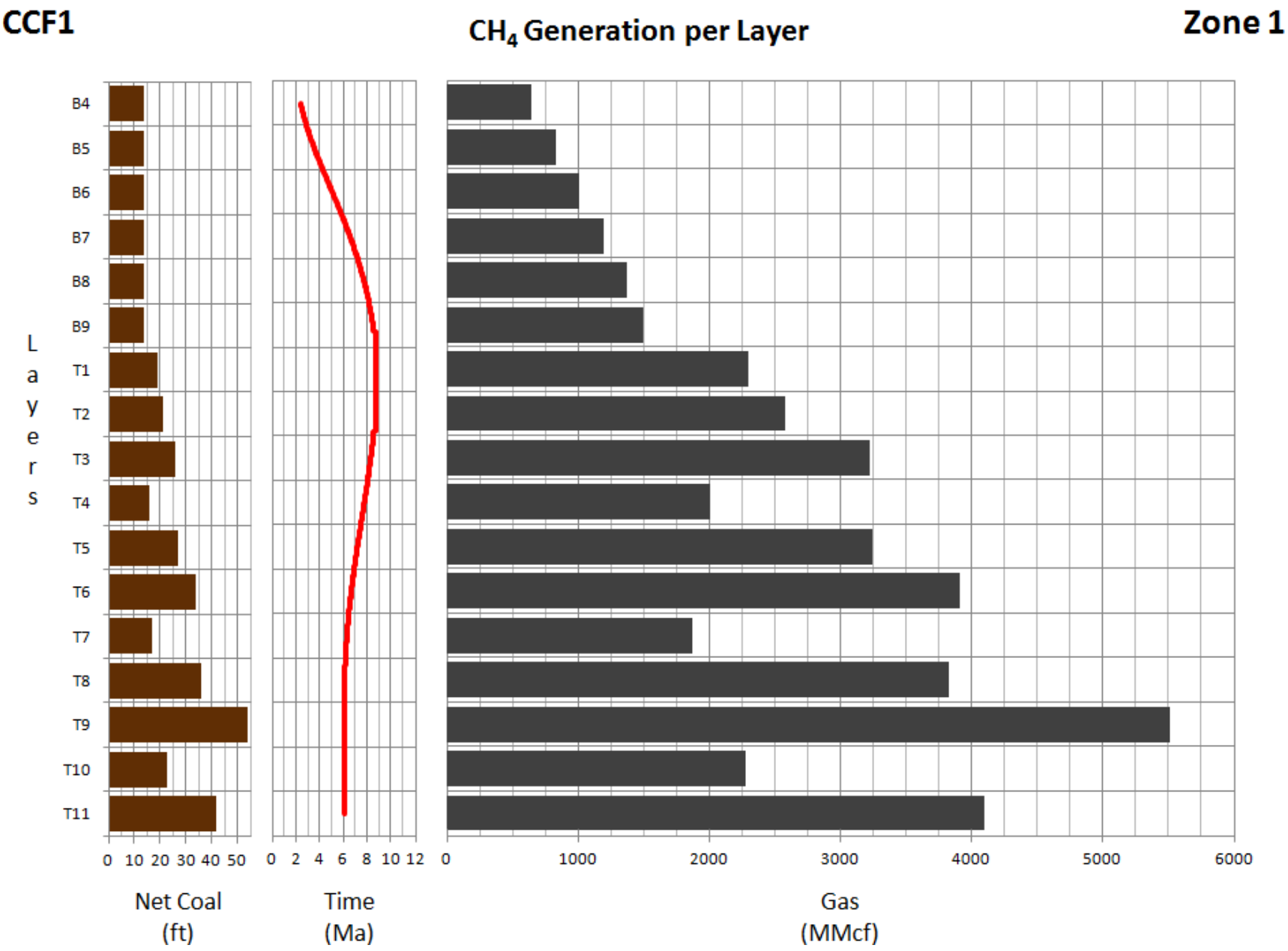
CCF1
CH4 Generation per Layer
Zone 1
Layers
B4
B5
B6
B7
B8
B9
T1
T2
T3
T4
T5
T6
T7
T8
T9
T10
T11
0 10 20 30 40 50
Net Coal (ft)
0 2 4 6 8 10 12
Time (Ma)
0 1000 2000 3000 4000 5000 6000
Gas (MMcf)

CCF1 **Zone 1**

CH_4 Generation per Layer (5 °C Temp Intervals)

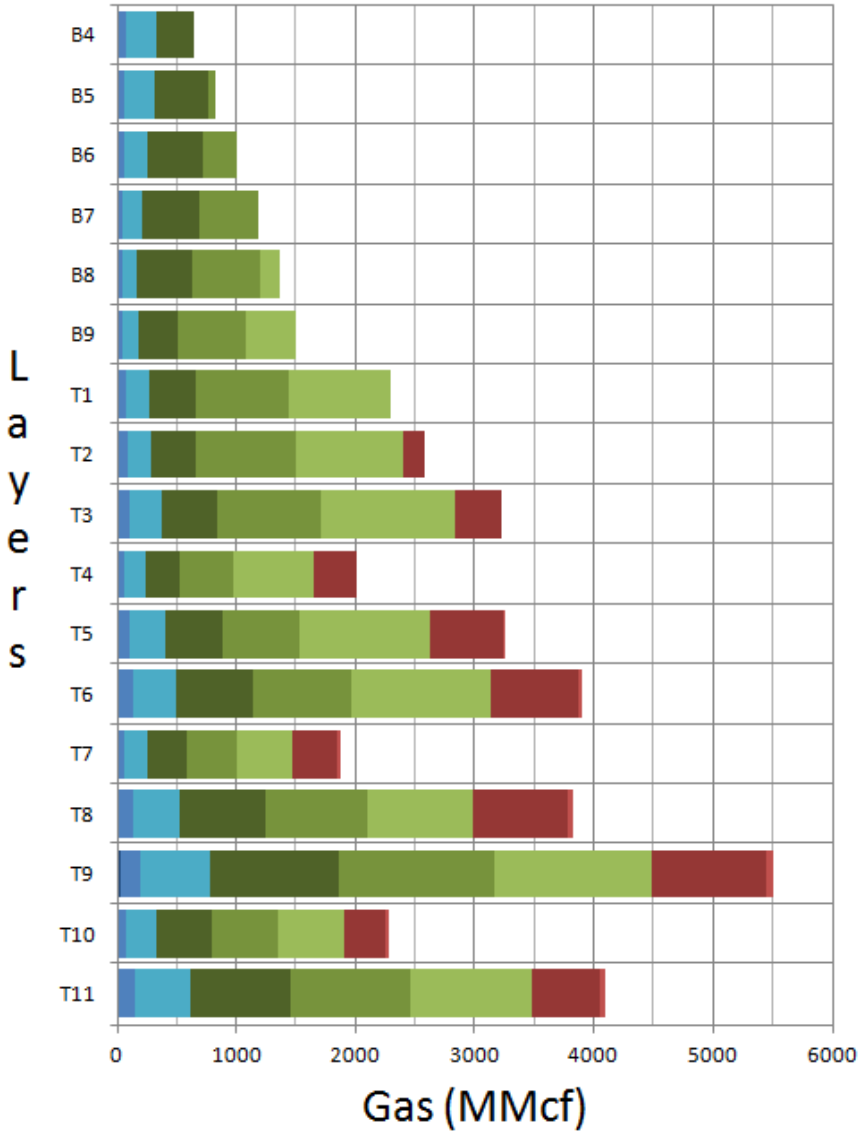

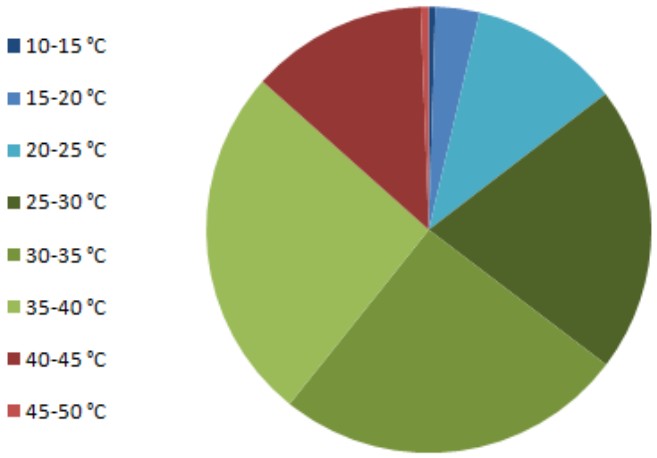

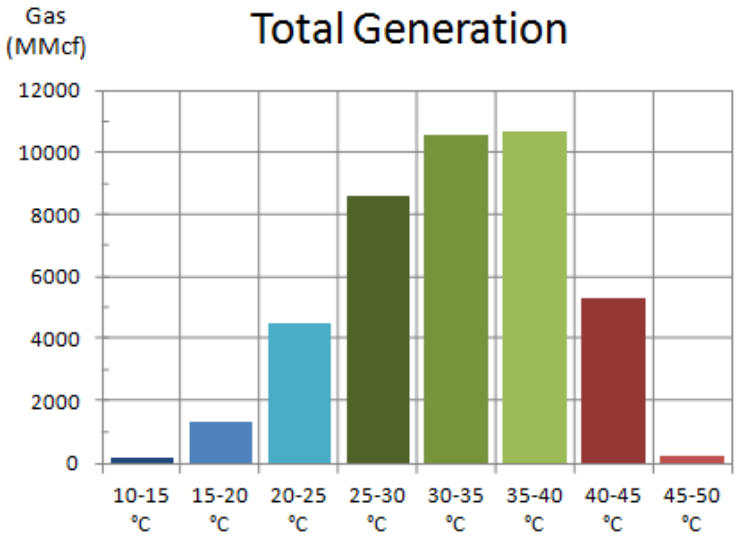

CCF1 **Zone 1**

CH_4 Generation per Layer (5 Ma Time Intervals)

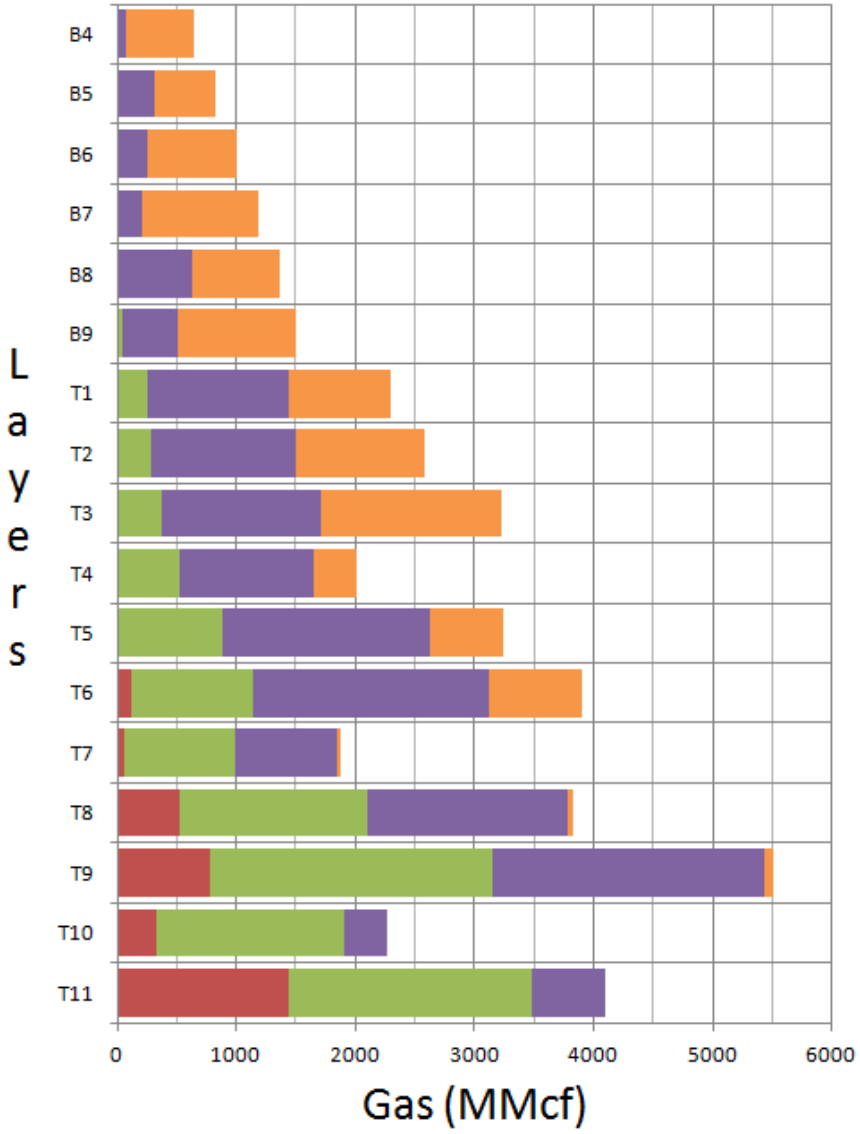

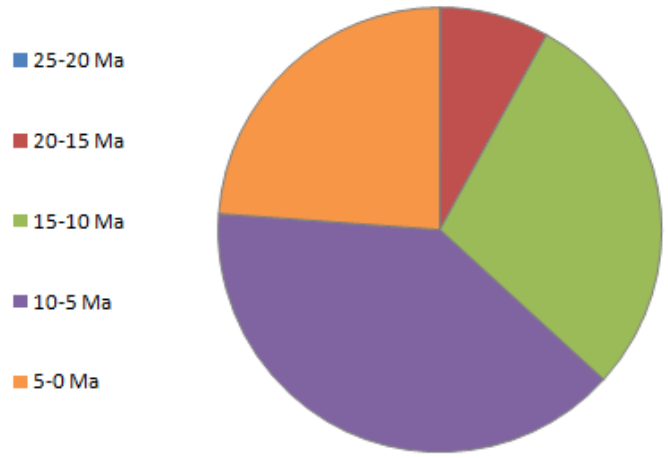

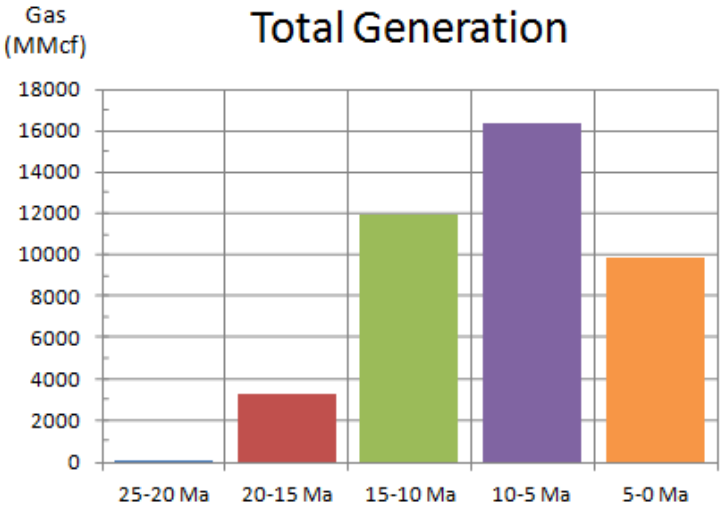

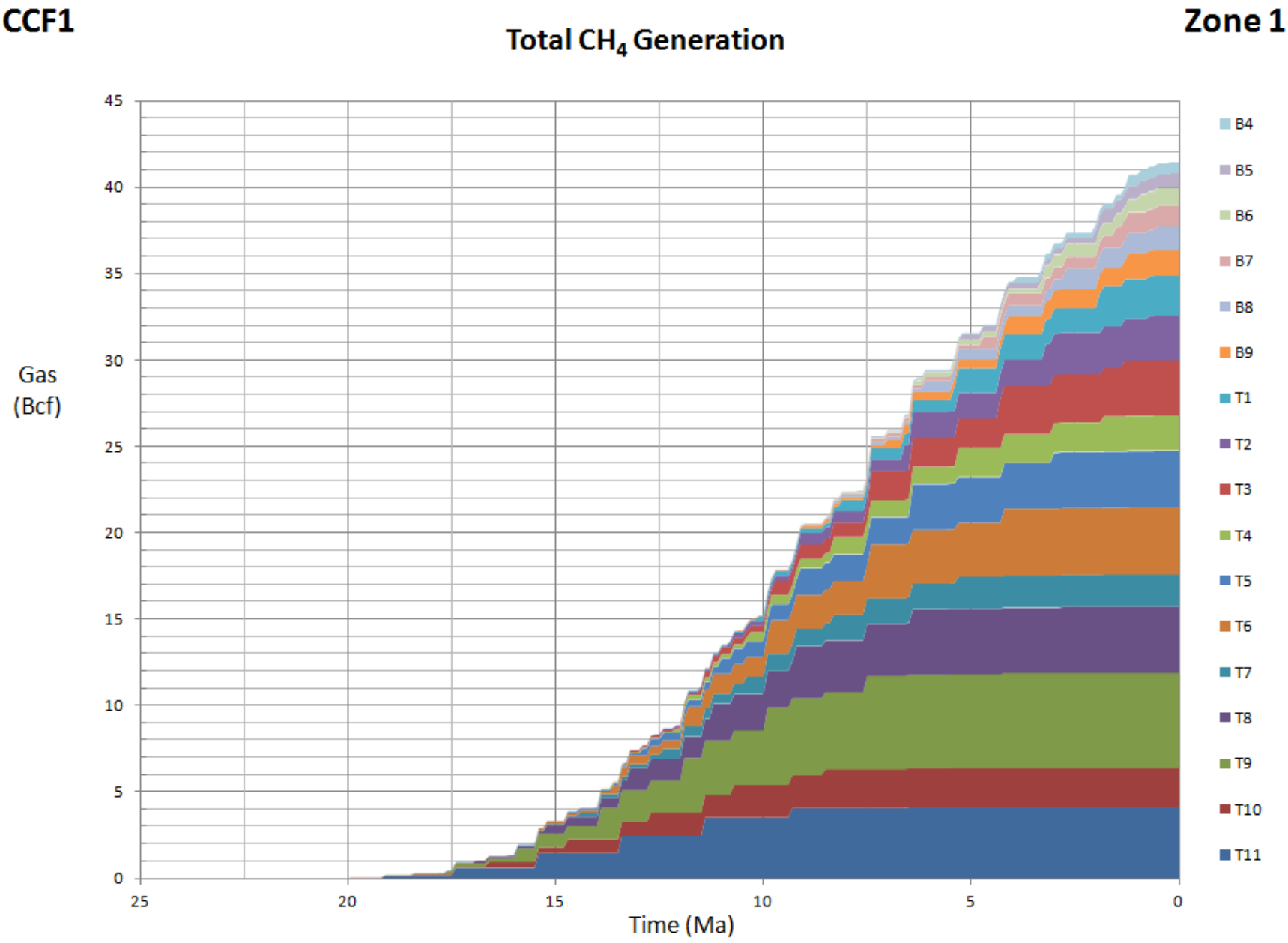
CCF1
Zone 1
Total CH_4 Generation
Gas (Bcf)
45
40
35
30
25
20
15
10
5
0
25
20
15
10
5
0
Time (Ma)
B4
B5
B6
B7
B8
B9
T1
T2
T3
T4
T5
T6
T7
T8
T9
T10
T11

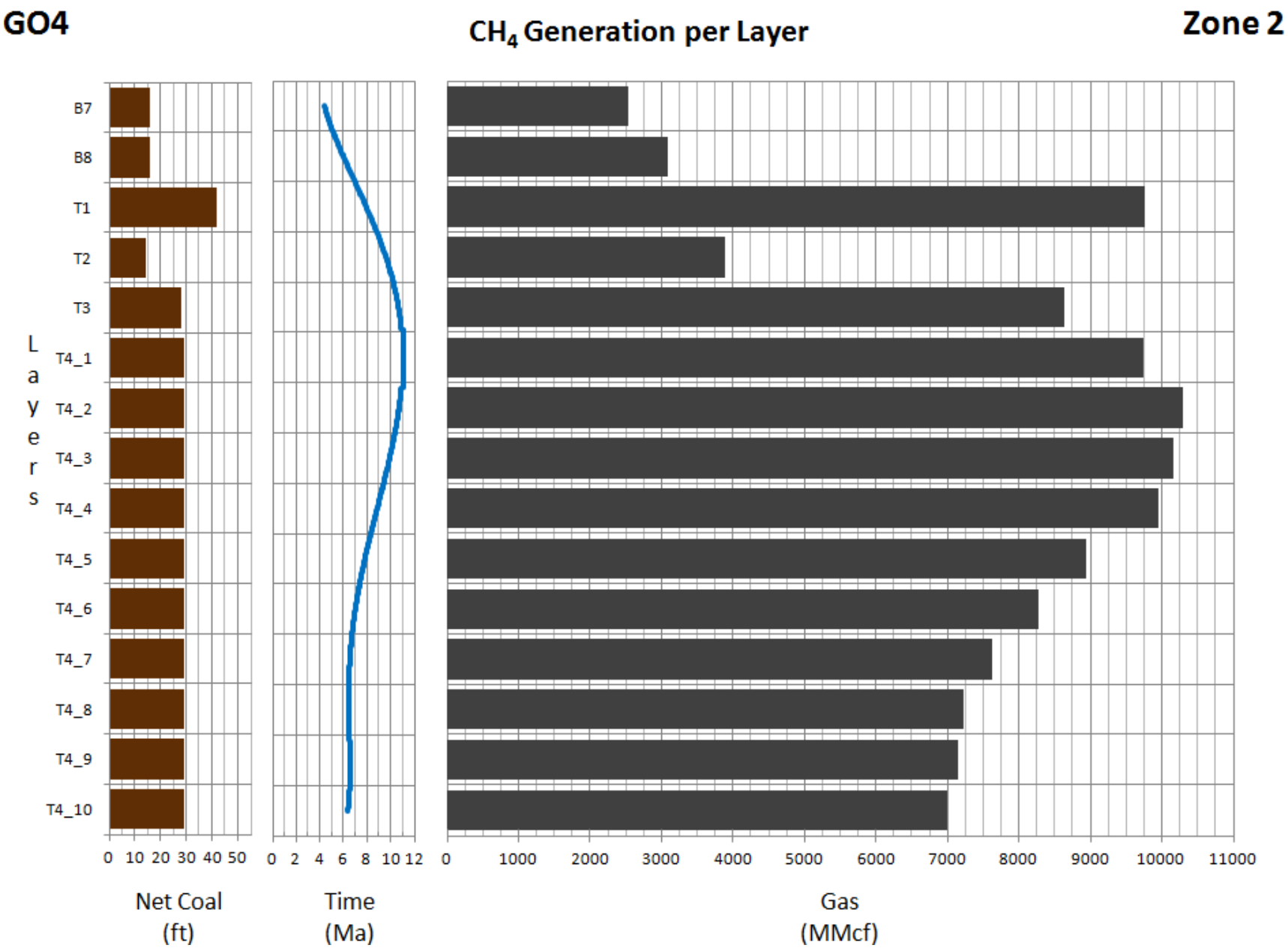
GO4
CH4 Generation per Layer
Zone 2
Layers
B7
B8
T1
T2
T3
T4_1
T4_2
T4_3
T4_4
T4_5
T4_6
T4_7
T4_8
T4_9
T4_10
0 10 20 30 40 50
Net Coal (ft)
0 2 4 6 8 10 12
Time (Ma)
0 1000 2000 3000 4000 5000 6000 7000 8000 9000 10000 11000
Gas (MMcf)

GO4 **Zone 2**

CH_4 Generation per Layer (5 °C Temp Intervals)

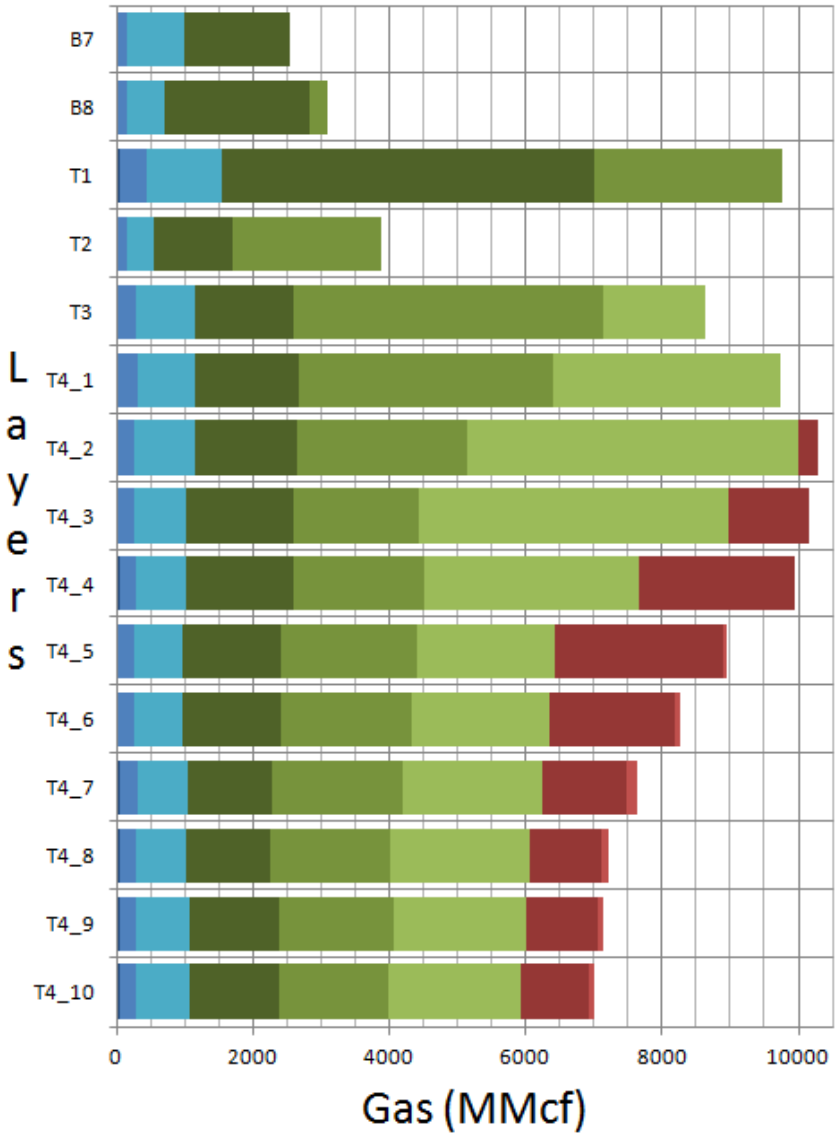

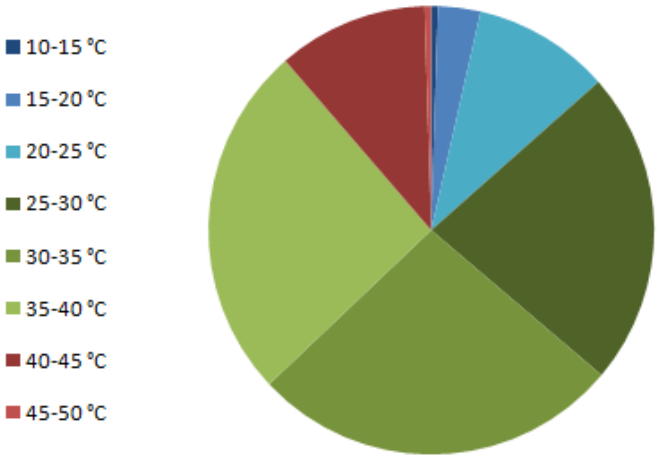

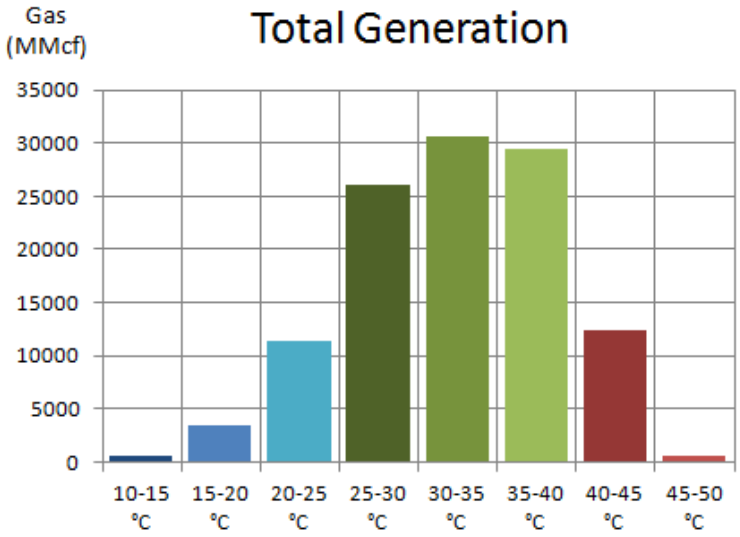

GO4 **Zone 2**

CH_4 Generation per Layer (5 Ma Time Intervals)

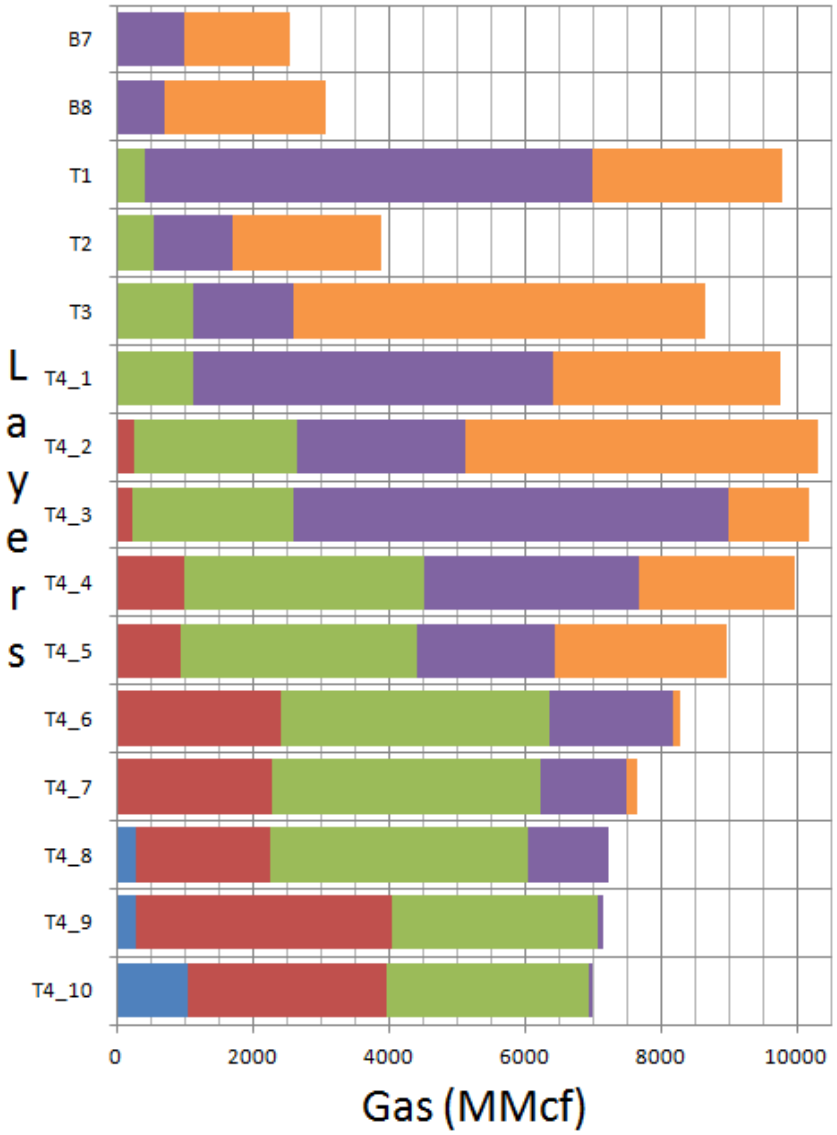

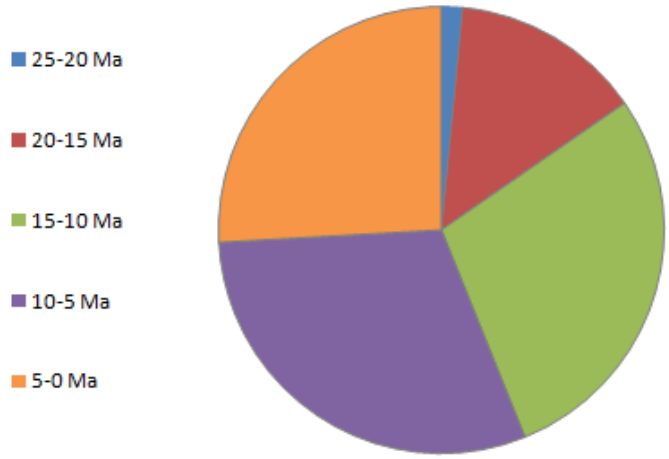

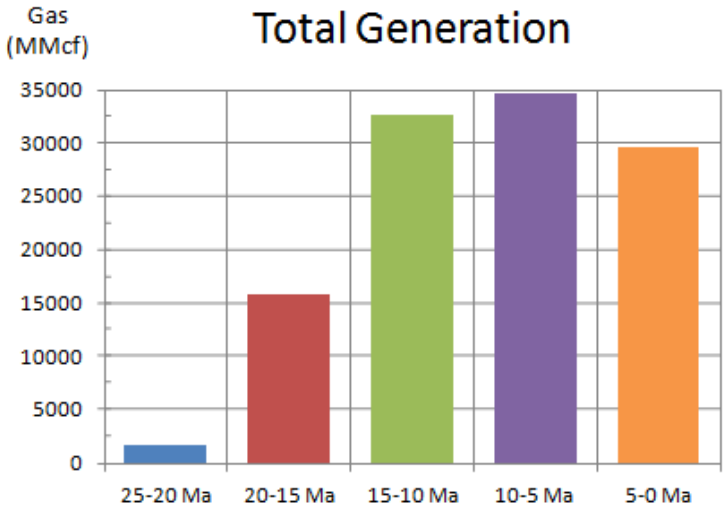

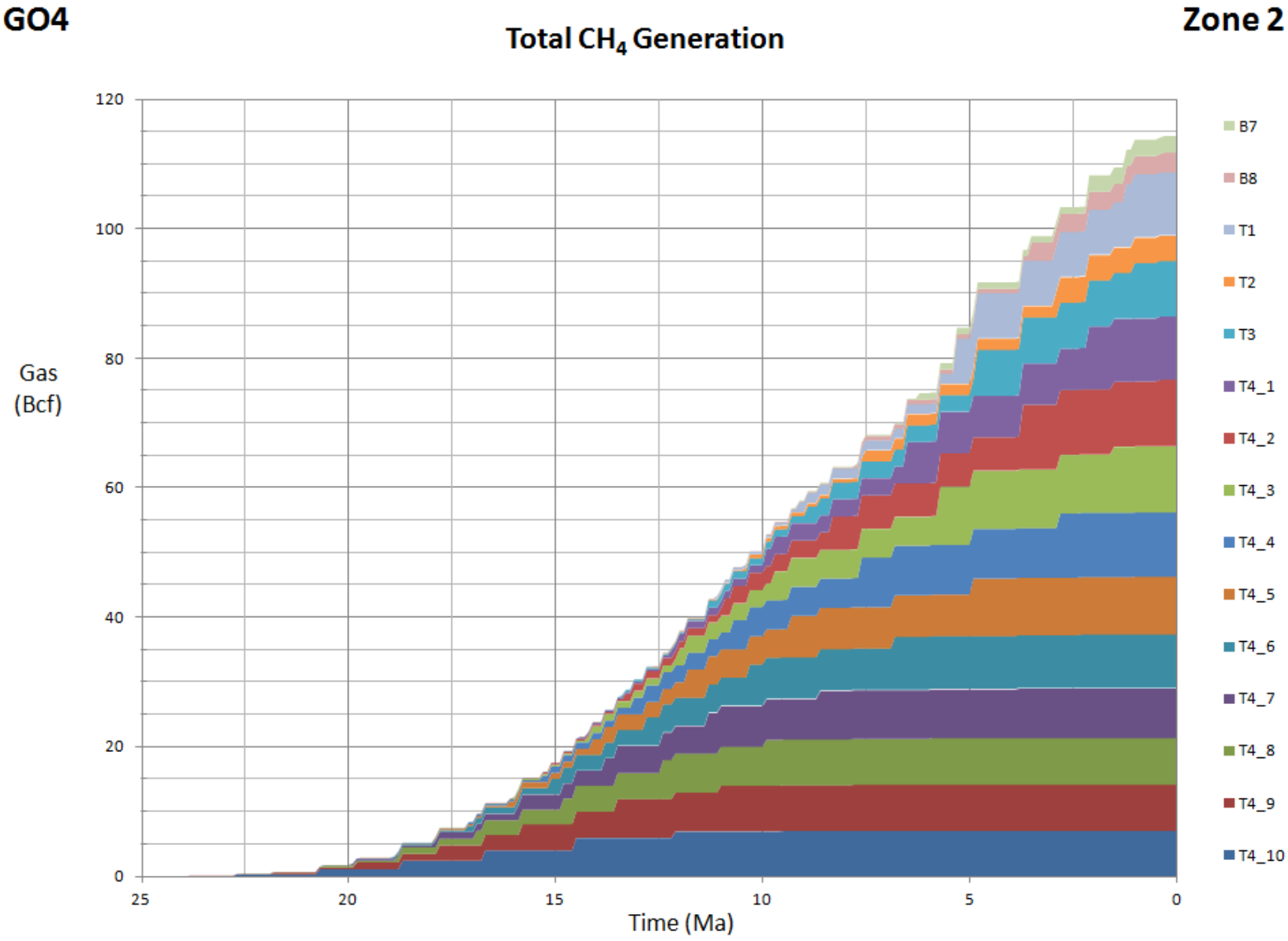
GO4
Zone 2
Total CH_4 Generation
Gas (Bcf)
120
100
80
60
40
20
0
25
20
15
10
5
0
Time (Ma)
B7
B8
T1
T2
T3
T4_1
T4_2
T4_3
T4_4
T4_5
T4_6
T4_7
T4_8
T4_9
T4_10

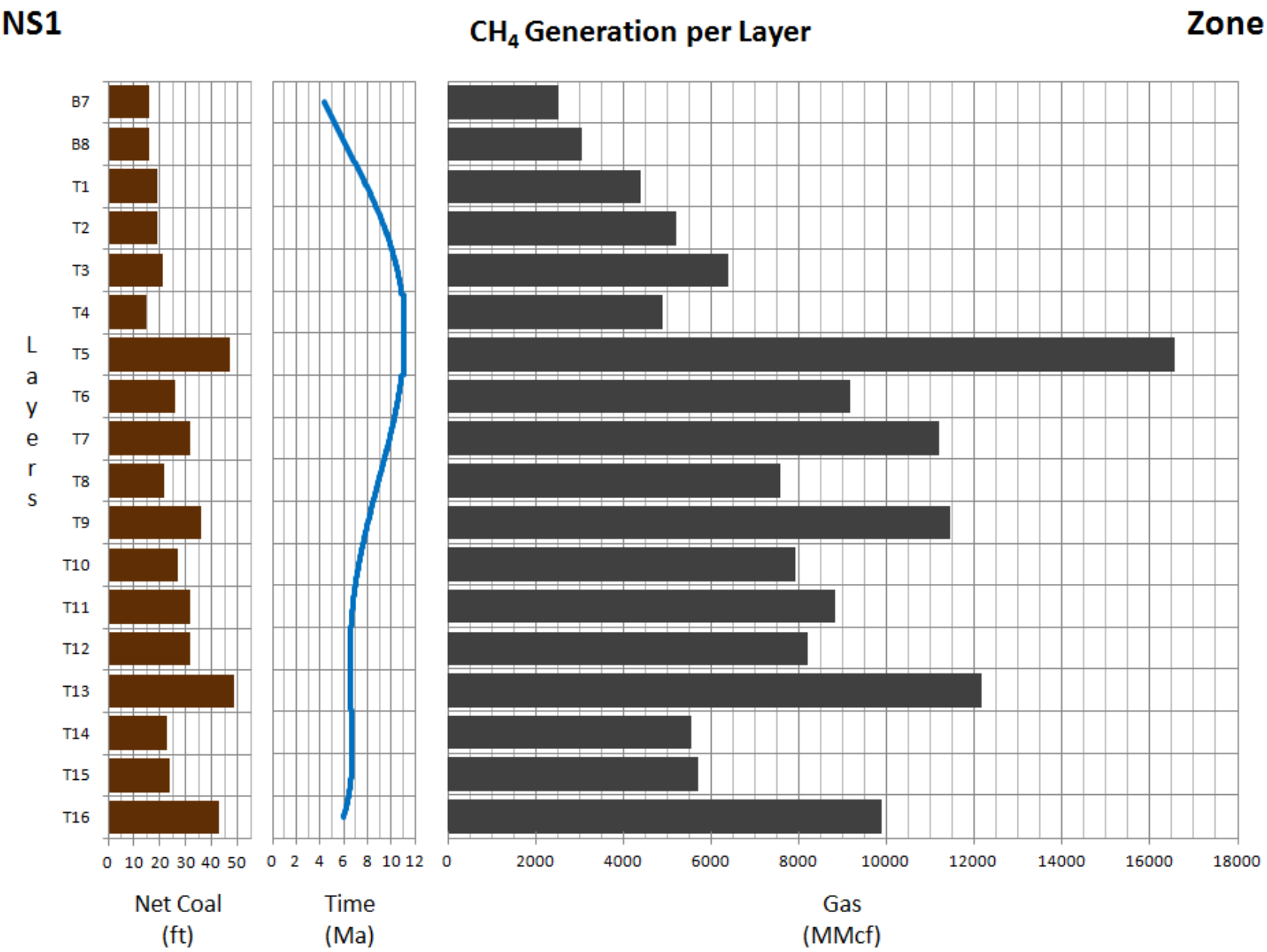
NS1
CH4 Generation per Layer
Zone 2
Layers
B7
B8
T1
T2
T3
T4
T5
T6
T7
T8
T9
T10
T11
T12
T13
T14
T15
T16
0 10 20 30 40 50
Net Coal (ft)
0 2 4 6 8 10 12
Time (Ma)
0 2000 4000 6000 8000 10000 12000 14000 16000 18000
Gas (MMcf)

NS1 **Zone 2**

CH_4 Generation per Layer (5 °C Temp Intervals)

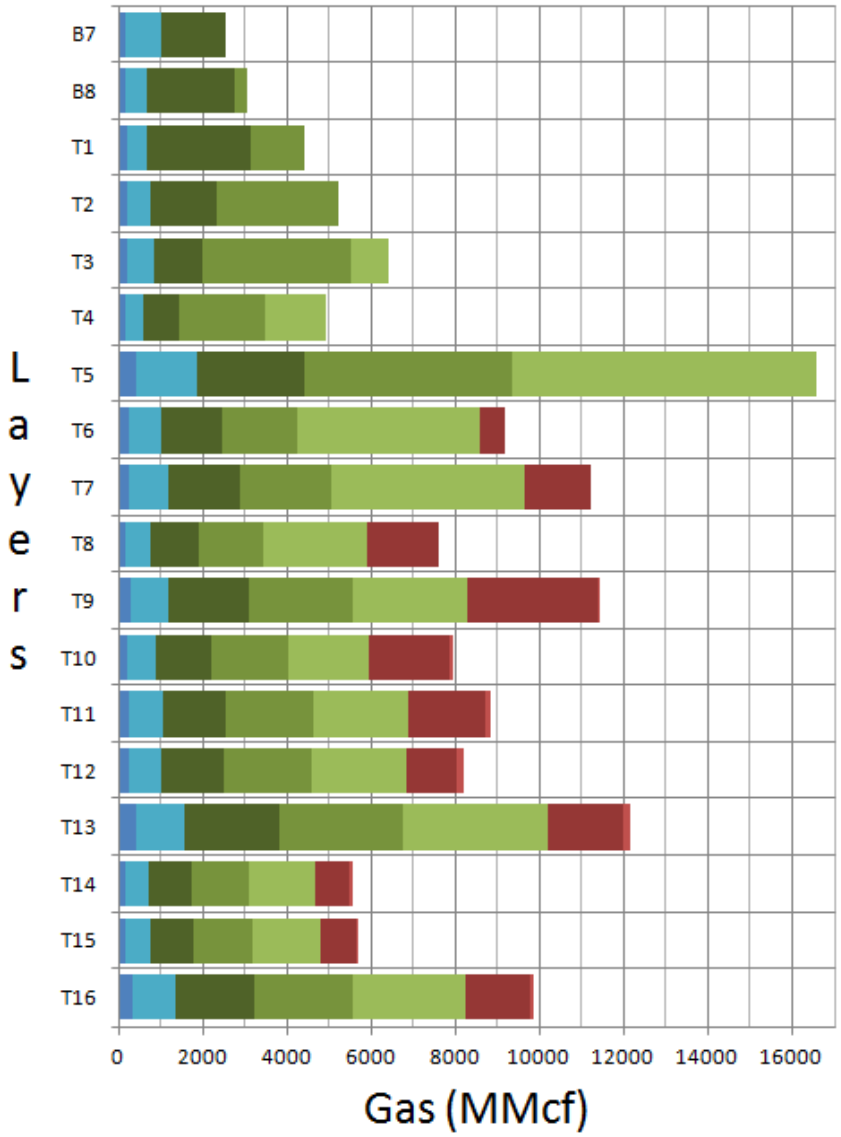

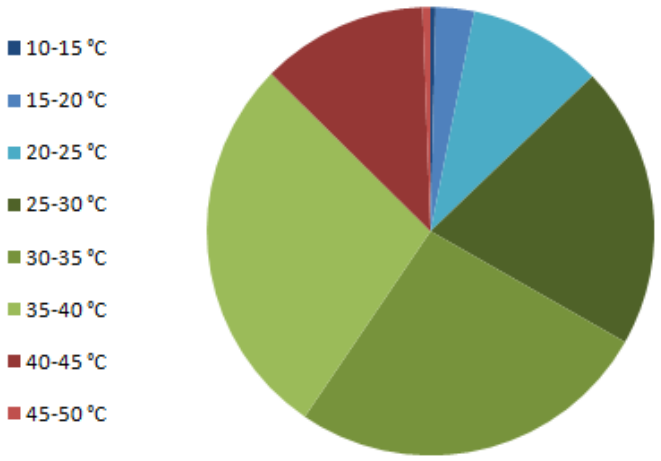

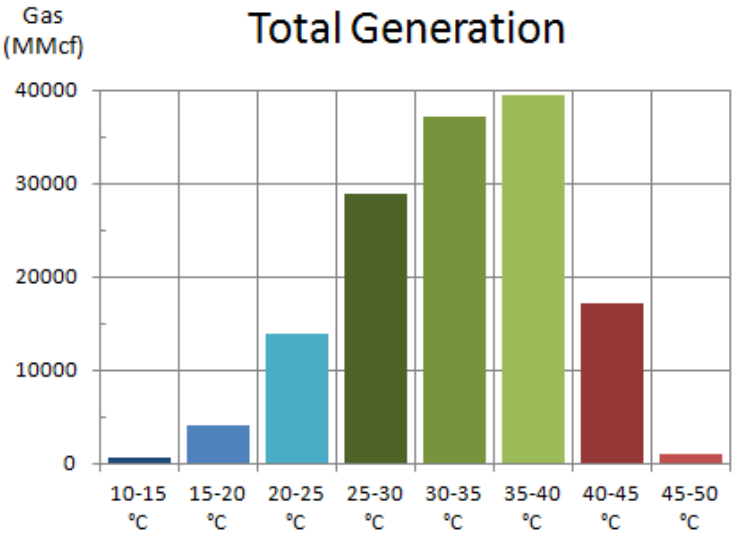

NS1 **Zone 2**

CH_4 Generation per Layer (5 Ma Time Intervals)

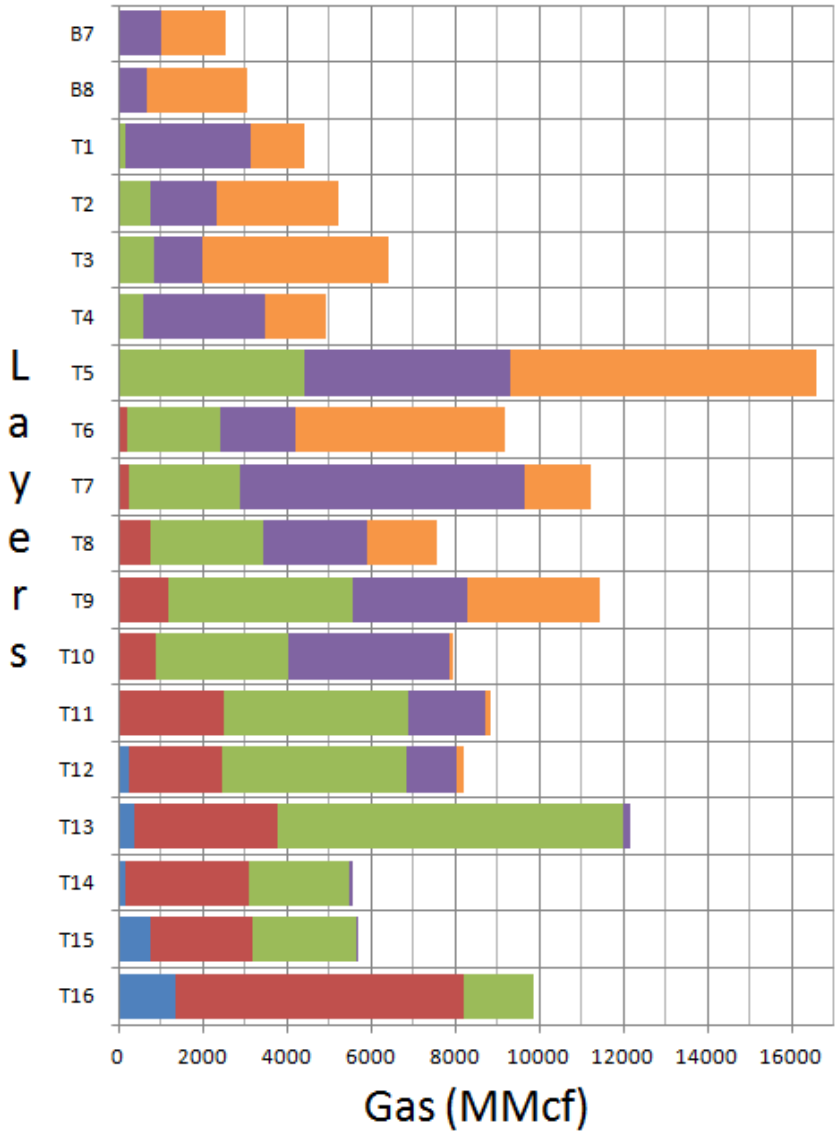

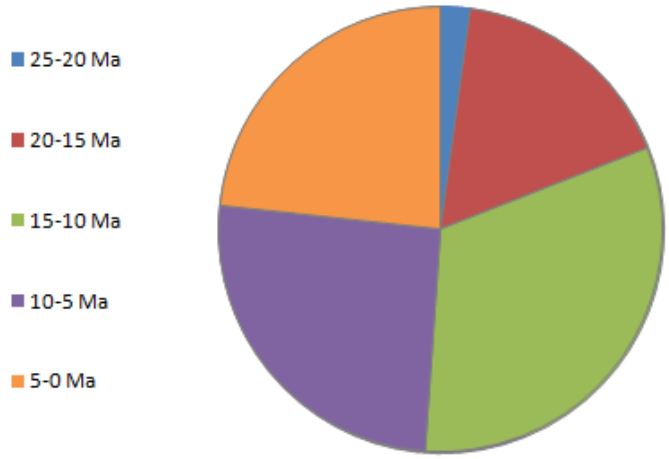

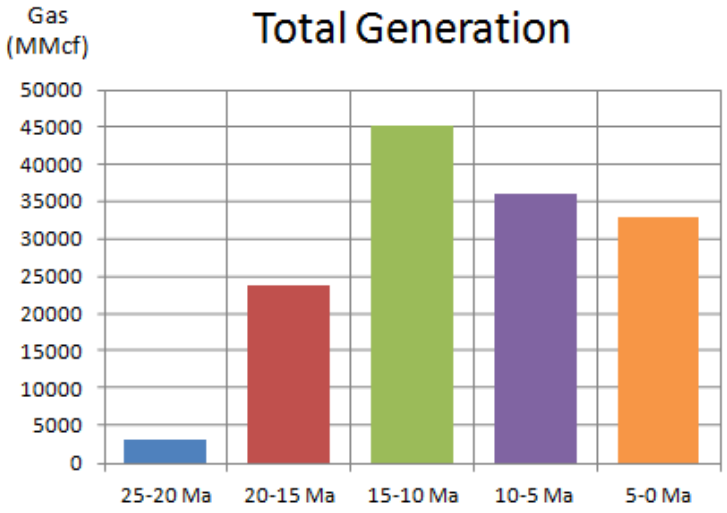

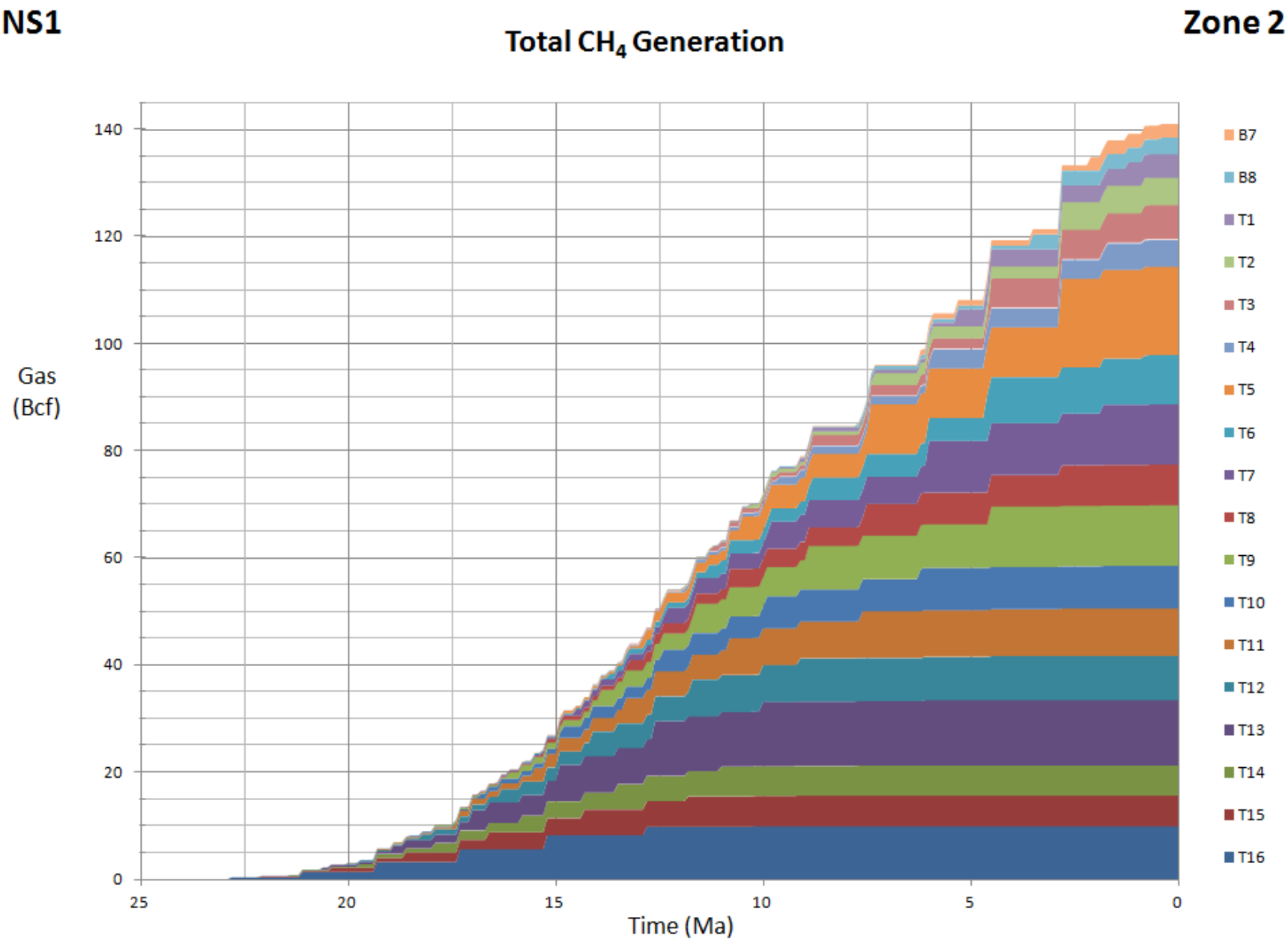
NS1
Zone 2
Total CH_4 Generation
Gas (Bcf)
140
120
100
80
60
40
20
0
25
20
15
10
5
0
Time (Ma)
B7
B8
T1
T2
T3
T4
T5
T6
T7
T8
T9
T10
T11
T12
T13
T14
T15
T16

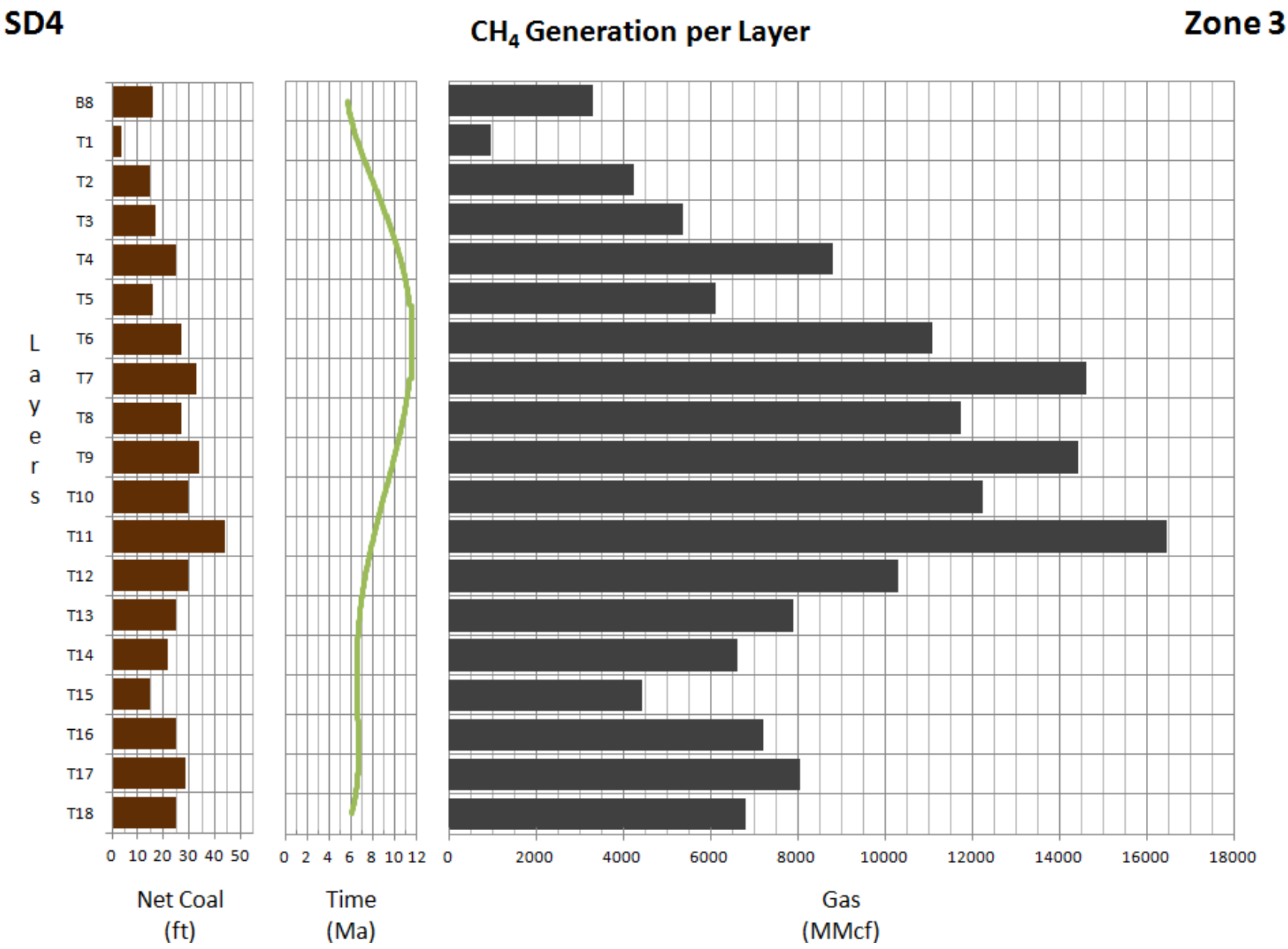
SD4
CH4 Generation per Layer
Zone 3
Layers
B8
T1
T2
T3
T4
T5
T6
T7
T8
T9
T10
T11
T12
T13
T14
T15
T16
T17
T18
0 10 20 30 40 50
Net Coal (ft)
0 2 4 6 8 10 12
Time (Ma)
0 2000 4000 6000 8000 10000 12000 14000 16000 18000
Gas (MMcf)

SD4 **Zone 3**

CH_4 Generation per Layer (5 °C Temp Intervals)

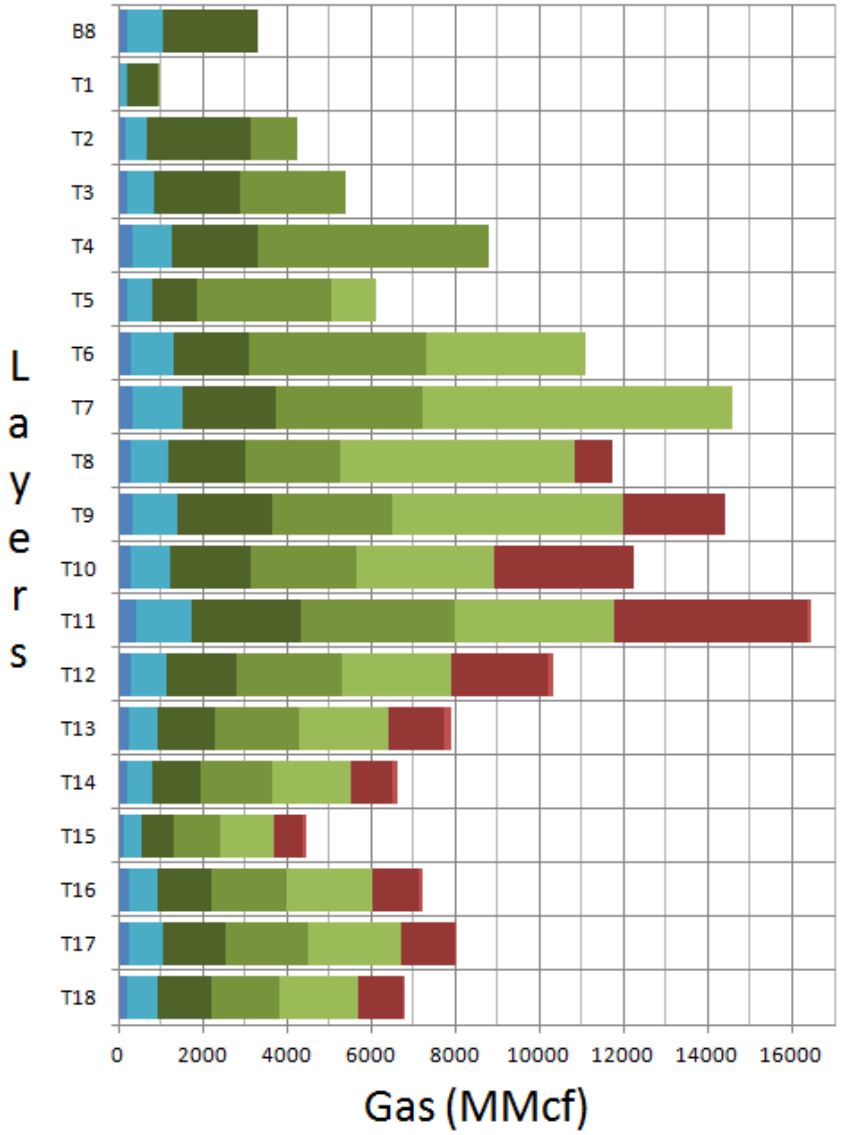

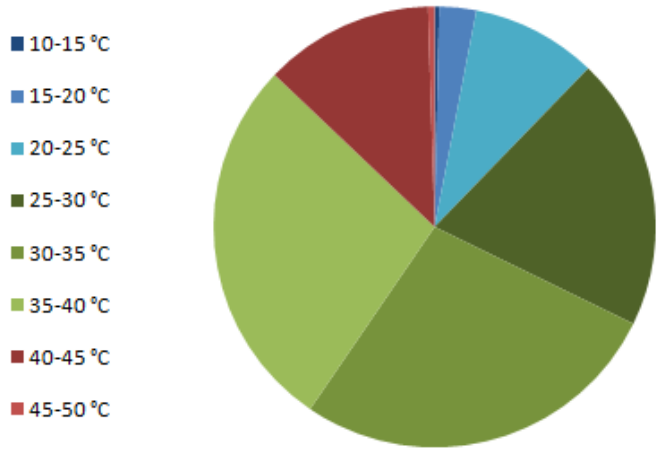

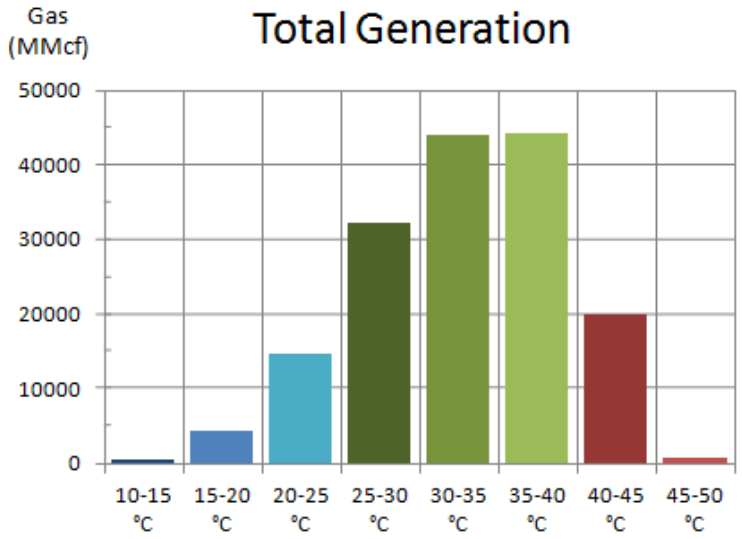

SD4 **Zone 3**

CH_4 Generation per Layer (5 Ma Time Intervals)

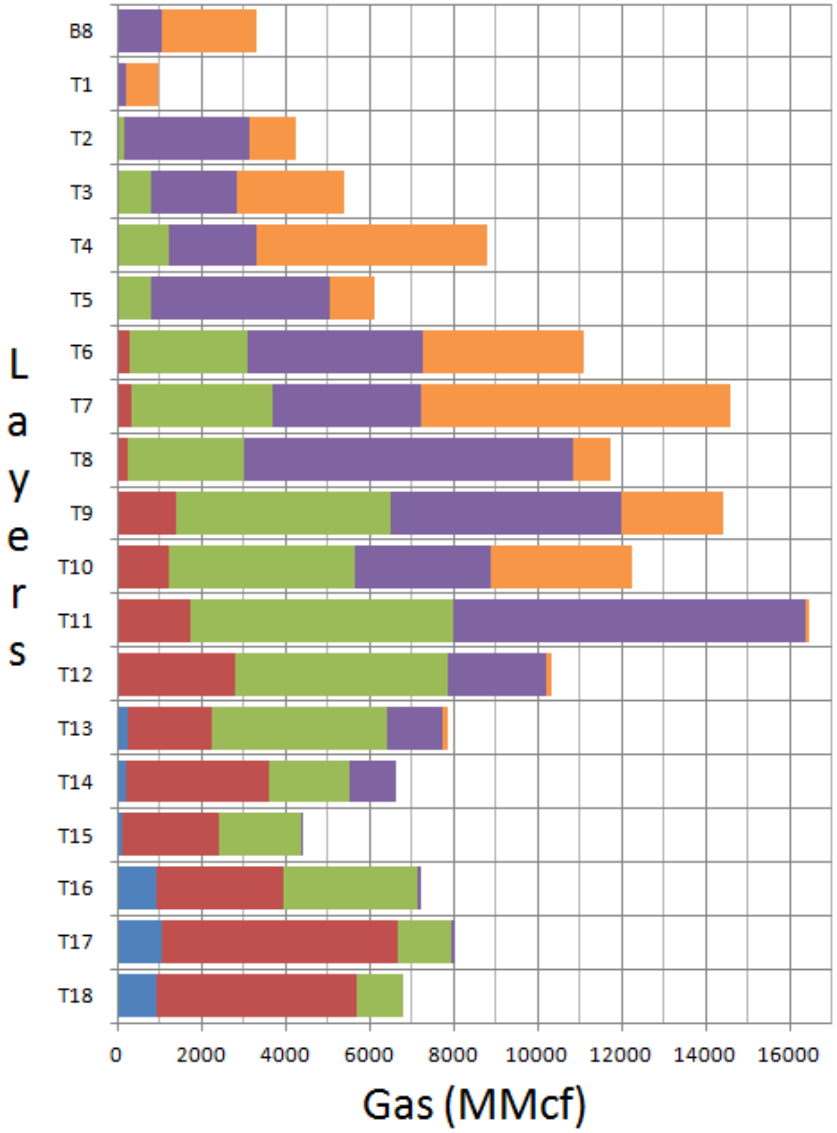

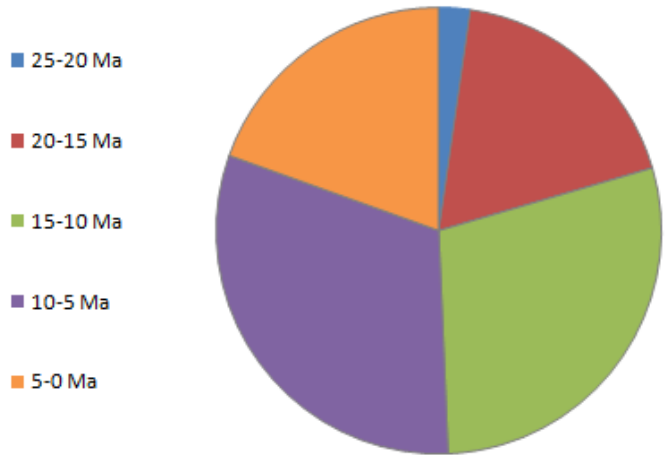

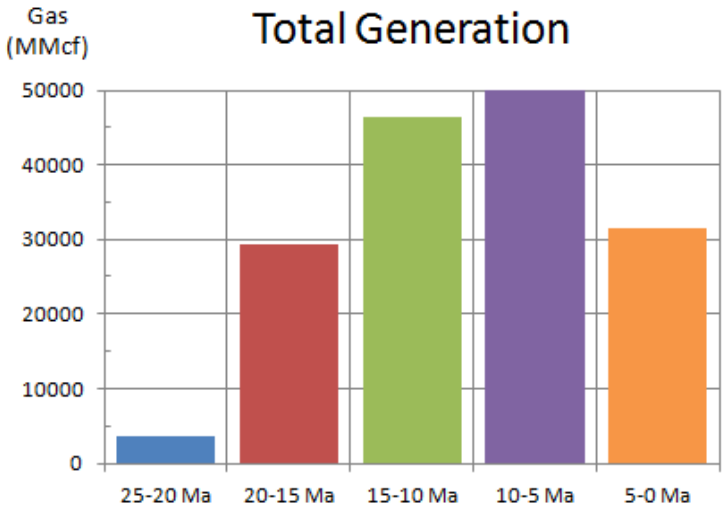

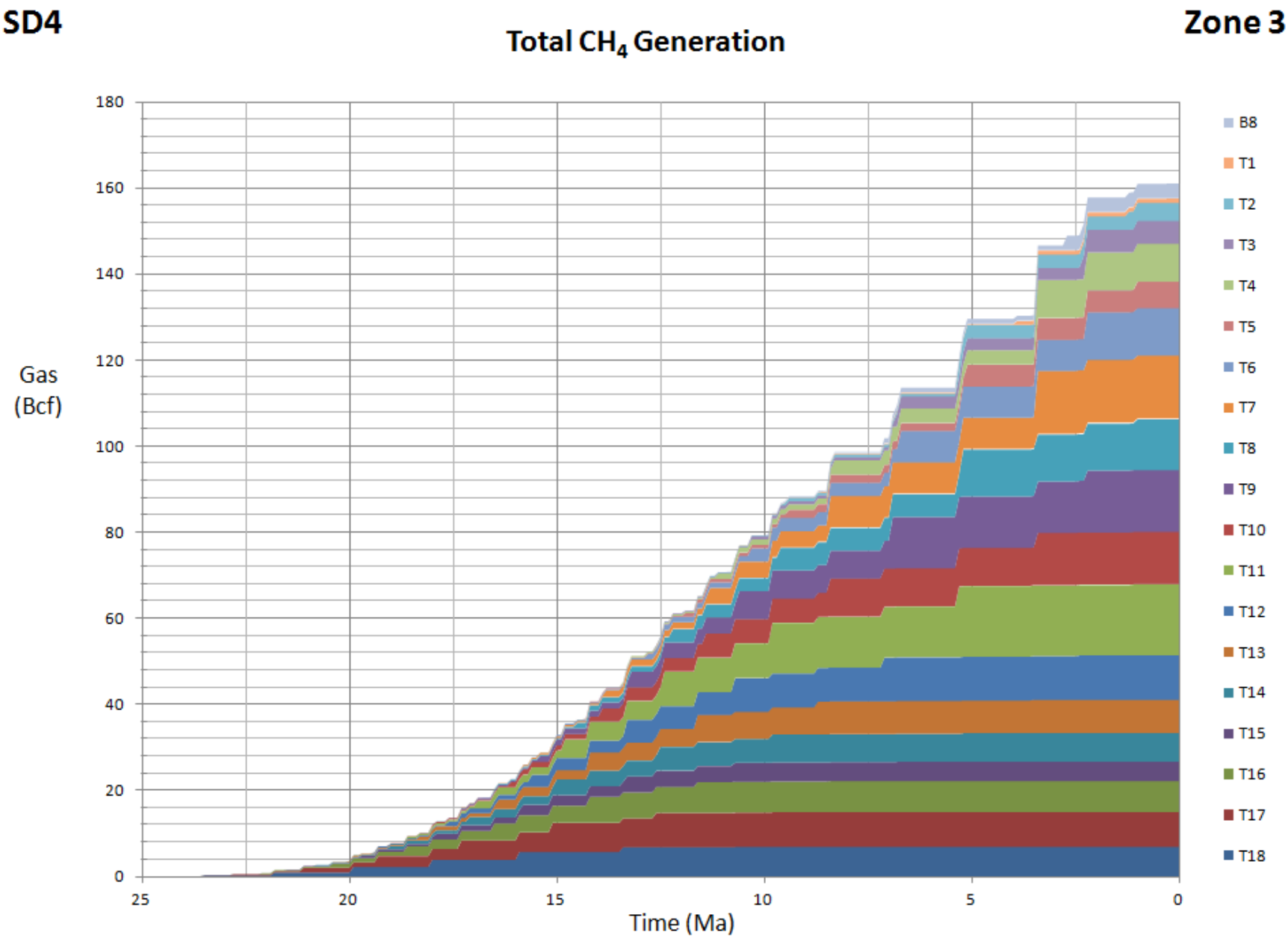
SD4
Zone 3
Total CH_4 Generation
Gas (Bcf)
180
160
140
120
100
80
60
40
20
0
25
20
15
10
5
0
Time (Ma)
B8
T1
T2
T3
T4
T5
T6
T7
T8
T9
T10
T11
T12
T13
T14
T15
T16
T17
T18

PAX2

PAX2: CH_4 Generation per Layer

Zone 3

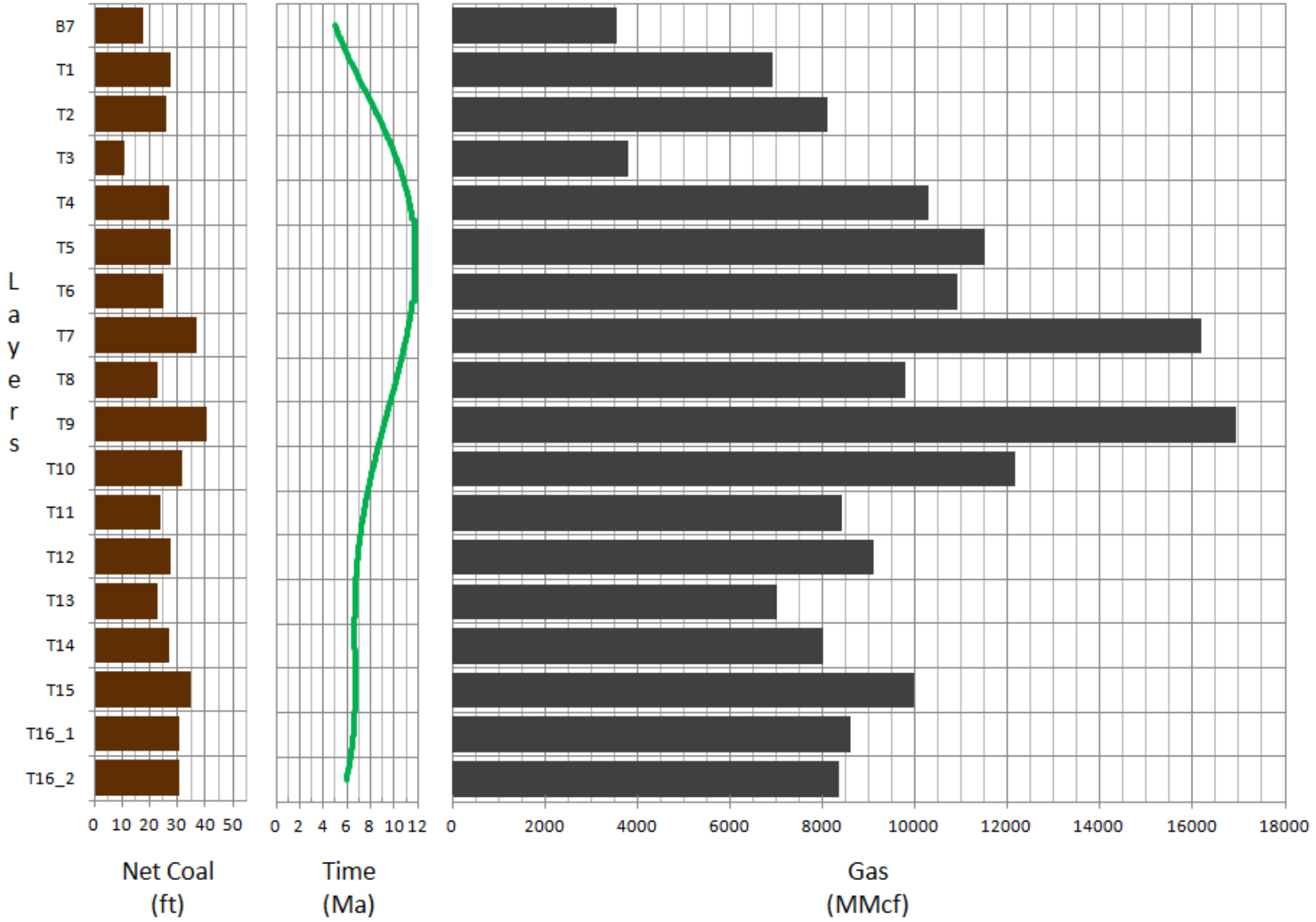

PAX2 **Zone 3**

CH_4 Generation per Layer (5 °C Temp Intervals)

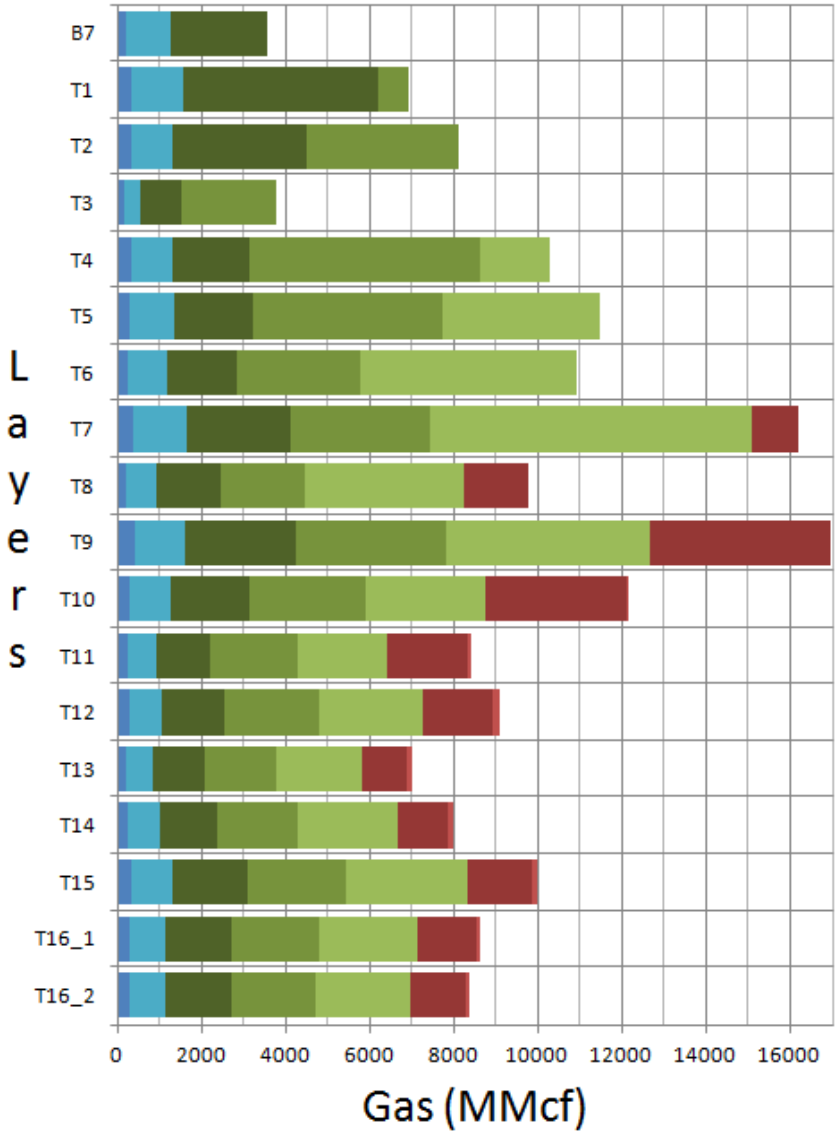

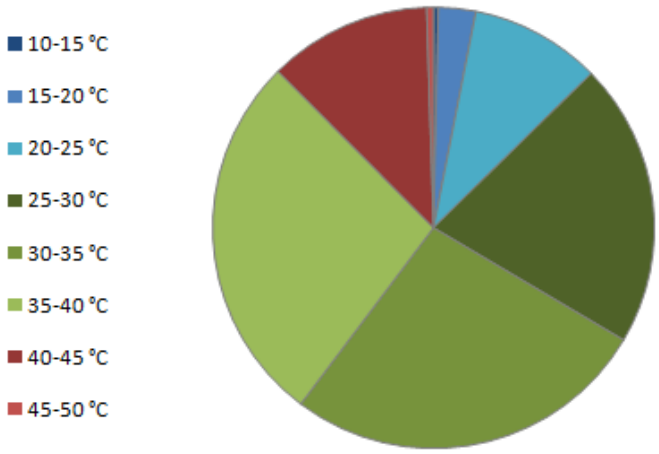

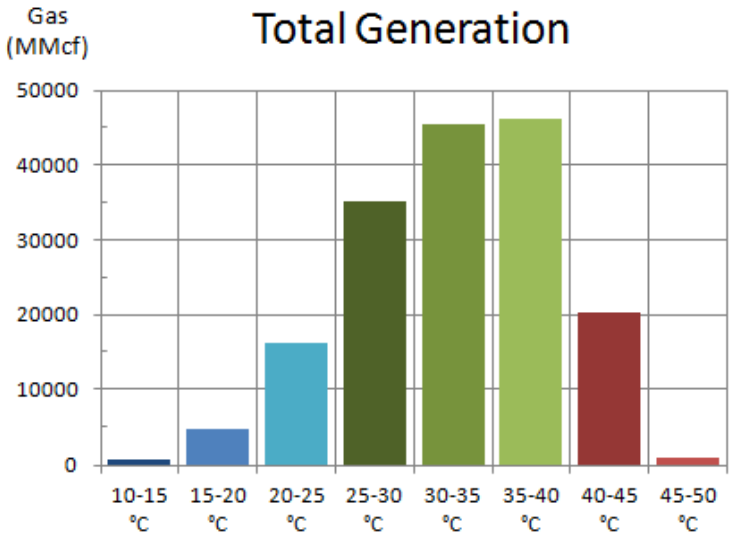

PAX2 **Zone 3**

CH_4 Generation per Layer (5 Ma Time Intervals)

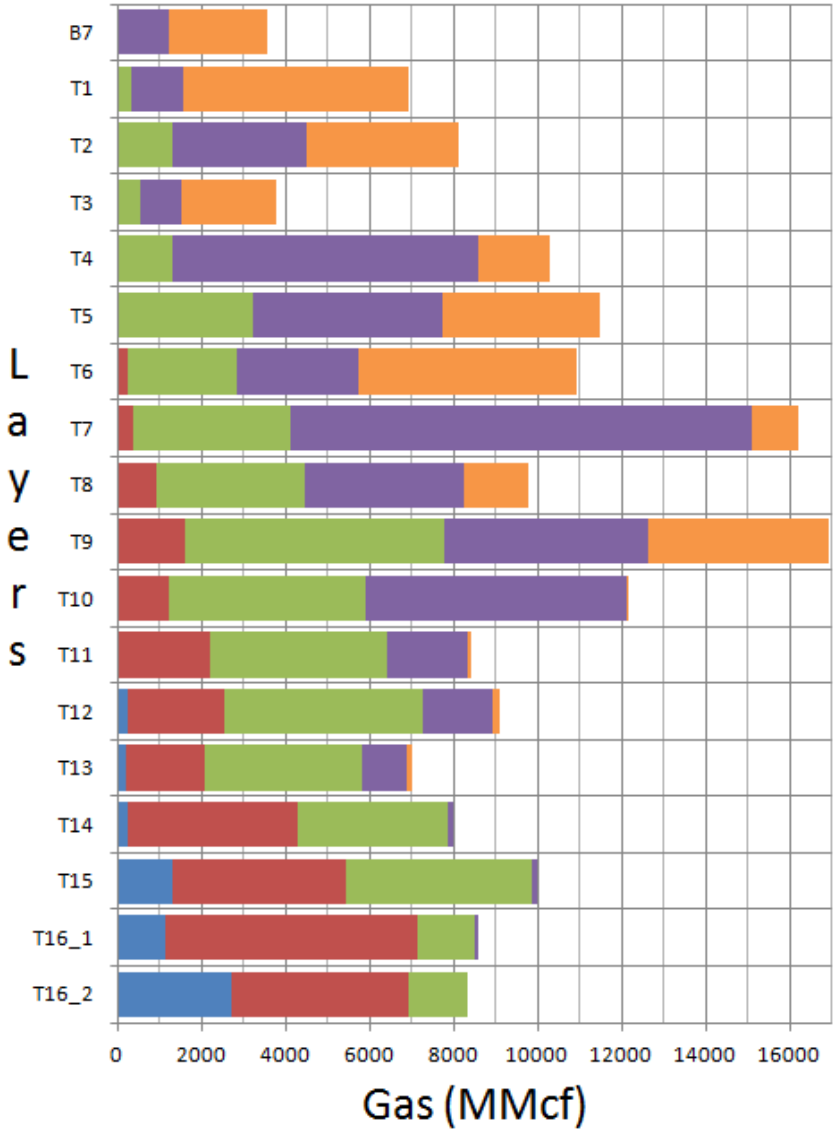

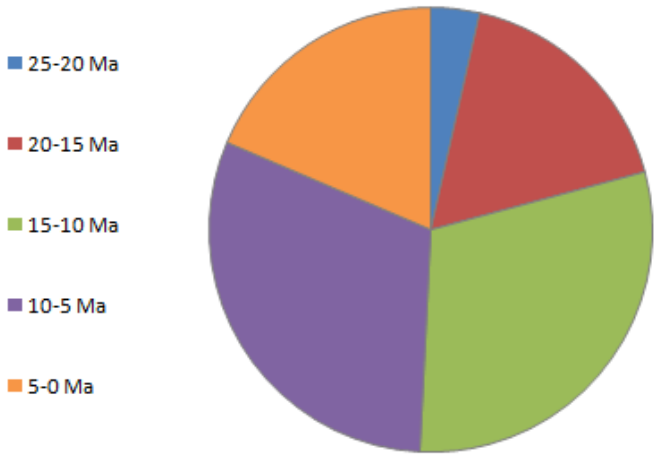

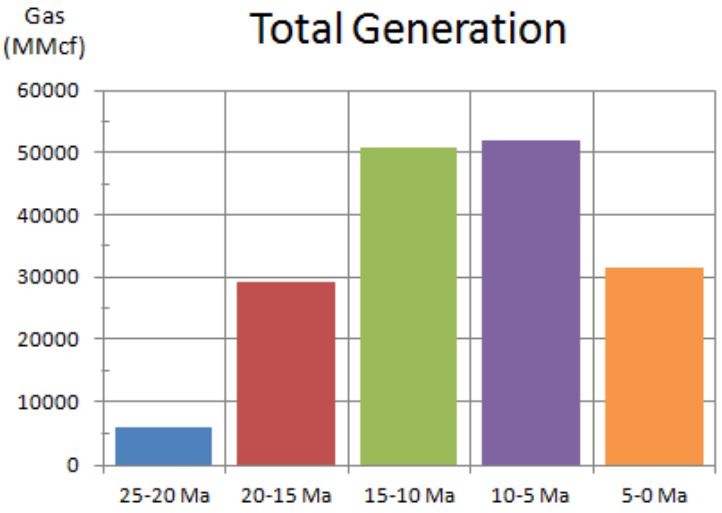

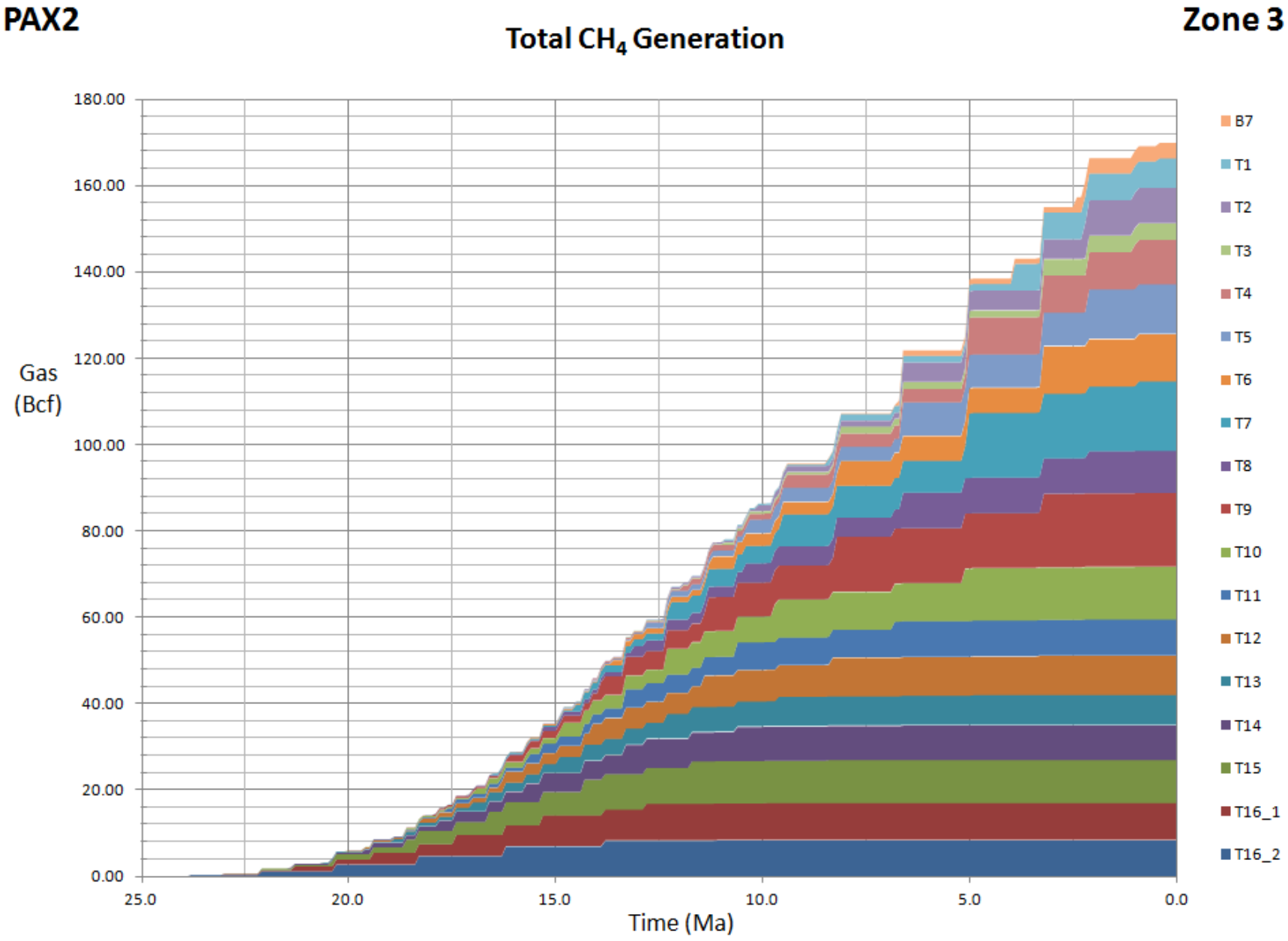
PAX2
Zone 3
Total CH_4 Generation
Gas (Bcf)
180.00
160.00
140.00
120.00
100.00
80.00
60.00
40.00
20.00
0.00
25.0
20.0
15.0
10.0
5.0
0.0
Time (Ma)
B7
T1
T2
T3
T4
T5
T6
T7
T8
T9
T10
T11
T12
T13
T14
T15
T16_1
T16_2

Appendix F: Geothermal Histories and Methanogenesis of the Sensitivity Analysis

Explanation of Appendix F abbreviations and labels:

SD4 = Susan Dionne #4 modeled well used in Sensitivity Analysis

High = Model produced using upper bound temperature parameters with original depositional ages

Low = Model produced using lower bound temperature parameters with original depositional ages

Ages = Model produced using original temperature parameters with alternate depositional ages

Ages High = Model produced using upper bound temperature parameters with altered depositional ages

Ages Low = Model produced using lower bound temperature parameters with altered depositional ages

Layers = ~250 ft layers of Tyonek (T) and Beluga (B) formations; orientation represents relative depths along wellbore

Net Coal (ft) = Thickness of coal measured within the layer

Graph of 'Time (Ma)' = Duration each layer spent within MBGW (25-40 °C)

Gas (mmcf) = Total gas generation for each layer in millions of cubic feet; colors designate distributions per 5 °C and 5 Ma

Graph of 'Gas (Bcf) vs Time (Ma)' = Each layers' cumulative gas contribution to the modeled well volume with time

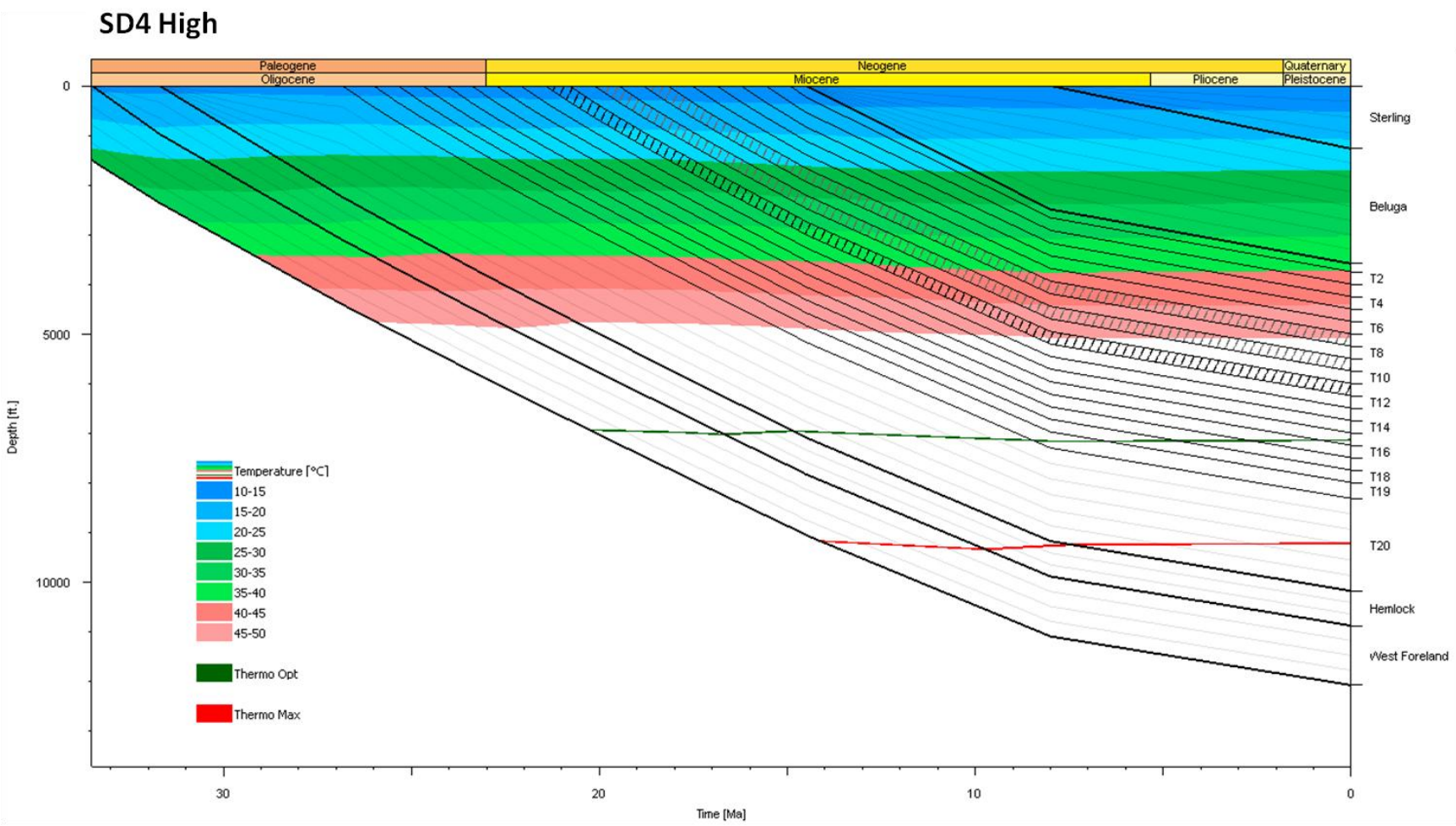
SD4 High
Paleogene
Oligocene
Neogene
Miocene
Pliocene
Quaternary
Pleistocene
0
5000
10000
Depth [ft.]
Temperature [°C]
10-15
15-20
20-25
25-30
30-35
35-40
40-45
45-50
Thermo Opt
Thermo Max
Sterling
Beluga
T2
T4
T6
T8
T10
T12
T14
T16
T18
T19
T20
Hemlock
West Foreland
30
20
10
0
Time [Ma]

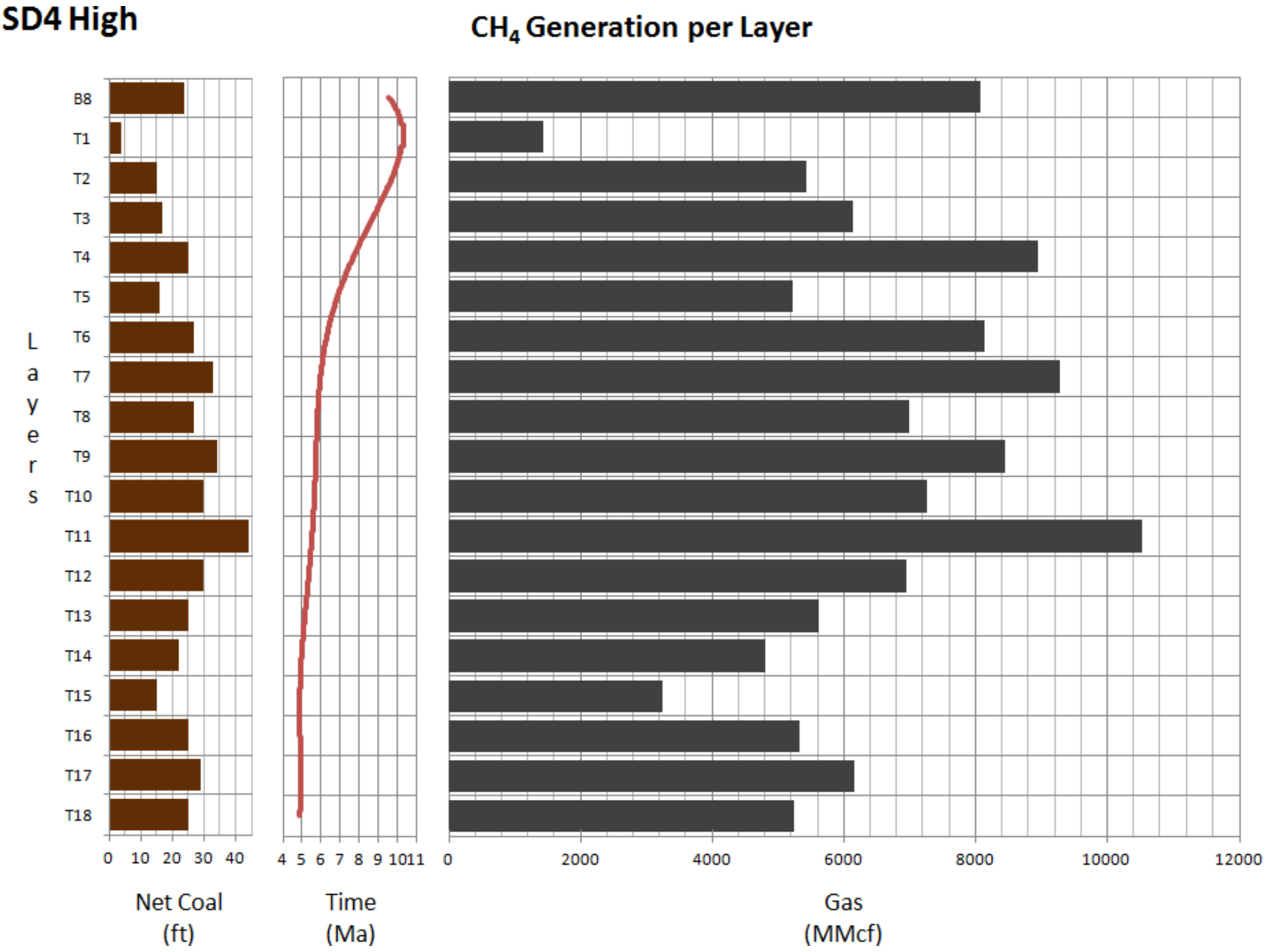
SD4 High
CH4 Generation per Layer
Layers
B8
T1
T2
T3
T4
T5
T6
T7
T8
T9
T10
T11
T12
T13
T14
T15
T16
T17
T18
0 10 20 30 40
Net Coal (ft)
4 5 6 7 8 9 10 11
Time (Ma)
0 2000 4000 6000 8000 10000 12000
Gas (MMcf)

SD4 High

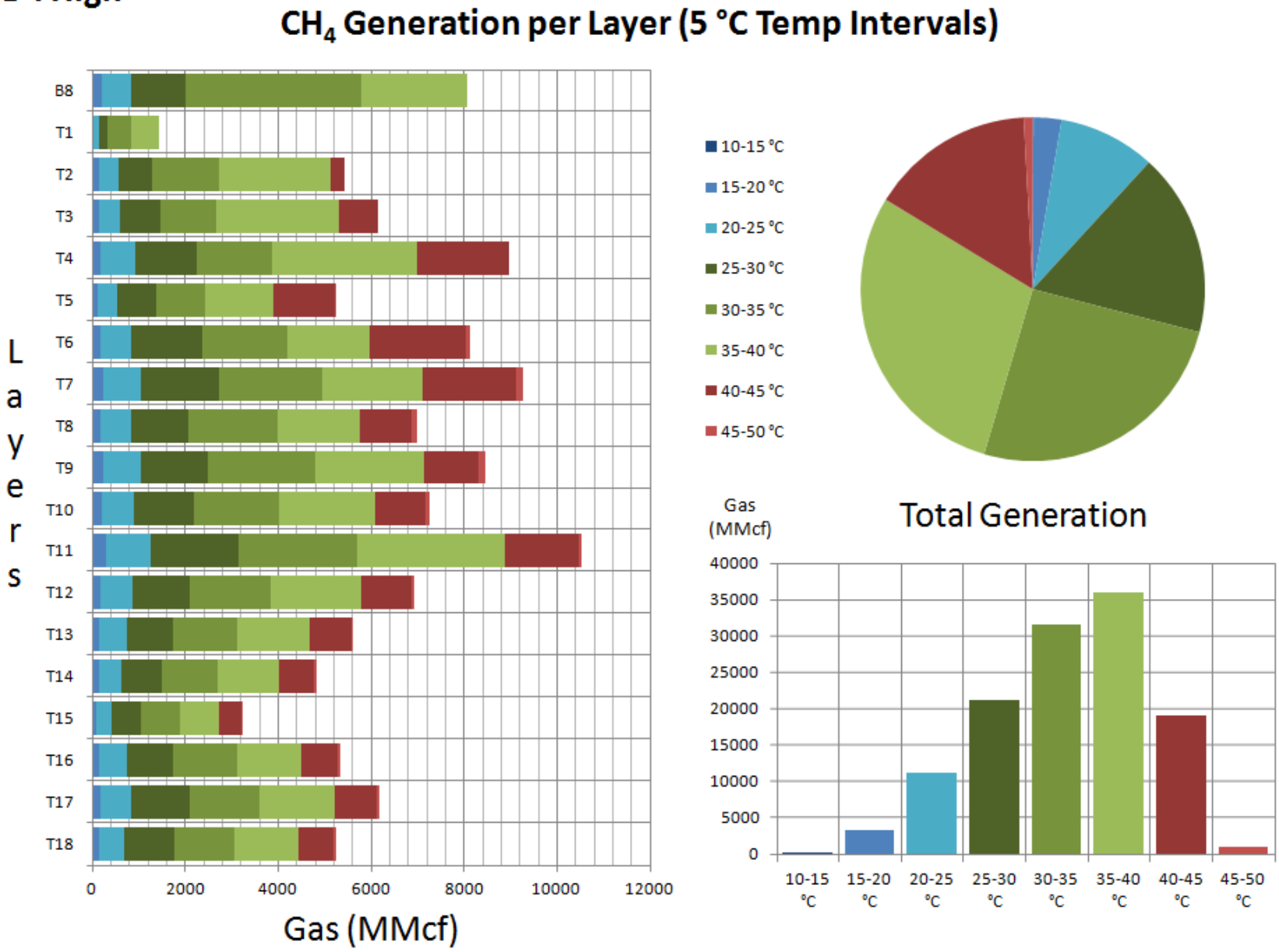
CH4 Generation per Layer (5 °C Temp Intervals)
B8
T1
T2
T3
T4
T5
T6
T7
T8
T9
T10
T11
T12
T13
T14
T15
T16
T17
T18
Layers
0
2000
4000
6000
8000
10000
12000
Gas (MMcf)
10-15 °C
15-20 °C
20-25 °C
25-30 °C
30-35 °C
35-40 °C
40-45 °C
45-50 °C
Total Generation
Gas (MMcf)
40000
35000
30000
25000
20000
15000
10000
5000
0
10-15 °C
15-20 °C
20-25 °C
25-30 °C
30-35 °C
35-40 °C
40-45 °C
45-50 °C

SD4 High

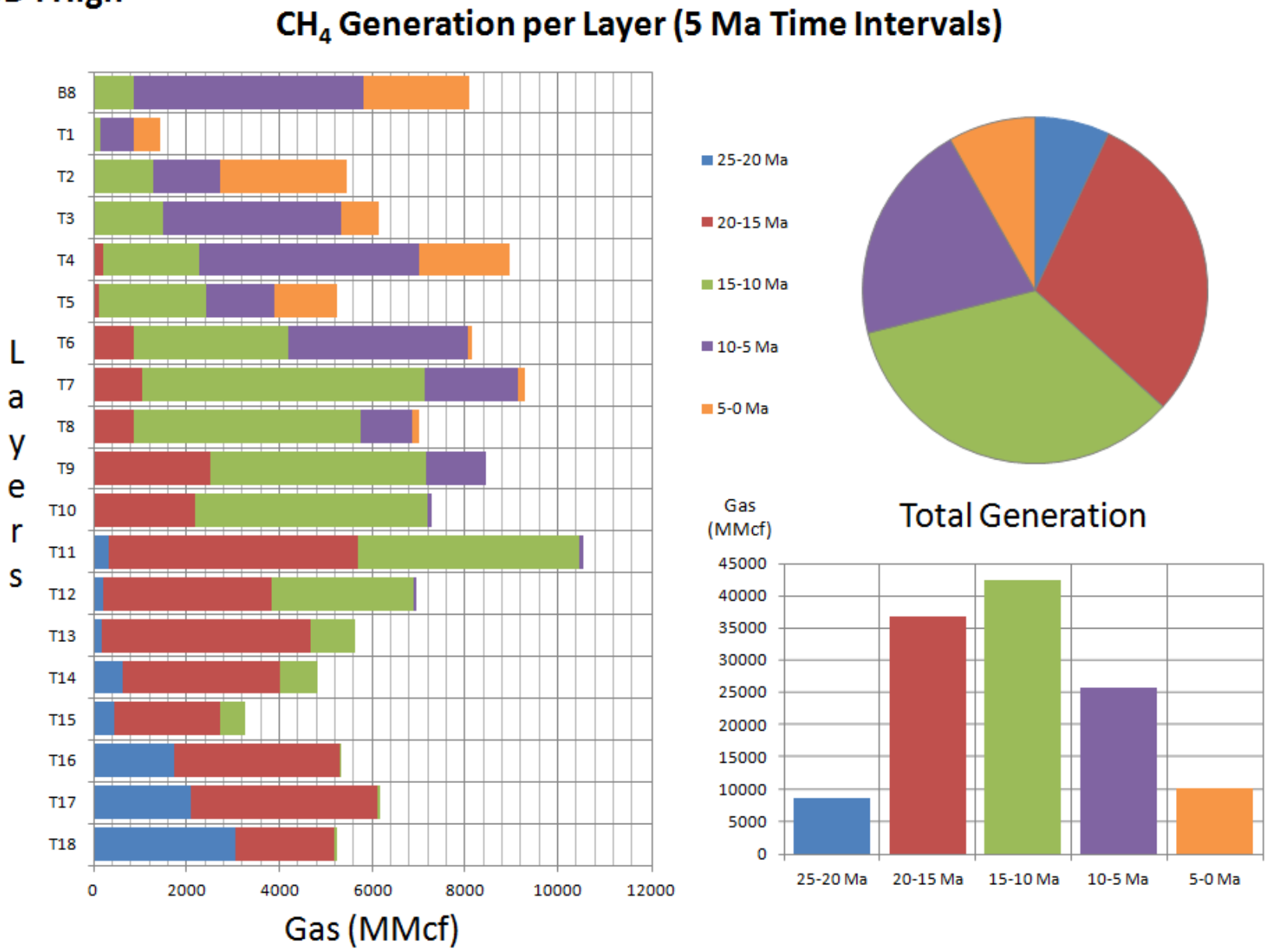
CH4 Generation per Layer (5 Ma Time Intervals)
Layers
B8
T1
T2
T3
T4
T5
T6
T7
T8
T9
T10
T11
T12
T13
T14
T15
T16
T17
T18
0
2000
4000
6000
8000
10000
12000
Gas (MMcf)
25-20 Ma
20-15 Ma
15-10 Ma
10-5 Ma
5-0 Ma
Total Generation
Gas (MMcf)
45000
40000
35000
30000
25000
20000
15000
10000
5000
0
25-20 Ma
20-15 Ma
15-10 Ma
10-5 Ma
5-0 Ma

SD4 High

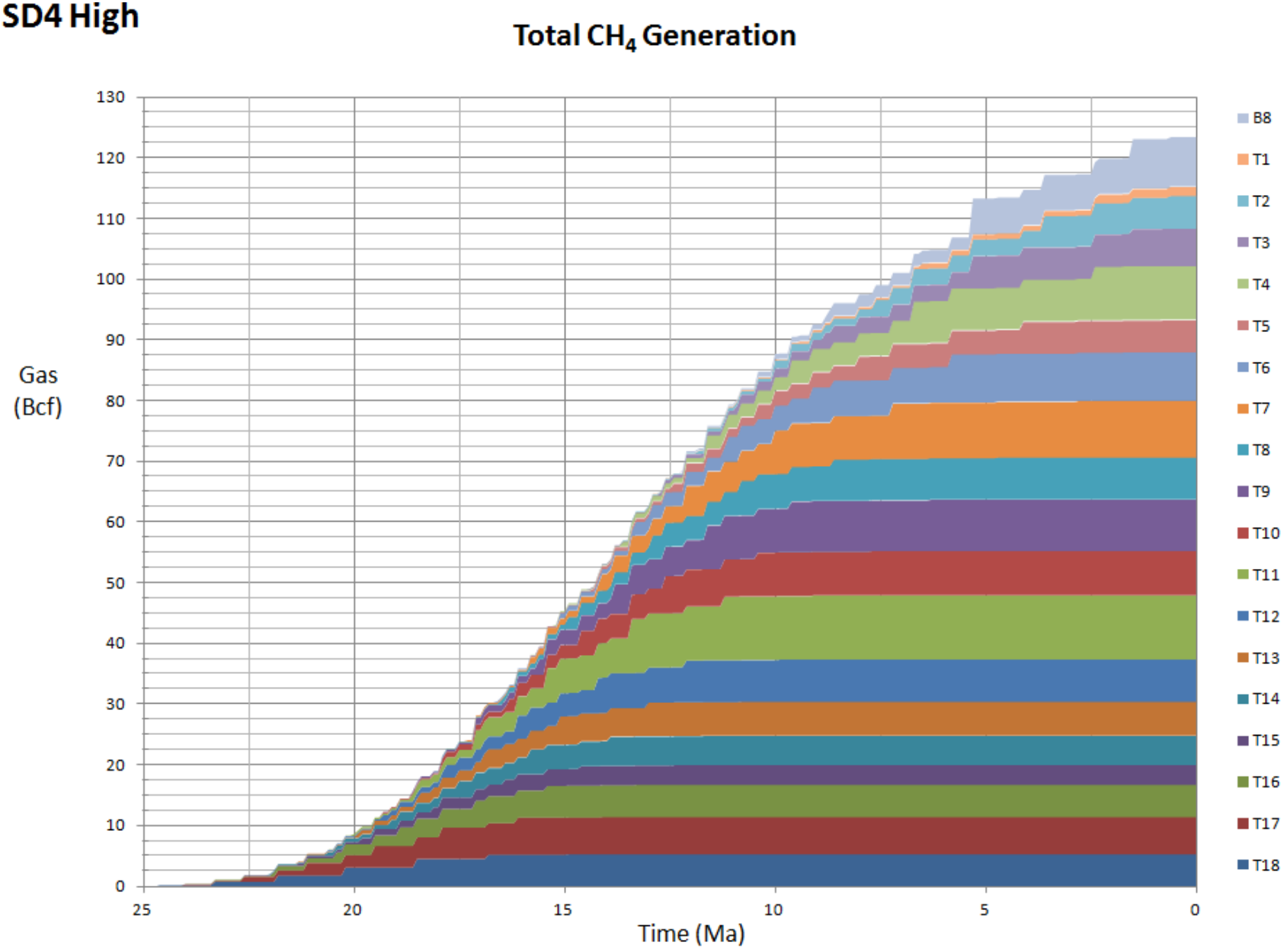
Total CH_4 Generation
Gas (Bcf)
130
120
110
100
90
80
70
60
50
40
30
20
10
0
25
20
15
10
5
0
Time (Ma)
B8
T1
T2
T3
T4
T5
T6
T7
T8
T9
T10
T11
T12
T13
T14
T15
T16
T17
T18

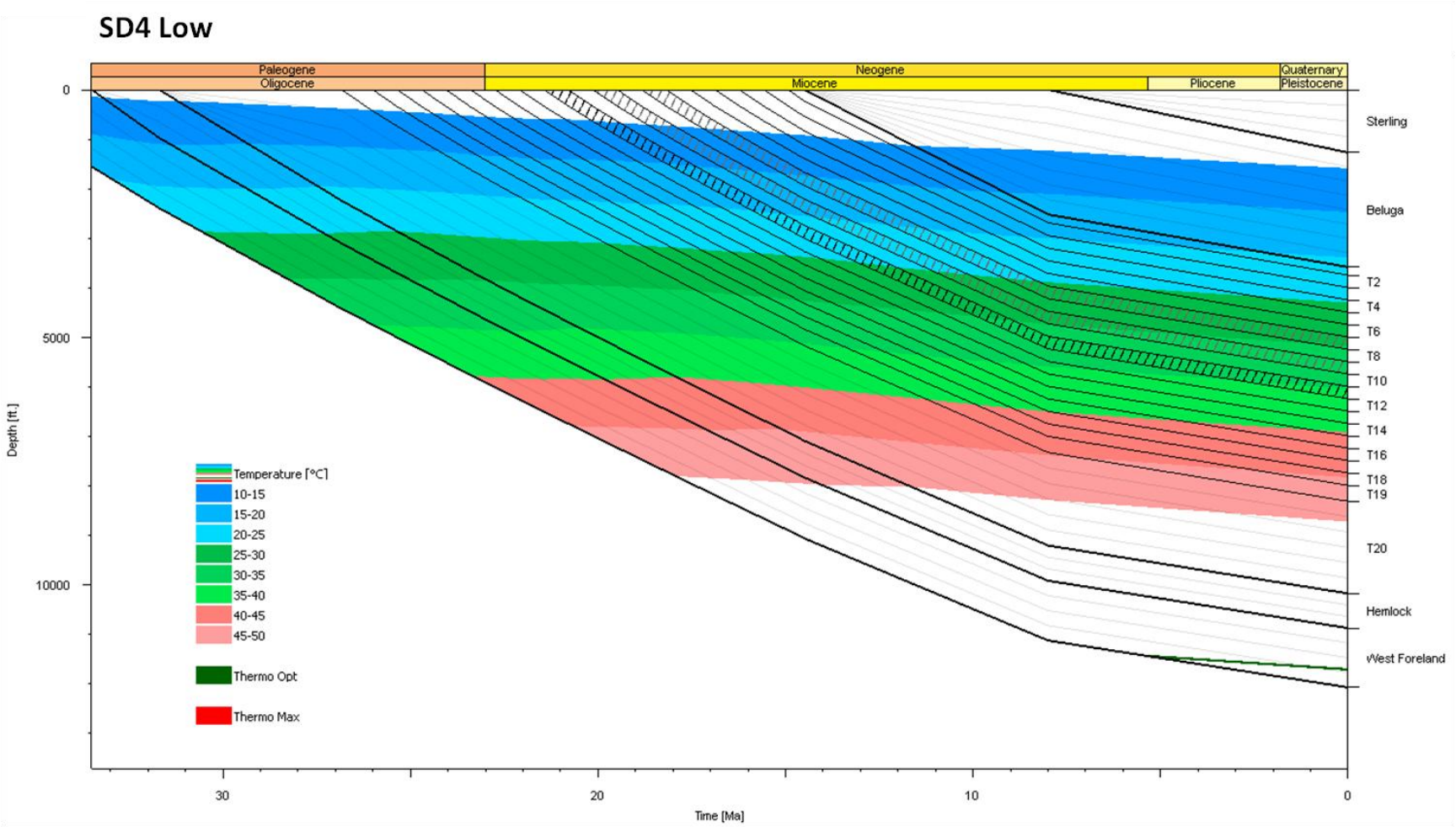
SD4 Low
Paleogene
Oligocene
Neogene
Miocene
Pliocene
Quaternary
Pleistocene
0
5000
10000
Depth [ft.]
Temperature [°C]
10-15
15-20
20-25
25-30
30-35
35-40
40-45
45-50
Thermo Opt
Thermo Max
Sterling
Beluga
T2
T4
T6
T8
T10
T12
T14
T16
T18
T19
T20
Hemlock
West Foreland
30
20
10
0
Time [Ma]

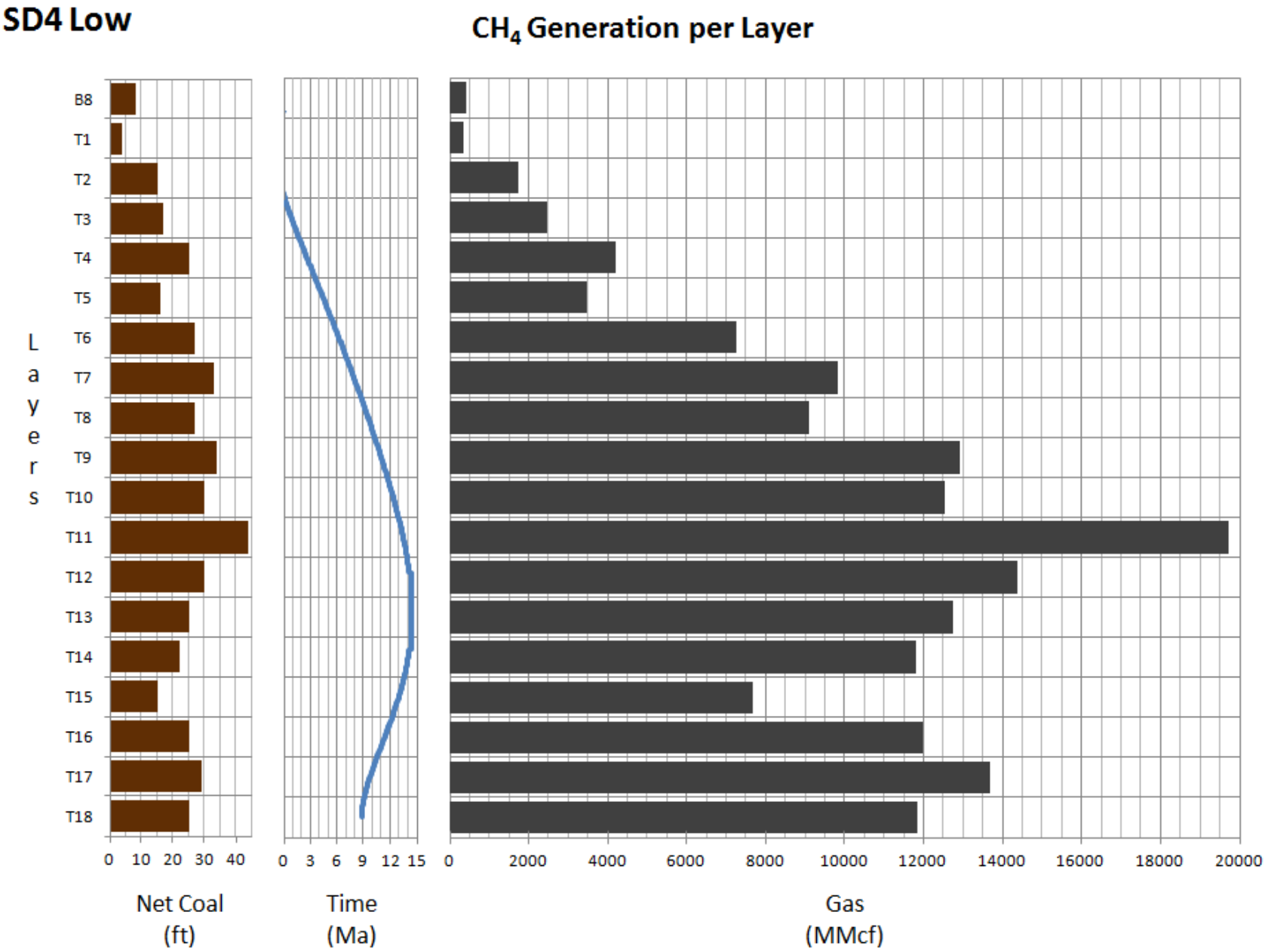
SD4 Low
CH4 Generation per Layer
Layers
B8
T1
T2
T3
T4
T5
T6
T7
T8
T9
T10
T11
T12
T13
T14
T15
T16
T17
T18
0 10 20 30 40
Net Coal (ft)
0 3 6 9 12 15
Time (Ma)
0 2000 4000 6000 8000 10000 12000 14000 16000 18000 20000
Gas (MMcf)

SD4 Low

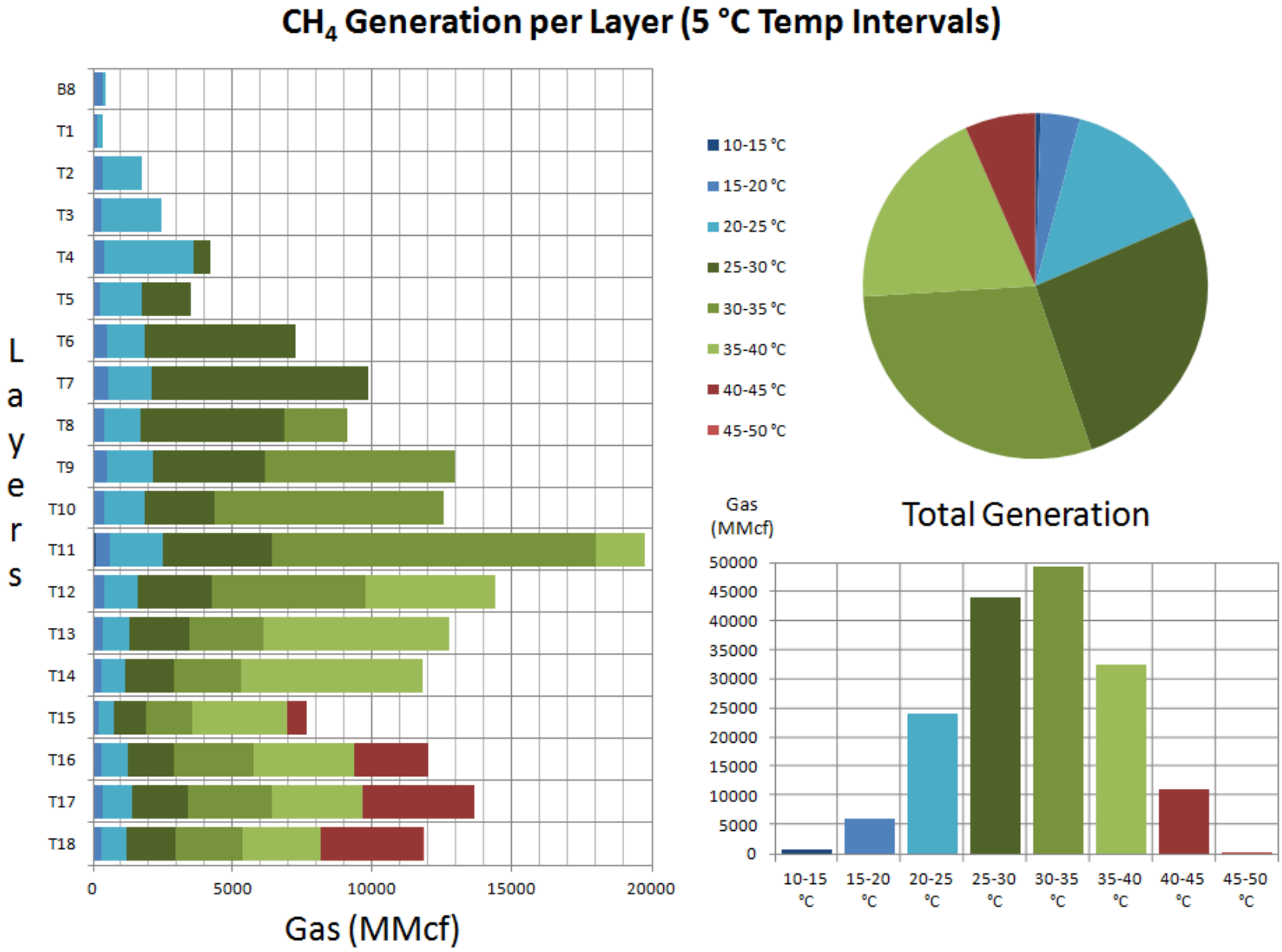
CH4 Generation per Layer (5 °C Temp Intervals)
Layers
B8
T1
T2
T3
T4
T5
T6
T7
T8
T9
T10
T11
T12
T13
T14
T15
T16
T17
T18
0
5000
10000
15000
20000
Gas (MMcf)
10-15 °C
15-20 °C
20-25 °C
25-30 °C
30-35 °C
35-40 °C
40-45 °C
45-50 °C
Gas (MMcf)
Total Generation
50000
45000
40000
35000
30000
25000
20000
15000
10000
5000
0
10-15 °C
15-20 °C
20-25 °C
25-30 °C
30-35 °C
35-40 °C
40-45 °C
45-50 °C

SD4 Low

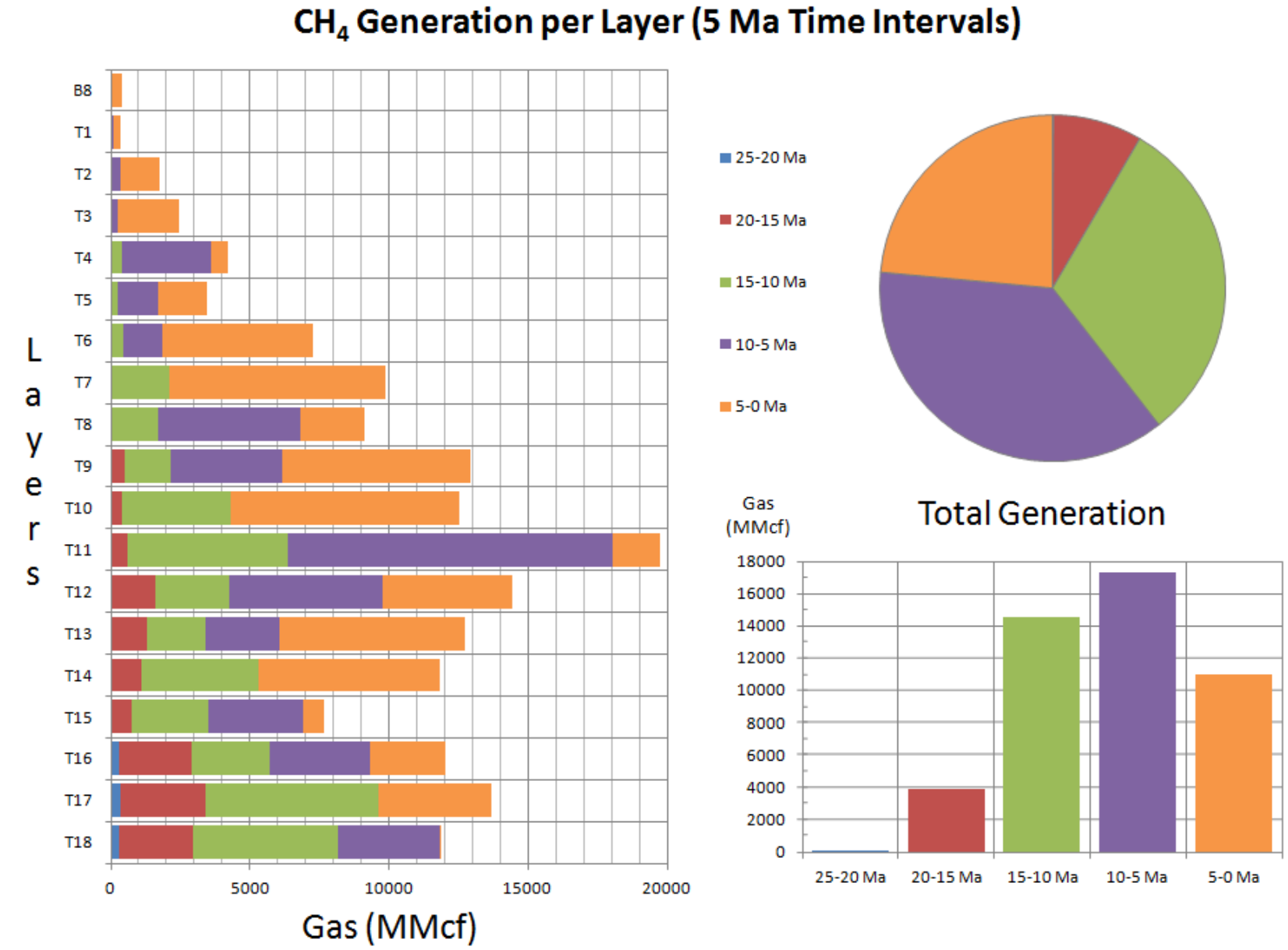
CH4 Generation per Layer (5 Ma Time Intervals)
B8
T1
T2
T3
T4
T5
T6
T7
T8
T9
T10
T11
T12
T13
T14
T15
T16
T17
T18
Layers
0
5000
10000
15000
20000
Gas (MMcf)
25-20 Ma
20-15 Ma
15-10 Ma
10-5 Ma
5-0 Ma
Total Generation
Gas (MMcf)
18000
16000
14000
12000
10000
8000
6000
4000
2000
0
25-20 Ma
20-15 Ma
15-10 Ma
10-5 Ma
5-0 Ma

SD4 Low

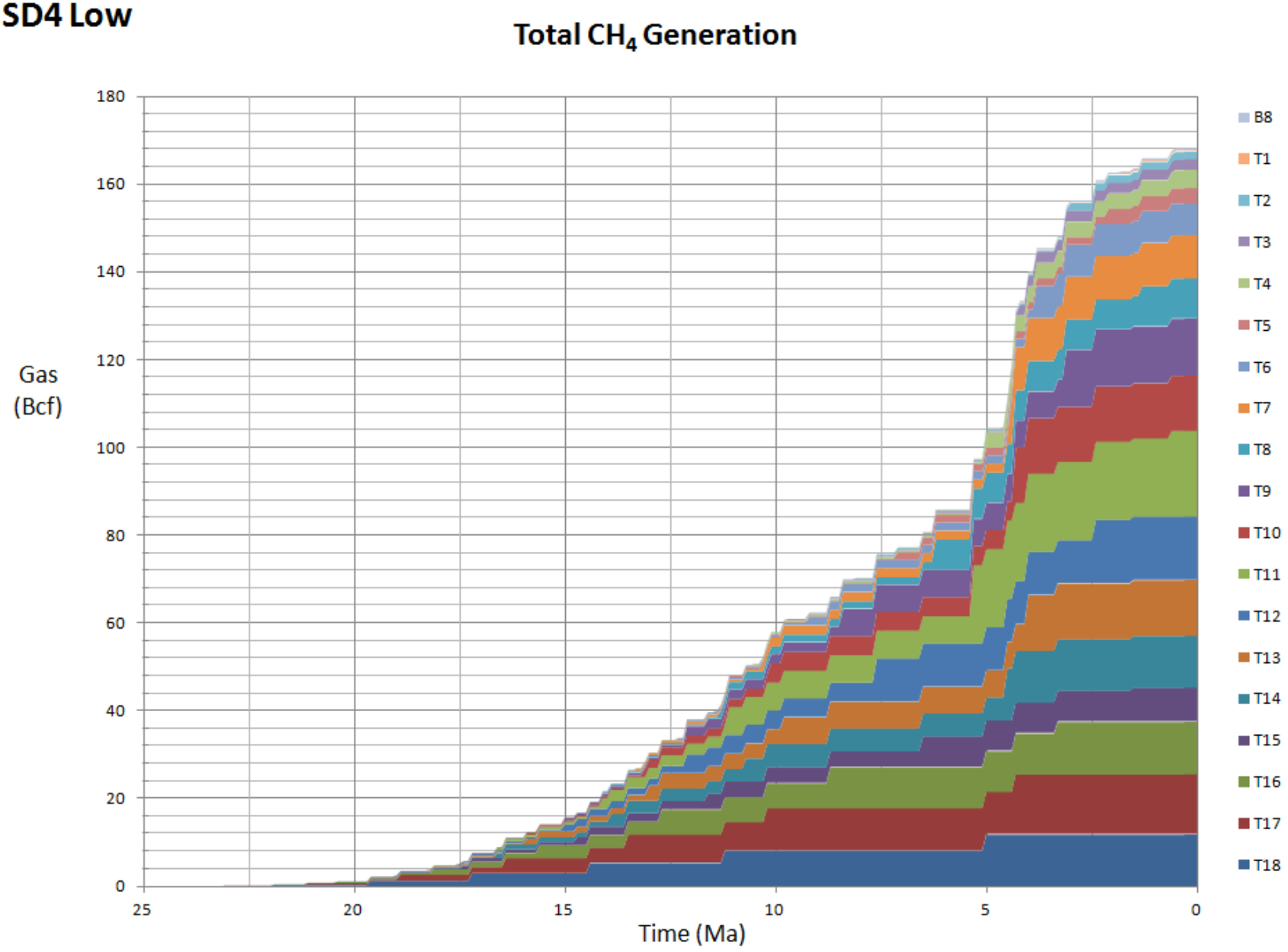
Total CH_4 Generation
Gas (Bcf)
180
160
140
120
100
80
60
40
20
0
25
20
15
10
5
0
Time (Ma)
B8
T1
T2
T3
T4
T5
T6
T7
T8
T9
T10
T11
T12
T13
T14
T15
T16
T17
T18

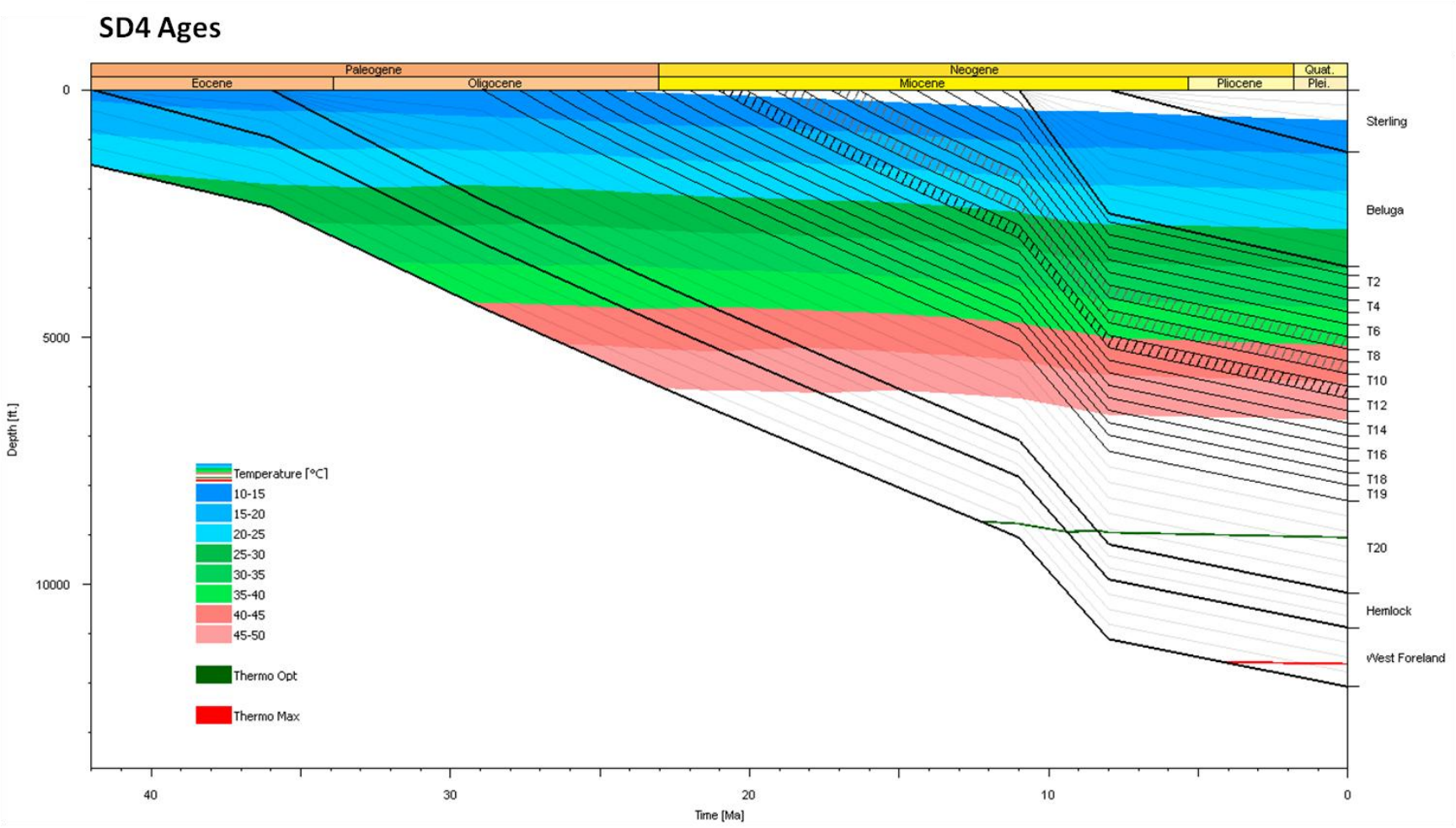
SD4 Ages
Paleogene
Neogene
Quat.
Eocene
Oligocene
Miocene
Pliocene
Plei.
0
5000
10000
Depth [ft.]
Temperature [°C]
10-15
15-20
20-25
25-30
30-35
35-40
40-45
45-50
Thermo Opt
Thermo Max
Sterling
Beluga
T2
T4
T6
T8
T10
T12
T14
T16
T18
T19
T20
Hemlock
West Foreland
40
30
20
10
0
Time [Ma]

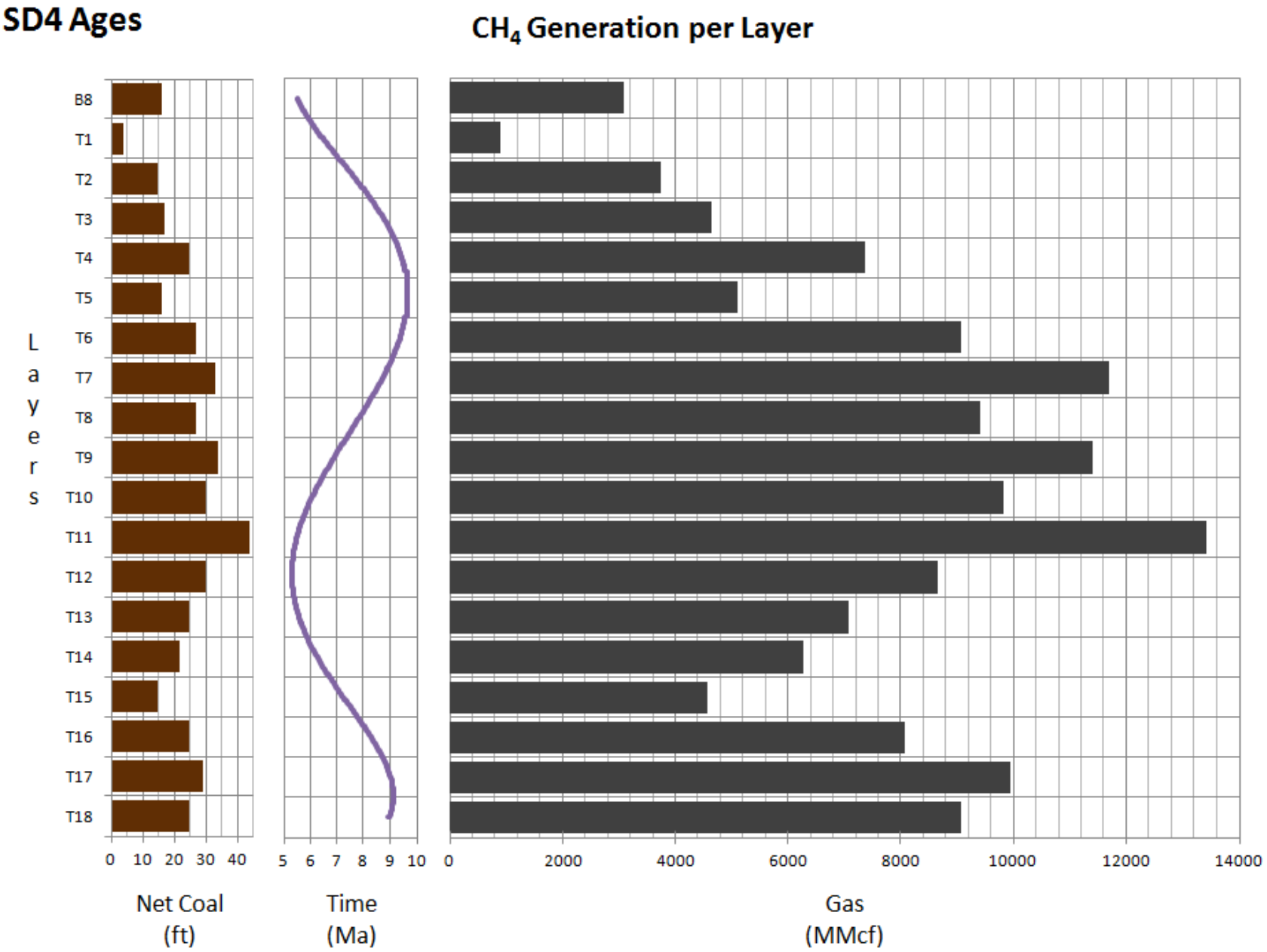
SD4 Ages
CH4 Generation per Layer
Layers
B8
T1
T2
T3
T4
T5
T6
T7
T8
T9
T10
T11
T12
T13
T14
T15
T16
T17
T18
0 10 20 30 40
Net Coal (ft)
5 6 7 8 9 10
Time (Ma)
0 2000 4000 6000 8000 10000 12000 14000
Gas (MMcf)

SD4 Ages

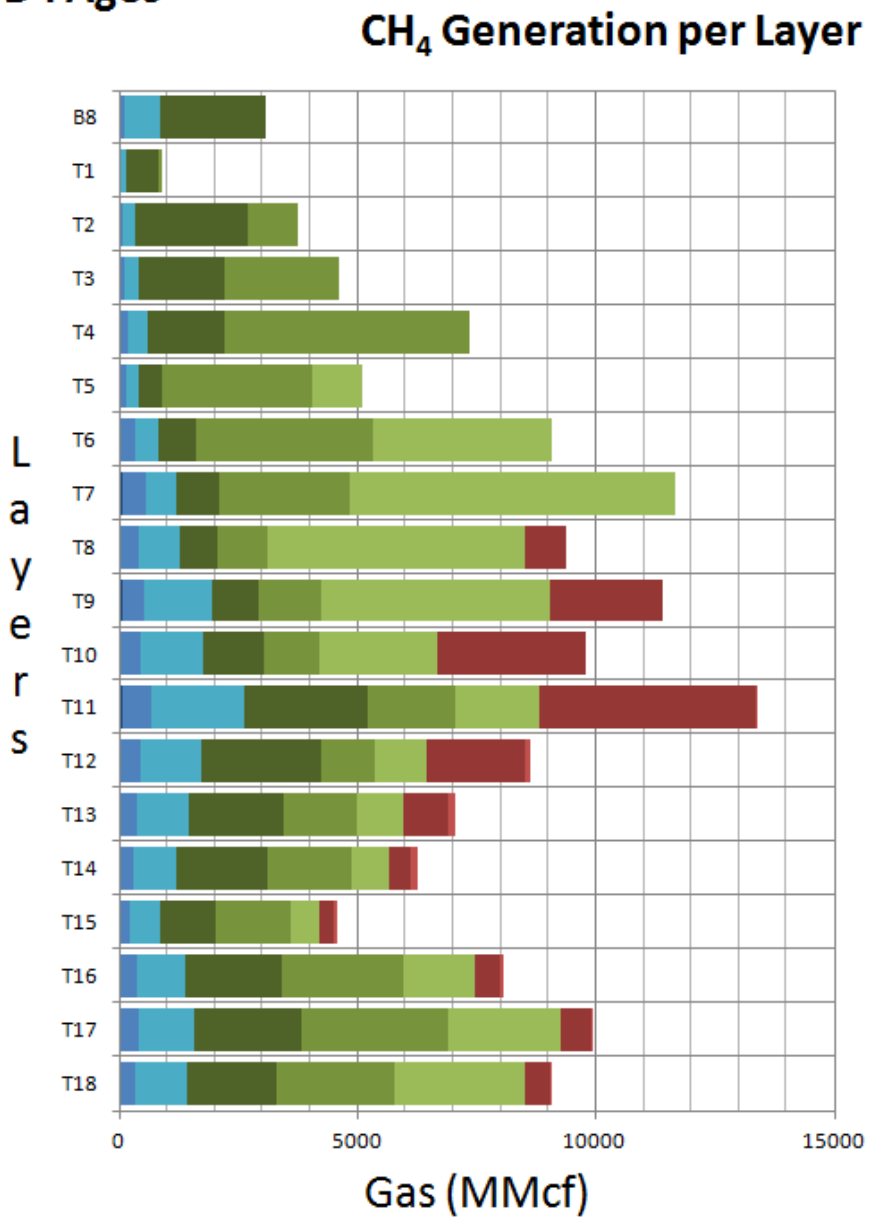
CH4 Generation per Layer (5 °C Temp Intervals)
Layers
B8
T1
T2
T3
T4
T5
T6
T7
T8
T9
T10
T11
T12
T13
T14
T15
T16
T17
T18
0
5000
10000
15000
Gas (MMcf)

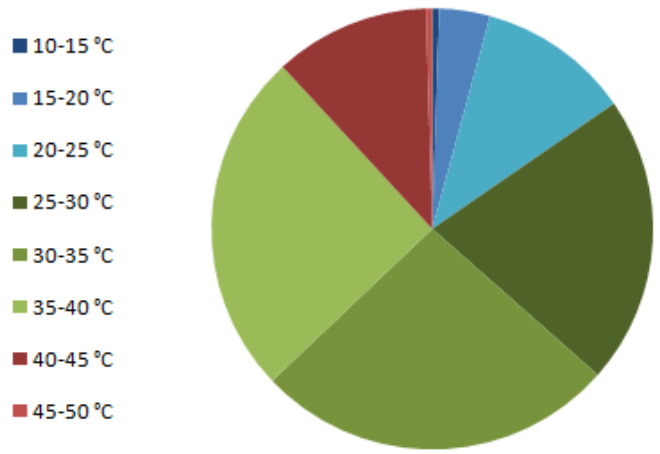
10-15 °C
15-20 °C
20-25 °C
25-30 °C
30-35 °C
35-40 °C
40-45 °C
45-50 °C

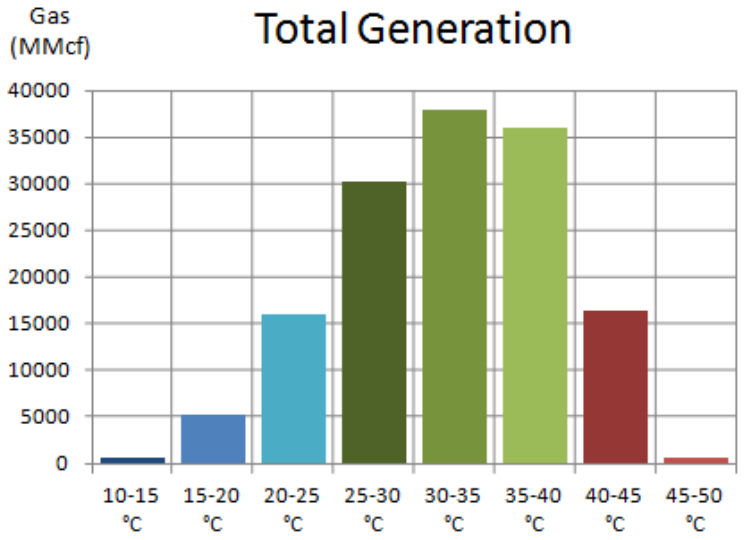
Total Generation
Gas (MMcf)
40000
35000
30000
25000
20000
15000
10000
5000
0
10-15 °C
15-20 °C
20-25 °C
25-30 °C
30-35 °C
35-40 °C
40-45 °C
45-50 °C

SD4 Ages

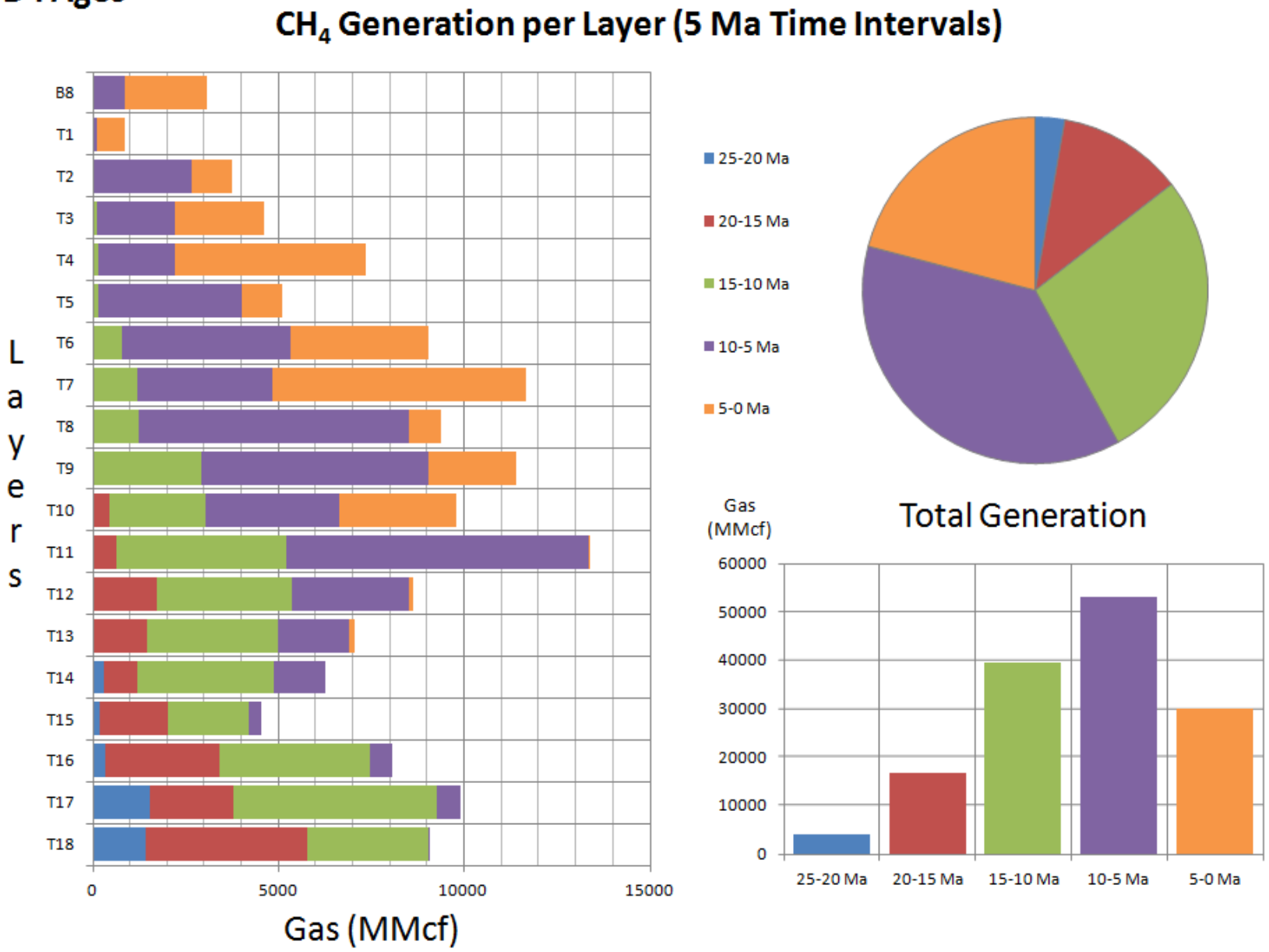
CH4 Generation per Layer (5 Ma Time Intervals)
B8
T1
T2
T3
T4
T5
T6
T7
T8
T9
T10
T11
T12
T13
T14
T15
T16
T17
T18
Layers
0
5000
10000
15000
Gas (MMcf)
25-20 Ma
20-15 Ma
15-10 Ma
10-5 Ma
5-0 Ma
Total Generation
Gas (MMcf)
60000
50000
40000
30000
20000
10000
0
25-20 Ma
20-15 Ma
15-10 Ma
10-5 Ma
5-0 Ma

SD4 Ages

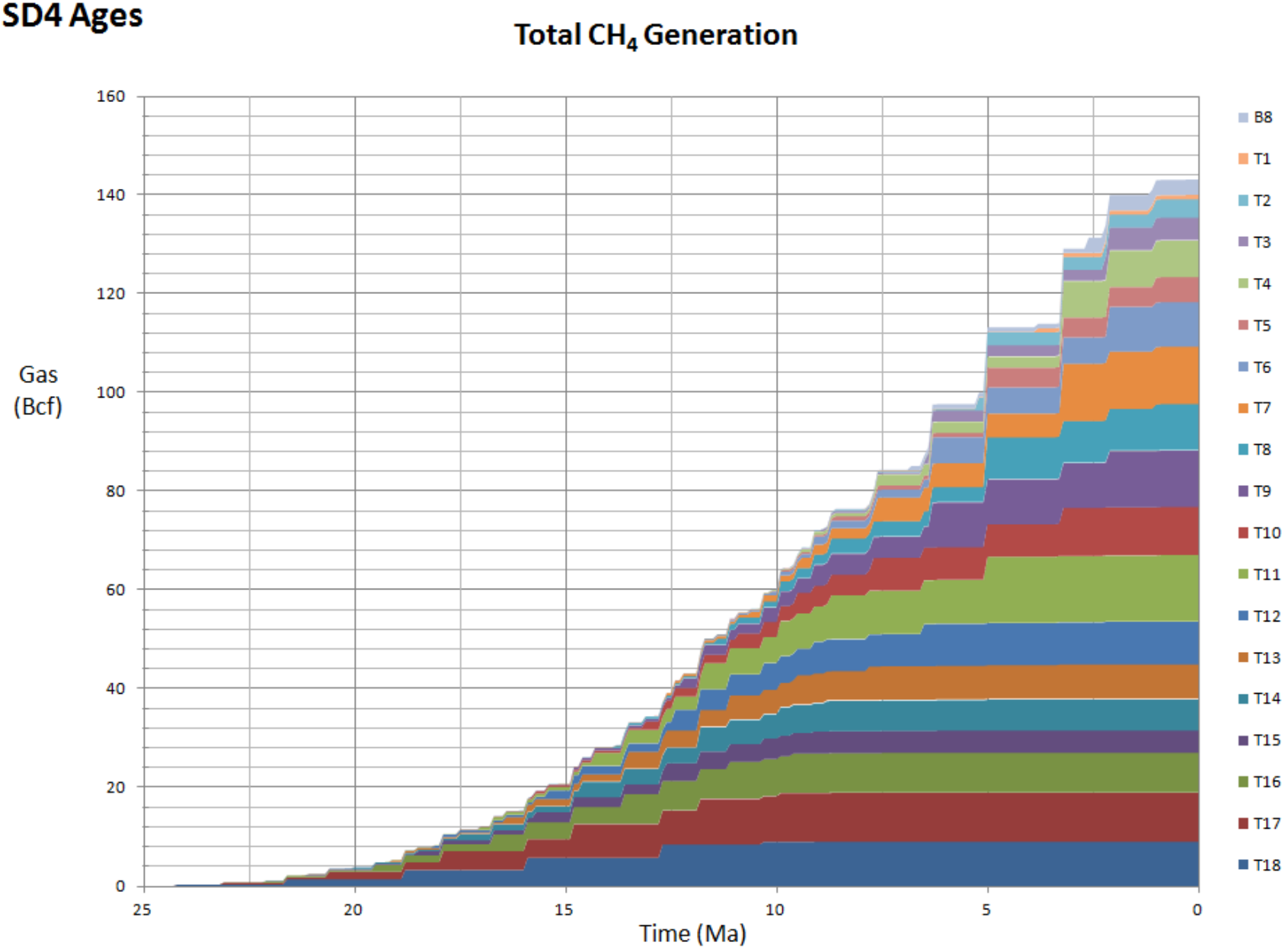
Total CH_4 Generation
Gas (Bcf)
160
140
120
100
80
60
40
20
0
25
20
15
10
5
0
Time (Ma)
B8
T1
T2
T3
T4
T5
T6
T7
T8
T9
T10
T11
T12
T13
T14
T15
T16
T17
T18

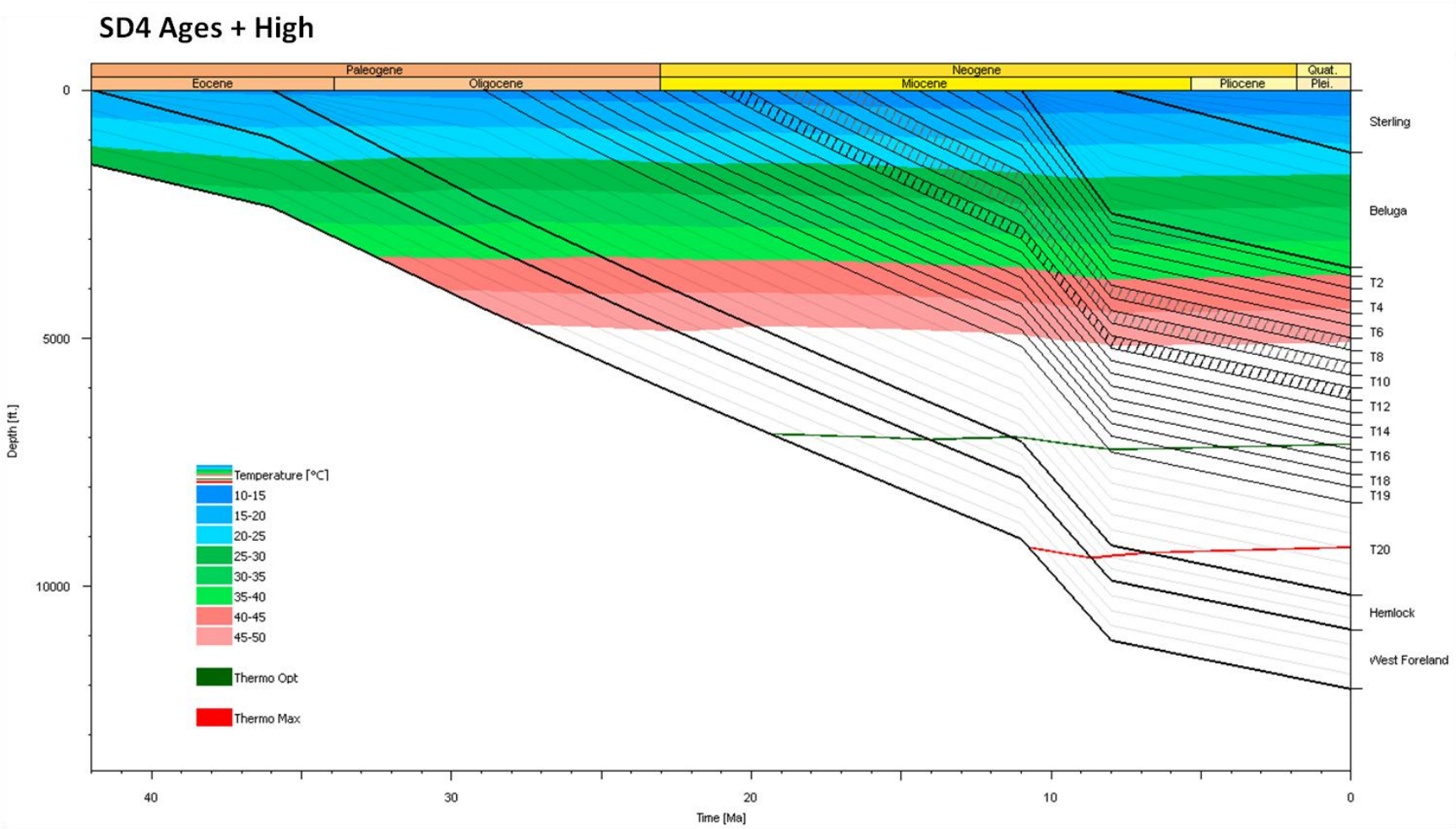
SD4 Ages + High
Paleogene
Neogene
Quat.
Eocene
Oligocene
Miocene
Pliocene
Plei.
0
5000
10000
Depth [ft.]
Temperature [°C]
10-15
15-20
20-25
25-30
30-35
35-40
40-45
45-50
Thermo Opt
Thermo Max
Sterling
Beluga
T2
T4
T6
T8
T10
T12
T14
T16
T18
T19
T20
Hemlock
West Foreland
40
30
20
10
0
Time [Ma]

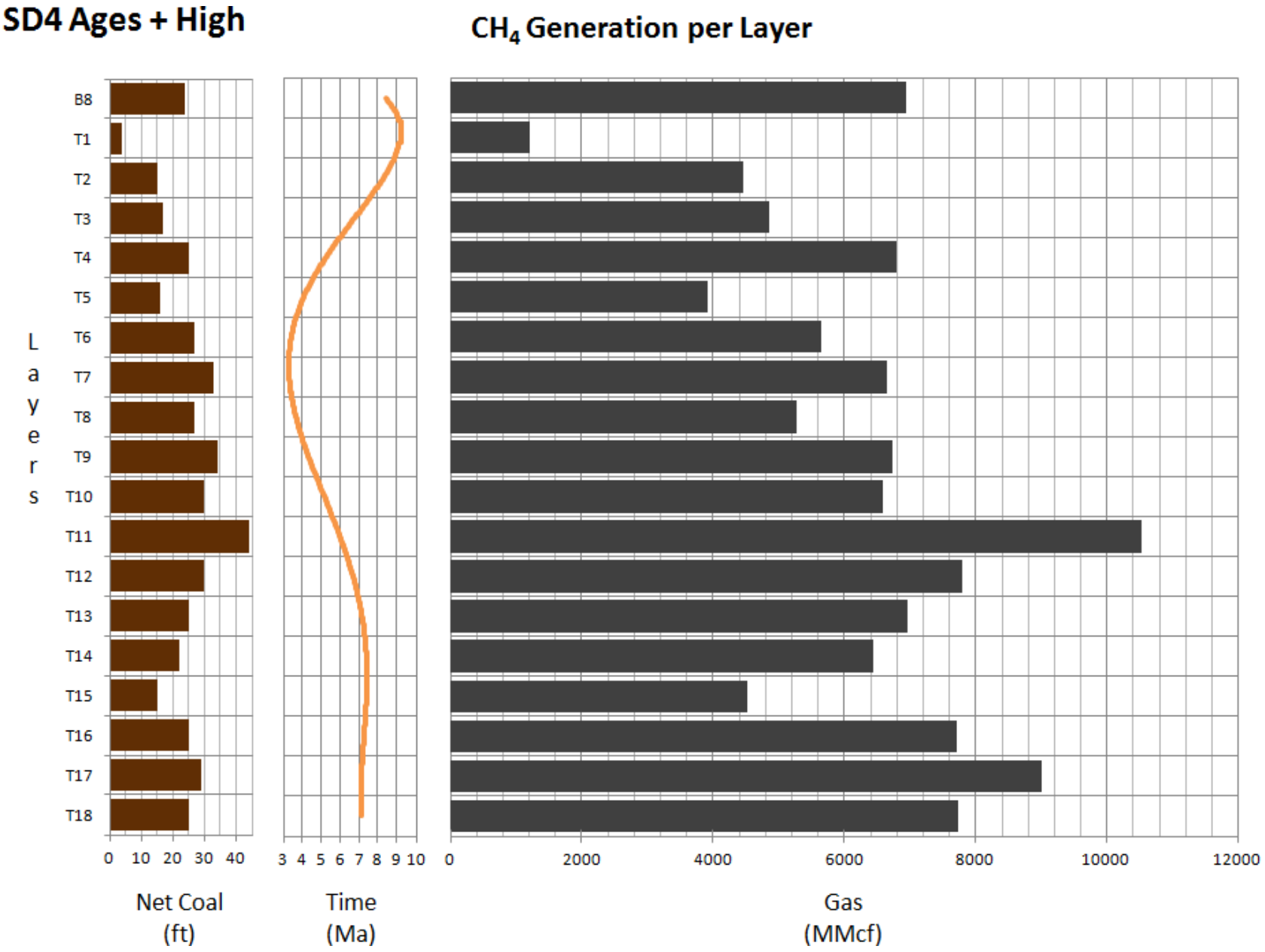
SD4 Ages + High
CH4 Generation per Layer
Layers
B8
T1
T2
T3
T4
T5
T6
T7
T8
T9
T10
T11
T12
T13
T14
T15
T16
T17
T18
0 10 20 30 40
Net Coal (ft)
3 4 5 6 7 8 9 10
Time (Ma)
0 2000 4000 6000 8000 10000 12000
Gas (MMcf)

SD4 Ages + High

CH_4 Generation per Layer (5 °C Temp Intervals)

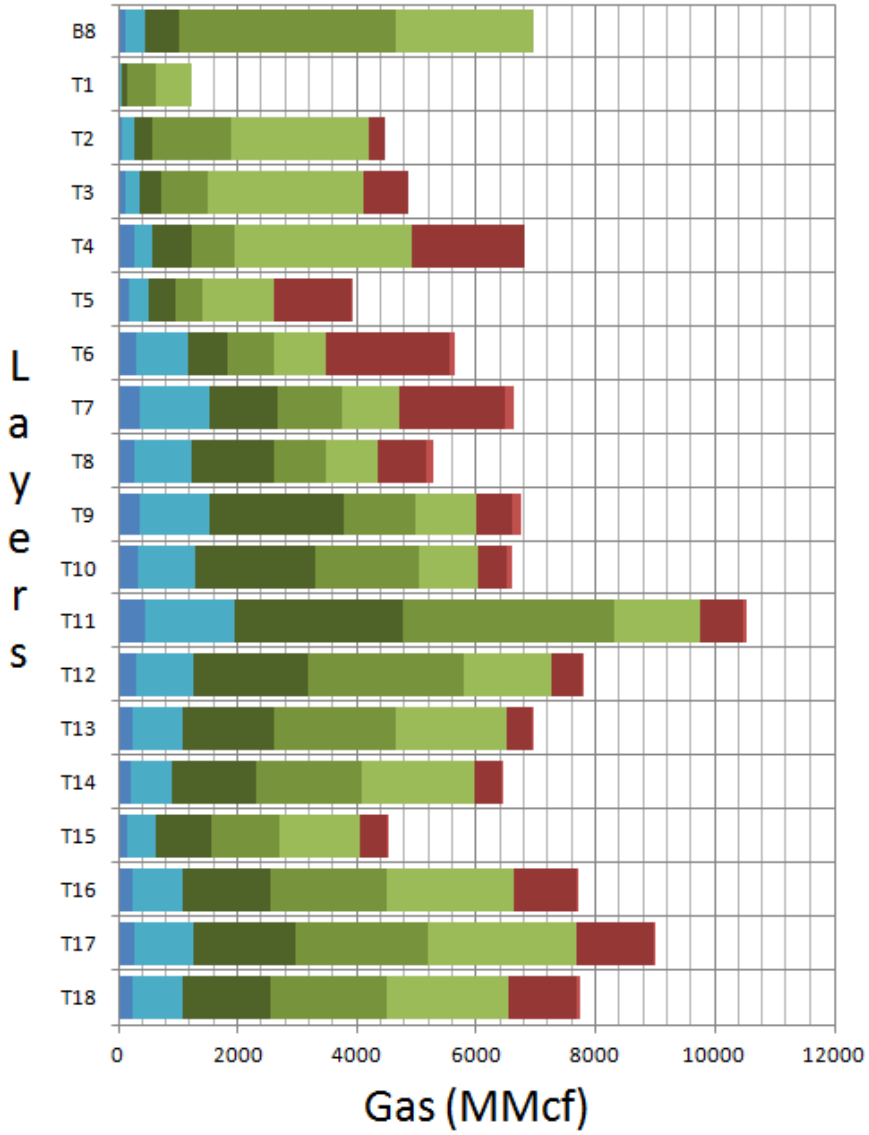

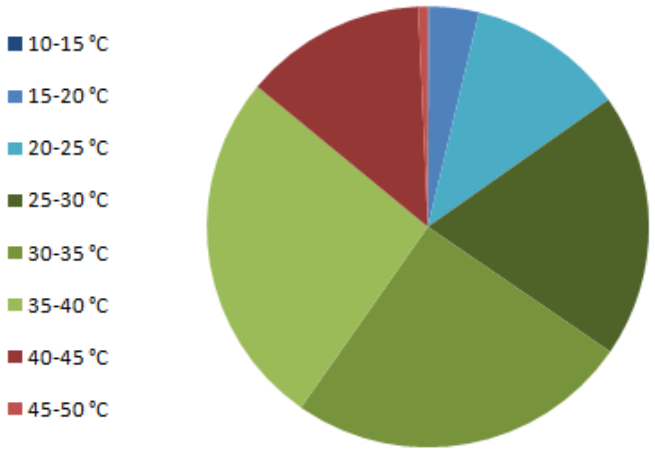

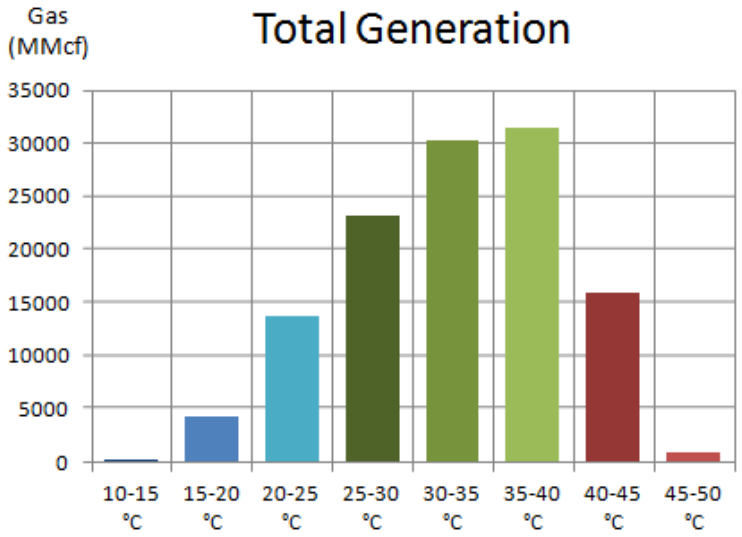

SD4 Ages + High

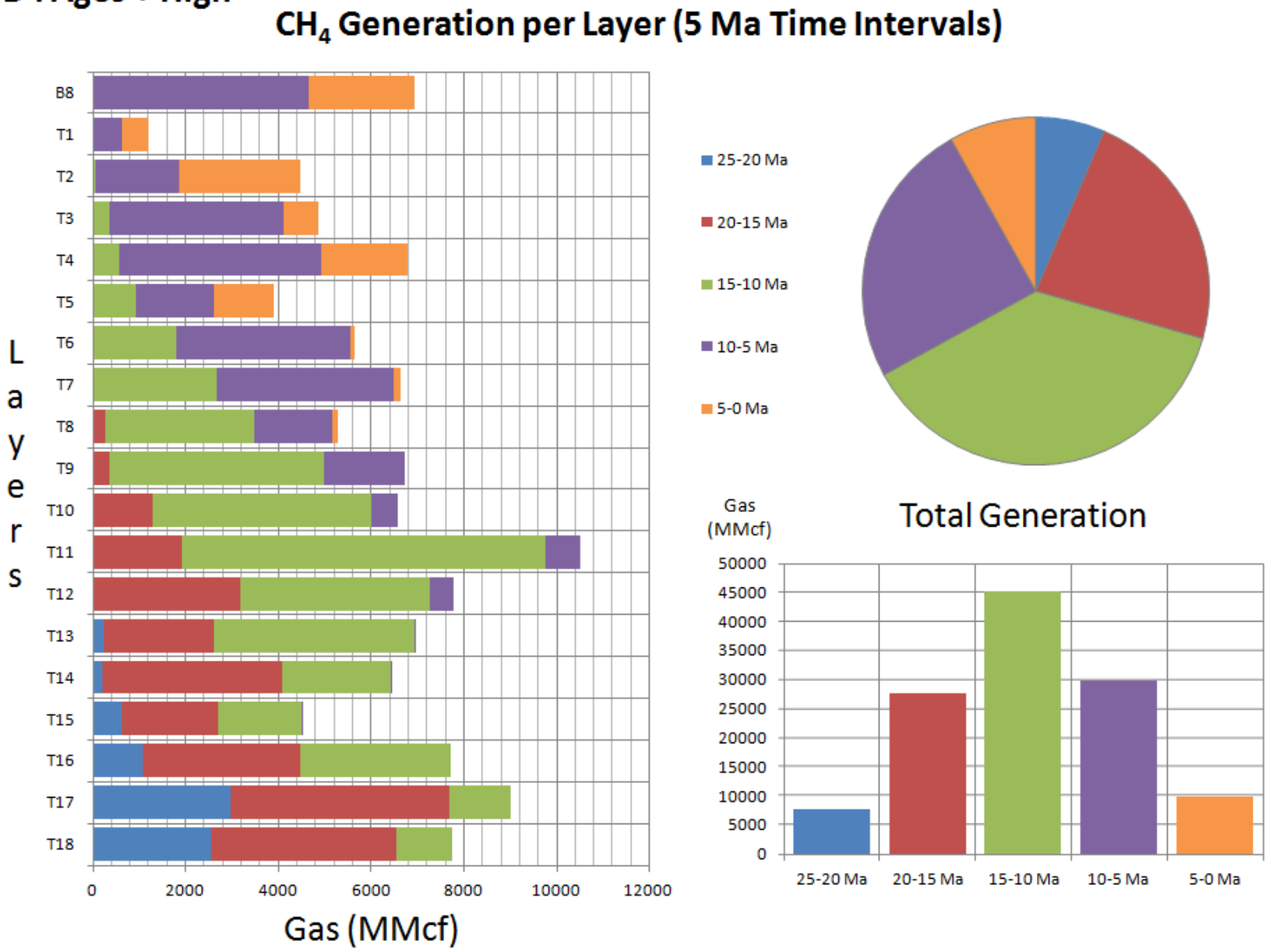

SD4 Ages + High

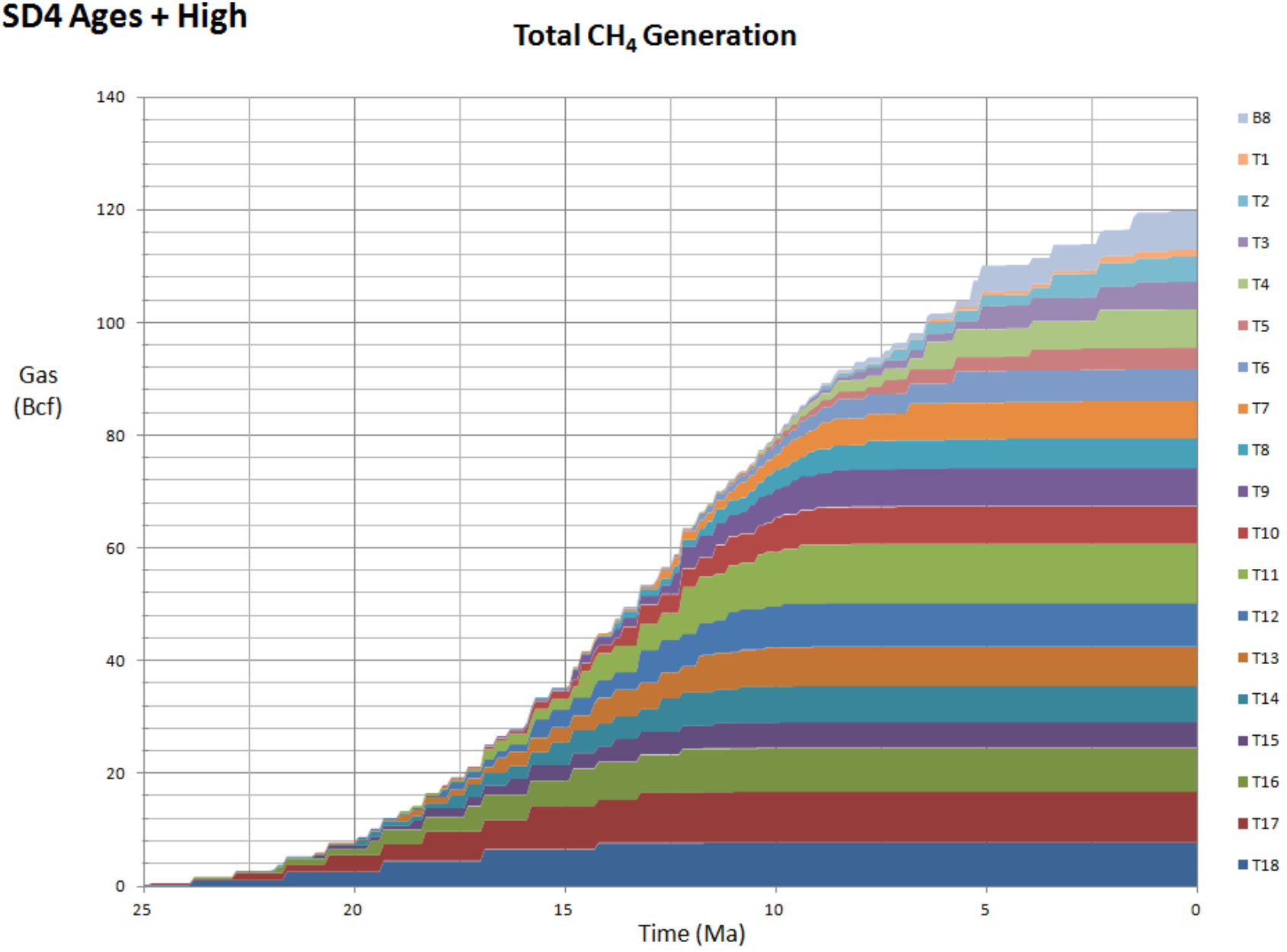

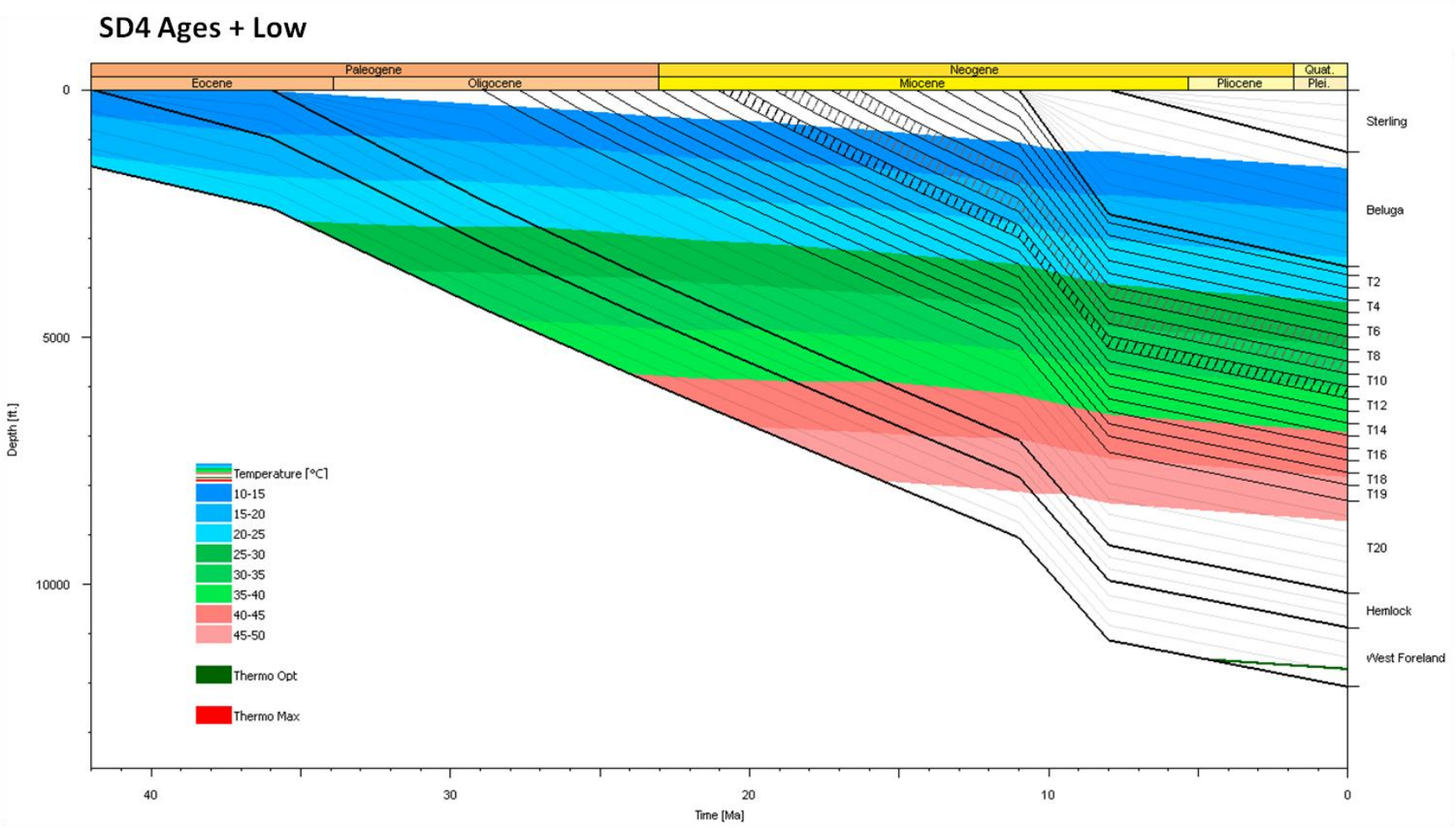
SD4 Ages + Low
Paleogene
Neogene
Quat.
Eocene
Oligocene
Miocene
Pliocene
Plei.
0
5000
10000
Depth [ft.]
Temperature [°C]
10-15
15-20
20-25
25-30
30-35
35-40
40-45
45-50
Thermo Opt
Thermo Max
Sterling
Beluga
T2
T4
T6
T8
T10
T12
T14
T16
T18
T19
T20
Hemlock
West Foreland
40
30
20
10
0
Time [Ma]

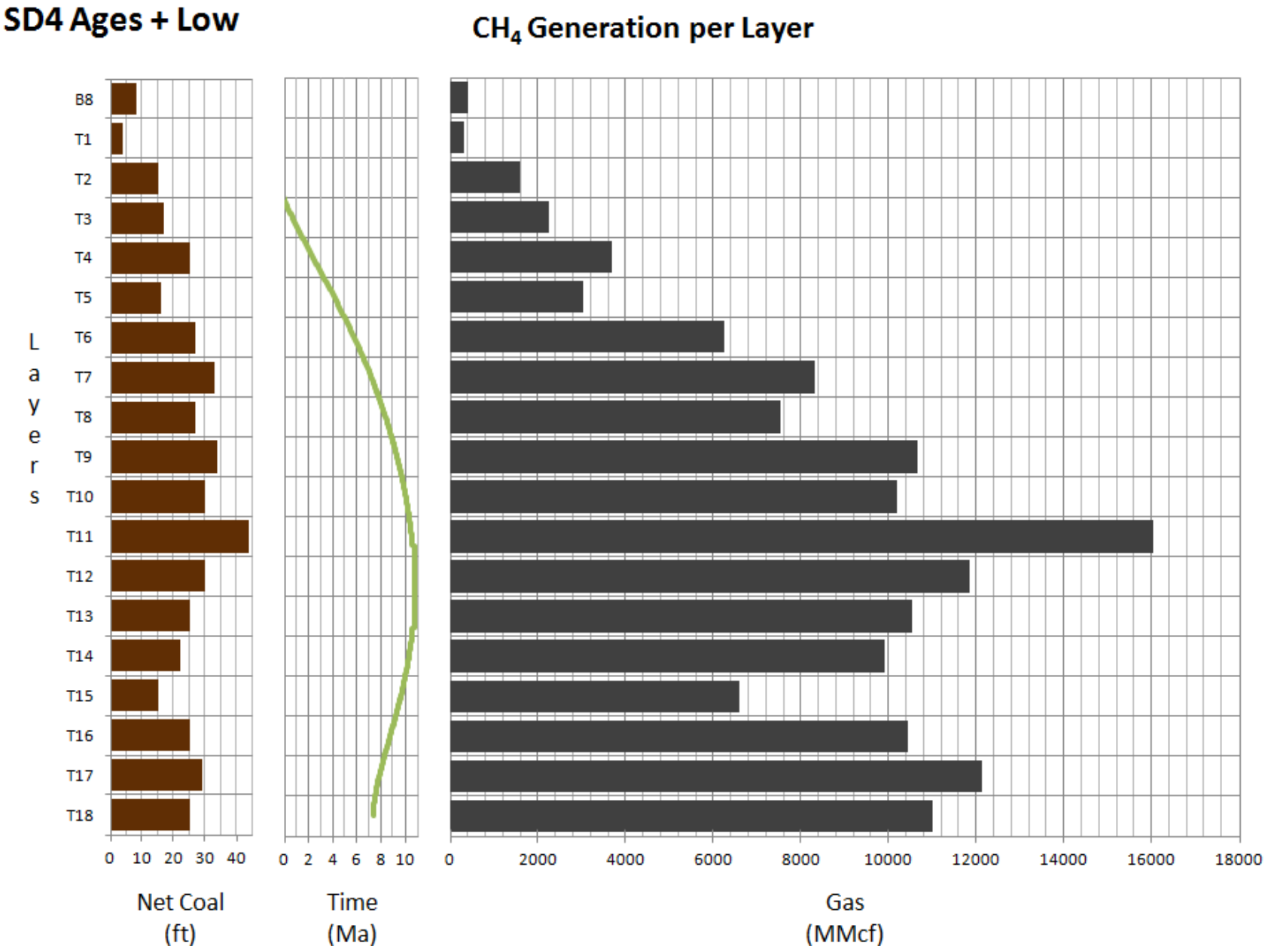
SD4 Ages + Low
CH4 Generation per Layer
Layers
B8
T1
T2
T3
T4
T5
T6
T7
T8
T9
T10
T11
T12
T13
T14
T15
T16
T17
T18
0 10 20 30 40
Net Coal (ft)
0 2 4 6 8 10
Time (Ma)
0 2000 4000 6000 8000 10000 12000 14000 16000 18000
Gas (MMcf)

SD4 Ages + Low

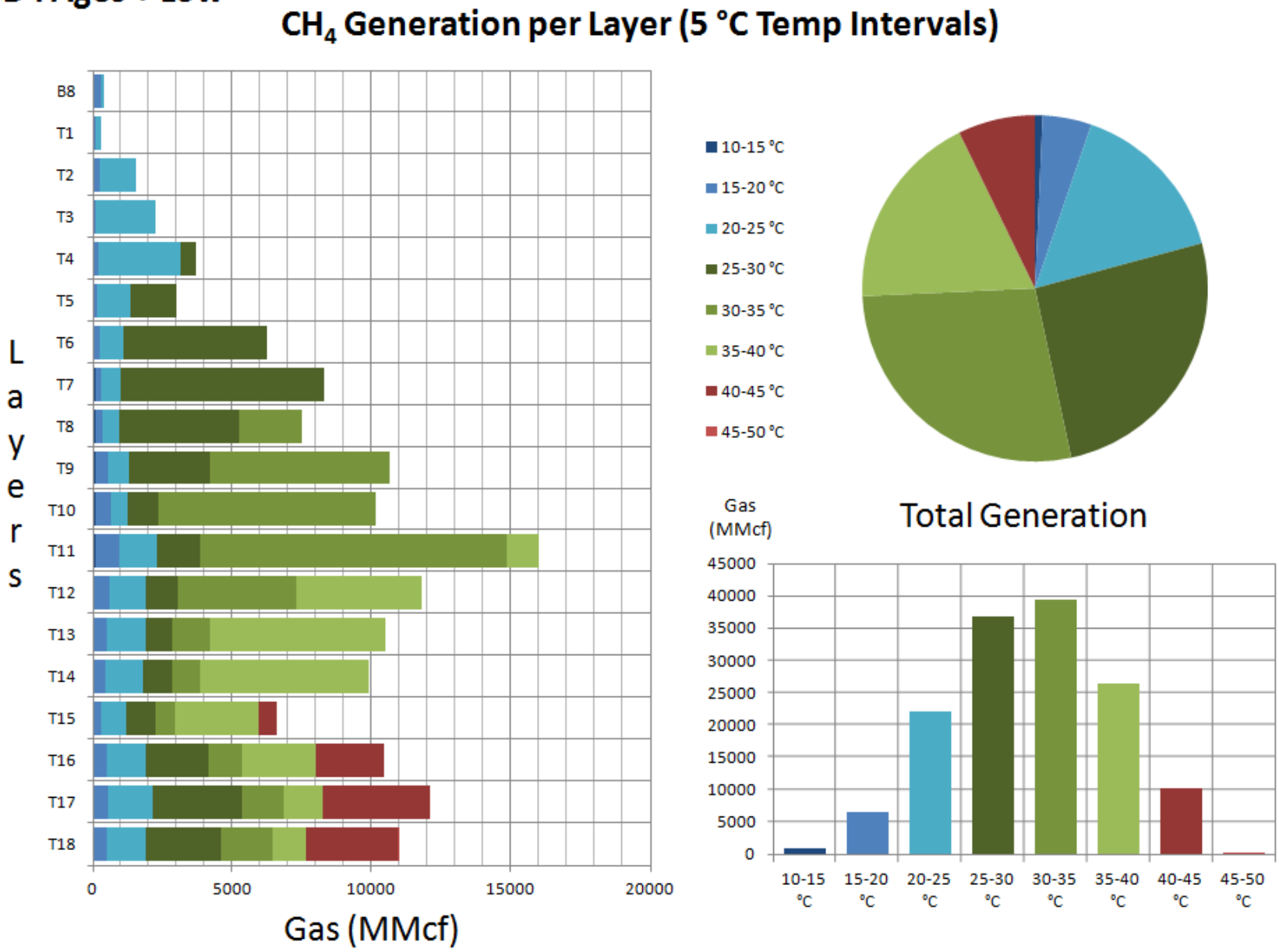
CH4 Generation per Layer (5 °C Temp Intervals)
B8
T1
T2
T3
T4
T5
T6
T7
T8
T9
T10
T11
T12
T13
T14
T15
T16
T17
T18
Layers
0
5000
10000
15000
20000
Gas (MMcf)
10-15 °C
15-20 °C
20-25 °C
25-30 °C
30-35 °C
35-40 °C
40-45 °C
45-50 °C
Total Generation
Gas (MMcf)
45000
40000
35000
30000
25000
20000
15000
10000
5000
0
10-15 °C
15-20 °C
20-25 °C
25-30 °C
30-35 °C
35-40 °C
40-45 °C
45-50 °C

SD4 Ages + Low

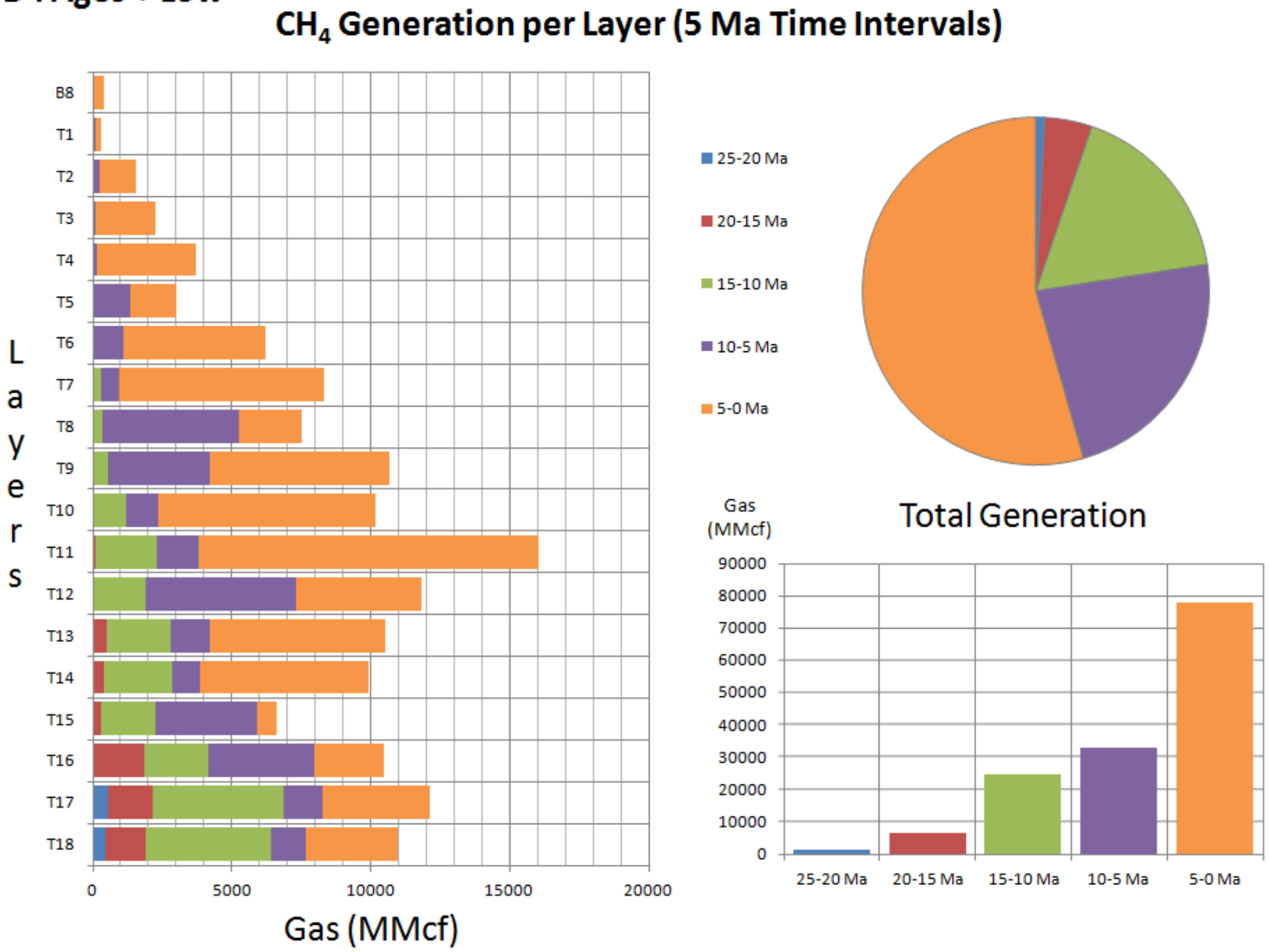
CH4 Generation per Layer (5 Ma Time Intervals)
Layers
B8
T1
T2
T3
T4
T5
T6
T7
T8
T9
T10
T11
T12
T13
T14
T15
T16
T17
T18
0
5000
10000
15000
20000
Gas (MMcf)
25-20 Ma
20-15 Ma
15-10 Ma
10-5 Ma
5-0 Ma
Total Generation
Gas (MMcf)
90000
80000
70000
60000
50000
40000
30000
20000
10000
0
25-20 Ma
20-15 Ma
15-10 Ma
10-5 Ma
5-0 Ma

SD4 Ages + Low

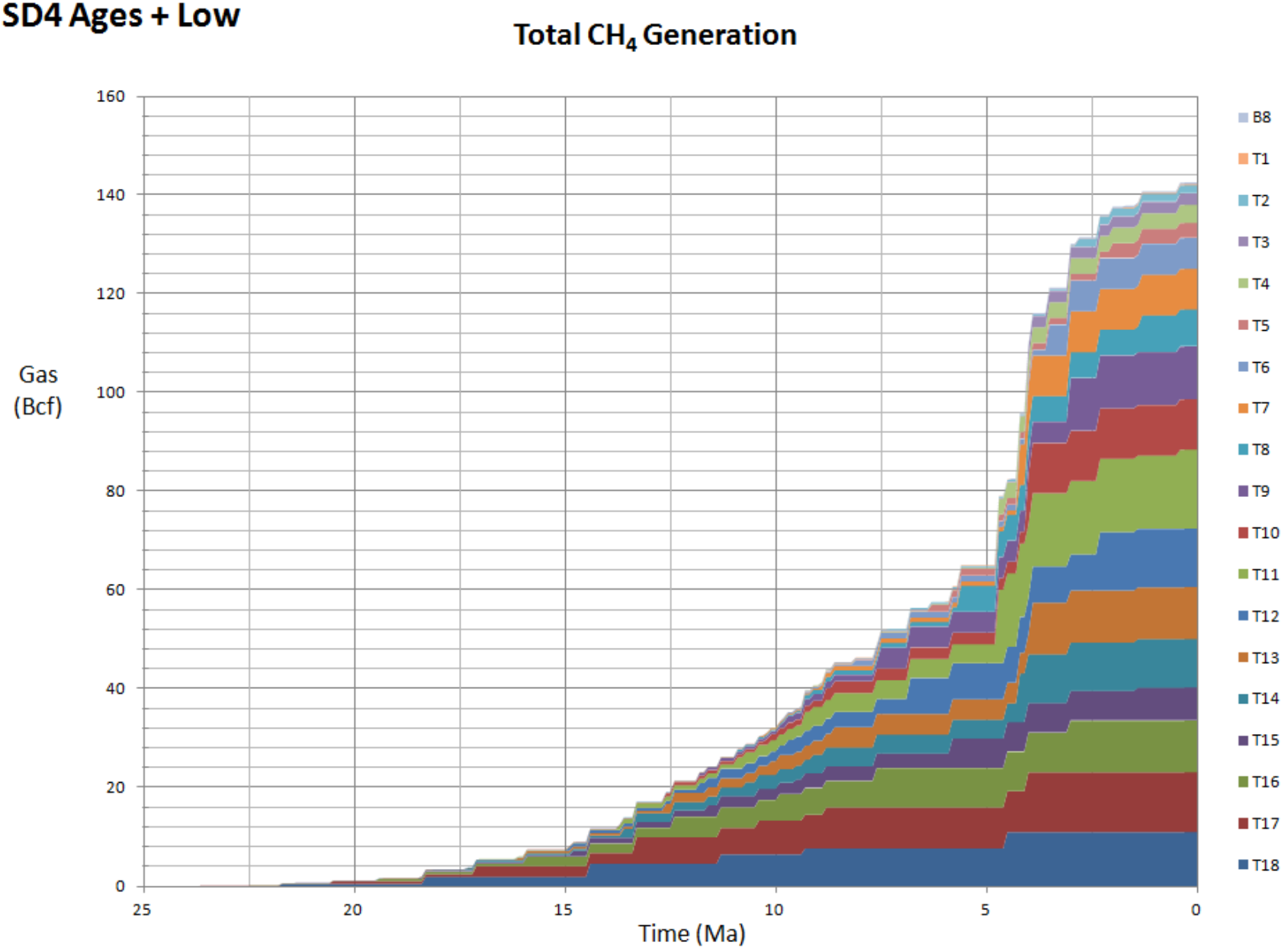
Total CH_4 Generation
Gas (Bcf)
160
140
120
100
80
60
40
20
0
25
20
15
10
5
0
Time (Ma)
B8
T1
T2
T3
T4
T5
T6
T7
T8
T9
T10
T11
T12
T13
T14
T15
T16
T17
T18

Vita

Eric Hart was born in Lafayette, Louisiana, in June of 1988 to parents Tom and Paula Hart. He attended high school at Lafayette High, and after graduating in 2006 he journeyed across the Atchafalaya Basin to Louisiana State University where he was named one of the top 100 students of his incoming freshman class. Not sure whether to pursue a career in petroleum engineering or geology, he enrolled in both curricula. Through his engineering courses, he landed two summer internships with Chevron Corporation, first as an offshore operations engineer on a platform in the Gulf of Mexico, and second as a reservoir engineer in their Lafayette office. Although irreplaceably educational opportunities, he decided that engineering was too technical for his liking and switched majors into his inherited passion and hobby, geology. Following junior year, he attended LSU field camp near Colorado Springs, Colorado, which proved to be another of his life's most singly defining events. It is said that field camp is the best experience that you hope to never go through again, but Eric would go back in a heartbeat if given the chance. After graduating from LSU in 2010 with a major in geology, a minor in anthropology, and a strong appreciation for petroleum engineering, he went to work as a geoscience intern for Devon Energy in Oklahoma City, Oklahoma. The following fall he returned to LSU to obtain his master's degree in geology and, more importantly, for two extra seasons of LSU football. During the next summer he completed his second geoscience internship at Devon (fourth overall), and was offered a full time position as a geophysicist in their new state of the art office tower which he gladly accepted. Eric has since relocated to OKC with his fiancée, Jance, and is very relieved to have finally begun his professional career after a tumultuous, yet eventful and extremely rewarding stint in academia.